10-18-2023

Cationic Frontal Polymerization: Front Kinetics, Effects of Additives, and Applications

Brecklyn R. Groce
Louisiana State University and Agricultural and Mechanical College

CATIONIC FRONTAL POLYMERIZATION: FRONT KINETICS, EFFECTS OF ADDITIVES, AND APPLICATIONS

A Dissertation

Submitted to the Graduate Faculty of the
Louisiana State University and
Agricultural and Mechanical College
in partial fulfillment of the
requirements for the degree of
Doctor of Philosophy

in

The Department of Chemistry

by
Brecklyn Ryleigh Groce
B.S. University of West Florida, 2019
December 2023

ACKNOWLEDGEMENTS

I want to thank my entire family for their support through my education. I am extremely grateful to my parents and sister who have supported me during my life—I would not be where I am or who I am without you. I'm thankful for my close friends back home who have always shown me support. In addition, thanks to my friends in the McGuire's Pipe Band, whom I've had the pleasure of continuing to play alongside even during my graduate studies.

I have had excellent professors during my undergraduate and graduate school experience who have led me to where I am in my academic career. To my advisor, Dr. John Pojman, I can't thank you enough for the guidance and support you've shown me during my time at LSU. You've allowed me to have many incredible experiences traveling to work with collaborators that have had such a positive impact on my career. I'm grateful for the opportunities you've given me to grow as a scientist and the kindness you've shown along the way which have made my time in graduate school so enjoyable. To my committee members, Dr. David Spivak, Dr. Víctor García-López, and Dr. Genevieve Palardy, thank you for your help, excellent suggestions, and knowledge you've passed on to me. To other collaborators and mentors I've worked with, Dr. Guy Van Assche, Dr. Robrecht Verhelle, Dr. Guoqiang Li, Dr. Mostafa Yourdkhani, Dr. Xiang Zhang, and Dr. Rafael Cueto, I'm grateful to have worked with all of you. Thank you also to Kim, Rachel, Kate, and everyone in the chemistry department office who have always been helpful and so kind.

Finally, to all my fellow graduate students and undergraduate students—thank you. I have made many wonderful friendships in graduate school that I cherish. To my fellow graduate students in the Pojman team, Anowar, Alex, Anthony, Daniel, Sam, Fahima, Maria, Dominic, and Mahmud, it's been fun working with all of you and I've appreciated all your help. To my

undergraduate colleagues, Joseph, Emma, Douglas, Dylan, Julia, Madison, Cristina, Madeline, and Imogen, it has been a pleasure working with you and thank you for all your help. The opportunity to serve as a mentor to you has had such a profound impact on my life.

TABLE OF CONTENTS

LIST OF ABBREVIATIONS

Frontal polymerization	**FP**
Radical-induced cationic frontal polymerization	**RICFP**
Frontal ring-opening metathesis polymerization	**FROMP**
Parts per hundred resin	**phr**
p-(octyloxyphenyl)phenyliodonium hexafluoroantimonate	**IOC-8**
1,1-Bis(tert-butylperoxy)-3,3,5-trimethylcyclohexane **(**Luperox 231)	**L231**
Benzopinacol	**TPED**
4-methoxyphenol	**MeHQ**
Trimethylolpropane triglycidyl ether	**TMPTE**
Tri(ethylene glycol) divinyl ether	**TEGDVE**
Trimethylolpropane triacrylate	**TMPTA**
1,4-cyclohexanedimethanol divinyl ether	**DVE-1,4**
1,4-butanediol vinyl ether	**BVE-1,4**
Ethylene glycol vinyl ether	**EGVE**
Bisphenol A diglycidyl ether	**BADGE**
3,4-epoxycyclohexylmethyl-3’-4’-epoxycyclohexanecarboxylate	**CE**
Neopentyl glycol diglycidyl ether	**NPDGE**
1,4-butanediol diglycidyl ether	**DGE**
Ethyl glycidyl ether	**EGE**
Dichloromethane	**DCM**
4,4’-methylenebis-(phenyl isocyanate)	**MBPDI**
Dicyclohexylcarbodiimide	**DCC**
4-dimethylaminopyridine	**DMAP**
Oleic acid	**OA**
PEG 600 Dicarboxylic acid	**PEGDCA**
Hexyl acrylate	**HA**
p-tert butylphenyl glycidyl ether	**PTBGE**
Propylene carbonate	**PC**

Dodecyl vinyl ether	**D12VE**
Vikoflex 7190	**V7190**
Epoxidized sucrose soyate	**ESS**
Fumed silica	**FS**
Carbon nanofibers	**CNF**
Carbon nanotubes	**CNT**
Calcium bentonite	**Ca-BNT**
Sodium bentonite	**Na-BNT**
Montmorillonite K10	**MMT-K10**
Speed mixed	**SM**
Differential scanning calorimetry	**DSC**
Infrared spectroscopy	**IR**
Attenuated total reflectance	**ATR**
Scanning electron microscopy	**SEM**
Energy dispersive x-ray spectroscopy	**EDS**
Thermogravimetric analyzer	**TGA**
Glass transition temperature	**Tg**

ABSTRACT

Cationic frontal polymerization broadens the potential application of frontal polymerization by allowing for use of monomers such as epoxies and vinyl ethers. In this work, the effects of monomer and initiator composition and additives including fillers on front kinetics, along with applications of cationic frontal polymerization were investigated.

Using a radical-induced cationic frontal polymerization (RICFP) method with a superacid generating salt and a thermal radical initiator, the addition of vinyl ethers to epoxy formulations was studied, where an increase of front velocity was seen with increase of divinyl ether to epoxy ratio. Other aspects of vinyl ether systems, such as pot life and functionality, were also investigated. With promising results of vinyl ethers, synthesis of novel vinyl ethers for frontal polymerization was attempted in Chapter 3. In Chapter 4, a hybrid system with the addition of acrylates, which have been well-studied in frontal polymerization, to epoxies and vinyl ethers was investigated, and it was demonstrated that the ratio of monomers can affect the material properties of polymers formed. The acrylates do not copolymerize with the epoxy or vinyl ether, resulting in a concave dependence of front velocity on acrylate percentage.

Adding fillers to formulations can improve mechanical properties, lower overall cost, and affect front velocity. In Chapter 5, clay minerals added to RICFP systems were found to reduce front velocity. Causes of this reduction were investigated, as were the effects of the fillers on mechanical and thermal properties of the polymer composites and clay dispersion in the polymer matrix. Drying the clays in an oven increased the front velocity, indicating water content inhibiting the cationic polymerization.

In a modification of RICFP presented in Chapter 6, it was found that a front was supported for epoxies and vinyl ethers in absence of a primary radical source and only addition

of the superacid generator. The superacid generating salt acts as a source of radicals, as indicated by the addition of radical inhibitor. Potential applications investigated for RICFP are shown in Chapter 7, which includes additive manufacturing, coatings, and use of bio-derived monomers.

CHAPTER 1. OVERVIEW OF FRONTAL POLYMERIZATION

1.1. Brief History of Frontal Polymerization

Frontal polymerization (FP) was discovered by Chechilo and Enikolopyan, who observed the spreading of methyl methacrylate polymerization in reactors under pressure. [1] Studies of the frontal process were continued in Russia by both their group and others through the 1970s and 80s, involving characterization, curing of epoxies and acrylates, and analysis and simulations of FP. [2-5] FP was finally rediscovered by Pojman in 1991 and thoroughly studied during the 1990s[6-8] and has seen recent rapid growth through applications such as composites, [9, 10] cure-on demand materials and adhesives, [11, 12] deep-eutectic solvents[13] and hydrogels. [14-18] Use of FP gives many advantages versus traditional autoclave or bulk curing methods, like reduced energy input, long pot lives, one-pot formulations, cure on-demand materials, and faster cure times.

1.2. Frontal Polymerization Process

In FP, an input of energy at a specific area initiates a propagating localized reaction zone that travels through the entire material, where monomer is converted into polymer as propagation occurs. [19, 20] A cartoon depicting FP is shown in Figure 1.1. There are two other recognized forms of FP: photofrontal polymerization which relies upon constant UV irradiation, and isothermal FP, which relies on the gel effect and a propagation from a solid polymer placed into a solution of monomer and initiator. [19] Thermal FP is the most common method in the literature, which relies on the coupling of Arrhenius rate kinetics of an exothermic reaction with heat diffusion, and is the studied FP process throughout this dissertation. The basic requirement of FP is to have a rate of heat generation that exceeds the rate of heat loss. Additionally, systems must be unreactive at room temperature and have a high activation energy while resulting in a large heat release while reacting to exceed heat loss.

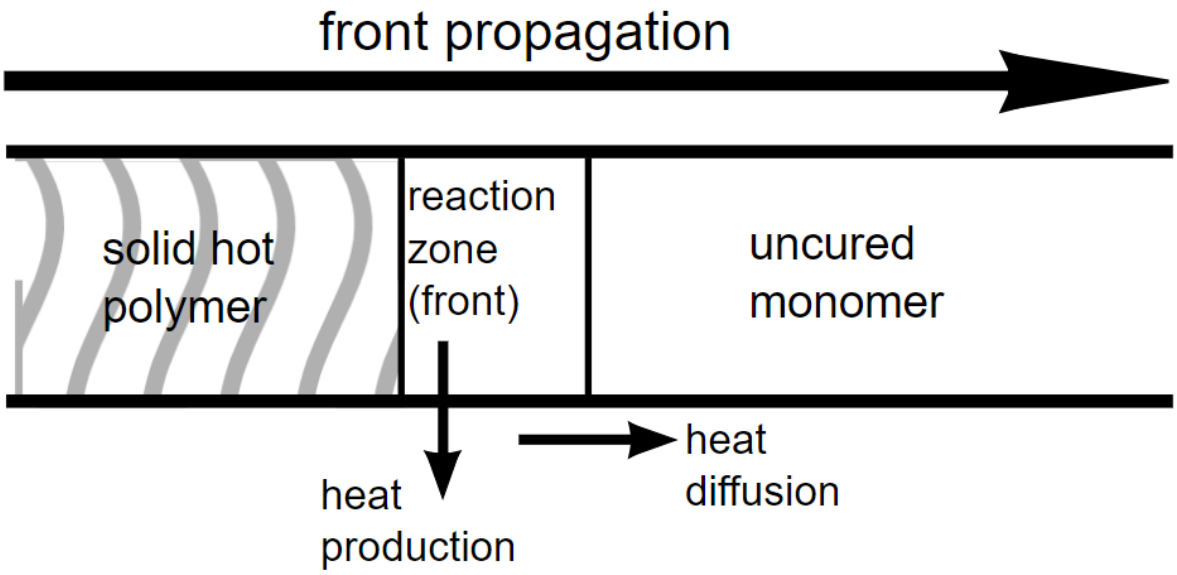

Figure 1.1. Illustration of a frontal polymerization process occurring.

Front-quenching can occur due to buoyancy-driven convection, but this can be avoided by increasing the viscosity through addition of fillers such as fumed silica. [21-23] Addition of fumed silica as an inorganic filler also allows for horizontal frontal polymerization in molds versus vertically in test tubes. [24] With unfilled, liquid monomers, FP in test tubes can suffer from convection if the fronts ascend. These conclusions are made based on forming solid product—if liquid product is formed, convection can mix cold monomer into a propagating front regardless of the reaction orientation, reducing front temperature. Reactions in test tubes sometimes can result in destruction of the test tube due to the pressure of any volatiles produced during FP, and FP of the viscous resin with fumed silica better replicates the practical applications of these cure on-demand materials. Excessive heat loss can also result in quenching of fronts.

FP kinetics are characterized by observing the front velocity and the front temperature. The front velocity is calculated by tracking the propagation of a front and taking the slope of front position versus time. It can be affected by many different factors, including initiator

concentration, monomer reactivity and functionality, and sources of heat loss in the system. Front temperature is directly related to the front velocity and can indicate heat loss present due to factors such as low boiling point monomers, additives that reduce thermal diffusion, or low reactivity of the system.

1.3. Monomer Systems for Frontal Polymerization

Typically, most monomers capable of supporting fronts proceed by free-radical mechanisms due to their high rate of reactivity and exothermicity. [19] Much of the early fundamental FP work was done with acrylate-based monomers. [6, 25, 26] These cure through chain-growth polymerizations initiated with peroxides such as benzoyl peroxide or Luperox 231, or azo-based initiators like azobisisobutyronitrile. Systems are usually initiated with a thermal energy source, such as a soldering iron or heat gun, or UV light, depending on what source is compatible with initiator decomposition and subsequent radical formation. Acrylate-based systems have been used to study the effects of functionality, initiator concentration, convection, and layer thickness for example. [7, 23, 27-29] With the use of peroxide-based radical initiators, voids can be an issue in these formulations as volatile compounds are typically produced upon decomposition of the initiator. [19]

One of the other major classes of monomers in FP are those monomers which can undergo frontal ring-opening metathesis polymerization (FROMP). [9, 30-32] These are mostly limited to norbornene and dicyclopentadiene-type monomers. Through combination with the ruthenium-based Grubbs' catalyst, these monomers will undergo a ring-opening metathesis polymerization with thermal or light-triggered initiation. Modified catalysts and monomers for FROMP systems have been studied extensively and demonstrated to successfully generate composites and be suitable for additive manufacturing. [9] Unfortunately, one of the disadvantages

with FROMP systems is their pot life, which have only reached ~30 hours at best. [33] The costs of Grubbs' catalysts are also a disadvantage.

1.4. Radical-Induced Cationic Frontal Polymerization (RICFP)

RICFP is a newer development in FP, where polymerization proceeds through a cationic mechanism rather than the typical free-radical polymerization. This process allows for FP of epoxies without using amine curing agents that give formulations short pot lives. [34, 35] Epoxies are commonly used in composites and adhesives. RICFP was developed by Mariani et al. in 2004, [36] and almost all focus has been on studying epoxy resins and composite materials. [37-41]

RICFP uses elements from radical FP through the integration of a thermal radical initiator, typically a peroxide or benzopinacol, [42] with a superacid generating salt used in cationic photopolymerization, typically an antimonate-based iodonium salt. Diaryliodonium salt photoacid generators were first discovered by Crivello et al. in 1977. [43] These salts generate acids upon UV irradiation and have since been shown to photopolymerize both epoxy[44-47] and vinyl ether monomers. [48-51] Their good thermal stability in ambient conditions led to increased use as photoinitiators. Now, the availability of these salts has widened, allowing commercially available onium salts to be common. When comparing RICFP to bulk photopolymerizations, the main advantage is the ability to cure thick samples through UV-irradiation, as opposed to only curing the surface; this is especially the case for filled or composite parts where UV penetration may be hindered.

Decomposition of onium salts with light begins through heterolytic or homolytic cleavage of the structure via photolysis, producing radical, cationic and radical-cationic species. Through proton abstraction, acid is generated that can initiate cationic polymerization. For the photoacid generator, the properties of the counterion determine the strength of the Brønsted

superacid formed; antimonium anions result in high strength superacids and higher polymerization rates due to large anion size and low nucleophilicity. [44, 52]

The mechanism shown in Figure 1.2 adapted from the original mechanism presented by Mariani et al. in 2004[36] displays the application of heat in step 1 rather than UV light. Throughout this dissertation, the photoacid generator will be referred to as a superacid generator.

In step 1, an input of heat will decompose the thermal radical initiator to form radicals that decompose and reduce the superacid generator, typically an iodonium hexafluoroantimonate salt as displayed in the figure, resulting in generation of the superacid in step 2. The superacid will then react with the monomer, propagating and generating heat to form radicals from the thermal initiator that cleave the iodonium salt (step 3) to once again form the superacid. This mechanism cycles as the front propagates, and the monomer is converted.

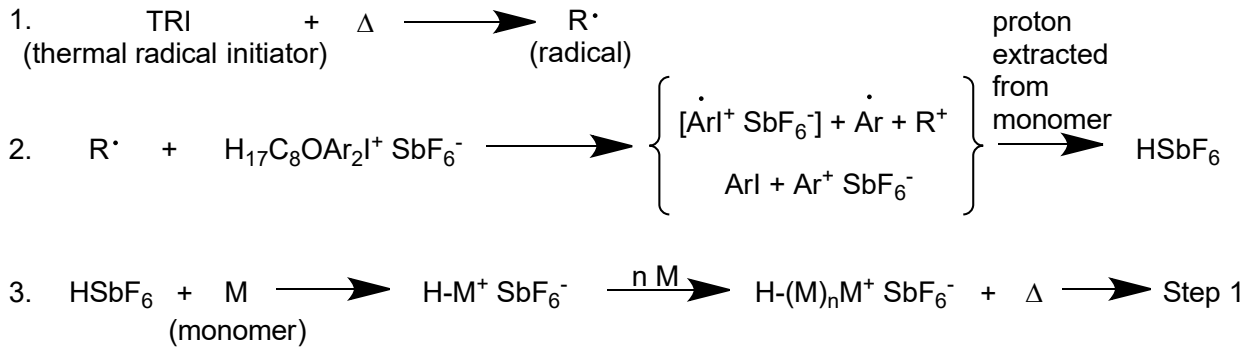

Figure 1.2. RICFP mechanism adapted from Mariani et al. [36]

Sulfonium-based salts have also been studied. [42, 53] UV-initiated RICFP has been demonstrated with a combination of sulfonium hexafluoroantimonate salts acting as both thermal and photoinitiators. [53] RICFP with sulfonium hexafluoroantimonate salts will not work in some cases due to the low redox potential of the sulfonium. [42, 54] Salts with aluminate-based counterions have displayed improvements over antimony-based salts in formulations with thermal radical initiator and bisphenol A diglycidyl ether (BADGE) and are available commercially at high cost to

volume. [55, 56] Taschner et al. studied the use of novel bismuthonium and pyrylium-based salts in RICFP, which had improved pot life over iodonium salts but otherwise performed unfavorably. [57]

Peroxides may be used as TRIs, though Bomze et al. discovered it was possible to use 1,1,2,2-tetraphenylethylenediol (benzopinacol, TPED) in lieu of peroxides. [42] This compound contains a labile C-C bond, and reversibly forms radicals; in formulations with BADGE and IOC-8, the TPED acts as a gas-free initiator. Extensive studies of the kinetic effects and potential applications of TPED as a bubble-free initiator have been published. [38, 54, 56, 58, 59] Bomze et al. additionally saw that many common TRIs could not support RICFP of BADGE. [42]

CHAPTER 2. RADICAL-INDUCED CATIONIC FRONTAL POLYMERIZATION OF VINYL ETHERS AND EPOXIES

2.1. Introduction to Vinyl Ethers in FP

Vinyl ether monomers are known to be highly reactive in cationic polymerization due to the contributions of the electron-donating oxygen adjacent to the double bond resulting in a highly nucleophilic double bond. [60] They typically see applications in coatings due to good adhesion with metal and wood, fast cure rate due to reactivity, low toxicity, insensitivity to oxygen and the cationic mechanism allowing for formulations with other comonomers. [52, 61] Cationic photopolymerizations of vinyl ethers have been studied extensively, both as homopolymers and comonomer systems. [62-68]

RICFP has been studied as a method to frontally polymerize mostly epoxide monomers. [37-42, 53, 54, 56, 69, 70] There has been recent work showing RICFP of pure divinyl ethers and divinyl ether/epoxy/acrylate hybrid systems with near-infrared sensitizers added to promote front initiation via near-infrared laser as well. [71] Use of vinyl ethers in small concentrations with pyrylium salts as a coinitiator system for photoinduced thermal FP has also been shown. [72] Epoxies are typically found in systems with vinyl ethers for existing photopolymerization reactions, as they can polymerize through a cationic mechanism like vinyl ether monomers. Addition of vinyl ether to epoxies has been shown to accelerate the photocuring process of the resin. [48]

This chapter was previously published as B. R. Groce, D. P. Gary, J. K. Cantrell and J. A. Pojman. Front velocity dependence on vinyl ether and initiator concentration in radical-induced cationic frontal polymerization of epoxies, Journal of Polymer Science, 2021, 59(15), 1678-1685. Reprinted with permission from Wiley.

Given that reactivity of photocured resins increases with vinyl ether addition, similar experiments were carried out with RICFP based resins. Enhancement of reactivity could prove useful for increasing the front speed with added vinyl ether. Likewise, the dependence of the front kinetics in respect to initiator concentration was studied to determine the best options towards optimization of RICFP resins.

2.2. Materials and Methods for RICFP

Trimethylolpropane triglycidyl ether (TMPTE), tri(ethylene glycol) divinyl ether (TEGDVE), 1,4-cyclohexanedimethanol divinyl ether (DVE-1,4) and 1,1-Bis(tert-butylperoxy)-3,3,5-trimethylcyclohexane (Luperox 231) were purchased from Sigma-Aldrich. 1,4-butanediol vinyl ether (BVE-1,4), and ethylene glycol vinyl ether (EGVE) were purchased from Beantown Chemical (Hudson, NH). *p*-(octyloxyphenyl)phenyliodonium hexafluoroantimonate (IOC-8) was purchased from abcr (Karlsruhe, Germany). All chemicals were used as received. Chemical structures of the monomers and initiators used are shown in Figure 2.1.

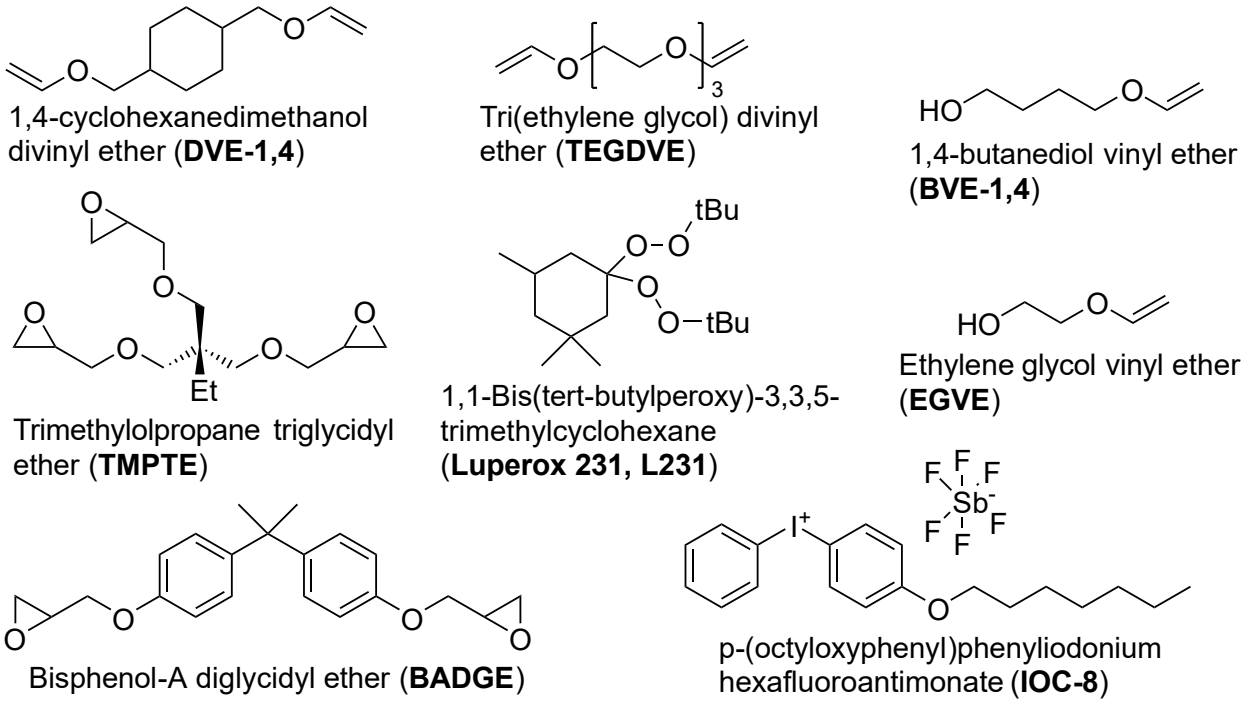

Figure 2.1. Chemical structures for all reagents used in vinyl ether kinetics studies.

Solutions were made for each formulation containing varying ratios of TMPTE (25-100 wt%) and vinyl ether (TEGDVE, DVE-1,4, BVE-1,4 or EGVE; 0-75 wt%) and varying concentrations in phr (parts per hundred resin) of Luperox 231 (0.50-1.50 phr) and IOC-8 (0.50-1.50 phr). Parts per hundred resin is a term meaning 1 gram of material for every 100 g of resin. Luperox 231 and IOC-8 were first added to and mixed with TMPTE for 1 hour to achieve near-complete dissolution of IOC-8 before the addition of vinyl ether. The solutions were then stirred overnight to ensure homogeneity. The system chosen for front kinetics studies utilizes TMPTE as the chosen epoxy comonomer. Low-viscosity TMPTE allows for easy solvation of the solid iodonium salt in addition to providing structural benefits such as the long glycidyl ether chains giving increased flexibility to the polymer.

To prepare samples for fronts, 15 g aliquots were taken from a formulation solution and 10 wt% fumed silica (Aerosil 200, Evonik Industries (Parsippany, NJ)) was added to form a

moldable putty. The putty was loaded into a wooden mold (13.5 cm × 2 cm × 0.6 cm) lined with wax paper for easy removal. A thermocouple connected to Logger Lite software from Vernier was then placed 2 cm into the length of the sample and approximately halfway into the sample depth to record front temperature. A soldering iron heated to approximately 200 ℃ (confirmed with an infrared thermometer) was used to initiate the fronts by brief contact with the sample. The fronts were tracked using a video camera placed directly above the sample. Front velocity was calculated from the slope of front position versus time. The mold was cooled to room temperature prior to subsequent experiments. Triplicate experiments were performed for each formulation from the same solution.

Thermal analysis of three samples was attempted using a TA Instruments Q100 differential scanning calorimeter (DSC). Samples of pure Bisphenol-A diglycidyl ether (BADGE), pure DVE-1,4 and a 1:1 ratio of both BADGE and DVE-1,4 were frontally polymerized with 0.50 phr IOC-8 and 1.00 phr Luperox 231 and 10 wt% fumed silica. A temperature ramp procedure of -40 ℃ to 400 ℃ with 2 cycles was utilized for each sample with differing heating rates depending on the sample. Infrared spectroscopy was performed with a Bruker FTIR and diamond ATR accessory for structural characterization and conversion determination. Parameters of 4 cm^{-1} resolution, 32 sample scans, and 16 background scans were used. The resin was placed directly on the ATR diamond. Polymer samples were instead ground into a powder using a mortar and pestle to place onto the ATR platform. By using a large amount of sample, the probe created a film on the platform. Triplicates of every IR spectrum were taken, and a background was taken before every measurement.

2.3. Effects of Vinyl Ethers in Epoxy RICFP

The vinyl ethers were first mixed in formulations with TMPTE to test the viability of front propagation. The initiator system consisted of 0.50 phr IOC-8 and 1.00 phr Luperox 231, which is approximately 1 mol% of the superacid generator and thermal initiator, previously reported by Bomze et al. to be sufficient to support fronts for epoxy-based RICFP systems. [42, 54]

Of the chosen vinyl ethers, DVE-1,4, TEGDVE and BVE-1,4 supported front propagation. When EVGE was added to formulations, no front was initiated but only local polymerization at the contact point of the soldering iron occurred. The polymers produced by TEGDVE-containing formulations were dark brown in color, soft, and flexible; those produced by DVE-1,4-containing formulations were lighter brown or orange, and less flexible. In DVE-1,4-containing polymers, a sharp decrease in flexibility was noted as the amount of vinyl ether was increased.

The front velocity increased monotonically with increasing fractions of DVE-1,4 to TMPTE, to a maximum front velocity of 26.3 cm min^{-1} at 75 wt% DVE-1,4 as shown in Figure 2.2. Front velocity increased sharply in DVE-1,4 formulations as a function of the amount of vinyl ether. In the same comparison, TEGDVE caused a small (1 cm min^{-1}) decrease in front velocity at 25 wt% compared but once again increased as the amount of vinyl ether increased in the formulation to a maximum of 29.2 cm min^{-1} at 75 wt% TEGDVE. The fraction of vinyl ether was limited to 75 wt% due to solubility issues initially encountered with IOC-8 and pure vinyl ether.

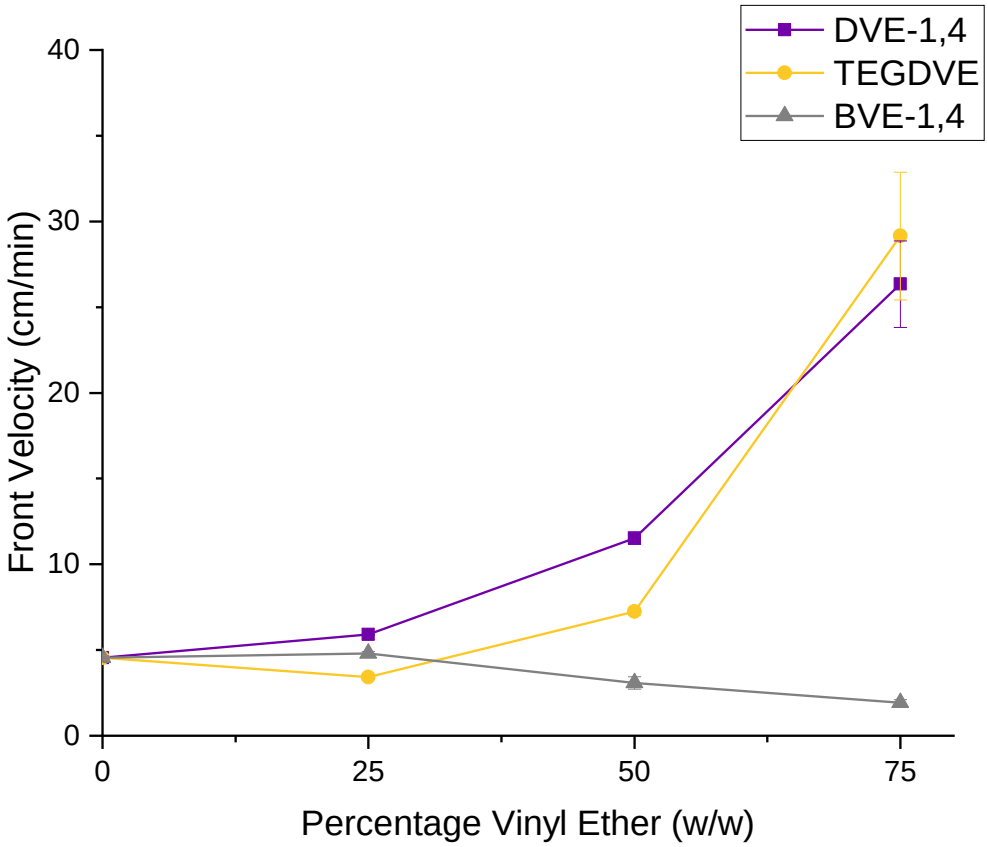

Figure 2.2. Front velocities for all front-supporting vinyl ethers as a function of vinyl ether percentage by weight, with a constant initiator concentration of 0.50 phr IOC-8 and 1.00 phr Luperox 231. Error bars are present in each formulation.

The formulations containing BVE-1,4 exhibited a minimal difference in front velocity (0.3 cm min^{-1}) at 25 wt% BVE-1,4, then the front velocity decreased as the amount of vinyl ether increased in the formulation. Propagating chains in cationic polymerization systems are known to undergo chain transfer reactions. [60] BVE-1,4 and EGVE are possible chain transfer agents in the epoxy system due to the presence of the hydroxyl group. The decrease in front velocity as the percentage of BVE-1,4 is increased is because the chain transfer reactions from the propagating chain end to the hydroxyl group of the monomer terminates the chain and results in the quenching of the front. In addition, there was observed boiling of the BVE-1,4 monomer as

the front propagated which will give a lower front velocity. According to the supplier, the boiling point of BVE-1,4 is 95 ℃ at 20 mmHg, and the boiling point at atmospheric pressure is unknown. The hypothesis for the inability for EGVE-containing systems to support a front is the chain transfer reactions, as there was no observed boiling of the monomer.

An increase of maximum front temperature was seen with increasing vinyl ether content and increasing concentration of IOC-8. As shown in Figure 2.3, at the constant concentration of initiators seen above (0.50 phr IOC-8 and 1.00 phr Luperox 231), for both DVE-1,4 and TEGDVE the front temperature increased as the percentage of the vinyl ether increased. The TEGDVE formulations experienced greater differences in front temperature than DVE-1,4 formulations. Inversely, formulations with BVE-1,4 showed a decrease in front temperature as the amount of vinyl ether increased, due to heat loss from the monomer boiling. The decrease in front temperature is consistent with the decrease in front velocity seen in these fronts.

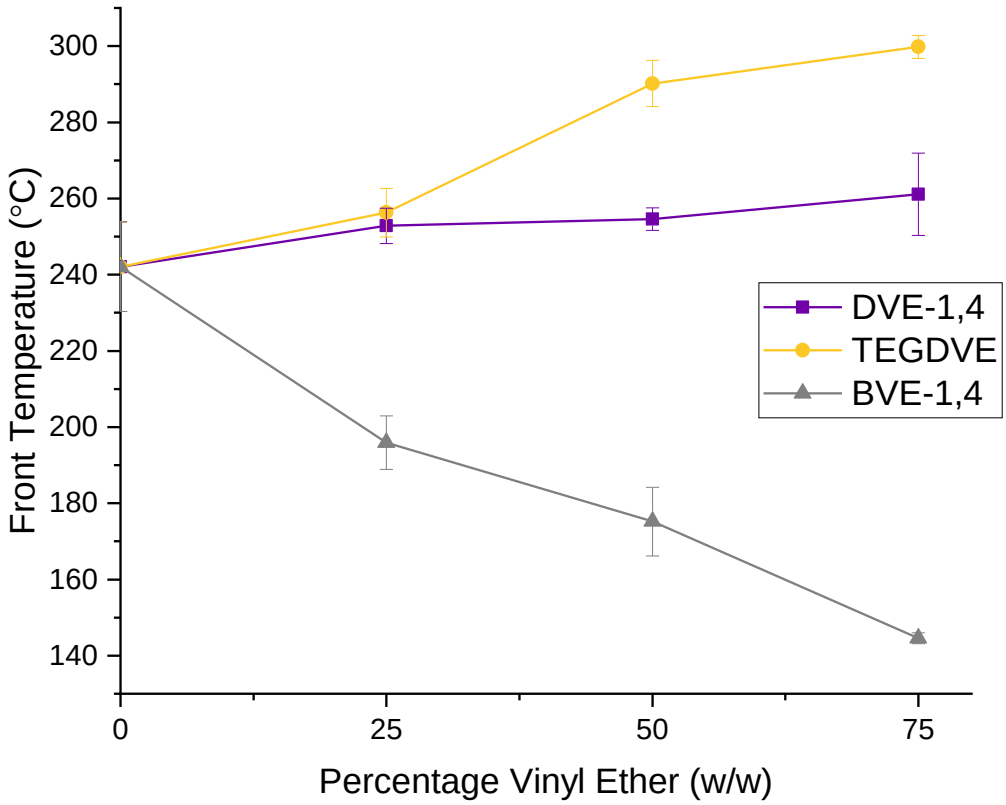

Figure 2.3. Maximum front temperature recorded for front-supporting vinyl ethers with constant initiator concentrations of 0.50 phr IOC-8 and 1.00 phr Luperox 231 as a function of vinyl ether percentage by weight.

In addition to increases in vinyl ether content, increases in IOC-8 concentration while keeping Luperox 231 concentration constant showed an overall increase in maximum front temperature. This is consistent with the increases in front velocity as IOC-8 concentration increased. An example of such is shown below in Figure 2.4 with 50 wt% DVE-1,4. Temperatures plateaued around 300℃ at all percentages of vinyl ether. Formulations containing 75 wt% DVE-1,4 had higher maximum front temperatures with lower concentrations of IOC-8 compared to the other vinyl ether percentages and experienced the smallest difference as the IOC-8 concentration

increased. No discernable trend in temperature was seen with increasing Luperox 231 concentration.

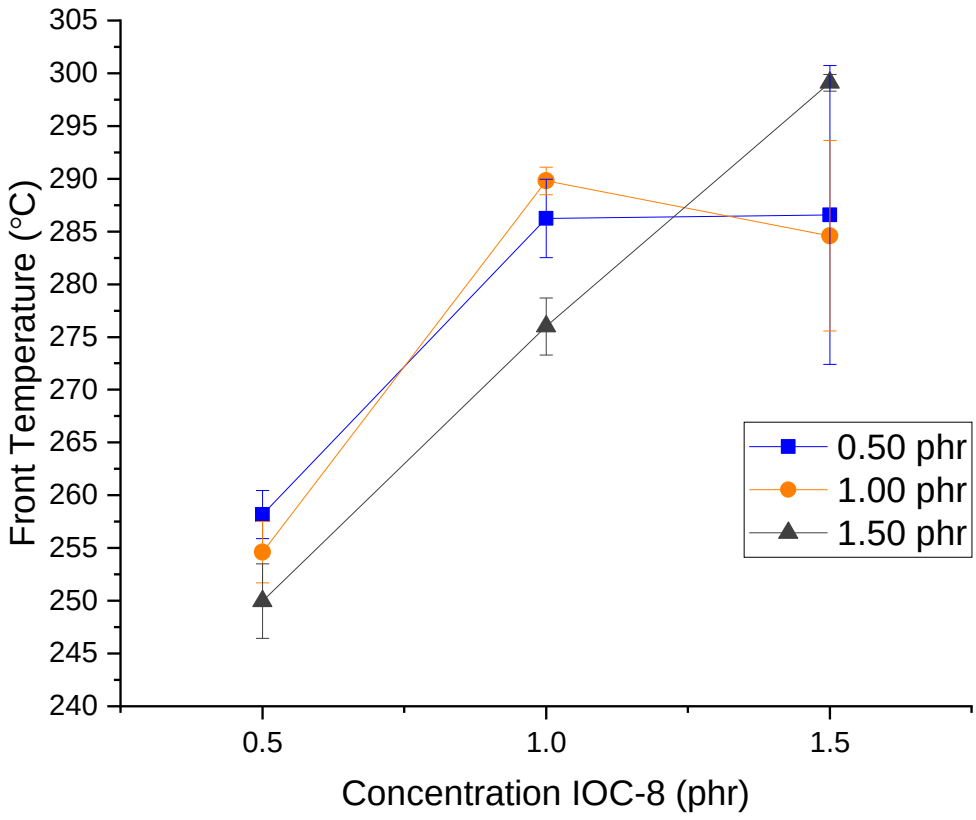

Figure 2.4. Maximum front temperatures observed for formulations of 50 wt% DVE-1,4 and 50 wt% TMPTE with constant Luperox 231 concentrations in legend, shown as a function of IOC-8 concentration.

2.4. Kinetic Effects of Initiators in RICFP with Vinyl Ethers

In typical frontal polymerizations, increasing initiator concentrations have been shown to increase front velocities. [7, 19, 23, 73] Studies have shown the same dependencies in RICFP. [54, 56]

Concentrations of initiators were varied in formulations containing a ratio of 25-100 wt% TMPTE and 0-75 wt% DVE-1,4. A range of 0.50, 1.00 and 1.50 phr was studied for both IOC-8

and Luperox 231 with initiator ratios ranging from 1:3 to 3:1. The physical properties, other than a darker color with increasing IOC-8 shown in Figure 2.5, did not visibly change with variations in initiator concentrations.

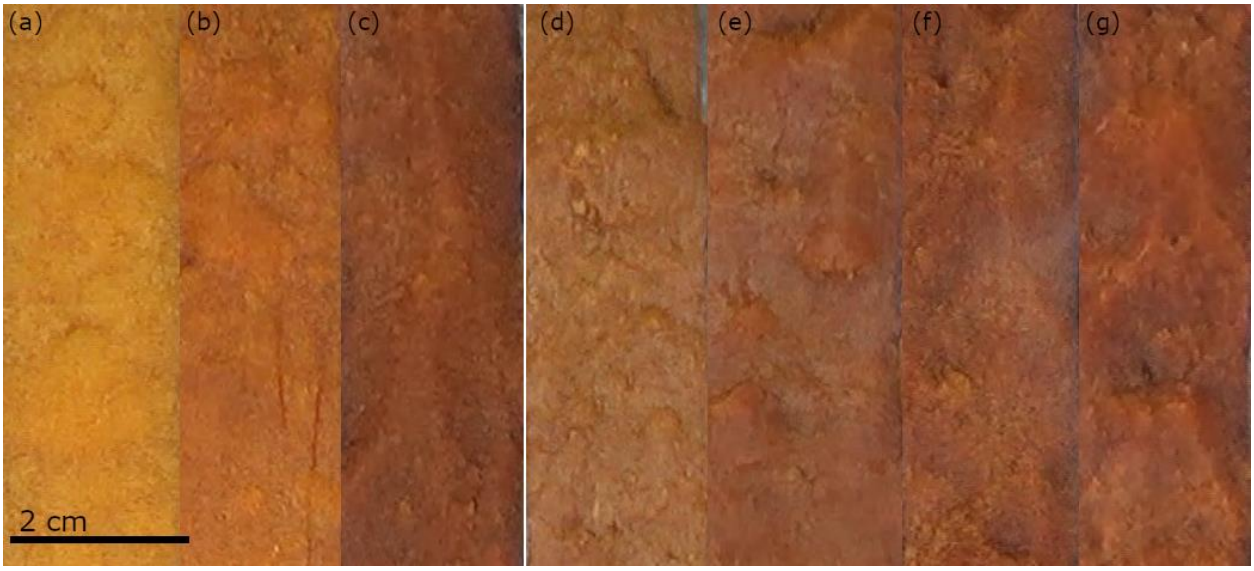

Figure 2.5. Range of colors seen for DVE-1,4-containing formulations. (a-c) show increases in IOC-8 concentration from 0.5 to 1.5 phr for 50 wt% DVE-1,4. (d-g) are formulations with 1.5 phr IOC-8 and Luperox 231 and increasing vinyl ether percentages.

As the concentration of both initiators increased in formulations, the front velocity increased for both vinyl ether systems. This is to be expected with regards to previous literature. [7, 54, 56]

The kinetic effects of each initiator on the front velocity were also studied. It was found that, similar to results seen by Bomze et al. for RICFP-cured epoxy resins, [54] the concentration of IOC-8 has a larger effect on front velocity at all vinyl ether percentages than the concentration of Luperox 231, which can be seen in Figure 2.6. Increases in 0.50 phr increments of IOC-8 showed average increases of 29-36 % in front velocity while the equivalent increments in Luperox 231 concentration resulted in average increases of 14-17 % in front velocity.

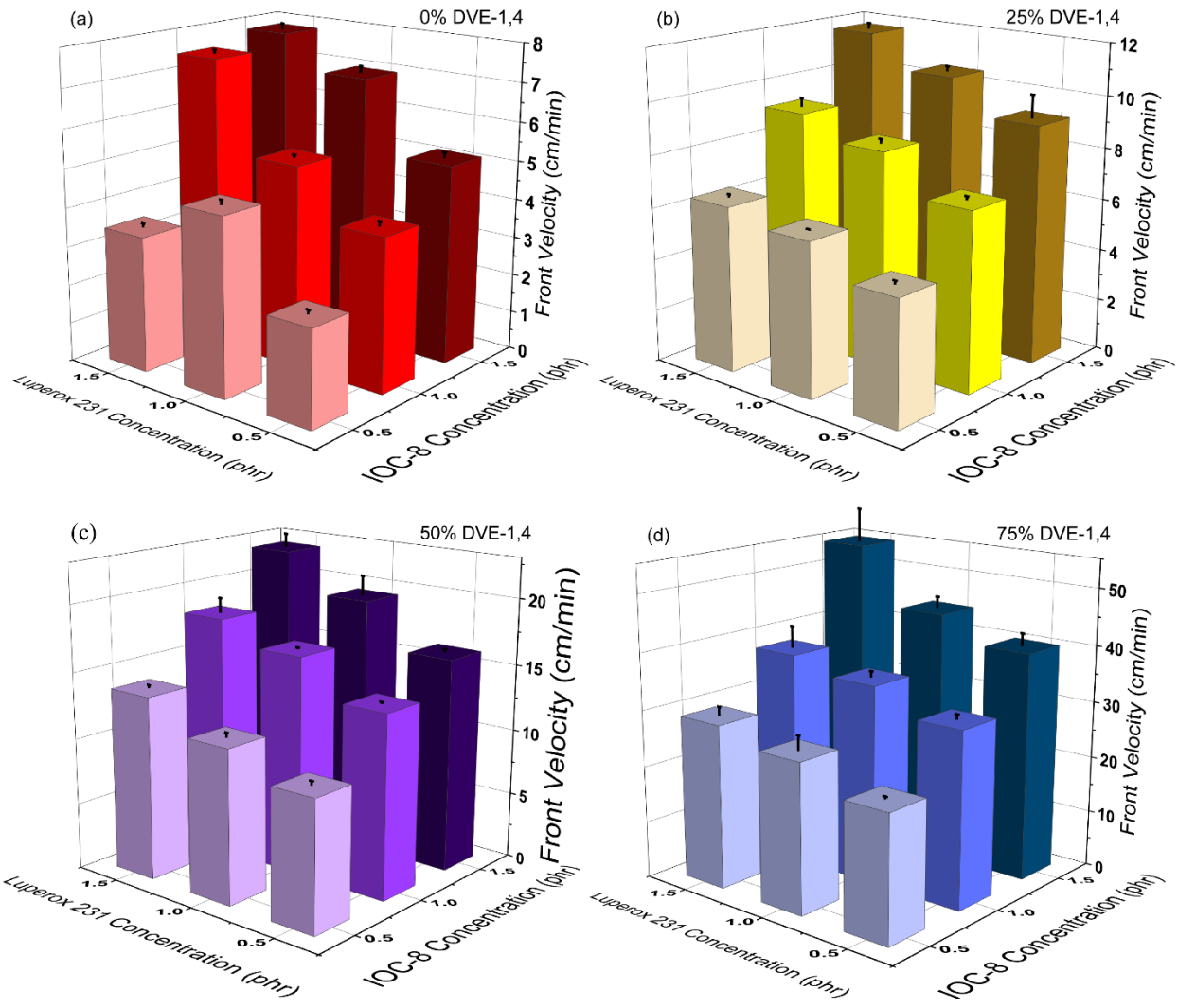

Figure 2.6. Front velocities versus Luperox 231 and IOC-8 concentrations from 0.5 to 1.5 phr, increasing on the bottom left axis from right to left for Luperox 231 and on the bottom right axis from left to right for IOC-8. Shown in increasing vinyl ether content from (a) to (d) with a maximum of 75 wt% DVE-1,4.

2.5. Pot Life of RICFP Samples

Since FP is carried out with one-pot formulations, pot life is a crucial parameter for formulations to be developed into commercial materials but also to maintain the possibility of FP over time. Thus, the pot life of the vinyl ether/epoxy formulations were studied. It was seen that samples would remain in the dark unreacted for months, with increasing vinyl ether content generally

reducing the time for spontaneous curing to occur. At room temperature, samples containing a high percentage of DVE-1,4 were found to suffer from pot life issues. Samples with pure DVE-1,4 and both 0.5 phr IOC-8 and 1.0 phr Luperox 231 would violently react within hours regardless of light exposure. Increasing the IOC-8 and Luperox 231 concentrations to 1.50 phr with DVE-1,4 resulted in a pot life of approximately 2 hours which resulted in a violent, exothermic polymerization of a dark, brittle material. Other formulations containing different concentrations of IOC-8 and Luperox 231 with pure DVE-1,4 all reacted at room temperature with stirring in less than 24 hours, even if stored in the dark. However, formulations containing at least 25 wt% TMPTE had a much longer pot life ranging from approximately 2 to 3 months.

At 90% DVE-1,4 and 10% TMPTE, small gel-like particles would be formed rapidly after dissolution of IOC-8 but remain stable up to approximately 60 days. The formation of small particles was more pronounced in those solutions containing 1.50 phr IOC-8. Solid IOC-8 was found to be only mildly soluble in vinyl ether, which presents issues of homogeneity at higher concentrations of superacid generator.

Inhibitors are frequently added to commercial monomers to prevent curing of the product from exposure to light or heat. Some vinyl ethers are shipped with added KOH as an inhibitor. Addition of 0.5 wt% KOH was found to increase the pot life to just under a week for pure DVE-1,4 with IOC-8 and Luperox 231 present.

To study the pot life with front kinetics on an accelerated time scale, solutions were placed into an oven at 50 °C. Initially, samples containing 0.5 phr IOC-8 and 1.0 phr Luperox 231 of 50 wt% TMPTE/50 wt% TEGDVE or 25 wt% TEGDVE/75 wt% TMPTE would react overnight in the oven, even with their long pot lives at room temperature. With the promising results of KOH addition with DVE-1,4 samples, 0.1 wt% KOH was added to the 50 wt%

TEGDVE/50 wt% TMPTE sample, but it still reacted overnight. Instead of KOH, 300 ppm 4-methoxyphenol (MeHQ), an inhibitor of free-radicals, was added to the 50 wt% TEGDVE/50 wt% TMPTE formulation which successfully stabilized the sample in the oven unlike KOH. The addition of MeHQ does reduce the initial front velocity of the 50/50 formulation (11.5 cm min^{-1} without and 7 cm min^{-1} with), highlighting the tradeoff of front velocity for increased pot life. Since the MeHQ was found to enhance the pot life through radical inhibition, similar samples were tested in the oven without Luperox 231 and MeHQ, with Luperox 231 being the primary radical source, and the formulation still polymerized after 3 days, indicating there is decomposition of IOC-8 resulting in the initiation of cationic polymerization. Samples with no IOC-8 would not polymerize. Additionally, samples containing no vinyl ether and only epoxy with the initiators and no MeHQ had pot lives of at least 35 days, indicating the vinyl ether reactivity is playing a significant role in the pot life. The viscosity over time was studied using a Brookfield viscometer in Figure 2.7, to displaying the spontaneous polymerization occurring slowly over time through an increase in viscosity.

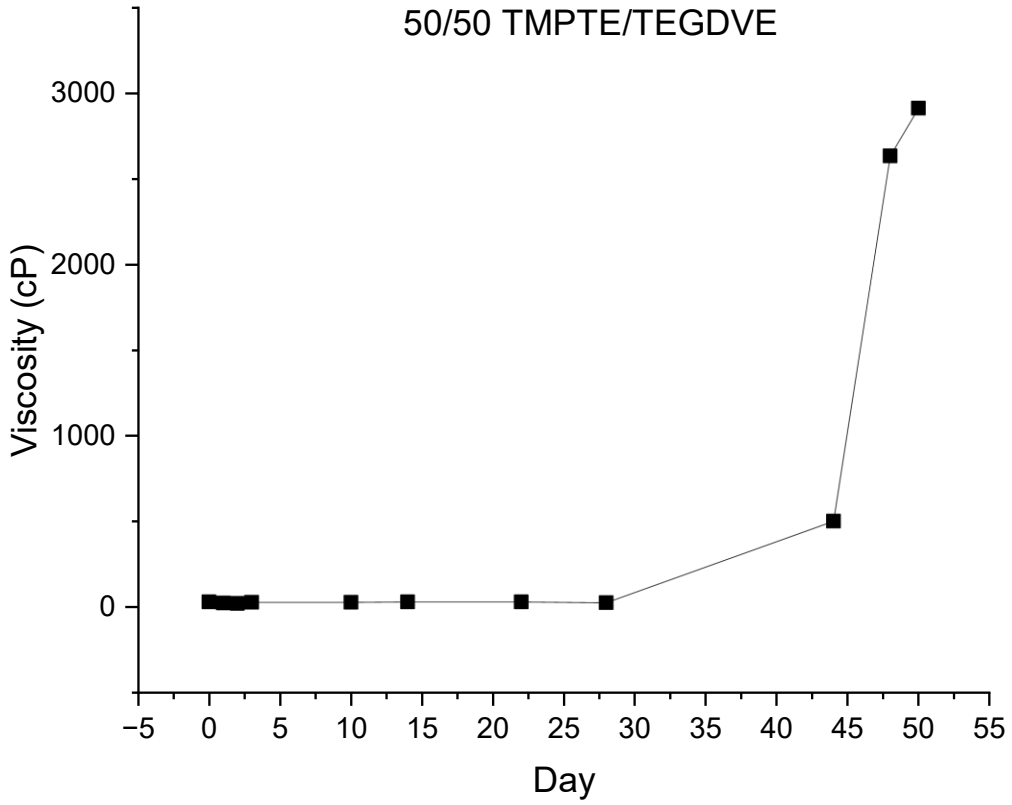

Figure 2.7. Viscosity over time of a 50 wt% TEGDVE/50 wt% TMPTE sample with 0.5 phr IOC-8 and 1 phr Luperox 231 with 300 ppm MeHQ kept in an oven at 50 ℃.

The front velocity of samples containing MeHQ in the accelerated pot life study are shown in Figure 2.8 for 50 wt% TEGDVE/50 wt% TMPTE and Figure 2.9 for 100% TMPTE. It is shown that for both samples with and without vinyl ether, the front velocity decreases over time, likely due to the decomposition of the Luperox 231 and subsequent inhibition of radicals that would support decomposition of IOC-8.

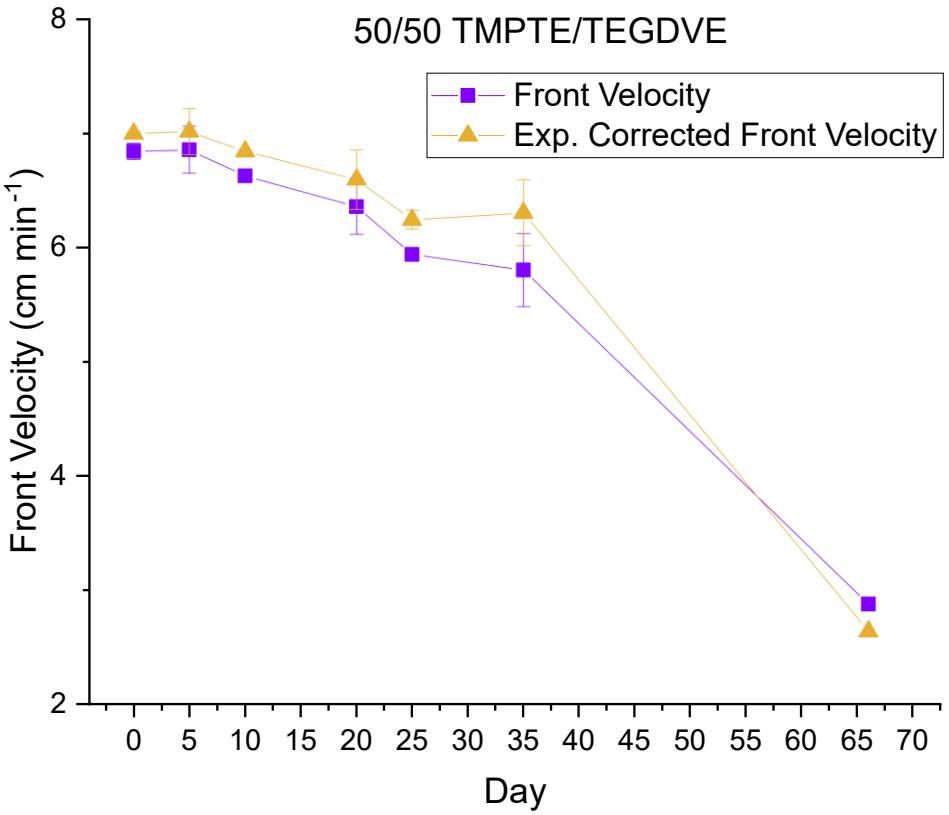

Figure 2.8. Front velocity over time of 50 wt% TEGDVE/50 wt% TMPTE with 0.5 phr IOC-8 and 1 phr Luperox 231 and 300 ppm MeHQ kept in an oven at 50 ℃.

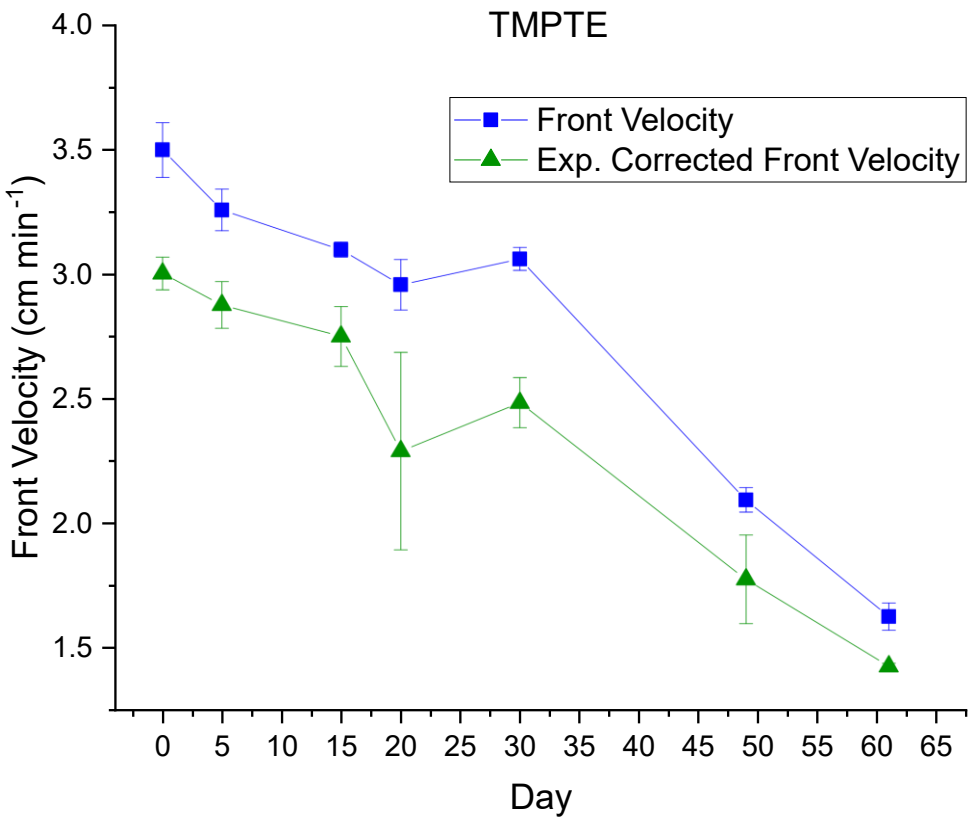

Figure 2.9. Front velocity over time of TMPTE with 0.5 phr IOC-8 and 1 phr Luperox 231 and 300 ppm MeHQ kept in an oven at 50 ℃.

2.6. Fast Fronts with Pure Vinyl Ethers

Despite the inhomogeneity of small particles present in pure DVE-1,4 solutions as described above, fronts were achieved with adding 0.50 phr and 1 phr IOC-8, with 1 phr Luperox 231 in each formulation. An average front velocity of 74.5 cm/min was observed for both these formulations.

Fronts with pure TEGDVE were also attempted. This monomer also suffered the same issues in pot life as DVE-1,4, which could be remedied through the addition of 3000 ppm MeHQ allowing for dissolution via sonication of the IOC-8 in TEGDVE. However, it was found that IOC-8 was readily soluble (approximately 1:1 by weight) in propylene carbonate, an inert aprotic solvent with a boiling point of 242 ℃. This allowed for the addition of a predissolved solution of

IOC-8 in propylene carbonate to the vinyl ether to rapidly prepare samples and reduce risk of spontaneous polymerization which occasionally occurred with IOC-8 dissolution into TEGDVE, even with MeHQ. The propylene carbonate will not interact with the propagation, and the high boiling point lessens the risk of heat loss to vaporization. There still exists an issue with the short pot life with this method but the timescale of sample preparation is much shorter.

Formulations with either 1 phr IOC-8 and 1 phr Luperox 231 or 2 phr IOC-8 and 2 phr Luperox 231 were carried out with TEGDVE. These had very fast front velocities of 110 cm min^{-1} and 256 cm min^{-1}, however there was a large volume of fumes during FP that blocked visibility of the front propagating. So, the values above were calculated by dividing the total length of the uncured resin by the time for the front to propagate through the material. This is different to the typical method for determining front velocity by taking the slope of front position over time. One possibility to still observe the front is by using a thermal camera, however this would likely capture the temperature of the fumes produced by the reaction. Instead, the fronts were carried out as normal but with air from a hose in the fume hood blowing over the mold to blow away most of the fumes so that the front is visible. This led to a much slower front (55 cm min^{-1} and 105 cm min^{-1} for 1 and 2 phr of the initiators, respectively) due to the cooling of the polymerization, but it allowed for viewing of the front propagation and calculation of front velocity via the slope of position versus time. The front velocities for these TEGDVE experiments are shown in Figure 2.10 for individual samples. In both pure TEGDVE and DVE-1,4 formulations, the resulting materials are weak and not ideal for practical applications. This could be improved with addition of fillers, but regardless the possibility of extremely fast fronts would widen the scope of applications that need rapid cure times.

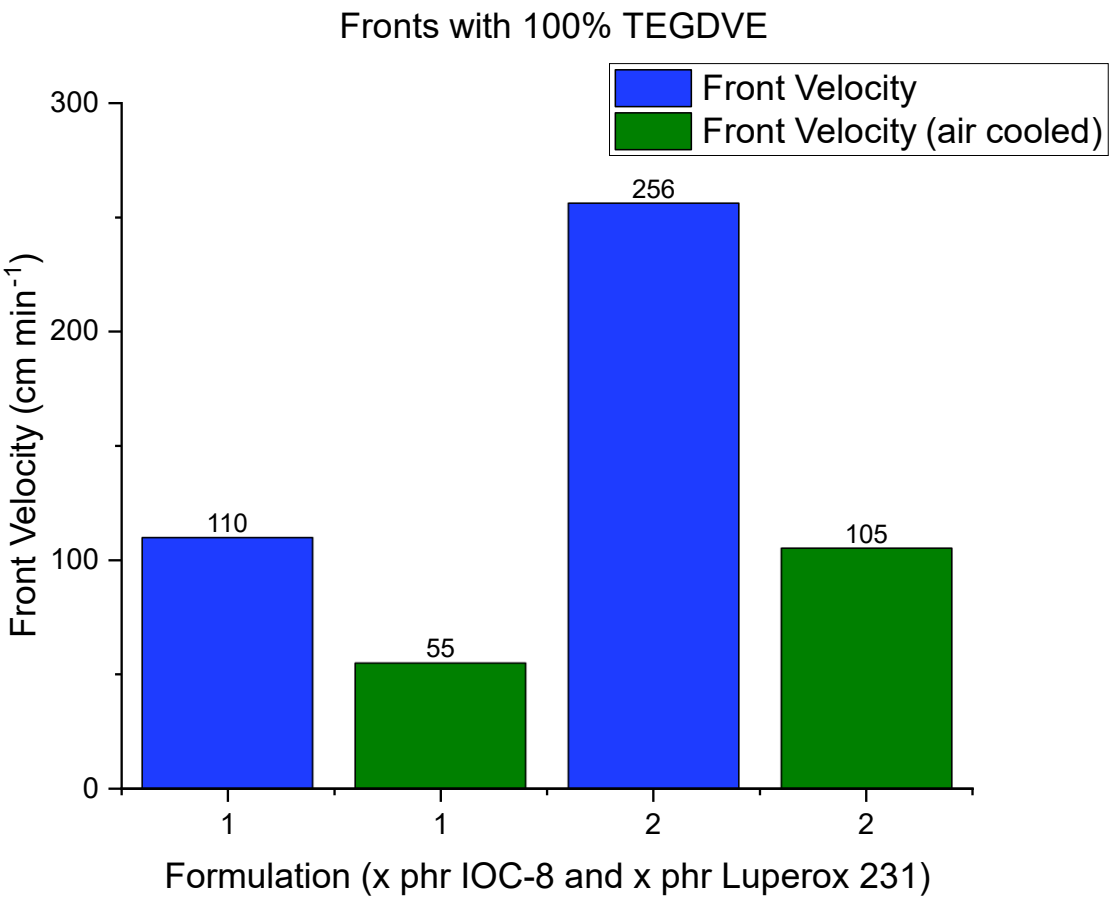

Figure 2.10. Front with pure TEGDVE formulations containing either 1 phr IOC-8 and 1 phr Luperox 231 or 2 phr IOC-8 and 2 phr Luperox 231. Formulations that were air cooled had air blowing over them with a hose to better witness front propagation.

2.7. Conversion of Epoxy-Vinyl Ether Polymers Produced via RICFP and Determination of Copolymerization

Due to the resulting thermoset materials with the studied monomers, the available characterization methods are limited. The polymers cannot be dissolved for use in nuclear magnetic resonance, and there are irregularities present such as voids that will affect results from dynamic mechanical analysis. A major motivator to characterization of the polymer is to determine whether the monomers are copolymerizing or generating interpenetrating polymer networks.

In the literature, there are a few conclusions drawn for epoxy-vinyl ether copolymerization. First, for the determination of copolymerization versus interpenetrating polymer networks from separate homopolymers using acrylates and epoxies, it was found that a minimum would occur in the front velocity when changing the ratio of one monomer to another when there is no copolymerization. [74, 75] There is no observed minimum in the increase of vinyl ether to epoxy for the results shown above. In photopolymerization studies of epoxies and vinyl ethers, it was concluded that epoxies and vinyl ethers do not copolymerize due to conversion of protonated vinyl ether species converting to protonated epoxide species which cannot initiate vinyl ether polymerization. [48, 76] Another study of photopolymerization kinetics reached different conclusions. In this paper, initially they concluded that there was no copolymerization between BADGE and TEGDVE initiated by a sulfonium salt due to the difference in each monomers polymerization profile when mixed. [77] However, with a more reactive cycloaliphatic epoxy and TEGDVE initiated with a sulfonium salt, they found similar polymerization profiles for the two monomers and an enhancement of the epoxide cure, which indicated that copolymerization was occurring. Therefore, the literature seems to give conflicting results on the occurrence of homopolymerization versus copolymerization.

One of the first attempts at determining copolymerization was to mix high functionality monomers that would give crosslinked materials, with monofunctional monomers that would result in linear polymers. If the monomers do not copolymerize, then after placing the polymer into solvent, the linear polymer should dissolve out leaving the crosslinked polymer. Dichloromethane (DCM) was used as solvent with two mixtures: 50 wt% TMPTE and 50 wt% dodecyl vinyl ether, and 50 wt% TEGDVE and 50 wt% p-tert butylphenyl glycidyl ether. With DCM, it seemed that the crosslinked network was partially dissolving as the polymer in either

case broke into many different pieces as opposed to just swelling with controls of pure TMPTE and TEGDVE. This could be due to low conversion of the functional group on the multifunctional monomer. The polymer consisting of TEGDVE and p-tert-butylphenyl glycidyl ether had to be filtered after dissolution, and the weight loss was 78.5%. In the case of TMPTE and dodecyl vinyl ether, 34.7% weight was lost. Unless a solvent which would preferentially dissolve the linear polymer without affecting the crosslinked network can be found, this method is unreliable for epoxy-vinyl ether copolymer determination currently.

Infrared spectroscopy (IR) was used to identify the effects of epoxy vinyl ether ratios on the conversion of the functional groups in RICFP systems. This could potentially give some idea whether copolymerization is occurring between the epoxy and vinyl ether. Unfortunately, given the similarity in repeat units of both poly(glycidyl ether) and poly(vinyl ether), which both produce ethers, IR cannot differentiate between homopolymers and potential copolymers.

In the literature, conversion of epoxy and vinyl ethers during photopolymerization has been studied. This is done through a few different methods, but mostly by either calculating the ratio of the area of peaks in the cured and uncured spectra, [78, 79] or a ratio of the absorbance value of peaks in the cured and uncured spectra. [48, 77] In this work, the conversion percentage was calculated as the area of the cured peak divided by the area of the uncured peak, as it seemed more accurate to include the broadness of the peaks in the calculation. Following similar results in the literature, the C=C peak centered at ~1618 cm^{-1} was studied for conversion of TEGDVE. For TMPTE, there are a few peaks which correspond to epoxy ring structural features at ~950-815 cm^{-1} and 880-750 cm^{-1}. [79, 80] The peak centered at 755 cm^{-1} for the epoxy ring was chosen to study as it did not overlap with any peaks from TEGDVE. The maximum of this peak slightly shifts from 745 cm^{-1} to 755 cm^{-1} after curing and the left and right bounds for the integration of

the peak shift by 5 cm^{-1}. Spectra for the TMPTE, TEGDVE, and 50 wt% TEGDVE/50 wt% TMPTE samples are shown below in Figures 2.11, 2.12, and 2.13. The ether peaks from the monomer structure and repeat unit are prominent in every spectrum at ~1090 cm^{-1}. The peak at ~471 cm^{-1}, which corresponds to fumed silica, is also visible.

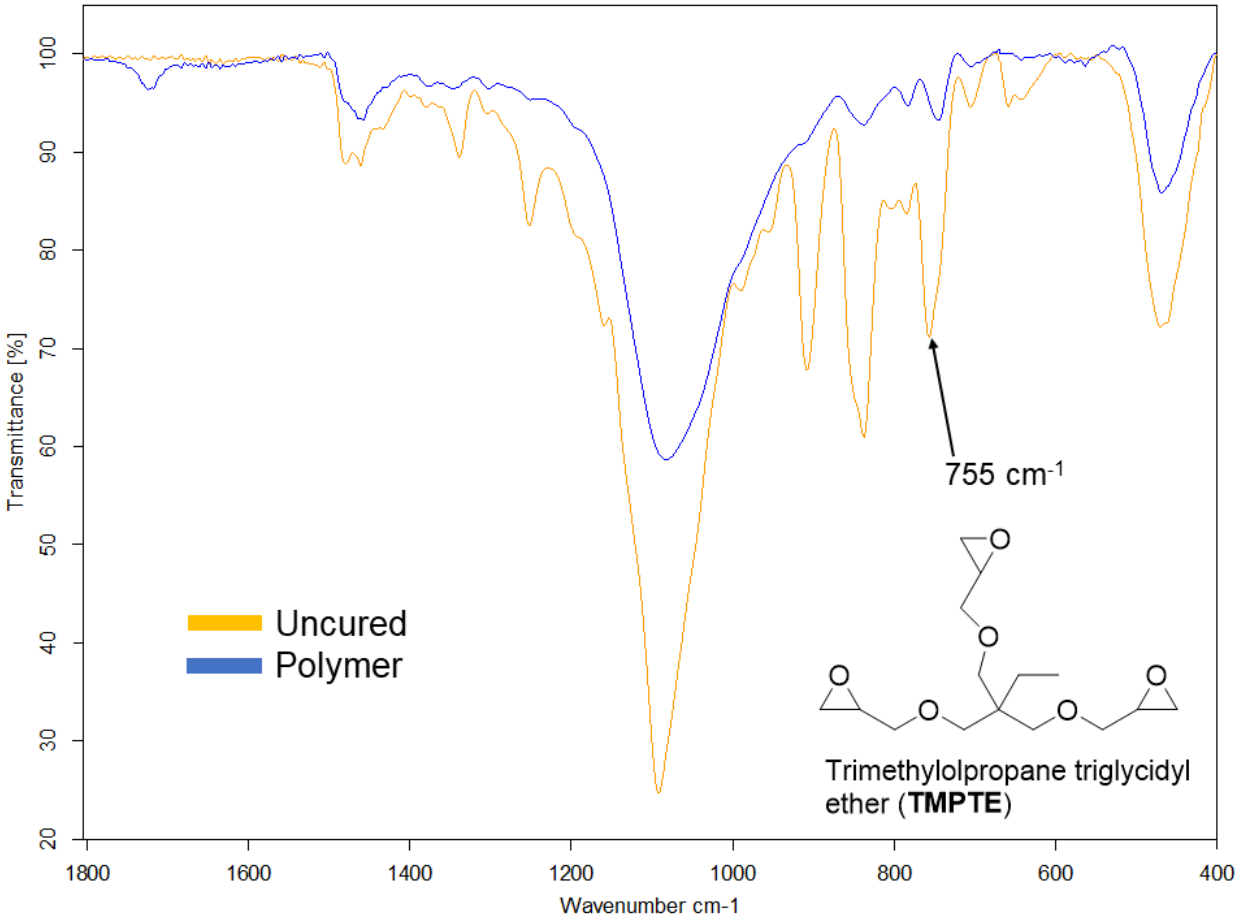

Figure 2.11. IR spectrum from 1800 to 400 cm^{-1} of TMPTE with 1 phr IOC-8 and 1 phr Luperox 231, with 10 wt% fumed silica. The orange spectrum is uncured while the blue spectrum is cured. The epoxy ring peak at 755 cm^{-1} is highlighted.

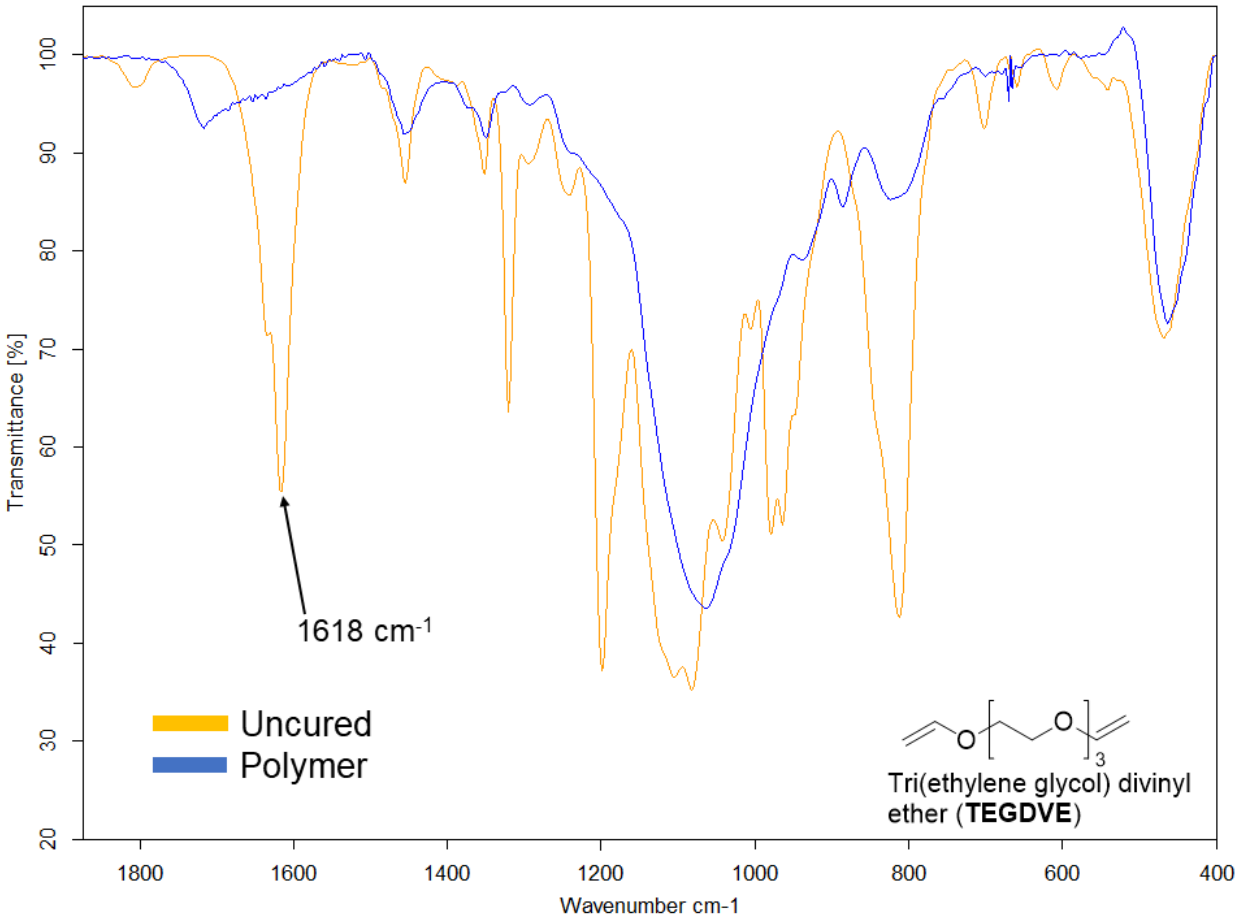

Figure 2.12. IR spectrum from 1800 to 400 cm^{-1} of TEGDVE with 1 phr IOC-8 and 1 phr Luperox 231, with 10 wt% fumed silica. The orange spectrum is uncured while the blue spectrum is cured. The vinyl ether peak at 1618 cm^{-1} is highlighted.

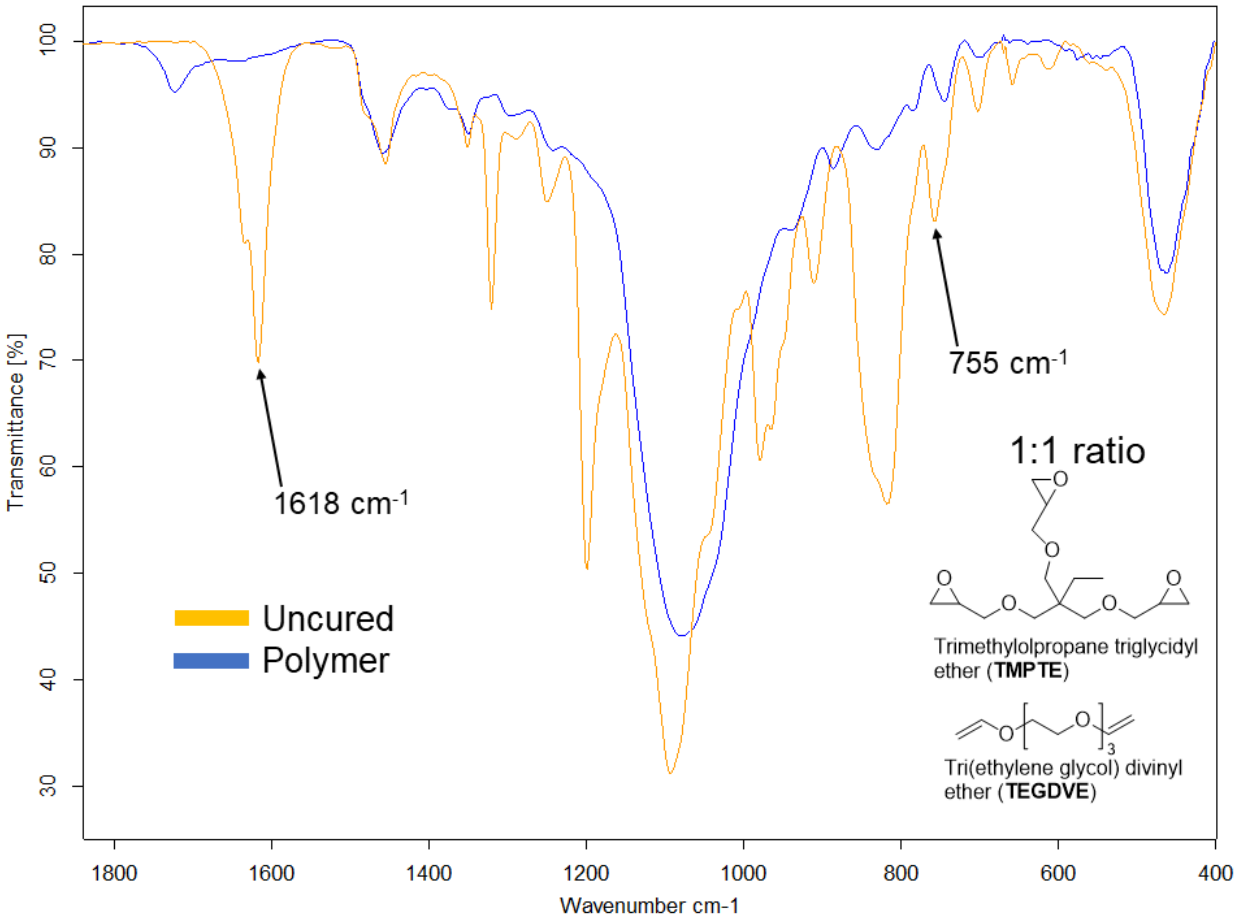

Figure 2.13. IR spectrum from 1800 to 400 cm^{-1} of a 50 wt% TEGDVE/50 wt% TMPTE mixture with 1 phr IOC-8 and 1 phr Luperox 231, with 10 wt% fumed silica. The orange spectrum is uncured while the blue spectrum is cured. The epoxy ring peak at 755 cm^{-1} and vinyl ether peak at 1618 cm^{-1} are highlighted.

Notably, there was a peak at 1715 cm^{-1} that appeared after curing in every spectrum. This is attributed to acetone that is generated during the decomposition of Luperox 231. Comparing the spectra of pure Luperox 231, where some small amounts of acetone is expected based on the smell of the compound, to the cured TEGDVE samples confirms this as shown in Figure 2.14. Additionally, there was a peak at ~3420 cm^{-1} that appeared in every spectrum but most intensely for formulations with vinyl ether. This is likely some termination, generating hydroxyl chain

ends or in the case of TMPTE the -OH chain ends from the initiation of the epoxy by the superacid. [60]

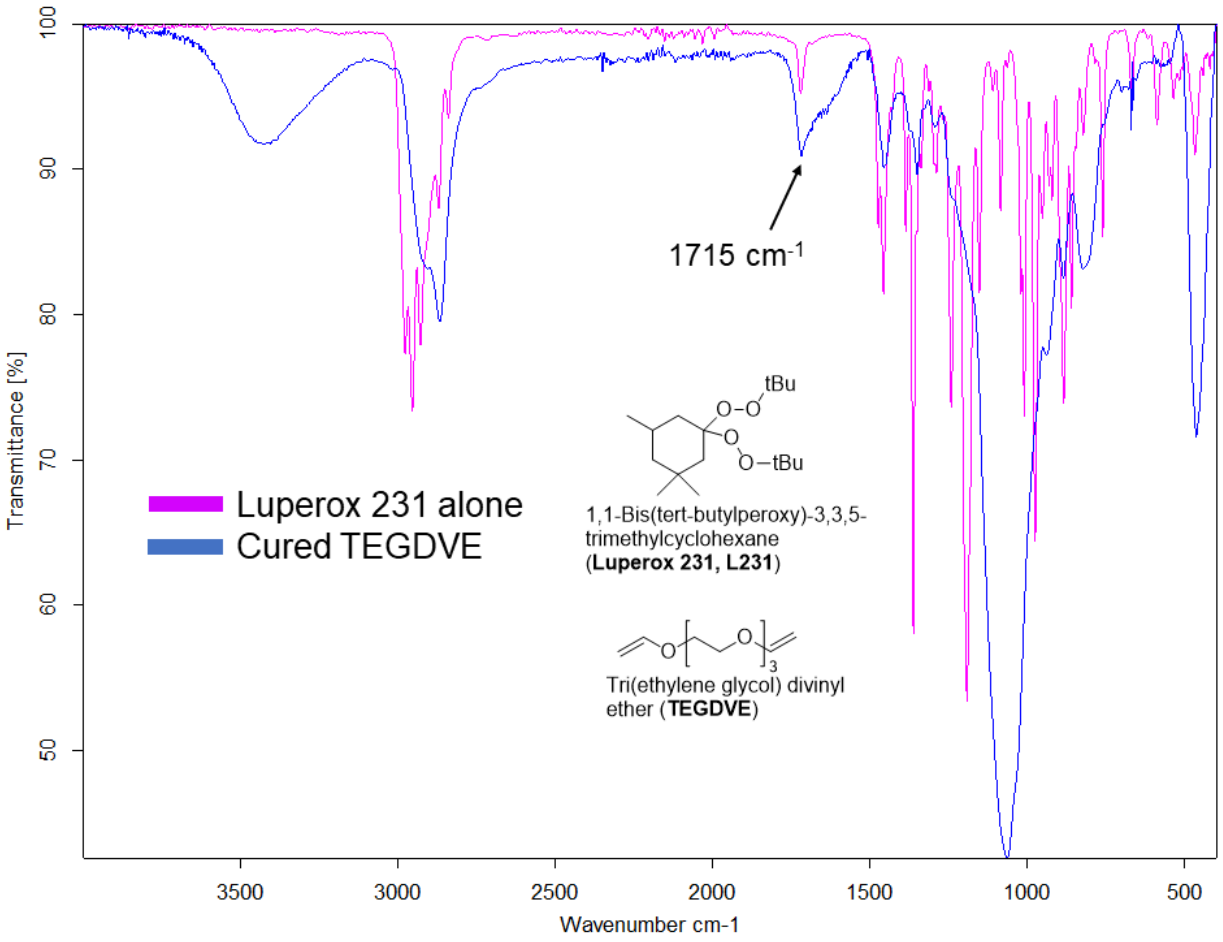

Figure 2.14. Spectra of pure Luperox 231 and cured TEGDVE with 1 phr IOC-8 and 1 phr Luperox 231, where the peak at 1715 cm^{-1} of acetone is visible in the spectra.

Initially, using the polymer sample placed directly resulted in a very low intensity spectrum and inhomogeneity. Grinding the polymer sample resulted in a more homogeneous sample and higher intensity, but the baseline of the polymer sample was at a lower transmittance than the uncured sample and suffered from some drift. This could be due to some inhomogeneity from the grinding of the polymer. An example of the difference in baselines between the resin and polymer of TMPTE is shown below in Figure 2.15. Since the conversion is calculated using the

area of the peaks, the difference in baseline will result in slightly different values than expected. Baseline correction using a rubber band correction method in OPUS software was used to make the baselines equal. One other error that may arise when calculating the conversion is the variance in the intensity of the same sample which could be caused by sample preparation. An example in Figure 2.16 shows three spectra for equivalent samples of 50 wt% TEGDVE/50 wt% TMPTE where the intensity of the peaks is shown to differ across the three samples.

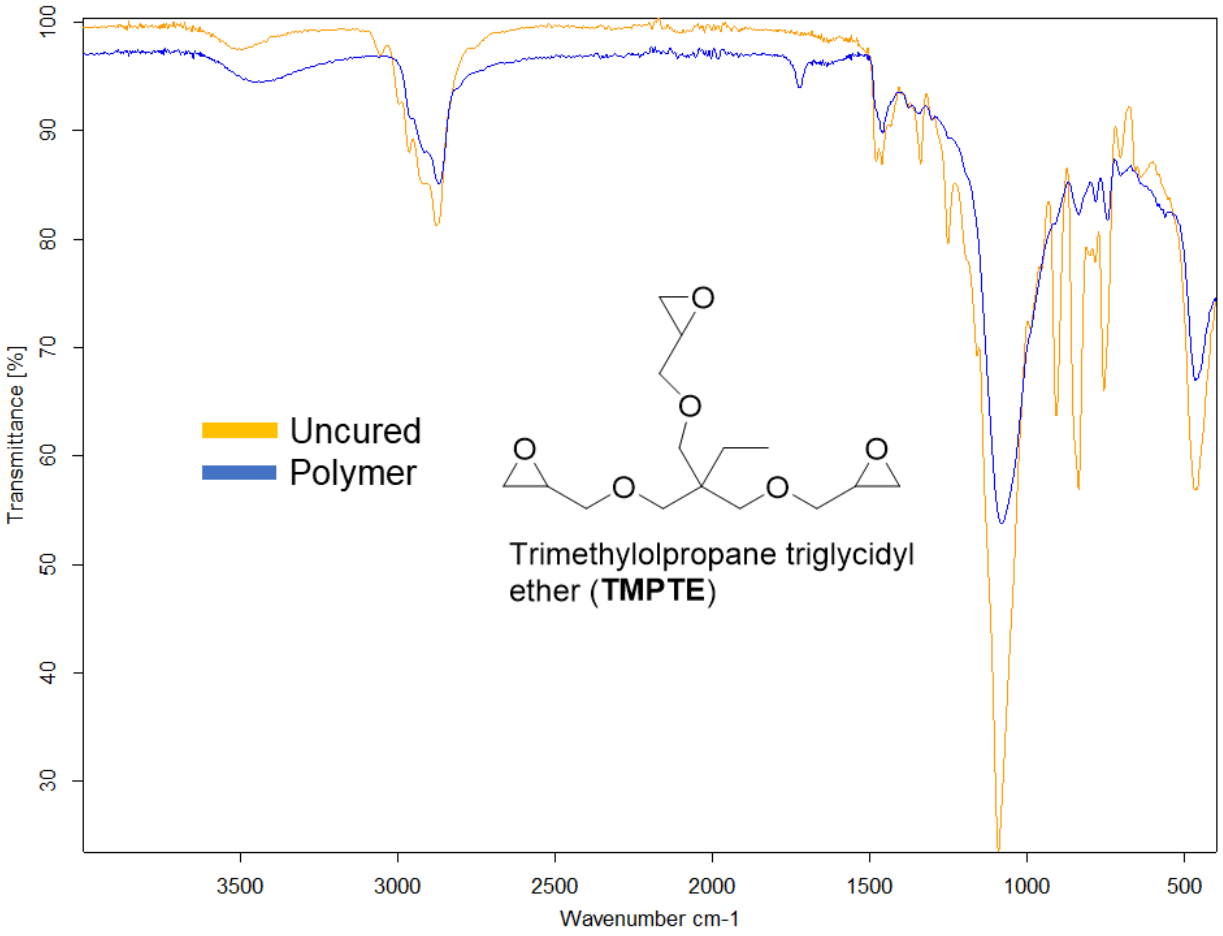

Figure 2.15. Spectra of TMPTE with 1 phr IOC-8 and 1 phr Luperox 231 before baseline correction. The orange spectrum is the uncured resin, and the blue spectrum is the polymer.

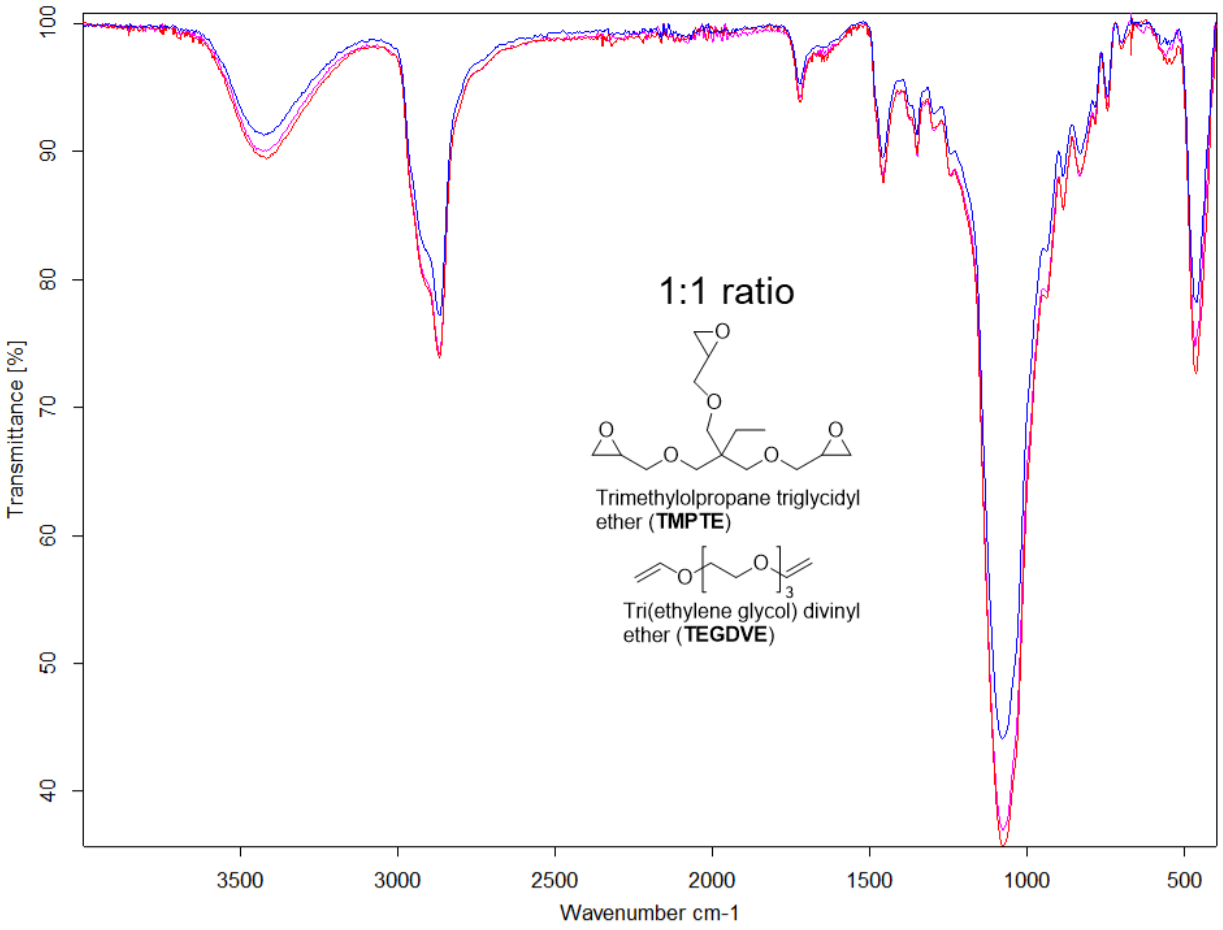

Figure 2.16. Spectra of three equivalent samples of cured 50 wt% TEGDVE/50 wt% TMPTE with 1 phr IOC-8 and 1 phr Luperox 231 to highlight the difference in peak intensity.

The area under the curves for the spectra of the uncured resin were averaged, and the ratio of the area of the indicated peaks for the three cured to the average of the uncured area was calculated as the conversion, which allowed for a standard deviation to be determined for the samples. OPUS software has an included plugin that integrates the area under the curve of a peak which was used. The results for conversion and limits of integration are shown in Table 2.1. Conversion was very similar for pure TMPTE and pure TEGDVE at 78.7% and 77.0%. When mixed 1:1, the vinyl ether conversion increased by ~10% to 84.7%, with epoxy conversion decreasing substantially to 57.3%. Decker et al. studied photopolymerizations of TEGDVE and BADGE

and saw TEGDVE polymerization inhibited BADGE polymerization and reduced epoxy conversion through rapid crosslinking of vinyl ethers restricting epoxy mobility, reduction of protons available for epoxy initiation, and preferential reactivity of vinyl ether carbocations with other vinyl ether carbocations. [77] The reduction in TMPTE conversion when mixed with TEGDVE seems to support this conclusion by Decker et al.; however, the increase in conversion of the TEGDVE instead indicates that a catalytic process may be occurring that involves the interaction of TMPTE and TEGDVE resulting in copolymerization. More studies to confirm the increase in conversion of TEGDVE are needed, in addition to structural identification of copolymers of TMPTE and TEGDVE versus homopolymers.

Table 2.1. Results from IR study of conversion with epoxy/vinyl ether resins.

Formulation	Conversion (%)	Integration Limits (cm^{-1})
100% TMPTE	78.7 ± 1.2	772 – 723 (uncured) 767 – 723 (cured)
50% TMPTE, 50% TEGDVE	57.3 ± 4.1 (epoxy) 84.7 ± 2.3 (vinyl ether)	772 – 723 (uncured) 767 – 723 (cured) 1703 – 1566[a]
100% TEGDVE	77.0 ± 1.2	1703 – 1566

[a]A baseline point of 1836 cm^{-1} was used with cured vinyl ether samples.

Thermal analysis was attempted for polymer samples containing BADGE and DVE-1,4 both as separate homopolymers and varying ratios of the two monomers. The hypothesis was that if copolymerization was occurring, one glass transition temperature would be present in a mixture as an average of the two homopolymers, while interpenetrating polymer networks would instead give two separate Tg. BADGE was chosen, as the rigid structure of the monomer was hypothesized to produce a much higher glass transition temperature than DVE-1,4, which would allow for easier determination of copolymerization. A strong glass transition peak in the DSC curve was observed for BADGE at ~105 °C, with a weak step change for the 1:1 mixture at ~71

°C and finally a broad, weak change observed in the pure DVE-1,4 sample centered around 73 °C. The DSC curves for DVE-1,4 are shown in Figure 2.17 and the 100% DVE-1,4, 100% BADGE, and 50/50 systems in Figure 2.18. A heating rate of 20 °C min^{-1} was chosen for the DVE-1,4 sample as it gave a stronger signal than 10 °C min^{-1}.

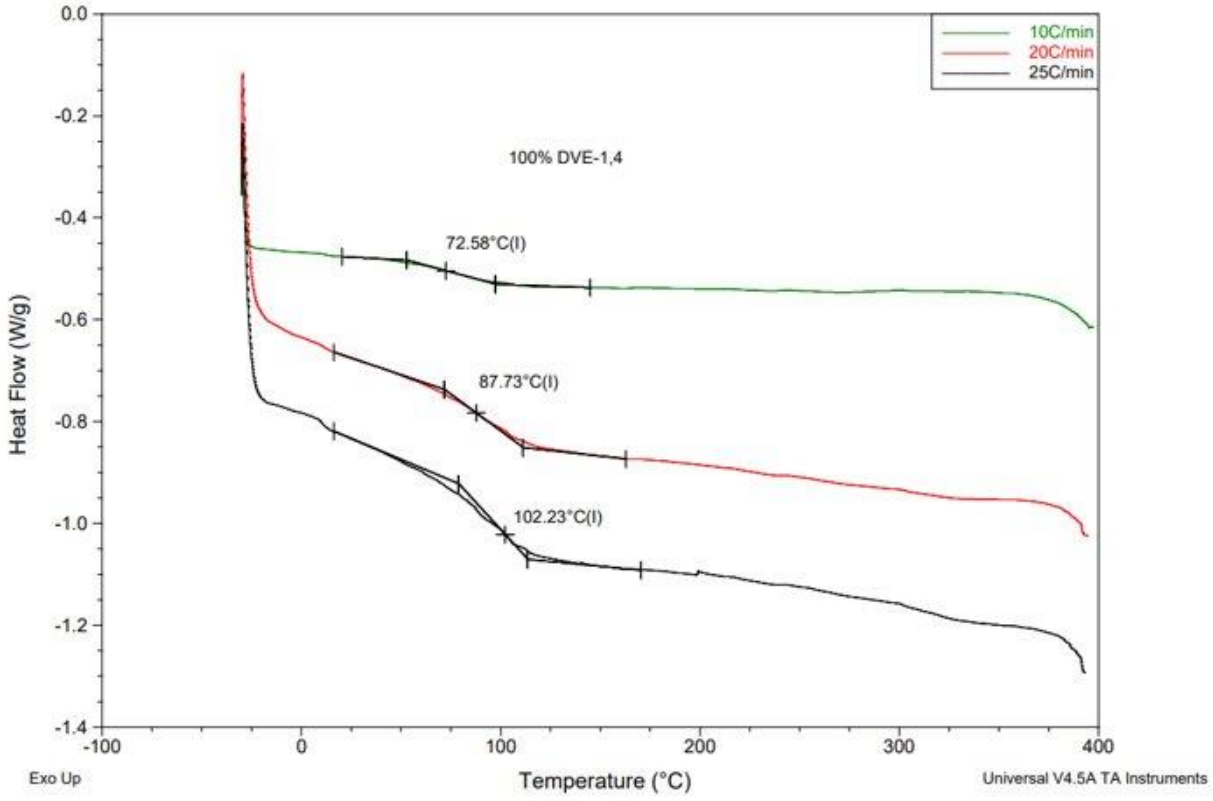

Figure 2.17. DSC curves of a polymerized 100% DVE-1,4 sample with 0.5 phr IOC-8 and 1.0 phr Luperox 231 with 10 wt% fumed silica, with increasing heating rates from 10 °C min^{-1} to 25 °C min^{-1}.

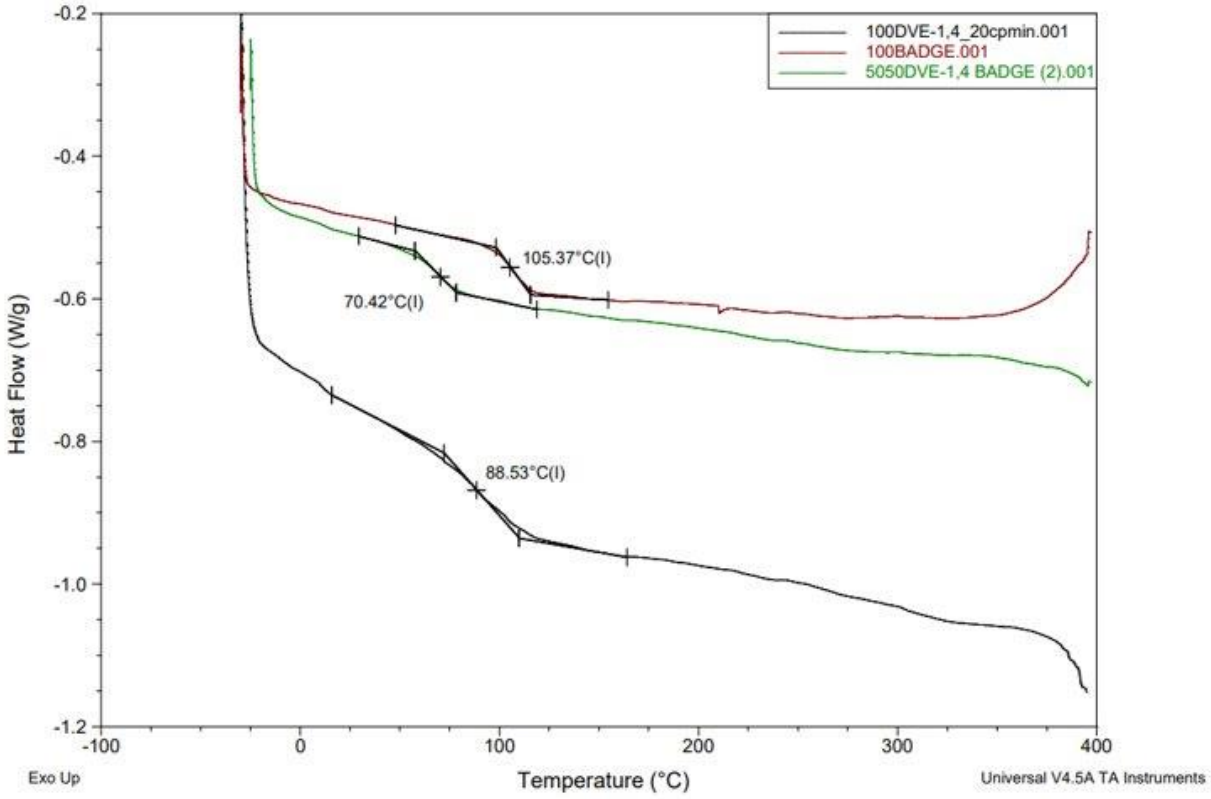

Figure 2.18. DSC curves of polymerized 100% DVE-1,4, 100% BADGE, and 50 wt% BADGE/50 wt% DVE-1,4 samples with 0.5 phr IOC-8 and 1.0 phr Luperox 231 with 10 wt% fumed silica, with a heating rate of 20 °C min^{-1} for the 100% DVE-1,4 sample, and 10 °C min^{-1} for the 100% BADGE and 50 wt% BADGE/50 wt% DVE-1,4 samples.

The results obtained from DSC were inconclusive in determining any presence of copolymerization between vinyl ether and epoxy monomers in RICFP, due to the weak and low temperature shift observed for the system containing both polymerized monomers. It was hypothesized that copolymerization would reveal itself through an average of the glass transition shifts appearing, while non-interactions between monomers or an interpenetrating polymer network of two homopolymers would be present as two separate glass transitions for the system. Even observing DSC curves of increasing wt% of DVE-1,4 below in Figure 2.19 shows that the glass transition appears to decrease to a near equivalent amount with mixtures. The homopolymers have higher glass transitions. This could be a result of increased chain mobility

due to a lack of crosslinking between the vinyl ether and epoxy groups. There may be more crosslinking with the homopolymers.

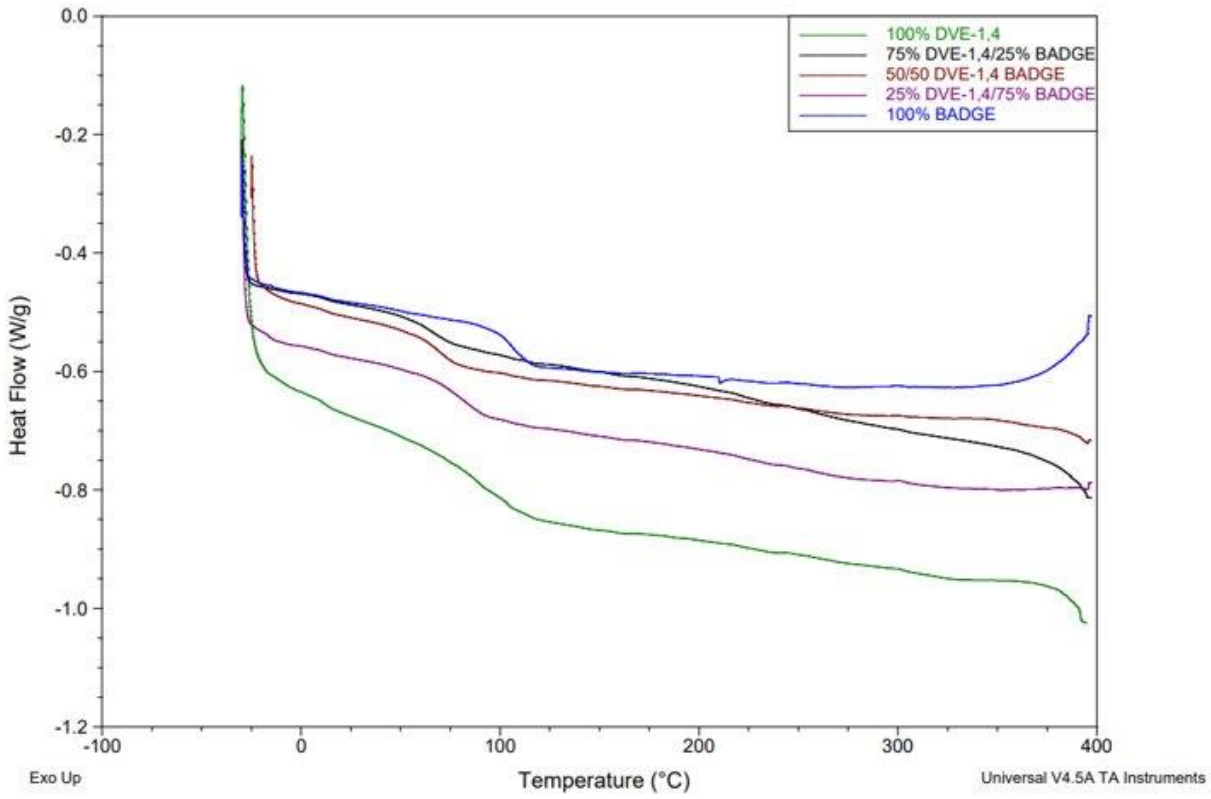

Figure 2.19. DSC curves of polymerized samples of differing ratios of BADGE:DVE-1,4 with 0.5 phr IOC-8 and 1.0 phr Luperox 231 with 10 wt% fumed silica, with a heating rate of 20 °C min^{-1} for the 100% DVE-1,4 sample and 10 °C min^{-1} for all other samples.

With regards to front kinetics, it has previously been shown that binary independent monomer systems in FP can exhibit a convex curve of front velocity with a minimum value as a function of monomer content due to dilution of one monomer system by the other. [74, 75] It is hypothesized that as the front velocity increases in vinyl ether and epoxy systems with increase of vinyl ether, that the monomers are not reacting independently but instead copolymerizing. However, the systems used by Pojman et al. utilized polymerized via free-radical and cationic mechanisms, while the RICFP systems in this work instead operate under identical cationic mechanisms.

For photopolymerization systems containing vinyl ethers and aromatic epoxides, arguments have been made against copolymerization, mostly on the basis of oxonium stability. [48, 76, 77] It has been proposed that due to the higher stability of oxonium ions in comparison to alkoxycarbenium ions, vinyl ethers would preferentially react with the carbenium ions formed from initiation of the vinyl ether monomer, leading to independent polymers. Rajaraman et al. [48] argue this is due to an equilibrium existing between alkoxycarbenium ions and oxonium ions, which are formed from interactions between carbenium ions and epoxide monomers. However, it is believed that the same arguments cannot be made for the RICFP system, as the photopolymerization studies are based on systems that polymerize at room temperature rather than high temperatures seen in RICFP. The high temperatures could affect the equilibrium explained above. For the studies of conversion in TMPTE and TEGDVE systems presented in this dissertation, a reduction in conversion of TMPTE when the monomers are mixed seems to indicate no copolymerization, though the increase of TEGDVE conversion indicates otherwise.

2.8. Effects of Functionality in RICFP Systems

The kinetic effects of functionality in acrylate-based free-radical FP systems have been previously published. [27] It was found that in formulations with increasing functionality of monomers, the front velocity increased. This was attributed to the gel effect, where rapidly increasing crosslinking density leads to a reduction in radical termination rates causing an increase in polymerization rate. To mimic this for cationic FP, three epoxy monomers were chosen which had nearly identical equivalent molecular weight per functional group, so that the specific heat release per gram was not the cause of any kinetic effects. Tetrafunctional epoxies are not commercially available, so this study was limited to trifunctional monomers at most. Results did not follow the same trend seen in free-radical FP. Instead, there existed a maximum

with difunctional 1,4-butanediol diglycidyl ether (DGE), shown in Figure 2.20. As a comparison of another difunctional monomer, DER 332, a bisphenol A diglycidyl ether based resin, has a 50% higher equivalent molecular weight per functional group, which is the likely cause of its much lower front velocity than DGE; in addition, the initiator loading for DER 332 was half that of the other monomers, which could be a cause for the reduction.

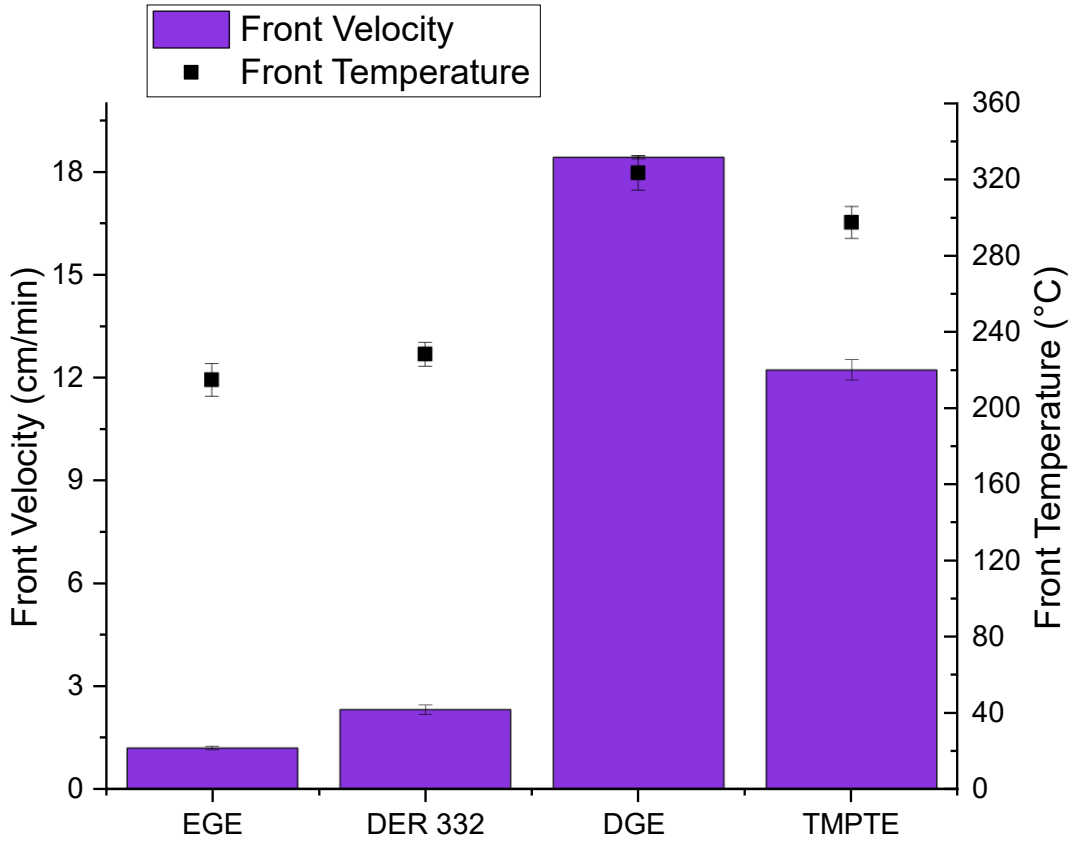

Figure 2.20. Front velocity and temperature for different glycidyl ether monomers with 2 phr IOC-8 and 2 phr Luperox 231 with 10 wt% fumed silica added.

One possible variable that could be affecting these results is the concentration of epoxy groups in the formulation. While the equivalent molecular weight per functional group is nearly identical for monofunctional ethyl glycidyl ether (EGE), DGE, and TMPTE, the concentration of epoxy groups is different mostly due to density differences. Using equation 1, the concentration of

epoxy groups in molarity can be calculated and are tabulated in Table 2.2. It is seen that the concentration of epoxy groups goes down as the functionality decreases. This still unfortunately does not explain the trend seen with the comparison of front velocities of the monomers. The epoxy group concentration can be equalized by dilution of the monomer. Propylene carbonate was chosen to dilute the monomers as it is inert to cationic systems and has a high boiling point. After dilution of the monomers to equal epoxy concentrations based on the epoxy group concentration of EGE, it was found in Figure 2.21 that the front velocity increases with increasing functionality, much like free-radical FP.

$$\text{Density} \times MW^{-1} \times 1000 = M_{epoxy} \qquad \text{Equation 2.1}$$

Table 2.2. Density, molecular weight per functional group, concentration of epoxy groups for different monomers, and wt% propylene carbonate added to equalize concentration.

Monomer	Density ($g\ mL^{-1}$)	MW per fn	Epoxy group concentration (M)	wt% PC added
TMPTE	1.16	100.8	11.5	25.7
DGE	1.10	101.1	10.9	19.9
EGE	0.90 (20 °C)	102.1	9.2	-
DER 332	1.16	170.2	6.82	-

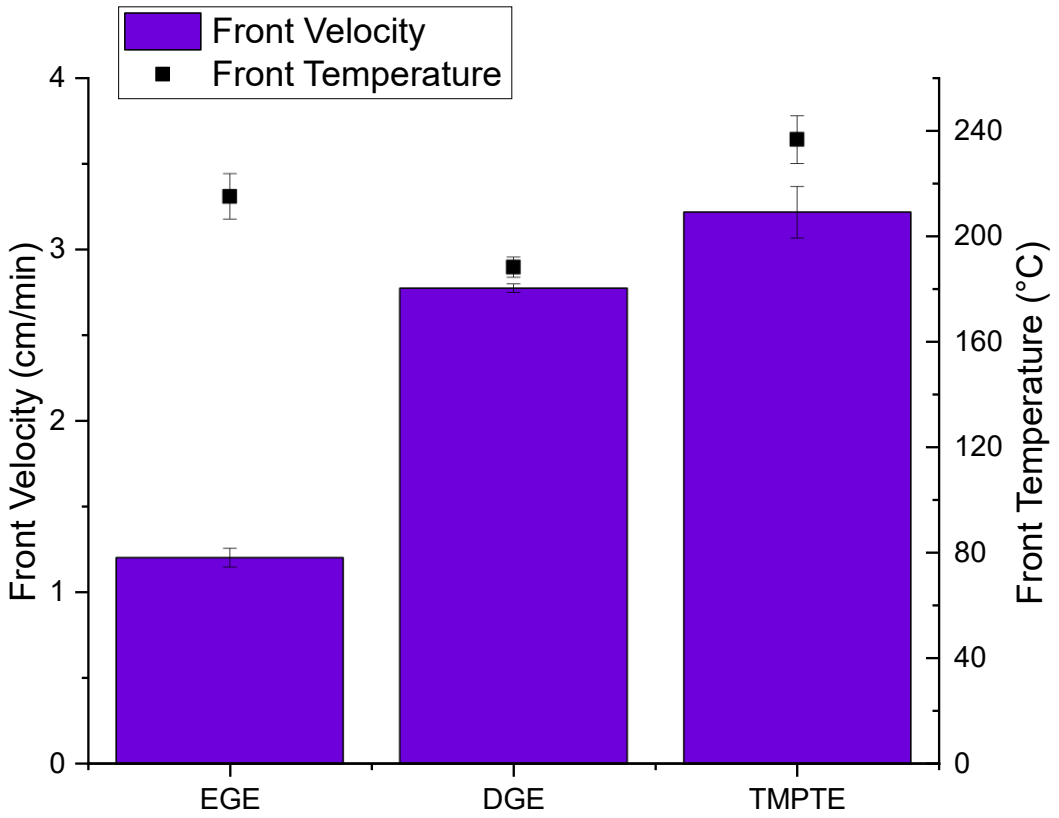

Figure 2.21. Front velocity and temperature of glycidyl ether monomers with increasing functionality that have been diluted to equal epoxy group concentrations using propylene carbonate, with 2 phr IOC-8 and 2 phr Luperox 231.

It is possible that crosslink density is affecting the front velocity. In photopolymerizations of epoxies, it has been shown that increasing crosslink density results in lower polymerization rate due to lower active center mobility that are responsible for propagation. [81] Just based on functionality, in the neat fronts difunctional DGE would have a lower crosslink density than TMPTE and the maximum in front velocity was with DGE. This changed with dilution, where potentially the crosslink density of TMPTE was lower than DGE even though the concentration of epoxy groups was equalized which led to the maximum front velocity of TMPTE. Outside of this hypothesis, it is not certain the cause of these results in functionality. For photopolymerization of epoxies, the rate of termination is so low that cationic centers are thought

to be non-terminating. [82, 83] Instead, the main mechanism of termination is chain transfer events to water or other impurities. [81] This is unlike free-radical polymerization, and thus the gel effect argument is not entirely analogous for cationic FP.

2.9. Conclusions and Future Outlooks

The radical-induced cationic frontal polymerization of vinyl ethers added to epoxies was studied. Using four separate vinyl ethers of varying structure with an epoxy (TMPTE) and through use of a superacid generator (IOC-8) with a radical thermal initiator (Luperox 231), a front was supported in three out of four vinyl ethers: BVE-1,4, DVE-1,4 and TEGDVE. With increasing increments of DVE-1,4 to epoxy, large increases in front velocity and front temperature were seen. The same trend occurred for TEGDVE, with an initial unexplained drop in front velocity at 25 wt%. Formulations with BVE-1,4 and EGVE, both hydroxy-functionalized monovinyl ethers, were unsuccessful in increasing the front velocity. BVE-1,4 reduced the front velocity with increasing addition, while EGVE did not support a front at any percentage. This is due to chain transfer to the hydroxyl for both monomers, and in the case of BVE-1,4, boiling also occurred which contributes to heat loss. TEGDVE-containing formulations produced soft and flexible materials, while DVE-1,4 formulations instead produced rigid materials at higher vinyl ether percentage.

The effects of the initiators on the front kinetics was studied with DVE-1,4 and TMPTE. It was found that IOC-8 had a larger effect on the front velocity than Luperox 231. This is hypothesized to be due to the IOC-8 being the generator of the superacid initiating species, while Luperox 231 exists to only decompose the iodonium salt into radical species that are reduced to the superacid.

Formulations containing pure DVE-1,4 successfully support a very fast front, but had a very short pot life in comparison to formulations containing at least 25% epoxy, experienced solubility issues with IOC-8, and presented inhomogeneity in the solution. Initially, a solution to these issues with pure TEGDVE was to add MeHQ, a radical inhibitor, which appeared to lengthen the pot life. A better solution was found by using propylene carbonate to dissolve the IOC-8 in a 1:1 ratio before adding to the monomer which allowed enough time to work with the resin. With 1 phr IOC-8 and 1 phr Luperox or 2 phr IOC-8 and 2 phr Luperox, extremely fast front velocities of 110 cm min^{-1} and 256 cm min^{-1} were found for TEGDVE. The materials produced from pure TEGDVE and DVE-1,4 are weak and impractical for applications. However, an optimal selection of fillers or addition of small amounts of another monomer could possibly strengthen these polymers.

Pot life of the formulations was also studied. It was found that even 10 wt% TMPTE added to DVE-1,4 resulted in a much longer pot life than pure DVE-1,4 which only would set at room temperature for a few hours before polymerizing violently. Addition of 0.5 wt% KOH increased this pot life to a little under a week. To instead study the pot life on an accelerated time scale, formulations were placed in an oven at 50 °C. Samples of TMPTE and TEGDVE were polymerizing overnight, but with addition of 300 ppm MeHQ the polymerization was inhibited. The addition of MeHQ increases the pot life at the cost of the reduction of front velocity. Formulations of 50 wt% TEGDVE/50 wt% TMPTE were studied up to 66 days and formulations of pure TMPTE were studied for 61 days where it was found that the front velocity decreases by approximately 42 % and 47 %, respectively. This is due to the generation of radicals by Luperox 231 and subsequent inhibition of the radicals by MeHQ, which then cannot decompose the IOC-8 to generate superacid. Formulations of TMPTE with no MeHQ did have a pot life of 35 days,

indicating the vinyl ether reactivity is partly responsible for the short pot life. Additionally, it was found that samples of 50 wt% TEGDVE/50 wt% TMPTE would react after 3 days without Luperox 231 and MeHQ and only IOC-8.

Studies to discern copolymerization of the resulting polymer using mixtures of linear and crosslinked epoxy-vinyl ether systems were unsuccessful, and studies with DSC were inconclusive in determining copolymerization. However, IR spectroscopy to determine conversion of the epoxy and vinyl ether groups showed a decrease in epoxy conversion from 78.7 % with only TMPTE to 57.3 % when mixed 1:1 with TEGDVE. Combined with reports in the literature of cationic epoxy-vinyl ether photopolymerization, this initially suggests that the two monomers are not copolymerizing. But there was also an increase of conversion of TEGDVE when mixed 1:1 with TMPTE, which indicates otherwise.

Regarding future outlooks for the addition of vinyl ethers to epoxies in radical-induced cationic frontal polymerization, detailed study into the variables affecting pot lives of these systems needs to be carried out. Initiator concentration, reactivity of the monomer, ambient temperature, and inhibitor choice and loading will all affect the pot life, and their study can optimize formulations especially in the case of practical applications. Analysis of mechanical properties and thermal properties of polymers produced by RICFP of vinyl ethers and epoxies will also be useful in optimization. Detailed analysis of monomer conversion and structural characterization to determine the presence of copolymerization is needed. Finally, the effects of the monomer functionality on front kinetics was studied, but requires more investigation to determine the mechanisms and causes of the results that were observed with thermal cationic FP.

CHAPTER 3. SYNTHESIS OF NOVEL VINYL ETHERS FOR FP

There are not many commercially available vinyl ethers. Moreover, vinyl ethers with greater than difunctionality are not available which makes direct comparisons of functionality and investigations of increasing crosslink density impossible. Therefore, there is an advantage to synthesize novel vinyl ethers that contain high functionality or other interesting structure-property relationships.

3.1. Solid Vinyl Ethers Based on Urethanes

The first attempt at synthesis of novel vinyl ethers was a solid vinyl ether based on urethane chemistry. Urethanes are formed from the alcoholysis of isocyanates. [60, 84] Solid monomers for FP could be useful for powder coatings, but there exists a major issue that the endothermic melting process can hinder front propagation through heat loss. A diisocyanate, 4,4'-methylenebis-(phenyl isocyanate) (MBPDI), a flaky white solid, was mixed with 1,4-butanediol vinyl ether (BVE-1,4) in a 1:2 molar ratio (MBPDI:BVE-1,4) in acetone. MBPDI was chosen so that the monomer produced by the reaction would give a crosslinked system rather than linear polymers that would be produced if the vinyl ether product was monofunctional. BVE-1,4 was in excess as it only has 1 hydroxyl group. The overall reaction is shown in Figure 3.1.

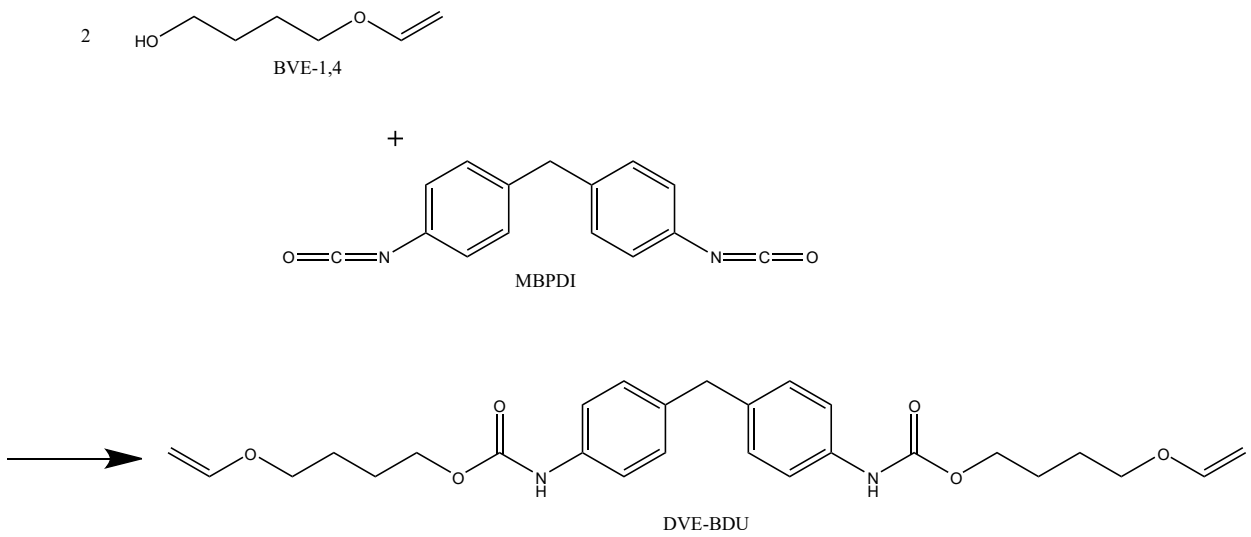

Figure 3.1. Reaction of BVE-1,4 with MBPDI to produce solid vinyl ether, DVE-BDU.

Upon mixing, there was some visible precipitation, likely to be the dissolved MBPDI, but the solution stayed light yellow with stirring. After ~30 minutes, there was sudden precipitation of a pale-yellow material. The material was extracted, and vacuum filtration was used to pull most of the acetone off, which left a white powder with a yield of ~84%. The product was analyzed using IR, which confirmed that urethane peaks were formed, and the hydroxyl groups of the vinyl ether reacted with the isocyanate. The IR spectra for the reagents and product is shown in Figure 3.2.

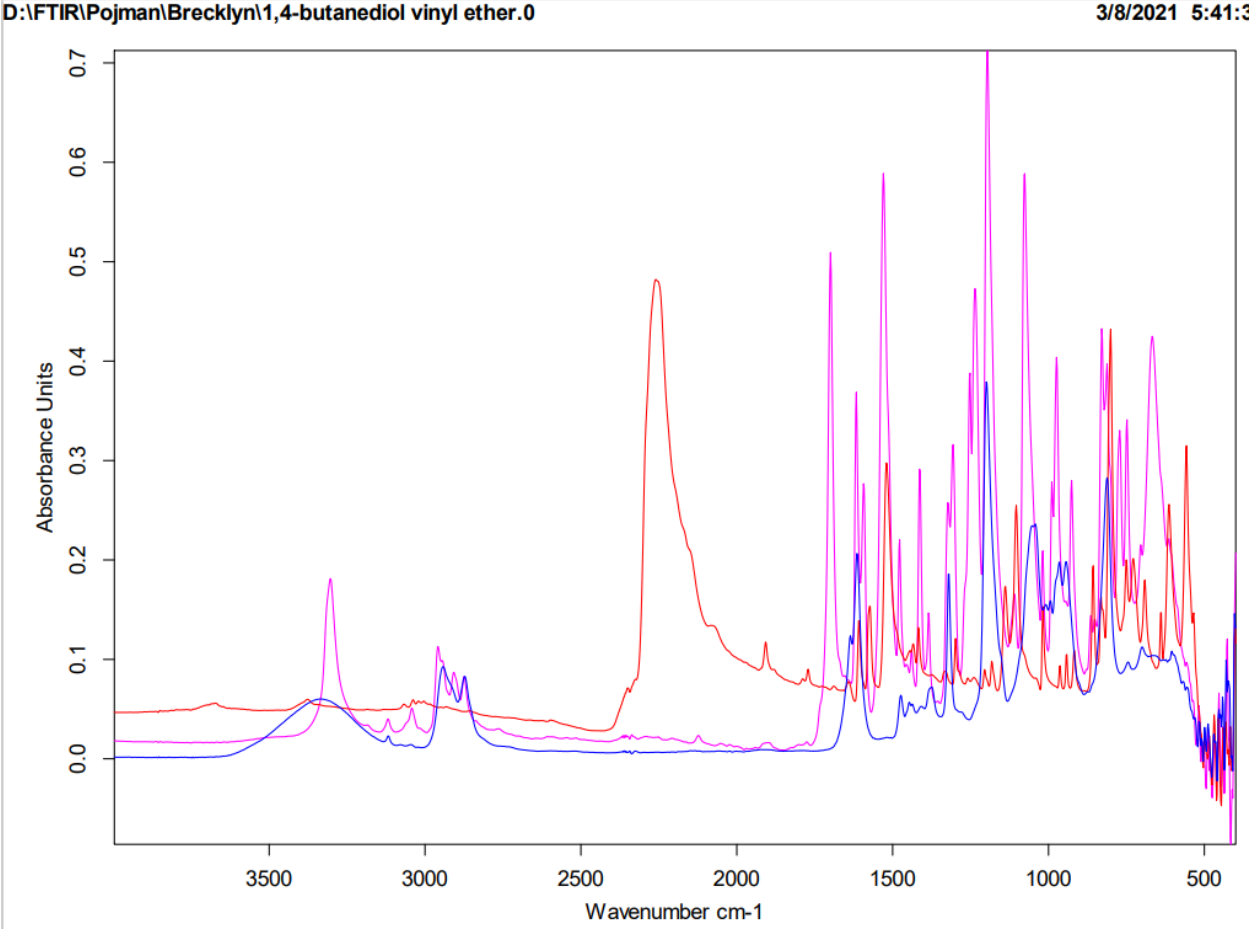

Figure 3.2. Combined IR spectra of MBDPI (red), BVE-1,4 (blue), and DVE-BDU (pink).

The most telling peak to confirm the product is the disappearance of the large peak around ~2200 cm^{-1} in the diisocyanate spectrum, which corresponds to the -N=C=O group. The peak is almost completely gone in the product spectrum, meaning the -N=C=O group has been converted to a urethane. Another peak associated with the urethane group is the sharp peak around ~3300 cm^{-1} in the product spectrum, which corresponds to an -NH that is present in the product but not the diisocyanate. Likewise, the disappearance of the broad peak in the hydroxy vinyl ether spectrum at ~3300 cm^{-1} indicates conversion of the hydroxyl groups to a urethane.

A liquid diisocyanate, isophorone diisocyanate, was also mixed with BVE-1,4. The liquid reagents were miscible, but nothing occurred as far as color changes or an exotherm upon

addition and stirring unlike the previous reaction. The solution stayed clear, even with external heating up to 70°C. The physical observations of this reaction including a lack of precipitate concluded no product was formed.

Another attempted synthesis of a solid vinyl ether was based on EGVE. Synthesis of this divinyl ether was very similar to the BVE-1,4-based vinyl ether. The overall reaction is shown in Figure 3.3. A 2:1 molar ratio of EGVE to MBPDI was used to balance out the functionality of the two reagents. To make the vinyl ether with initiators already integrated, approximately 2 phr IOC and 3 phr L231 was added to a solution of liquid EGVE. An appropriate amount of MBPDI (to achieve the 2:1 ratio) was dissolved in nearly double its mass in acetone. With stirring, the MBPDI solution was added to the EGVE solution. An immediate exothermic reaction occurred, with the solution bubbling for a couple seconds before settling down. The solution, originally yellow, also turned orange. Within 5 minutes an off-white solid was formed. The solid was left in a Buchner funnel overnight to eliminate all solvent. A yield of 64% was obtained.

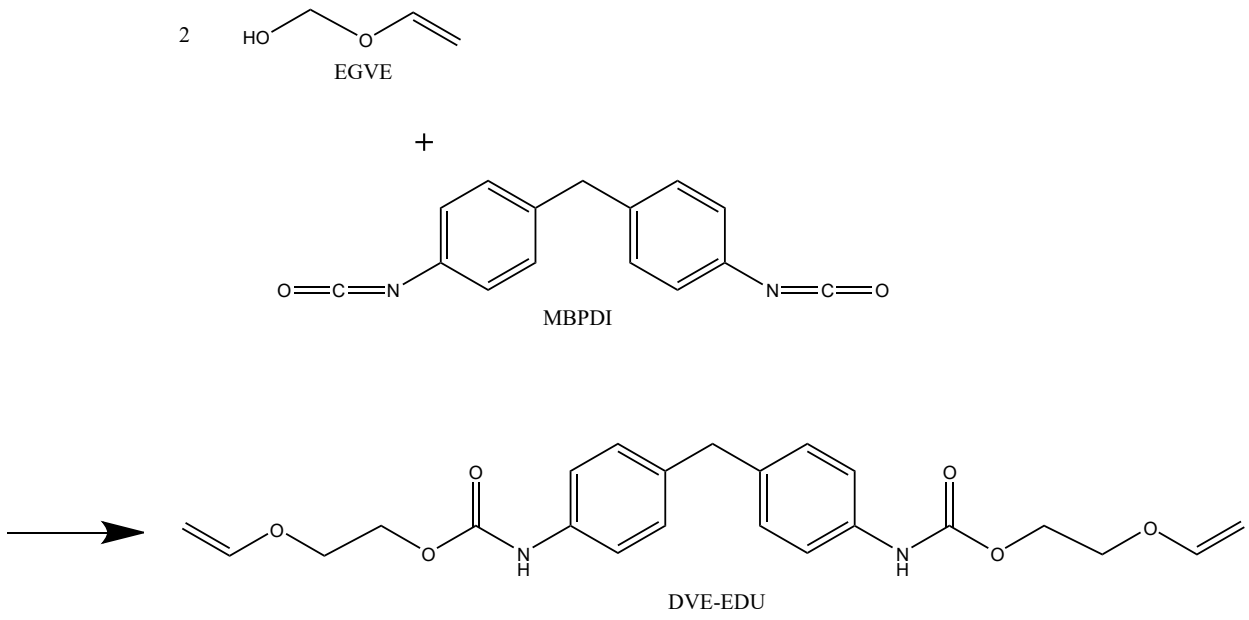

Figure 3.3. Synthesis of DVE-EDU by reaction of EGDVE and MBPDI.

Like the other solid vinyl ether, IR was used to confirm the product. The IR spectrum for the DVE-EDU product is shown below in Figure 3.4. This spectrum is similar to the one shown for the DVE-BDU, as expected. Similarly, the appearance of a sharp amine peak at ~3300 cm^{-1} in the spectrum with the absence of any broad -OH peaks or -N=C=O peaks at ~3500 cm^{-1} and ~2200 cm^{-1}, respectively, confirm the product was formed. The near complete absence of the -N=C=O peak may also indicate that the purity is adequate and minimal amounts of unreacted isocyanate remain.

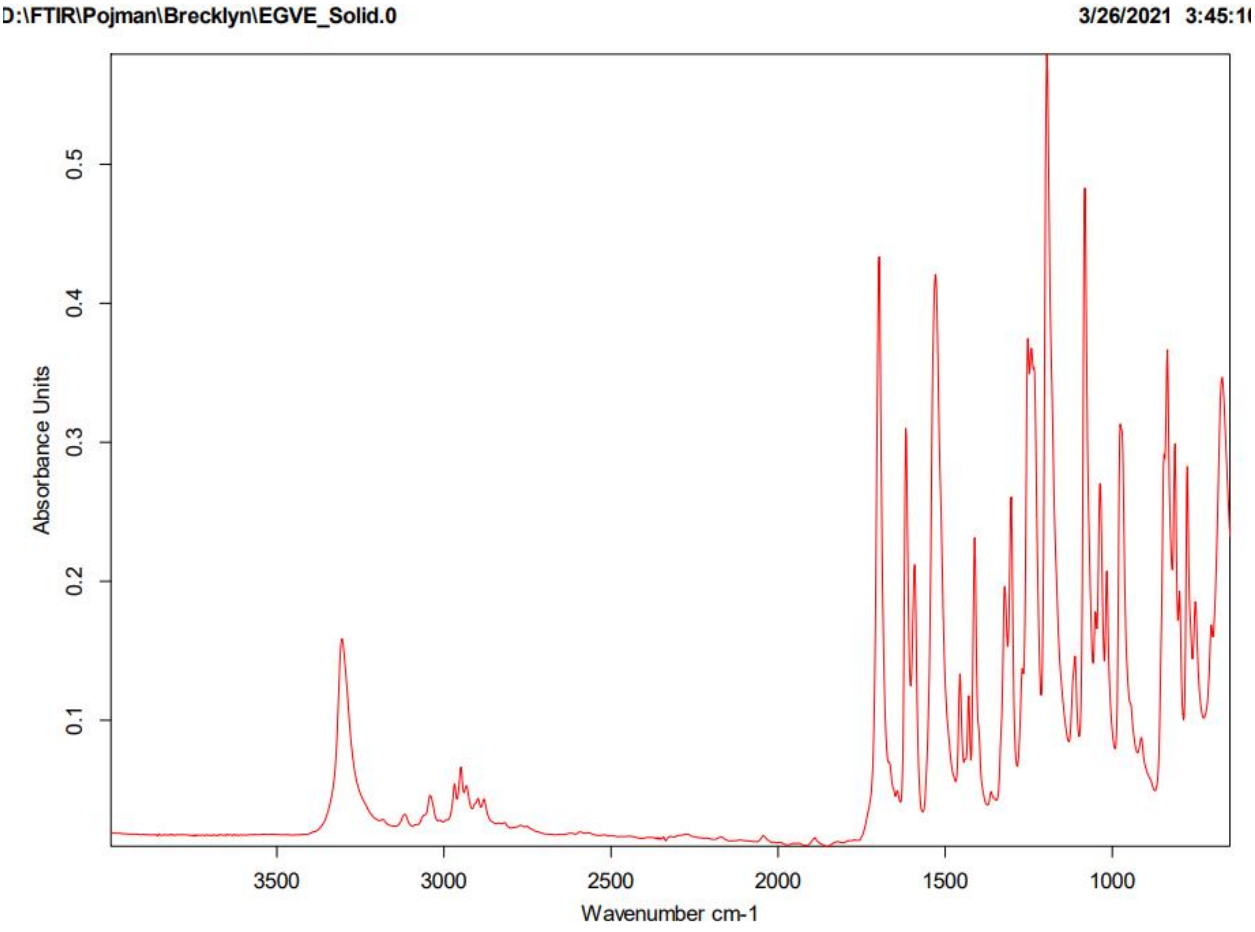

Figure 3.4. IR spectrum of DVE-EDU product from reaction of EGVE and MBPDI.

There was also an attempt to synthesize DVE-BDU with the initiator system already integrated. Following a similar synthesis method, the diisocyanate was dissolved in acetone and added to a solution of excess BVE-1,4 that contained approximately 1.0 phr IOC-8 and 2.0 phr Luperox 231. The IOC-8 readily dissolved with stirring. A reaction visibly occurred as the solution turned from a pale-yellow solution to orange with some moderate bubbling after about 5 minutes. The solution was placed on ice to suppress thermal decomposition of the Luperox 231 and after 10 minutes more of stirring, a white solid formed rather suddenly, like before. Vacuum filtration was used to pull off the acetone from the solid and what resulted was a white powder much like the pure DVE-BDU synthesized before. However, the potential issue is that the exothermic reaction that occurred caused the Luperox 231 to completely decompose, rendering it useless.

Frontal polymerization of these solid vinyl ethers was attempted. Three formulations were used: first, DVE-BDU with the initiator system added during synthesis as above. The next formulation contained DVE-BDU but the solid was dissolved in acetone and 1 phr IOC-8 and 10 phr Luperox 231 were added while in solution, then the solvent was evaporated. Both formulations did not support a front but did polymerize locally with heat after melting of the solid. The confirmation of polymerization was shown by heating the solid vinyl ether with absence of initiator, which did not result in any change. Additionally, IOC-8 and Luperox 231 were mixed with the DVE-BDU as a powder instead of in solution in acetone as above—it polymerized but also did not support a front. The final formulation contained DVE-EDU as described above. This formulation melted to form a brown liquid which then hardened upon cooling. It is likely that this material polymerized given the color and property changes.

A MelTemp device was used to analyze the melting points of DVE-BDU, the DVE-BDU that was synthesized with initiator, and DVE-EDU. For fronts with solid monomer, it is

important to have a low melting point so that less heat loss occurs from melting of the solid. It was found that the melting point of DVE-BDU without initiator was a wide range, where the appearance of a phase change started around 150 ℃, and the solid had completely melted at 219 ℃. This shows some impurity in the solid, likely being unreacted vinyl ether, as the diisocyanate was the limiting reagent. The DVE-BDU with initiator had a narrower melting point of 102.9-105 ℃, as did the DVE-EDU, which had a melting point of 126.8-129.4 ℃. The hypothesis for the lower melting point of the DVE-BDU with initiator is perhaps the initiator also acts as an impurity which lowers the melting point. This analysis shows how low of a temperature is required for the localized reaction zone during FP to melt the material ahead of it.

Finally, as an attempt to initiate FP with these monomers, DVE-BDU and DVE-EDU, both with initiator added during synthesis, were packed into a test tube and heated using a soldering iron. This did not support a front and only localized reactions occurred in both cases. DVE-BDU with initiator that was integrated during synthesis was added to TMPTE to act as a reactive filler. ~40 wt% DVE-BDU was added to TMPTE and mixed to form a slightly viscous, but spreadable material. This mixture did not support a front. The material only lowered in viscosity with heat and polymerized around the soldering iron tip. Addition of another ~1 phr IOC-8 and Luperox 231 was added to this solution and mixed. Addition of 1 wt% fumed silica to this to increase viscosity gave the same localized polymerization as before. Using a heat gun on the surface of the material formed a brown, weak, but very flexible film, only on the surface. Another 2 wt% fumed silica was added to the remaining unpolymerized solution until it became viscous—this also did not support a front and produced the same brown film when a heat gun was used.

One possibility for why FP with these materials is unsuccessful is that there is boiling once the solid melts due to the soldering iron. There is also boiling when the TMPTE was added along with fumed silica. Perhaps more initiator needs to be added or integrated into the solids. It could be very possible that decomposition of the Luperox 231 is occurring with the exothermic isocyanate-hydroxyl reaction, though the solid vinyl ethers will polymerize locally without adding additional Luperox 231. It also could be possible that the exotherm from the initial reaction is not sufficient to melt the solid ahead of the localized reaction zone. Another explanation for the suppression of FP is the urea group of the urethane linkage interfering with the cationic polymerization. The urea group is basic and could be neutralizing the acid formed from IOC-8 decomposition. Regardless, to form solid vinyl ethers in the future, different reagents must be chosen that are compatible with cationic polymerization.

3.2. High Boiling Point Vinyl Ethers Based on Esterification of Carboxylic and Fatty Acids

Propagating fronts can be quenched by boiling of monomer, as it leads to heat loss in the system. This is evident in the previously mentioned studies of hydroxy-functionalized vinyl ethers, which had lower boiling points than the studied divinyl ethers and resulted in decreasing front velocities and temperatures as they were increasingly added to epoxies. Therefore, synthesis of a monofunctional vinyl ether based on fatty acids was attempted as a means of increasing the boiling point of these monomers. This synthesis followed a Steglich esterification reaction shown below in Figure 3.5, where the hydroxy functionalized vinyl ether reacts with oleic acid and dicyclohexylcarbodiimide (DCC) with 4-dimethylaminopyridine (DMAP) as a catalyst. Using oleic acid results in a liquid product due to the unsaturation or the long aliphatic chain.

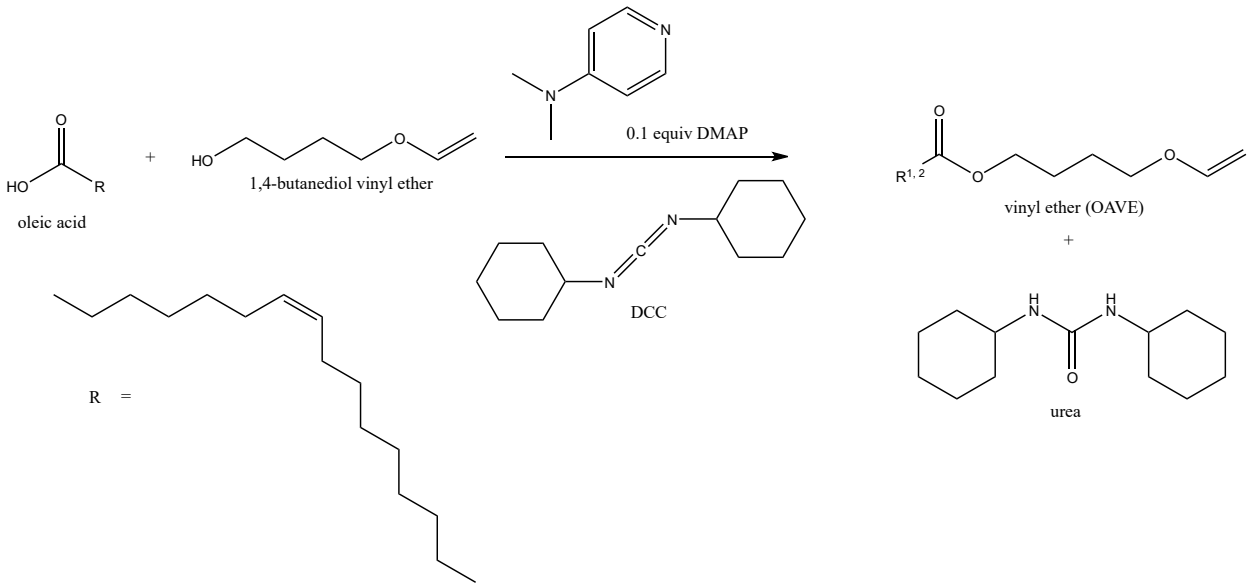

Figure 3.5. Synthesis of vinyl ether (OAVE) through esterification, based on oleic acid and BVE-1,4.

In a flask, 1 equivalent of BVE-1,4 was dissolved in chloroform, then 1 equivalent oleic acid (OA) was added along with 1.1 equivalents of DCC. After 5 minutes, a stable intermediate would form. 0.1 equivalents of 4-dimethylaminopyridine (DMAP) was then added as a catalyst. The reaction was left to stir overnight where a white solid had precipitated. The solid, a urea byproduct, was filtered off and the aqueous layer was extracted with chloroform and remaining organic layer was washed with saturated $NaHCO_3$ twice to remove acid, then saturated NaCl once to remove water. It was dried over $MgSO_4$ to remove any remaining water. The remaining solvent was evaporated off with a rotovap.

FP of the product after extraction, a viscous yellow liquid, was attempted with 1 phr IOC-8 and 1 phr Luperox 231. The IOC-8 dissolved readily in the liquid. Polymerization was first tested of the liquid monomer using a heat gun, where the yellow solution turned black and slightly more viscous after boiling. The boiling was likely to be leftover solvent. FP was attempted with fumed silica added to make a viscous putty, but no visible front was observed. A

control sample with equivalent initiator amounts but 50/50 BVE-1,4 and oleic acid was then tested to confirm that the product was formed. Upon heating this sample, a similar product, a brown viscous liquid, was observed.

Fronts of 50/50 TMPTE/OAVE, 50/50 TEGDVE/OAVE and 80/20 TEGDVE/OAVE were attempted with no success. These were all formulations with 1 phr of both IOC-8 and Luperox 231. It may be possible that OAVE must be added in small amounts as a flexibility promoter rather than a monomer all its own, since it has almost triple the equivalent weight per vinyl ether group as TEGDVE, which will lead to lower reactivity. Basic impurities such as DMAP or the urea byproduct could be inhibiting the cationic polymerization and not allowing a front to propagate. The product was dissolved in cold ethyl acetate to extract any remaining urea byproduct, but this did not result in any additional precipitation. There could also be an inherent flaw with the monomer such as low heat production, but a system of 80/20 TEGDVE/OAVE also would not support a front. This problem warrants more investigation as a high ratio of TEGDVE would be expected to still support FP unless the OAVE was actively inhibiting cationic polymerization.

Analysis of the pure OAVE, the polymerized OAVE, and the control sample of BVE-1,4 with oleic acid with IR gave the following spectra in Figure 3.6.

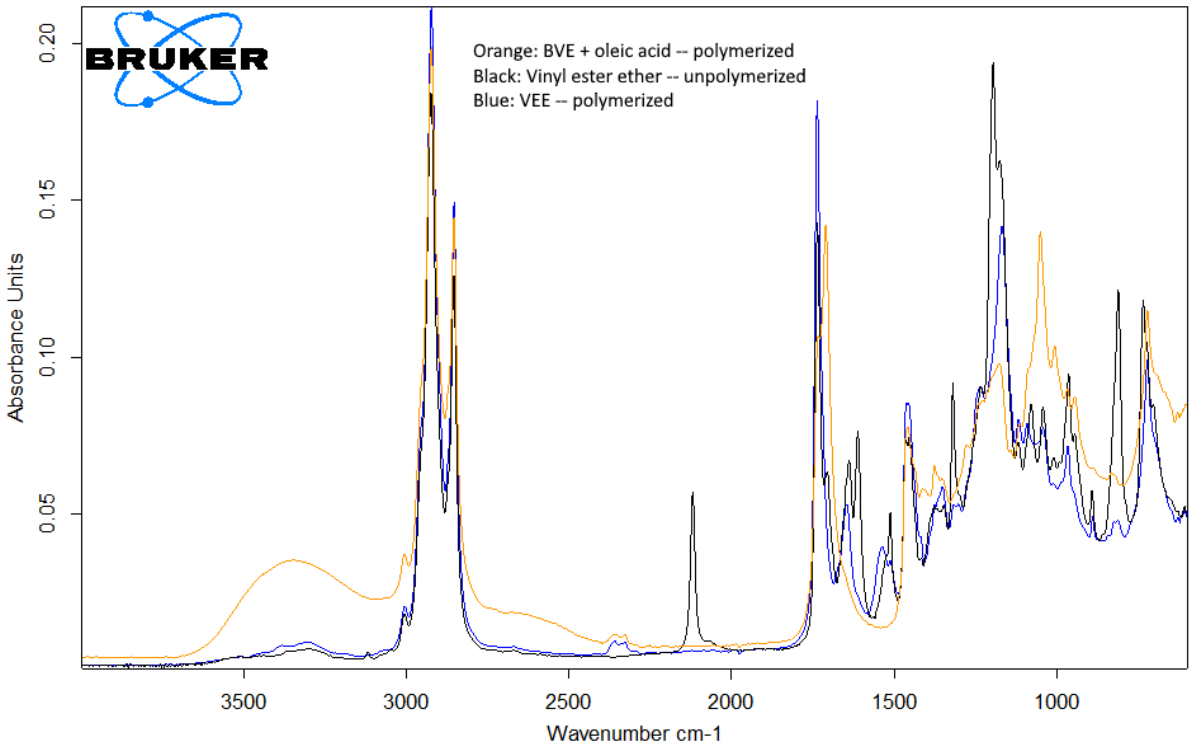

Figure 3.6. Spectra of OAVE, polymerized OAVE, and a control of BVE-1,4 with oleic acid. The spectra seem very similar save for the broad -OH peak shown in the BVE-1,4/oleic acid control sample that was to be expected due to the hydroxy functionalization of BVE-1,4, and a sharp peak in the unpolymerized OAVE at ~2100 cm^{-1}. It is not certain what structural feature is shown by this peak. Typically in this range is alkynes (C≡C) and allenes (X=X=X). The only possibility is that this is residual DCC left in the product. No other structural features of the OAVE, BVE-1,4, oleic acid, DCM or DMAP match the functional groups presented in this range. The issue is that remains is why the DCC peak would show in the unpolymerized product but not the polymerized product nor BVE-1,4/oleic acid control.

There were also attempts to synthesize a divinyl ether based on an esterification product of PEG-600 diacid and BVE-1,4, which is shown in Figure 3.7. This is a dicarboxylic acid that is liquid at room temperature. The synthesis method followed a similar procedure to the DCC

coupling (esterification) with oleic acid but used a 2:1 molar excess of BVE-1,4 to the PEGDCA (PEG dicarboxylic acid) due to the difunctionality of the PEGDCA. After a similar workup as above, the product was a clear, slightly yellow liquid with a viscosity higher than water. The product was analyzed using IR, shown below in Figure 3.8.

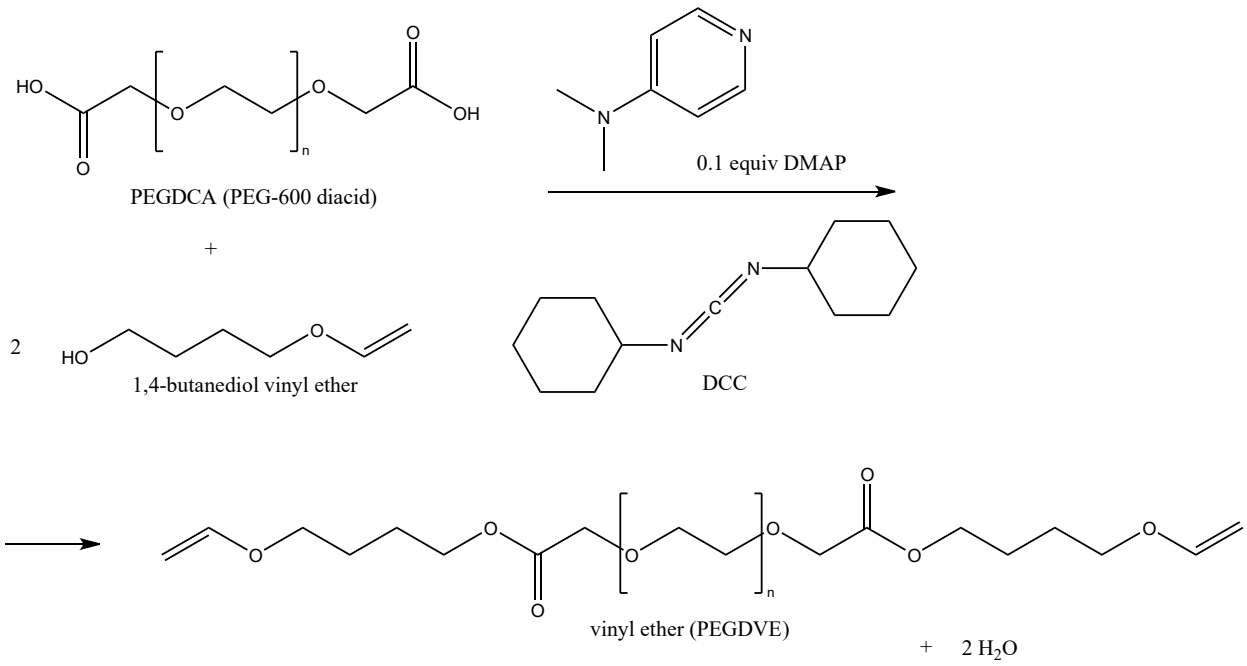

Figure 3.7. Synthesis of PEGDVE monomer from BVE-1,4 and PEGDCA.

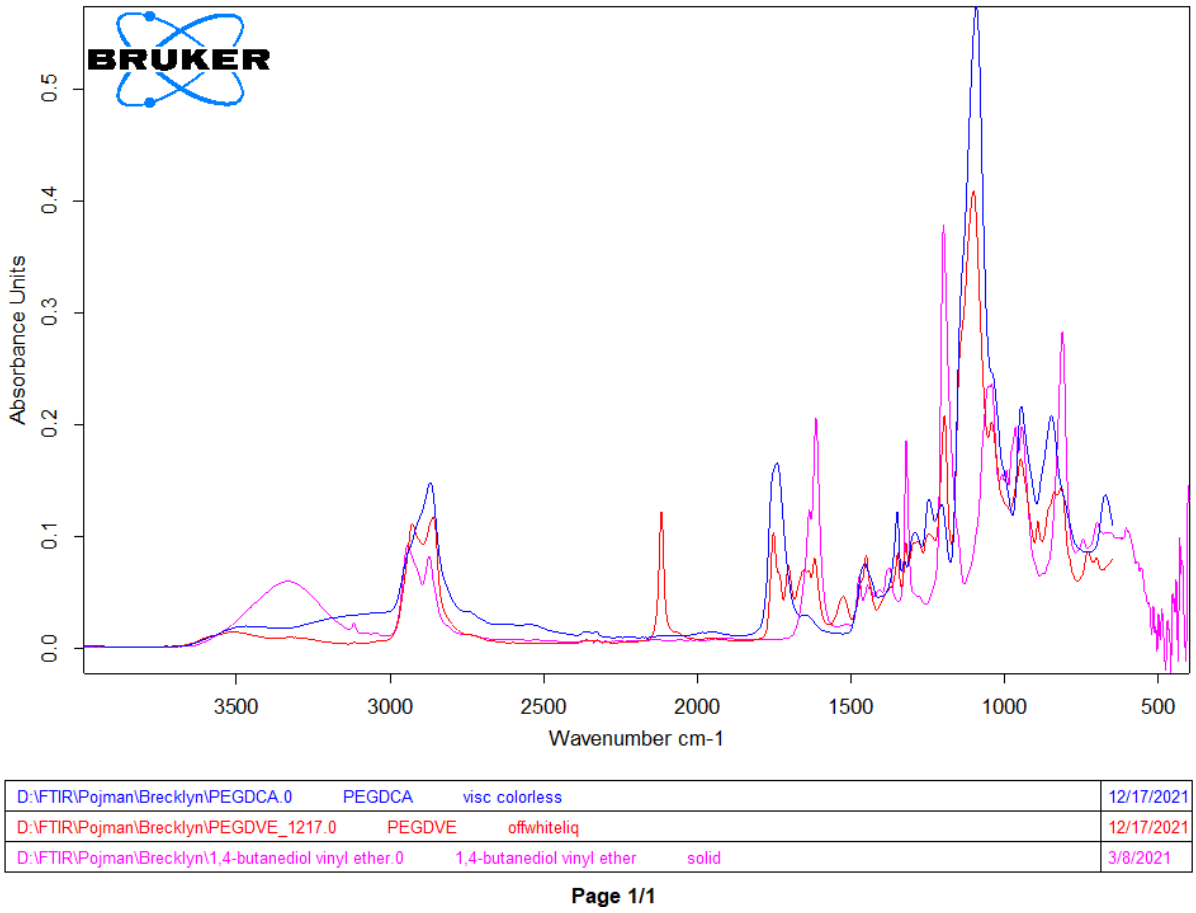

Figure 3.8. Spectra of BVE-1,4 (pink), PEGDCA (blue), and the synthesized PEGDVE vinyl ether (red).

The promising feature of the spectrum that would indicate conversion to a divinyl ether is the absence of an -OH stretch at ~3400 cm^{-1} for the product, PEGDVE. However, carboxylic acids appear at 1100 cm^{-1} and this peak is still present in the PEGDVE indicating there is residual diacid left in the solution. The other impurity present is DCC, which is likely the sharp peak at 2100 cm^{-1}.

Polymerization of the material in a test tube with 1 phr IOC-8 and Luperox 231 was attempted first with a heat gun. This resulted a very viscous brown liquid after a few minutes of heating. The problem with this outcome is that the expected difunctional monomer would produce a solid crosslinked thermoset and not a viscous liquid. Next, 10 wt% fumed silica was

added to a solution also containing 1 phr of both IOC-8 and Luperox 231 and FP was attempted, to no avail. Some changes in the material that was on the tip of the soldering iron were observed though. It is believed that there are unconverted carboxylic acid groups in the product, and this could be affecting the relative heat production by having only monofunctionality. This would also lead to the production of a liquid rather than a solid polymer. Future work into this synthesis would need to detailed characterization of the product to confirm the conversion of both carboxylic acid groups to vinyl ether groups. If the conversion is low then the reaction may need to be modified. The resulting divinyl ether, if achieved, could be beneficial to producing materials with a high degree of flexibility due to the long chain present in the PEG, while maintaining higher reactivity than equivalent epoxies because of the vinyl ether group.

3.3. Vinyl Ethers of Alcohols using Calcium Carbide

There are reactions in literature which describe vinylation of alcohols using calcium carbide.[85] In these processes, calcium carbide generates acetylene in situ through a reaction with water. This could be utilized to generate multifunctional vinyl ethers based on readily available alcohols, such as pentaerythritol or glycerol shown in Figure 3.9. Collaborators in the García-López group at LSU carried out this reaction, with some success and quantitative yields, but purification of the product is difficult to its volatility.

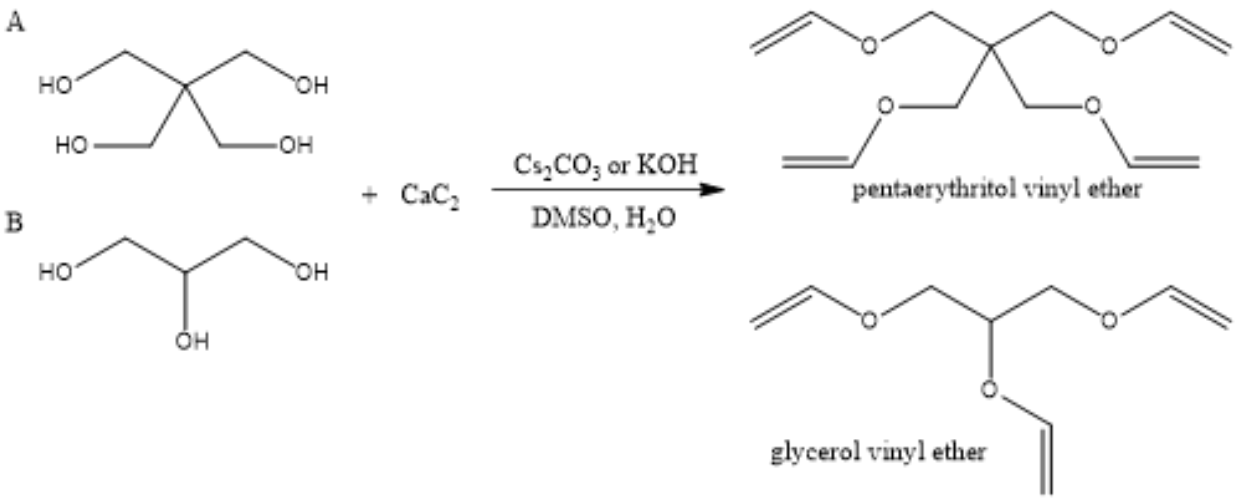

Figure 3.9. Synthesis of tri and tetrafunctional vinyl ethers based on commercially available alcohols pentaerythritol (A) and glycerol (B), using calcium carbide.

Vinyl ethers are traditionally synthesized using acetylene gas, therefore there is promise with using calcium carbide which is easier to handle. However, the reaction still is dangerous with the production of acetylene in situ which will make scaling up difficult. Nonetheless, future work with this reaction requires optimization and careful consideration of the properties of the product to generate desirable multifunctional vinyl ethers.

3.4. Conclusions and Future Work

Overall, it is shown that synthesis of novel vinyl ethers will require more careful planning of compatibility with cationic polymerization and synthetic optimization. The volatility of monomers remains an issue, in addition to obtaining desired conversion of reagent functional groups when synthesizing vinyl ethers with high functionality. Structural features, such as urea linkages, can interfere with cationic polymerization and should be avoided. Obtaining vinyl ethers with greater than difunctionality could prove useful to increasing crosslink density to potentially improve mechanical properties of pure vinyl ether systems, which are typically weak and brittle. Additionally, modification of the polymer backbone through synthesis of novel

monomers can also produce poly(vinyl ether) materials that are comparable in material properties to existing epoxy systems.

CHAPTER 4. HYBRID RICFP SYSTEMS WITH ACRYLATES

4.1. Background and Significance

Acrylates are very common in FP, due to their high reactivity, commercial availability, and generally low cost. [19] However, the physical properties of the polymers produced from acrylates can be poor. In addition, free-radical polymerization can suffer from oxygen inhibition, unlike cationic polymerization, and epoxides encounter less shrinkage than acrylates due to the ring opening process. An example of a polymer produced by FP of trimethylolpropane triacrylate (TMPTA) with only fumed silica added as a filler versus TMPTE with only fumed silica is shown below in Figure 4.1; in contrast to TMPTE, the TMPTA polymer is very brittle, and the material is unusable. While material properties of acrylate-based systems can be improved with addition of filler, [22, 86, 87] it is desirable to have systems that need the least components as possible. One solution is to add epoxy or vinyl ether to acrylate systems to tune the material properties with properties of the cationically-curing monomers. Epoxies and acrylates will polymerize via different mechanisms and will not copolymerize.

Figure 4.1. Comparison of polymer properties between formulations containing (a) TMPTE with 1 phr IOC-8 and 1 phr L231 with 10 wt% fumed silica and (b) TMPTA with 1 phr L231 and 10 wt% fumed silica, both with an ongoing front.

Hybrid epoxy-acrylate systems have been previously studied in FP. [74, 75, 88] Crivello studied the thermal FP of hybrid films generated by photopolymerization. [88] The epoxy/acrylate formulation, which contained an iodonium salt and 2,2-dimethoxy-2-phenylacetophenone as radical initiator, was photopolymerized with suppression of the cationic polymerization to generate a film based only on the acrylate, which then was thermally ignited to undergo FP of the epoxy. They found that FP was only supported with low concentration of TMPTA in a TMPTE/TMPTA system. It is important to note that in these systems, there is a sequential polymerization of the acrylate followed by FP of the epoxy aided by generation of cationic species through irradiation. Therefore, this study is not entirely analogous to the work shown in this dissertation.

A formulation studied by Pojman et al. used a bisphenol A diglycidyl ether resin cured by a combination of an alkyl amine and BCl_3-NR_3 complex mixed with triethylene glycol

dimethacrylate that polymerized via a peroxide, Luperox 231. [75] The alkyl amine cures epoxy via a step-growth mechanism, while the boron trichloride-amine complex acts as a cationic initiator. It was found that the two polymerizations occur independently generating an interpenetrating polymer network (IPN), indicated through a concave dependence of front velocity on the monomer ratio. The concave dependence indicates an IPN, since if only one monomer were reactive a monotonic increase in front velocity with an increase in the ratio of that monomer would be expected. Further studies using ethylene glycol dimethacrylate and bisphenol F diglycidyl ether with BCl_3-NR_3 and Luperox 231 instead indicated that BCl_3-NR_3 could be interacting with the decomposition of peroxide and did not exhibit the same concave dependence on monomer ratio. [74] The two monomers cured with an alkyl amine and Luperox 231 did however exhibit the concave dependence. The overall conclusion from both studies was that a minimum in front velocity will appear if two polymerizations are independent of one another and simultaneously occurring. It is assumed that if copolymerization is occurring in a binary system, the dependence of front velocity on monomer ratio will be convex, with a maximum appearing at the optimal ratio of the two monomers.

4.2. Materials and Methods of Frontal Polymerization of Hybrid Systems

Trimethylolpropane triglycidyl ether (TMPTE), tri(ethylene glycol) divinyl ether (TEGDVE), and trimethylolpropane triacrylate (TMPTA) were studied as the monomer systems. For the gravimetric studies of copolymerization, hexyl acrylate (HA), p-tert butylphenyl glycidyl ether (PTBGE), and dodecyl vinyl ether (D12VE) were used as monofunctional monomers. 1,1-Bis(tert-butylperoxy)-3,3,5-trimethylcyclohexane (Luperox 231) and p-(octyloxyphenyl)phenyliodonium hexafluoroantimonate (IOC-8) were used as the initiating

system. All chemicals were used as received. Chemical structures of the monomers and initiators used are shown in Figure 4.2.

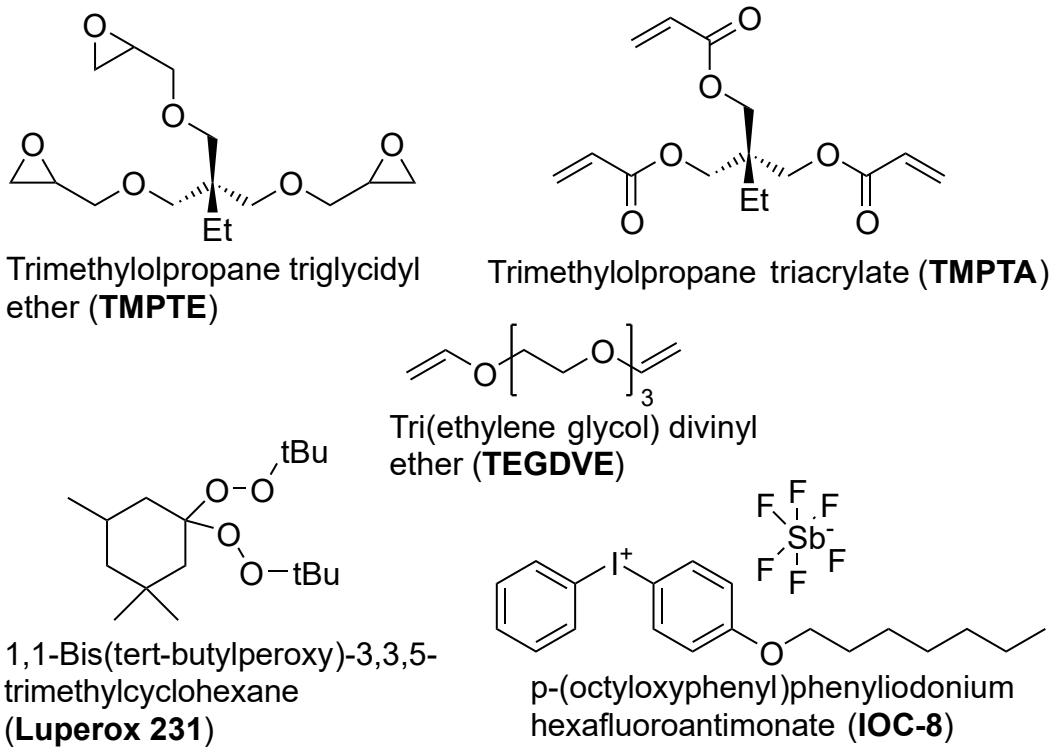

Figure 4.2. Structures of chemicals used in hybrid studies of acrylate and epoxy or vinyl ether systems.

Formulations were prepared with different ratios of TMPTA to TEGDVE or TMPTE, and different ratios of IOC-8 and L231. First, IOC-8 was dissolved in TMPTA using a heated sonicator at approximately 30 ℃. TMPTE or TEGDVE and L231 was then added. The mixture was stirred using a vortex mixer to ensure homogeneity. 10 wt% Aerosil E805 fumed silica was then added to increase viscosity and hand mixed.

The putty was loaded into a wooden mold (13.5 cm × 2 cm × 0.6 cm) lined with wax paper for easy removal. Fronts were initiated by brief contact with the resin using a soldering iron heated to 200 ℃. A Seek Thermal CompactPRO FF infrared camera was used to observe the evolving thermal field as the front propagated. The fronts were tracked using a video camera,

and front velocity was calculated from the slope of a position versus time plot. Expansion-corrected front velocity was calculated by multiplying the front velocity by a ratio of initial resin length to final resin length. Triplicate experiments from the same batch of resin were conducted. Infrared spectroscopy was performed with a Bruker FTIR and diamond ATR accessory for structural characterization and conversion determination. The technique used was equivalent to Section 2.7. Parameters of 4 cm^{-1} resolution, 32 sample scans, and 16 background scans were used. The resin was placed directly on the ATR diamond. Polymer samples were instead ground into a powder using a mortar and pestle to place onto the ATR platform. By using a large amount of sample, the probe created a film on the platform. Triplicates of every IR spectrum were taken, and a background was taken before every measurement.

4.3. Frontal Polymerization of Hybrid Epoxy/Acrylate Systems

TMPTE and TMPTA were chosen as monomers to study with IOC-8 and Luperox 231 acting as the initiating system. Shown in Figure 4.3, it was found that increasing the percentage of TMPTE to TMPTA resulted in a decrease in front velocity with a minimum at 10 wt% TMPTE. This indicates that the TMPTE is much less reactive than the TMPTA with two independent polymerizations occurring, forming an IPN similar to previous FP literature. [75]

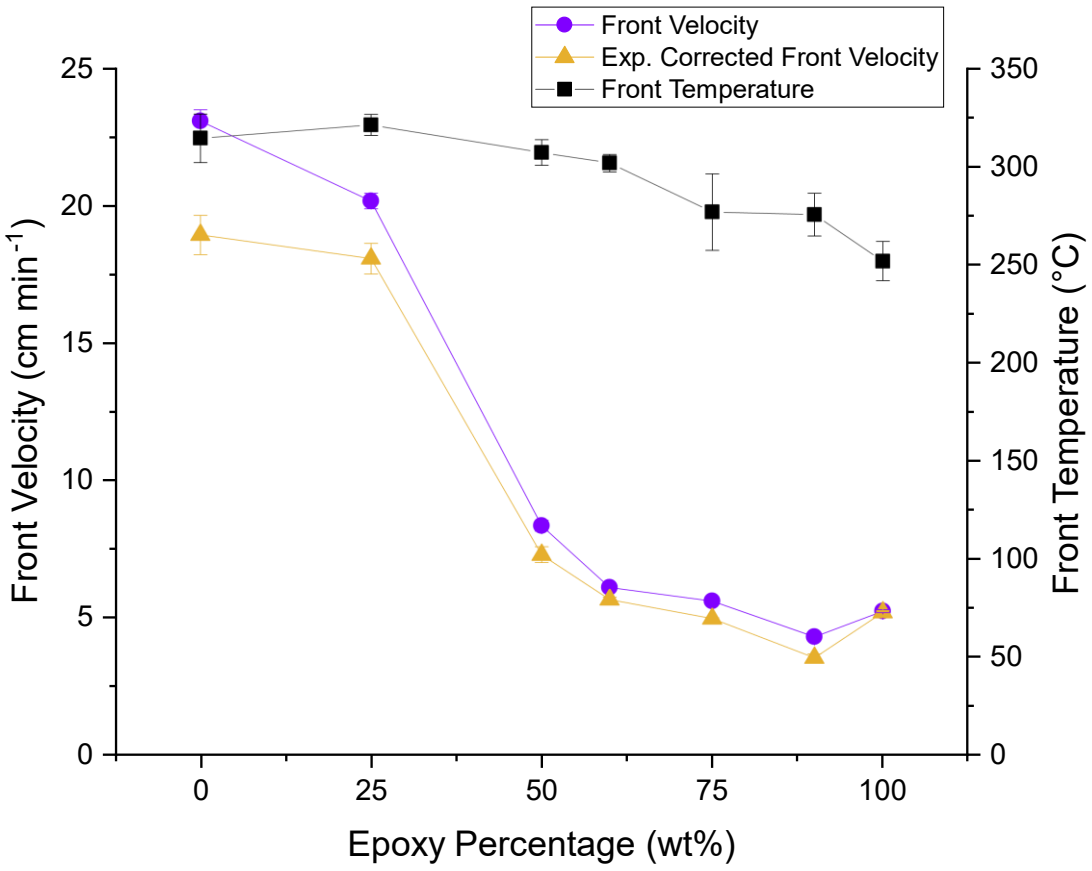

Figure 4.3. Front velocity, expansion corrected front velocity, and temperature as a function of epoxy percentage in a hybrid TMPTE/TMPTA system with 1 phr IOC-8 and 1 phr L231 with 10 wt% fumed silica.

There have been many studies of photopolymerization of hybrid epoxy-acrylate systems. [46, 89-91] These studies give some insight into the kinetics, but FP occurs at much higher temperatures and the trends in kinetics may be affected by this. It is suggested that addition of acrylate can accelerate the slower curing of epoxy. [46] A thesis by Dillman[90] saw that in photopolymerization of hybrid cycloaliphatic epoxy-acrylate systems using an iodonium salt and radical photoinitiator, similar epoxy conversion was achieved with or without radical initiator which implies that there is no copolymerization occurring.

By increasing the IOC-8 concentration in this system, the minimum in front velocity shifts to a lower TMPTE percentage as seen in Figure 4.4. This is because TMPTA is the more reactive monomer, but with more IOC-8 the TMPTE polymerization becomes more reactive as it proceeds by cationic polymerization, which is evidenced by the higher front velocity of 100% TMPTE versus 100% TMPTA with 5 phr IOC-8 and 1 phr Luperox 231. At 1 phr IOC-8 and 1 phr Luperox 231, the TMPTA reaction is dominant. It can also be seen that the front velocity for 100% TMPTA is lowered as the IOC-8 concentration is increased, which is due to the consumption of radical species to induce decomposition of IOC-8 and generate superacid for TMPTE polymerization.

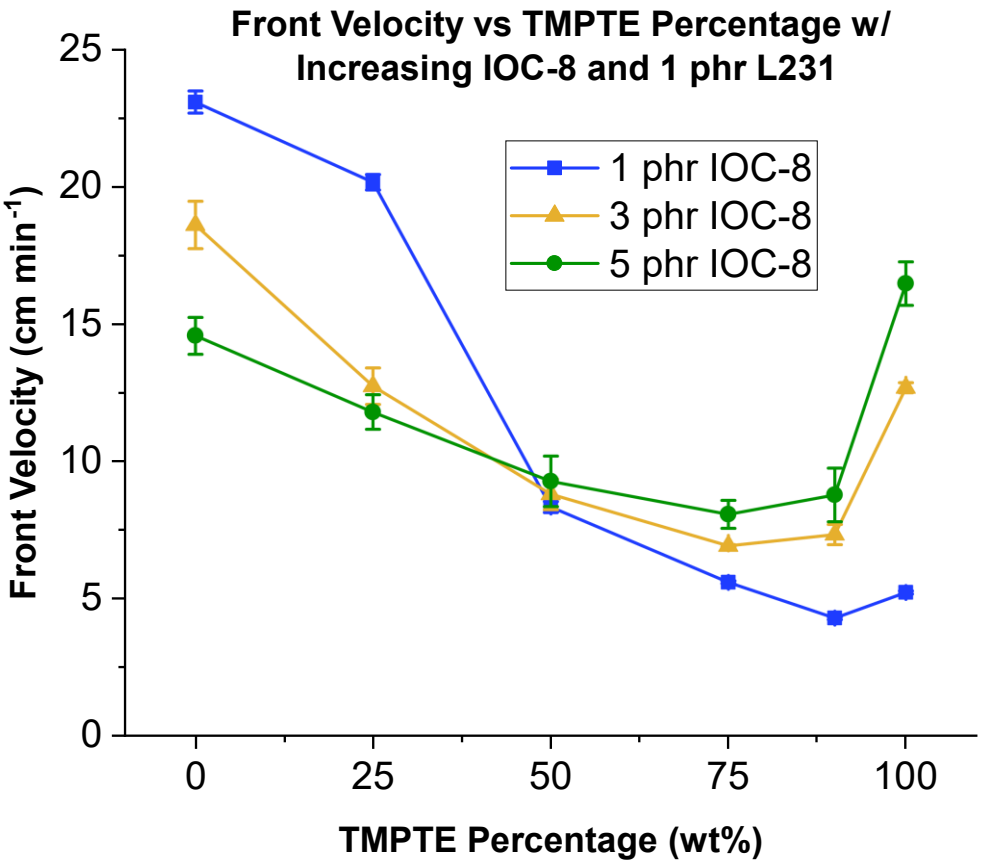

Figure 4.4. Front velocity versus increasing TMPTE to TMPTA ratio, with an increasing IOC-8 concentration.

Infrared spectroscopy (IR) was used in this study to try to examine the conversion of both the epoxy and acrylate components in the formulation for comparison with the results seen in the thesis by Dillman. [90] There are peaks unique to either the double bond in the acrylate or stretching of the epoxy ring. The epoxy peak at 755 cm^{-1} and acrylate peak at 1635 cm^{-1} were chosen to compare for conversion. However, every attempt to obtain an IR spectrum for polymers containing acrylate was unsuccessful. In each case, the spectrum for the polymer was much lower in intensity than the uncured spectrum, which can be seen by comparing the group of peaks associated with alkane C-H in Figure 4.5. The alkane peaks are much lower in intensity

for the cured spectrum, which should be largely unaffected as seen in previous IR studies in Chapter 2. This will affect the area of the peak and the calculation of the conversion. Many different adjustments were attempted to solve this, including grinding the polymer to a finer powder, increasing the resolution, increasing the scan rate, and using less sample on the diamond plate of the ATR. The issue with attempting another method such as KBr pellet is that the intensity could be affected which would change the calculated conversion.

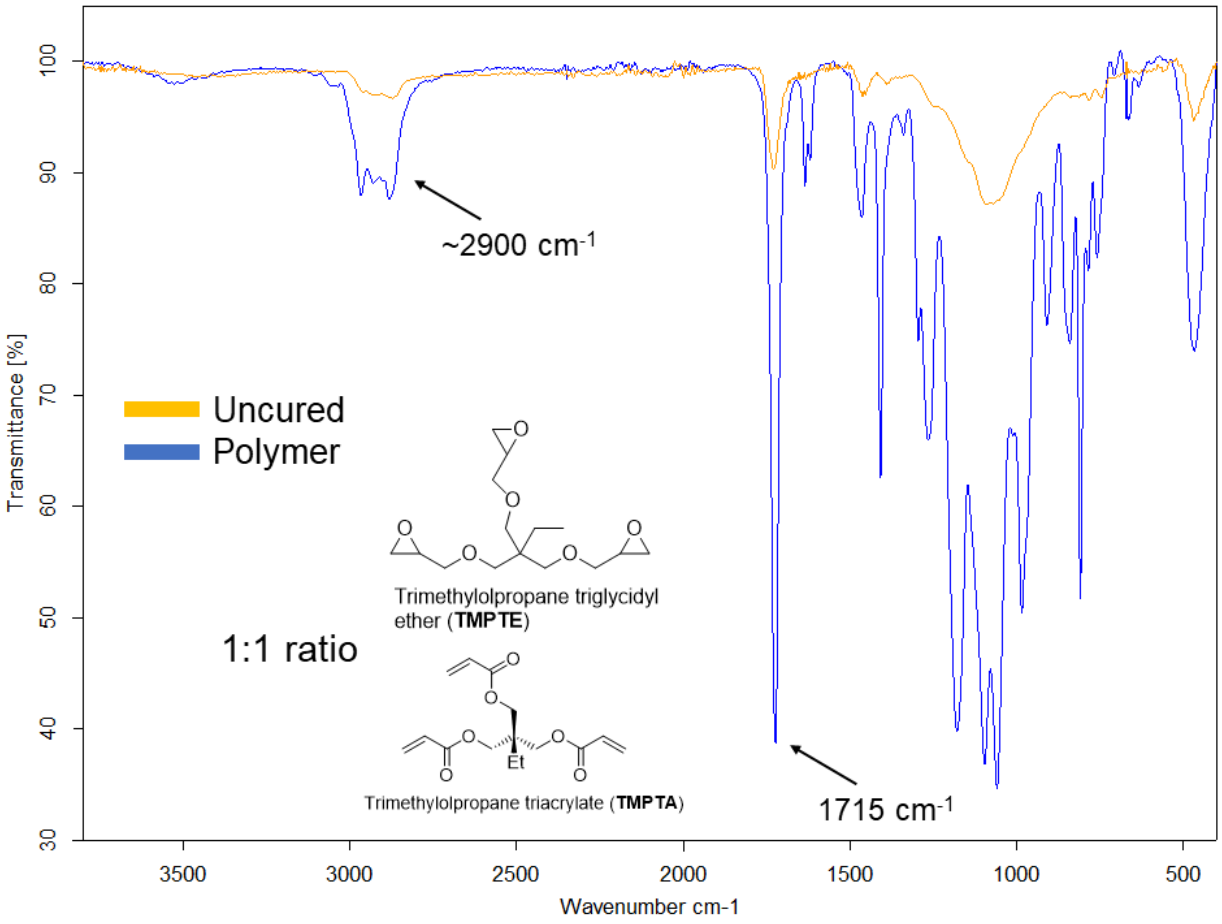

Figure 4.5. IR spectra of 50 wt% TMPTE/50 wt% TMPTA with 1 phr IOC-8 and 1 phr Luperox 231, with 10 wt% fumed silica. The orange spectrum is uncured while the blue spectrum is cured. The carbonyl peak at 1715 cm^{-1} and alkane peaks at ~2900 cm^{-1} is highlighted.

4.4. Frontal Polymerization of Hybrid Vinyl Ether/Acrylate Systems

Vinyl ethers involve more interesting phenomena than epoxies in hybrid formulations. They are known to be unable to homopolymerize radically. [60] This is because there is no potential for resonance stabilization of the radical, leading it to be a very unstable radical that undergoes many side reactions that can terminate polymerization. Compare this below to acrylates, which have resonance stabilization shown in Figure 4.6.

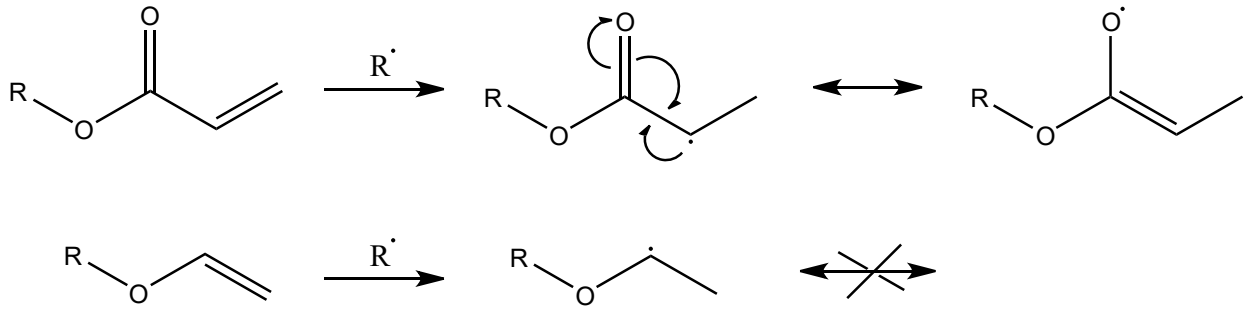

Figure 4.6. Resonance stabilization of radicals in acrylates versus vinyl ethers.

However, it has been proposed that vinyl ethers will copolymerize radically with acrylates, [60] though there are studies that indicate the contrary. [92, 93] Thus, there exists a need to investigate the resulting polymers of vinyl ether-acrylate blends produced via FP and the kinetic trends of these systems. Once again, the introduction of vinyl ethers, which produce typically rubbery, soft materials, can alter the mechanical properties of the acrylate.

Using a system of TEGDVE and TMPTA with 1 phr IOC-8 and 1 phr L231, with 10 wt% fumed silica, the front kinetics with increasing vinyl ether percentage were analyzed. It was found that a minimum in front velocity is present in this system at only 10 wt% TEGDVE, shown in Figure 4.7. This indicates that there are two separate polymerizations occurring rather than copolymerization.

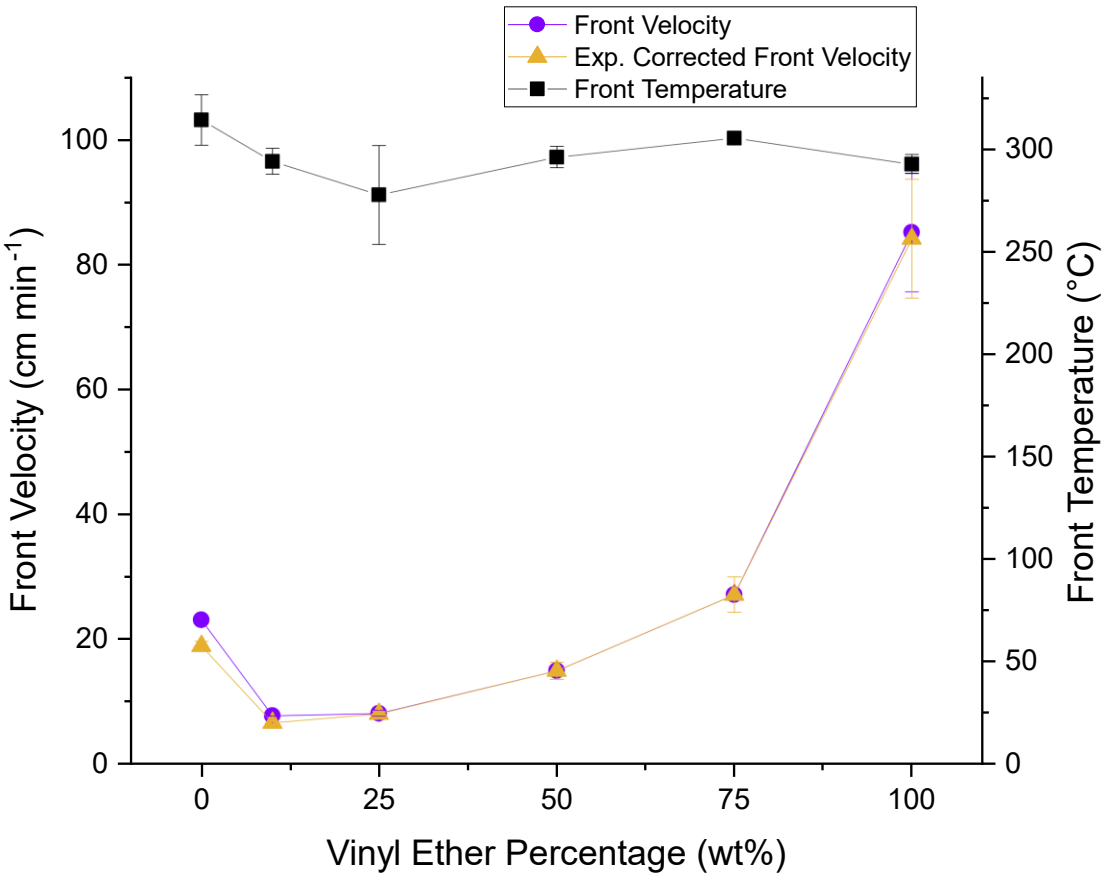

Figure 4.7. Front kinetics as a function of TEGDVE percentage in a TEGDVE/TMPTA system containing 1 phr IOC-8 and 1 phr L231 with 10 wt% fumed silica as a filler.

There are a few options to confirm the suspicions of simultaneous independent polymerizations considering previous indications of copolymerization. First, removal of IOC-8 in the system will show whether radical copolymerization is occurring between the vinyl ether and acrylate moieties. Using the same system but in absence of IOC-8 in Figure 4.8 shows a monotonic decrease in front velocity as the percentage of TEGDVE is increased, until a front is not supported at 100% TEGDVE. The monotonic decrease in front velocity indicates that TEGDVE is acting as an inert diluent in the system that cannot participate in the reaction. The decrease in

front temperature also supports this conclusion, given that the TEGDVE would be acting as a factor in heat loss.

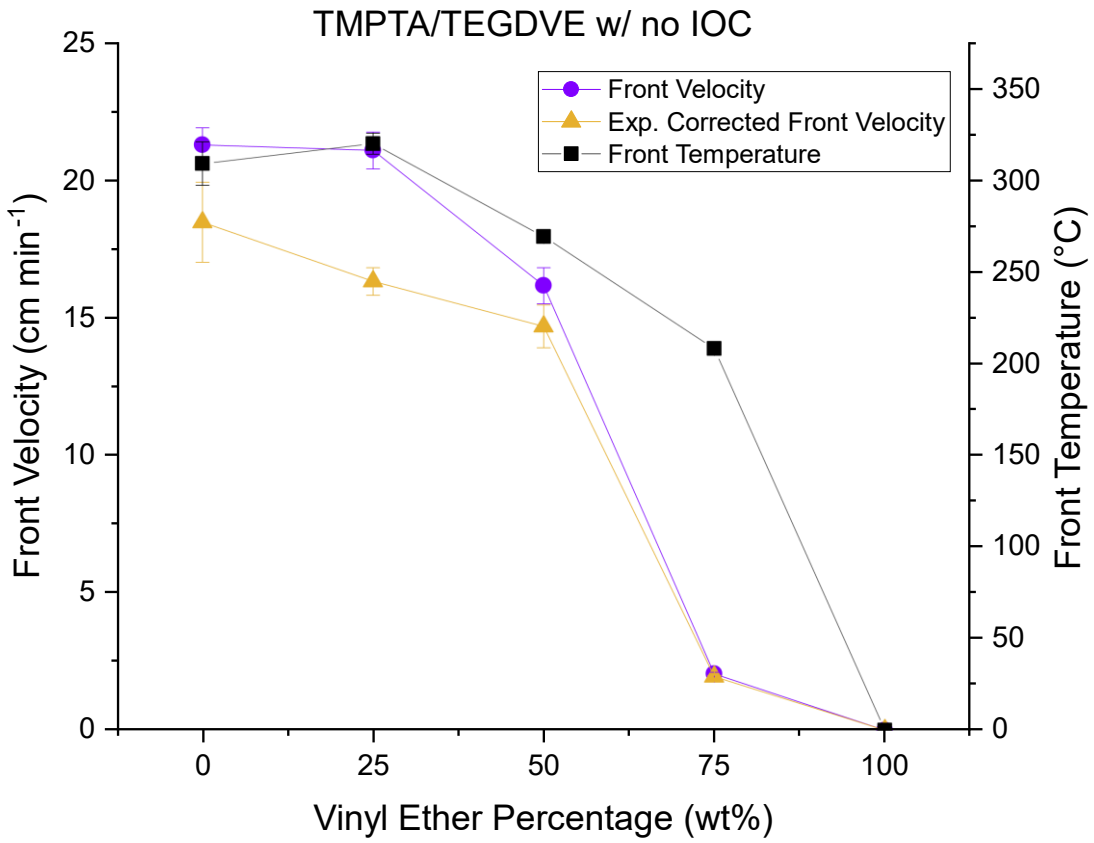

Figure 4.8. Front kinetics as a function of TEGDVE in a TEGDVE/TMPTA system with only 1 phr L231 and 10 wt% fumed silica added.

Comparing the front velocities of the TEGDVE/TMPTA system with and without IOC-8 results in the Figure 4.9 below. It can be seen there is a clear divergence in the trends as the vinyl ether percentage increases.

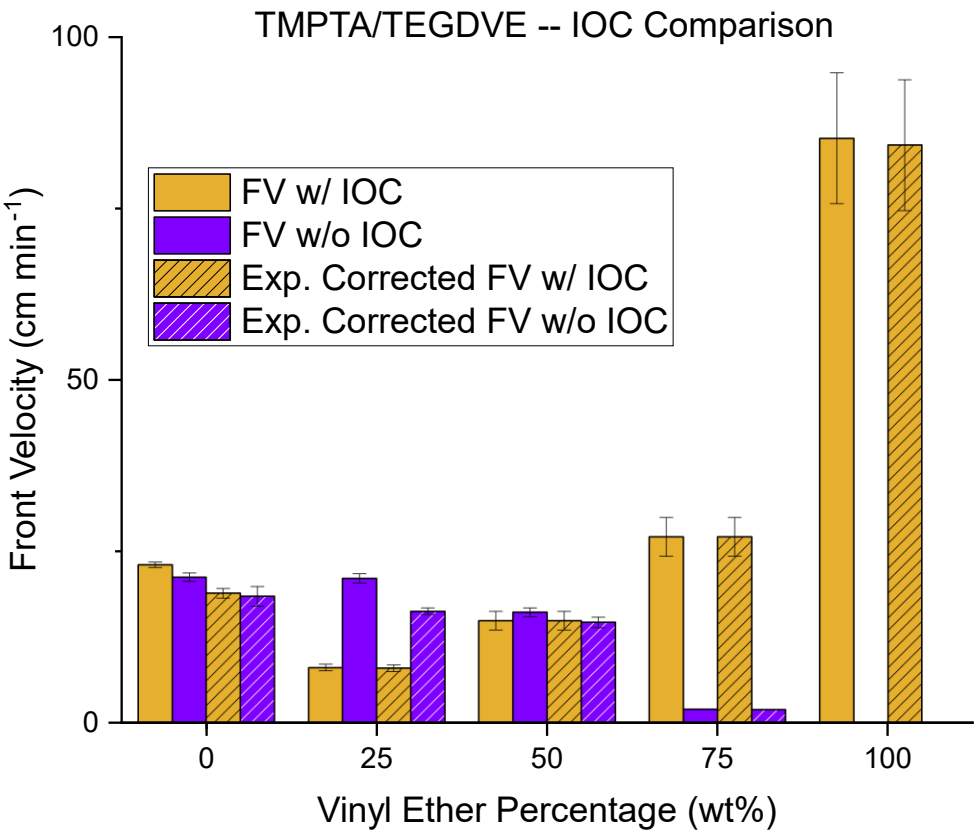

Figure 4.9. Comparison of front velocities and expansion corrected front velocities with a TEGDVE/TMPTA system with 10 wt% fumed silica and 1 phr L231 with and without IOC-8.

Unlike conversion determination with IR spectroscopy as shown for the epoxy-vinyl ether formulations, it is difficult for the vinyl ether-acrylate formulations. This is due to the overlap of the primary C=C peak from the acrylate and vinyl ether at 1635 cm^{-1} and 1617 cm^{-1}, respectively. Spectra comparing pure TMPTA, pure TEGDVE, and a 50 wt% TMPTA/50 wt% TEGDVE mixture are shown in Figure 4.10 with this peak annotated.

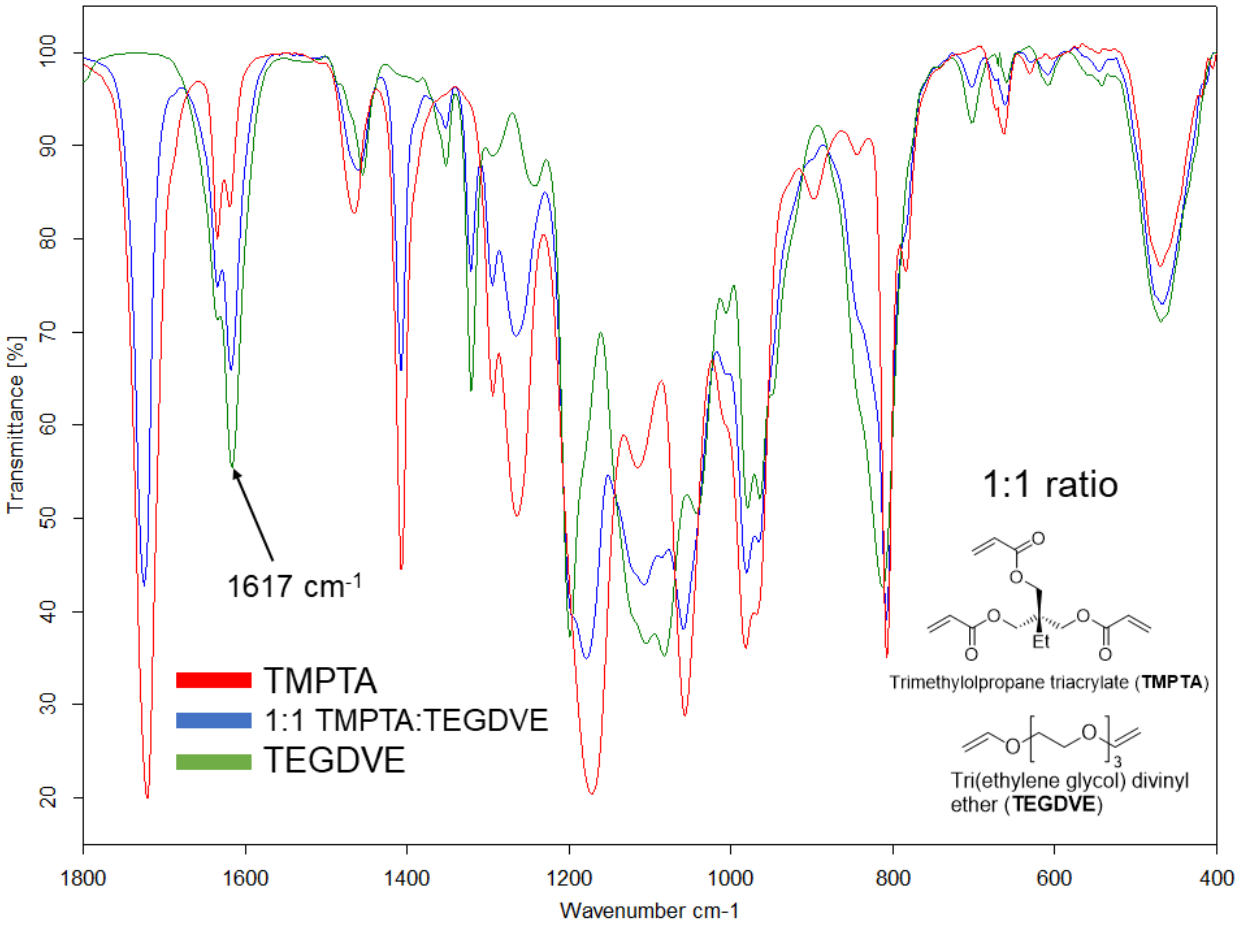

Figure 4.10. IR spectra from 1800 to 400 cm^{-1} of uncured TMPTA, TEGDVE, and 50 wt% TMPTA/50 wt% TEGDVE with 1 phr IOC-8 and 1 phr Luperox 231, with 10 wt% fumed silica. The overlapped C=C peak from TMPTA and TEGDVE at ~1617 cm^{-1} is highlighted.

Another experiment was to swap monomers out for propylene carbonate (PC), an inert solvent with a high boiling point. Using propylene carbonate can give insight into the behavior of the monomers with inert components mixed in. Initial studies were to determine the potential for front propagation when mixing with propylene carbonate and various combinations of initiators, shown in Table 4.1 as Y or N.

Table 4.1. Feasibility of front propagation with TMPTA, TEGDVE, or PC mixtures and pure monomers with a 1 phr IOC-8 and/or 1 phr L231 system. Mixtures were 50/50 by weight.

Binary Systems	TMPTA	TMPTA/PC	TMPTA/TEGDVE	PC/TEGDVE	TEGDVE
IOC-8	N	N	N	Y	Y
L231	Y	Y	Y	N	N
Both	Y	Y	Y	Y	Y

Table 4.2 indicates many expected results, such as the inability of TEGDVE to polymerize via free-radicals or TMPTA to polymerize via IOC-8. Interestingly, it is found that 50/50 TEGDVE/PC with IOC-8 and no L231 will support a front, while 50/50 TMPTA/TEGDVE will not. This implies that the PC is acting as an inert diluent while the TMPTA is actively inhibiting the cationic polymerization of TEGDVE. The front velocities of 100% TMPTA with and without IOC-8 are similar, which does not explain this phenomenon. On the contrary, 50/50 TMPTA/TEGDVE with only L231, the initiator responsible for free-radical FP, will support a front alongside a 50/50 TMPTA/PC system containing only L231. Analyzing the front kinetics with PC mixtures in Figure 4.11 shows that the front velocity is much lower with PC added in place of either monomer. This could simply be due to the independent polymerizations occurring and removal of a monomer that contributes to the overall front speed. The front velocity with TMPTA/PC is also half that of TEGDVE/PC, which can also be explained with the higher reactivity of TEGDVE or perhaps a difference in heat capacity of the two monomers. There is a negligible difference in front velocity for a system with TMPTA/PC and 1 phr L231, with and without IOC-8: 1.63 cm min^{-1} without IOC-8 and 1.50 cm min^{-1} with IOC-8 similar to what is seen with the undiluted system.

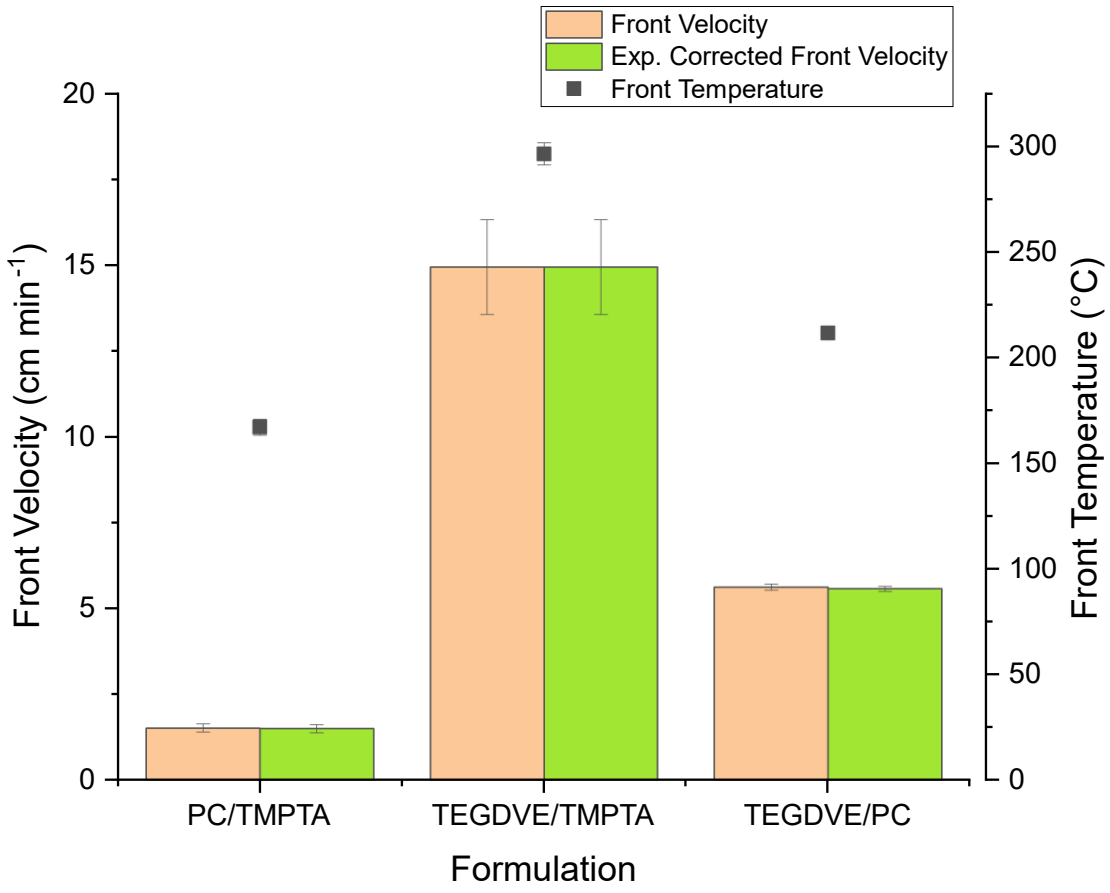

Figure 4.11. Front kinetics of formulations with 50/50 mixtures of the indicated components, along with 1 phr IOC-8 and 1 phr L231 with 10 wt% fumed silica.

4.5. Determination of Copolymerization Gravimetrically Through Generation and Dissolution of Linear and Crosslinked Networks

It was previously stated that due to the appearance of the front velocity dependence on ratio of monomers that copolymerization is not occurring with the hybrid systems, but rather an interpenetrating polymer network of homopolymers is forming. As another method to try and confirm that copolymerization is not present in the case of either acrylate-epoxy or acrylate-vinyl ether blends, combinations of monofunctional and higher functionality monomers were frontally polymerized. With these 1:1 mixtures, linear polymers are formed from the monofunctional monomers that could be dissolved from the non-dissolvable crosslinked network formed from

the higher functionality monomer. If copolymerization were to happen, it would be expected that very little to no weight loss would occur with dissolution as the network would be crosslinked. Conversely, approximately 50% of the weight should be lost from the polymer in the case of two independent polymerizations. The monomers used in this study are shown in Figure 4.12 below.

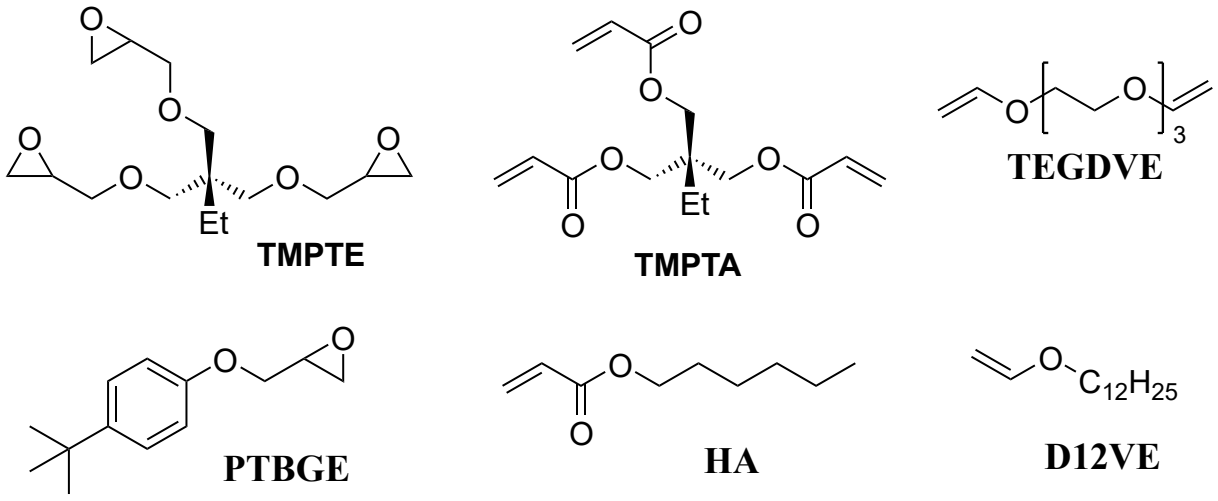

Figure 4.12. Structures of high functionality and monofunctional epoxies, acrylates, and vinyl ethers used in gravimetric dissolution study.

The monomers were mixed 1:1 with 1 phr IOC-8 and 1 phr Luperox 231. After adding fumed silica, they were frontally polymerized similar to previous methods, and a piece from the center of 3 to 4 cm length was removed. The polymer was placed into DCM and soaked for 4 hours, then dried overnight. Controls of only TMPTE, TMPTA, or TEGDVE were also made to make sure that weight was not lost from the crosslinked networks due to impurities or unreacted starting material dissolving. To calculate weight loss, Equation 4.1 was used.

$$\text{Weight loss \%} = [(\text{Starting weight} - \text{Final weight}) \times \text{Starting weight}^{-1}] \times 100 \qquad \text{Equation 4.1}$$

The gravimetric results of weights are shown below in Table 4.2. All the vinyl ether containing formulations resulted in solutions that were dark brown and dark yellow. The rest of the acrylate

and epoxy based formulations gave colorless solutions. Pictures of polymers in DCM are shown in Figure 4.13, where the color of solutions is visible.

Figure 4.13. Hybrid acrylate and epoxy or vinyl ether polymers of mixed functionality produced by FP submerged in DCM to dissolve linear components. Solutions shown are a) TMPTE/HA; b) TMPTA/PTBGE; c) TEGDVE/HA; d) TMPTA/D12VE.

Overall, the polymers did not lose 50% weight but they still all lost significant amounts after sitting in the DCM. The <50% weight loss could be a kinetic effect where more time is needed to completely dissolve out the linear polymer. This might be related to chains being entangled in the crosslinked network. Alternatively, perhaps there is a very small portion of the monomer that is copolymerized. TMPTE and TMPTA swelled with DCM resulting in a negative weight loss, which is a much different result from the formulations that contained either monomer with monofunctional monomers. On the other hand, TEGDVE lost 10.5% weight. Given the yellow

color of the solution after polymerization versus colorless TMPTA and TMPTE solutions, this could be unreacted starting material. This is still less than the 35.8% loss from the TEGDVE/HA formulation, which does not confirm but indicates that it is possible that linear polymer was dissolved.

Table 4.2. Results from dissolution of polymer produced from monofunctional and high functionality monomers.

Formulation	Initial Weight of Polymer (g)	Final Weight of Polymer (g)	Weight Loss (wt%)
TMPTE/HA	2.63	2.13	19.0
TMPTA/PTBGE	2.10	1.34	36.2
TEGDVE/HA	2.43	1.56	35.8
TMPTA/D12VE	3.46	2.31	33.2
TMPTE	4.35	4.48	-3.0
TMPTA	3.49	3.72	-6.6
TEGDVE	2.48	2.22	10.5

IR was used to analyze the solution and the polymer generated for evidence of peaks attributed to either monomer. The distinguishing feature that can be used to identify compounds in the solution and polymer is the peak at ~1730 cm^{-1}, which is the carbonyl peak that is only present in acrylate. Unfortunately, it seems that in the IR spectra of every hybrid mixture, this peak is present. This means that there is some quantity of acrylate present in both the solution and polymer. For the formulations having TMPTE or TEGDVE in Figures 4.14 and 4.15, this could indicate either some degree of acrylate copolymerization or inadequate dissolution of the linear polymer.

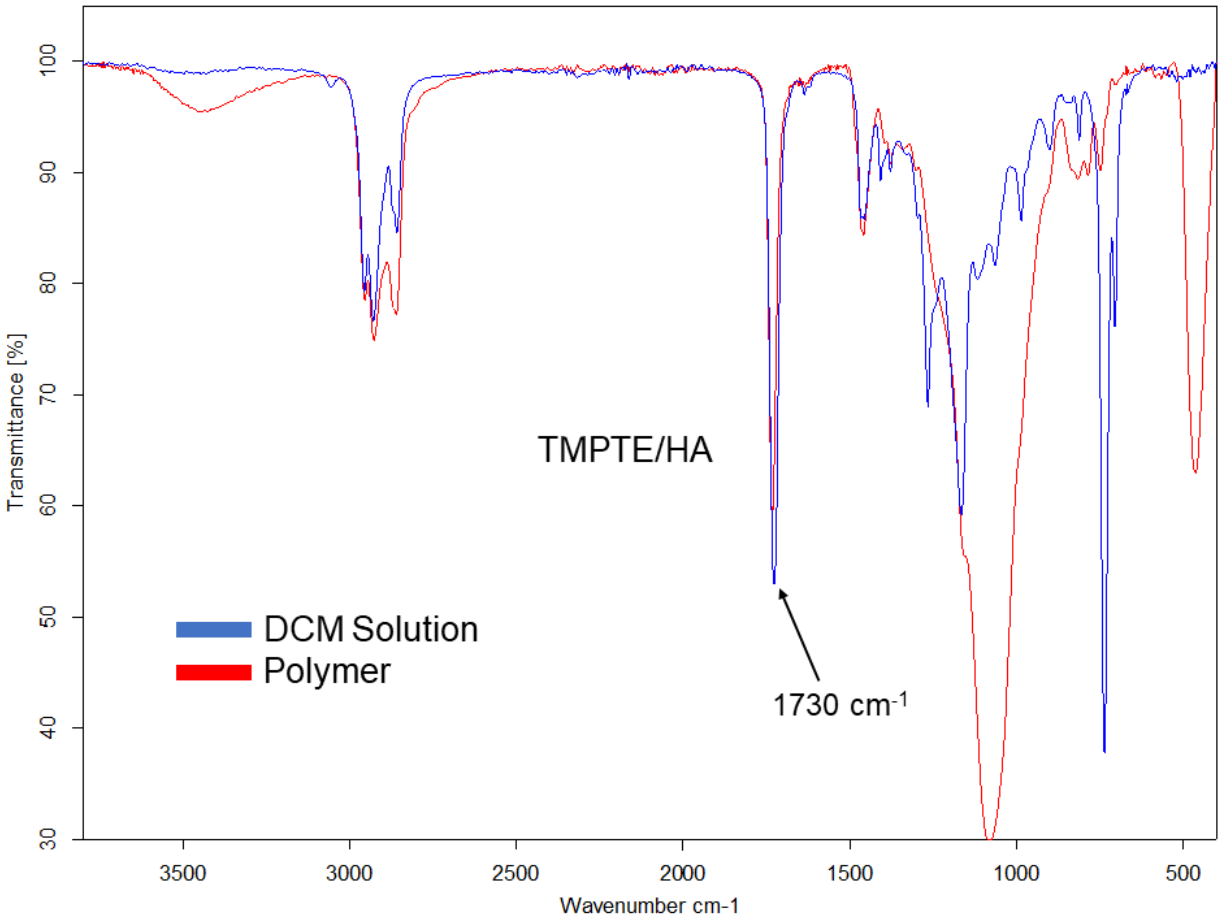

Figure 4.14. IR spectra of 50 wt% TMPTE/50 wt% HA with 1 phr IOC-8 and 1 phr Luperox 231, with 10 wt% fumed silica. The C=O peak from the acrylate functional group at ~1730 cm^{-1} is highlighted.

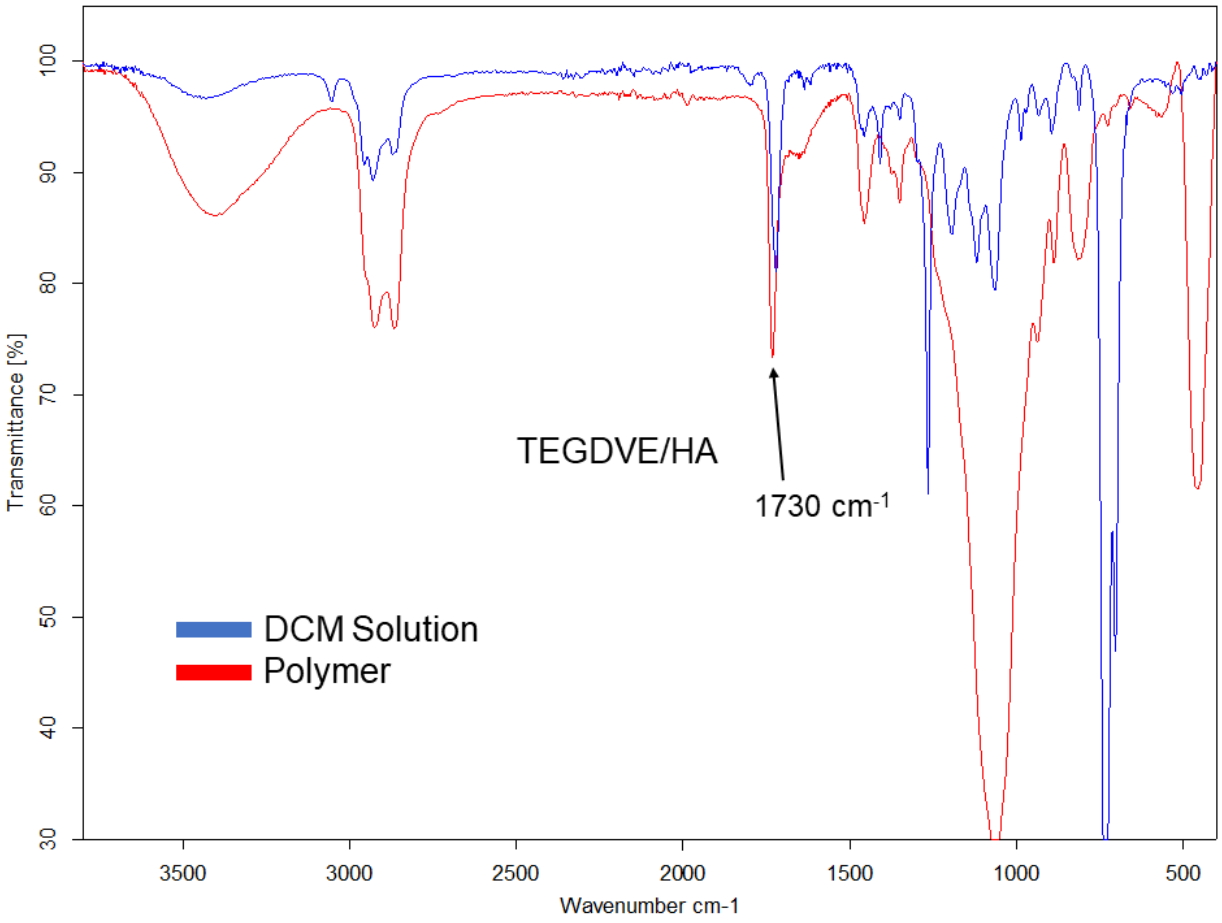

Figure 4.15. IR spectra of 50 wt% TEGDVE/50 wt% HA with 1 phr IOC-8 and 1 phr Luperox 231, with 10 wt% fumed silica. The C=O peak from the acrylate functional group at ~1730 cm^{-1} is highlighted.

For the formulations of TMPTA, the presence of the carbonyl in the solution would mean that unreacted starting material is dissolved into the DCM solution. The spectra of formulations containing TMPTA are shown below, in Figure 4.16 and Figure 4.17. Once again, the overlap in vinyl ether and acrylate peaks makes identification difficult in the spectra shown for TMPTA/D12VE. For the spectra of TMPTA/PTBGE, there are many peaks in the range associated with epoxy rings, 750 cm^{-1} to 950 cm^{-1}, which would only confirm that PTBGE is present in the DCM solution.

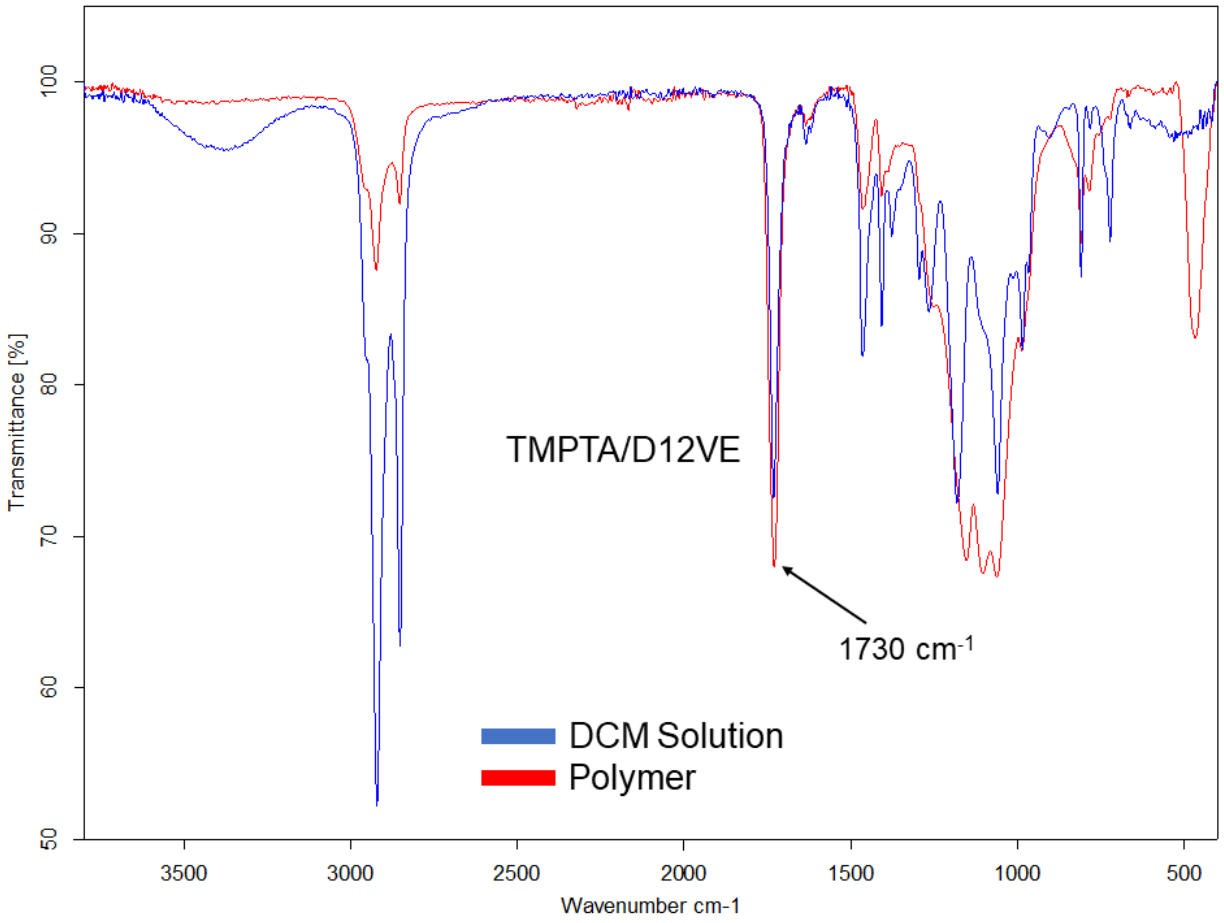

Figure 4.16. IR spectra of 50 wt% TMPTA/50 wt% D12VE with 1 phr IOC-8 and 1 phr Luperox 231, with 10 wt% fumed silica. The C=O peak from the acrylate functional group at ~1730 cm^{-1} is highlighted.

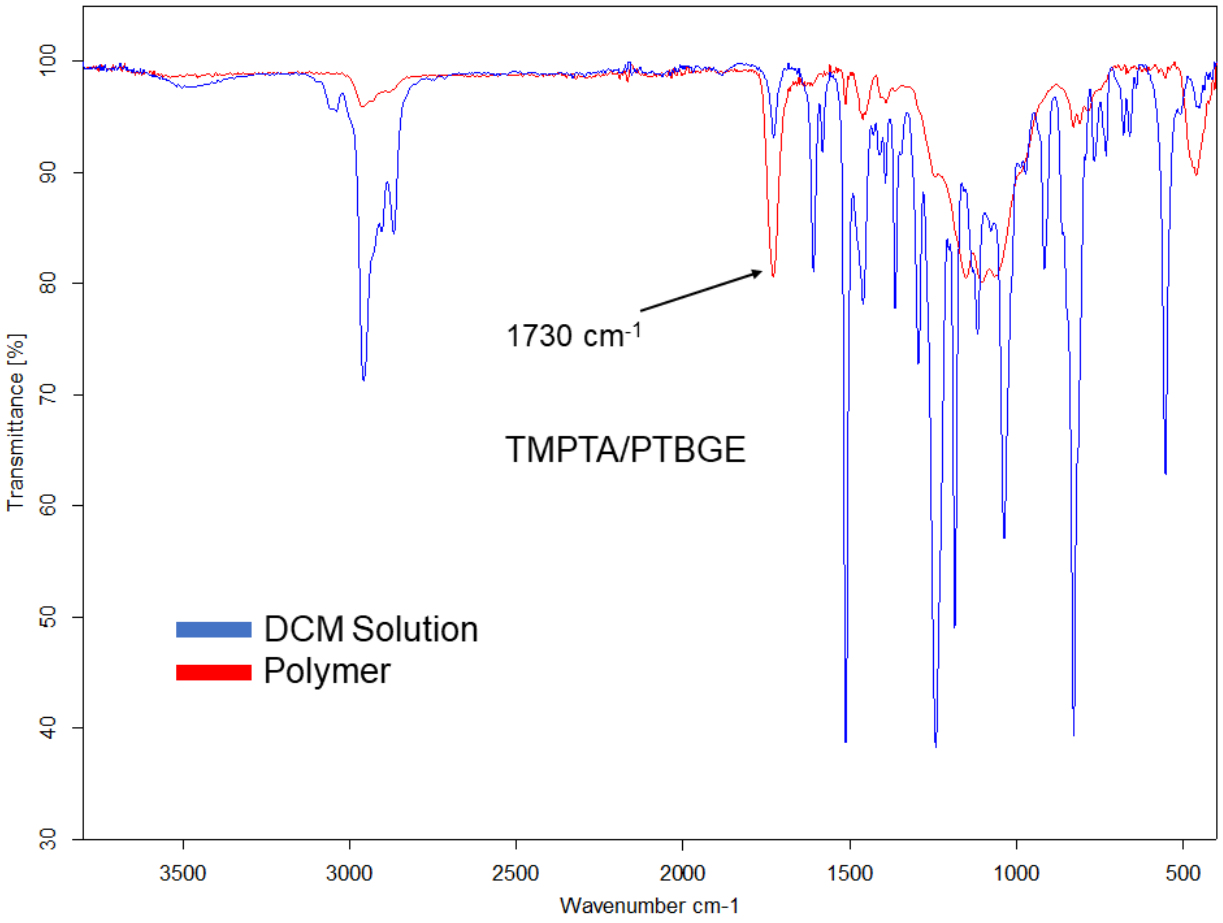

Figure 4.17. IR spectra of 50 wt% TMPTA/50 wt% PTBGE with 1 phr IOC-8 and 1 phr Luperox 231, with 10 wt% fumed silica. The C=O peak from the acrylate functional group at ~1730 cm^{-1} is highlighted.

With the results from the IR data, the conclusion of linear polymer dissolved into the DCM is uncertain. As mentioned before, it could be possible that small amounts of linear polymer did not dissolve, or that unreacted starting material is in solution. The similarity in structure of the HA to TMPTE and TEGDVE, all three being aliphatic in structure, does not aid in the identification of each monomer. Another possibility is that acetone formation from the decomposition of the Luperox 231 is present in the 1730 cm^{-1} peak, though the peak has a high intensity in all but the spectra of TMPTA/PTBGE.

4.6. Conclusions and Outlook

Hybrid systems allow for adjustment of advantageous properties of each monomer while balancing the reactivity of each system. It was shown through analysis of front kinetics that epoxy and vinyl ether will not copolymerize with acrylates during frontal polymerization. A minimum in front velocity exists as the ratio of epoxy or vinyl ether to acrylate is increased. There was an attempt at discerning copolymerization through dissolution of a linear polymer from a crosslinked polymer, which was unsuccessful. This was partly due to the chosen monomers being similar in structure. With monomers that have unique structural features, this method could be used in combination with IR spectroscopy. More detailed study needs to be conducted into analyzing the conversion of these systems, which was difficult due to issues with IR spectroscopy of acrylates. Knowing the kinetics of hybrid systems allows for more careful optimization of resins. There are reports that have looked at photopolymerization of monomers containing both acrylate and epoxy functionality to generate grafted polymer networks that are both entangled and covalently bonded.[94] These monomers could be advantageous to add in binary FP systems to enhance strength of the polymer and potentially affect the kinetics of front propagation.

CHAPTER 5. EFFECTS OF CLAYS AND OTHER FILLERS IN RADICAL-INDUCED CATIONIC FRONTAL POLYMERIZATION

5.1. Introduction to Fillers and Frontal Polymerization

A phenomenon that can quench a propagating front is convection. Buoyancy-driven convection is always present in fronts carried out horizontally due to the large gradients of temperature and concentration. [19] An increase of viscosity can suppress the effects of convection. [8, 19, 27, 95-98] The addition of fumed silica is a simple way to raise the viscosity. Fumed silica has been applied to both free-radically and cationically-curing resins to stop convection. [22, 99] The addition of fillers can suppress convection, enhance mechanical properties, modify rheological properties, and reduce cost through a reduction of resin needed. [100, 101]

Gary et al. have previously studied the effects on acrylate free-radical FP. [22] They found that kaolin, talc, and calcium carbonate behaved similarly and were chemically inert, while bentonite reduced the front velocity due to both a lower thermal diffusivity and presence of water contributing to heat loss. In addition, it was found that acid-activated clays such as montmorillonite K10 inhibit free-radical FP.

As mentioned before, the minimum requirement for any FP process, irrespective of the mechanism of polymerization, is that heat generation sufficiently exceeds heat loss to both the system and the surroundings. [19] One source of heat loss can be added fillers, which act as a heat sink. [86] Evaporation of water in swelling clays during FP absorbs heat generated from the system, also contributing to heat loss. Drying clays can eliminate the water present and increase front

---

This chapter was previously published as B. R. Groce, E. E. Lane, D. P. Gary, D. T. Ngo, D. T. Ngo, F. Shaon, et al. Kinetic and Chemical Effects of Clays and Other Fillers in the Preparation of Epoxy–Vinyl Ether Composites Using Radical-Induced Cationic Frontal Polymerization, ACS Applied Materials & Interfaces, 2023, 15, 19403-19413. Reprinted with permission from ACS.

velocity. [22] However, removing water from clays opens acidic sites that can act as radical inhibitors or catalyze cationic polymerizations. [102, 103] Two forms of bentonite (Na-bentonite and Ca-bentonite) were found by Gary et al. to affect the front velocity differently through this phenomenon, with the Ca-bentonite likely being more acidic and resulting in a lower front velocity. [22]

For RICFP, there have been few studies that examined the addition of fillers. Bomze et al. looked at the addition of mica to prove that RICFP is applicable in UV-initiated fronts with filler added. [54] One of the problems with adding filler to systems is that fillers reduce UV light penetration. [104-106] Bomze et al. found that up to 15 phr of mica could be added to BADGE resins with sensitizer added and still support a front. The front velocity did decrease with increasing loadings of mica, explained by the heat absorbed by the filler and the decreased fraction of monomer present. Thermal initiation allowed FP of the epoxy with 15 phr mica and no sensitizer. Klikovits et al. saw reductions in front velocity as SiO_2 nanopowder was added to BADGE, up to a 10% reduction with 3 phr SiO_2. [69] They attributed the inhibition to the low thermal conductivity of the filler, while the insulating properties of the SiO_2 made initiation of the front quicker. Finally, Tran et al. carried out large studies of fillers with varying thermal properties. [38] Using BADGE resins with reactive diluent added, they successfully used RICFP to cure polymers with high volume percentages, including 74 vol% glass microspheres. They saw that adding thermally conductive fillers, such as aluminum, short carbon fibers, and graphite, resulted in a smaller front velocity reduction than mica, a mineral which is less conductive. These results are similar what has been seen for free-radical FP, where milled carbon fibers are shown to increase front velocity as loading increases. [22] Adding graphite and aluminum to acrylate systems has been shown to reduce the front velocity due to radical scavenging. [22]

With the mechanistic differences between RICFP and free-radical FP, plus the desire to develop practical materials using RICFP, there exists a need to explore more effects of clays on front reactivity with cationic systems. In addition to the differences in thermal characteristics between clays, there are variations in chemistries of clays that could affect propagating cations but not free-radical polymerization. For this study, a monomer system of trimethylolpropane triglycidyl ether and tri(ethylene glycol) divinyl ether was used. Vinyl ethers have been shown to significantly increase front velocity in RICFP systems and were chosen for this purpose. [99] Using fumed silica as an inert viscosity enhancer allowed controlled amounts of clays to be added to systems. Zoltek® milled carbon fibers and pine wood flour were used to study the effect of differing thermal properties. Drying the clays to increase Lewis acidity and addition of acid-activated clays were investigated to see any possible chemical effects with the RICFP mechanism.

5.2. Materials and Methods of RICFP with Clays

5.2.1. Materials

Trimethylolpropane triglycidyl ether (TMPTE) and tri(ethylene glycol) divinyl ether (TEGDVE) were the monomers used, and 1,1-bis(tert-butylperoxy)-3,3,5-trimethylcyclohexane (Luperox® 231) with (4-(octyloxy)phenyl)(phenyl)iodonium hexafluorostibate(V) (IOC-8) was the initiator system. All chemicals were used as received. Chemical structures of the components used in the resin are shown in Figure 5.1. The clay fillers studied were talc, Hectalite® 200 (hectorite), bentonite HPM-20 (Na-bentonite), Bentolite L10 (Ca-bentonite), and Polygloss® 90 (kaolin). Hubercarb® Q3 (calcium carbonate) was also studied. Fulcat® 435 and montmorillonite K10 were studied as acid-treated clay fillers. Zoltek® PX35 milled carbon fiber and wood flour (60 mesh pine flour) were also used. For studies of surface area and aspect ratio, Nyad® G, 10 ES

Wollastocoat®, Nyad® 1215 from Imerys Performance Additives and Fibertec 520S, Microglass 7204, Microglass 9114 and FRM provided by Fibertec, Inc. were used, along with samples of untreated wollastonite from Imerys Performance Additives.

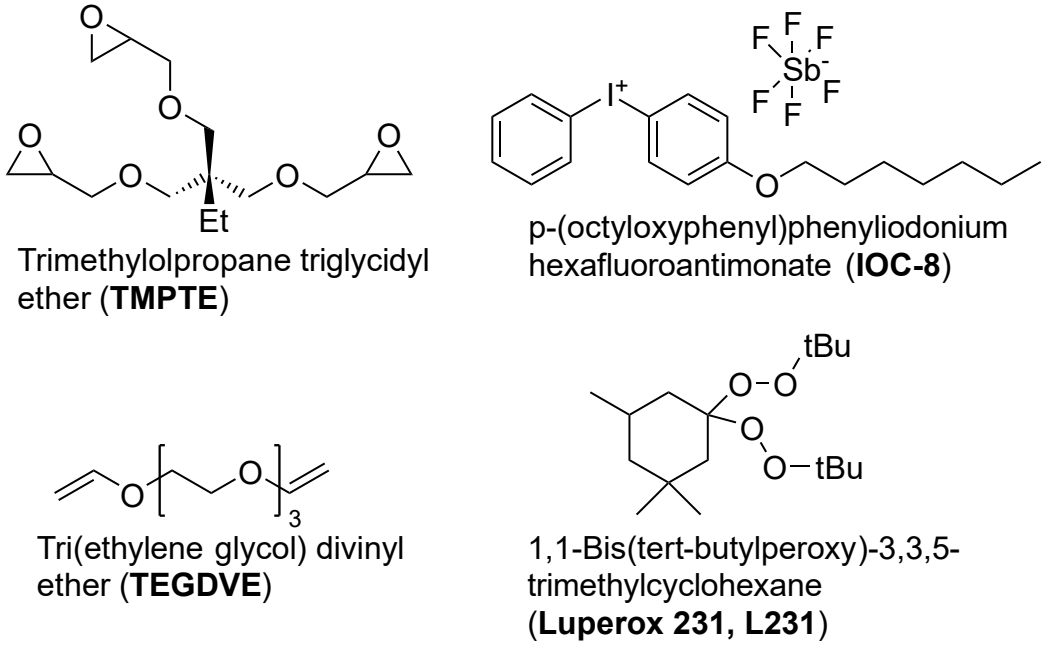

Figure 5.1. Chemical structures of monomers and initiators used in this study.

5.2.2. Formulation Preparation and Frontal Polymerization

Typical formulations consisted of 75 wt% TMPTE and 25 wt% TEGDVE, along with 1 phr (parts per hundred resin) of IOC-8 and 1 phr of Luperox® 231, unless otherwise indicated. IOC-8 was first mixed with TMPTE and sonicated for approximately 15 minutes to fully dissolve the IOC-8, before addition of TEGDVE and Luperox® 231. The solution was then mixed using a vortex mixer for approximately 30 seconds to ensure homogeneity.

To prepare samples for FP, aliquots were taken from a stock formulation solution and typically 5 wt% fumed silica (Aerosil® 200, Evonik Industries (Parsippany, NJ)) and 30 wt% of the other filler were added to form a moldable putty when hand mixed. Other separate filler loadings were hand mixed with the appropriate amount of filler added as described. Where

specified, some formulations were mixed using a FlackTek DAC 515-200 SE speed mixer. The putty was loaded into a wooden mold (13.5 cm × 2 cm × 0.6 cm) lined with wax paper for easy removal of the polymer. A type K thermocouple connected to a handheld thermometer device (Benetech® GM1312, purchased from Amazon) was then placed 2 cm into the length of the sample and approximately halfway into the sample depth to record the front temperature. A soldering iron heated to approximately 200 ℃ (confirmed with an infrared thermometer) was used to initiate the fronts by making brief contact with the sample. The fronts were tracked using a video camera placed directly above the sample. Front velocity was calculated from the slope of front position versus time. The front velocity after expansion, shown in the manuscript as "Exp. Corrected Front Velocity" was calculated by first taking the initial length of the resin in the mold and dividing by the final length of the cured material. The front velocity from the slope of front position versus time was then multiplied by this factor to result in the "Exp. Corrected Front Velocity." The mold was cooled to room temperature prior to subsequent experiments. Triplicate experiments from the same stock were performed for each formulation.

5.2.3. Drying Clays

To dry clays, the clays were placed in an oven containing desiccant at 200℃ for 3 hours before being removed and added to samples once cooled to approximately 30℃ to prevent spontaneous polymerization. The water loss percentage was measured both gravimetrically with a lab balance after the 3 hour heating period and using a TA Instruments TGA 550 thermogravimetric analyzer and a Hi-Res™ heating method.

5.2.4. Instrumental Characterization of Resin and Polymer

Uncured sample viscosity was determined using a TA Discovery HR-2 rheometer. Initially, the plate height was set to 550 μm, excess sample was removed, and then reduced to 500 μm to

ensure total probe coverage. The viscosity (Pa·s) measurements were performed at low (1 Hz) and high (10 Hz) shear rates. The first step was at 1 Hz for 60 s, followed by an increase to 10 Hz for 60 s, and returning to 1 Hz for 60 s. Recovery percent was calculated by comparing the viscosities of the first (1Hz) and last steps (1Hz) for all formulations. Three replicates were evaluated for each formulation and the data are presented as the mean ± SD.

Samples of the cured composites for scanning electron microscopy (SEM) and energy dispersive X-ray spectroscopy (EDS) to determine filler distribution were analyzed with a Thermo Scientific Helios G4 PFIB CXe electron microscope. A TA Instruments DSC Q100 differential scanning calorimeter (DSC) was used to determine the glass transition temperature of the cured composite, using a scan rate of 10 ℃ min^{-1} from -40 ℃ to 150 ℃ and 3 scan cycles. A sample size of approximately 5.5 – 9.5 mg was used.

Flexural testing was performed on an Instron 5969 universal testing machine. Samples for testing were cut from sheets perpendicular to the direction of front propagation with sizes according to ASTM D790. Crosshead speed was calculated based on the ASTM standard and the thickness and width of each sample. Support span length was set from 78 – 85 mm based upon the sample length.

5.3. Comparison of Clays

Clays were first tested for their effects on front kinetics in RICFP systems. Talc, hectorite, Na-bentonite, Ca-bentonite, kaolin, and calcium carbonate were added in 30 phr amounts to formulations containing the resin system along with 5 phr fumed silica as an additive to increase viscosity and suppress convection. Formulations with clays added are shown in Figure 5.2 placed in molds with propagating fronts in each sample. The differences in color can be seen in Figure 5.2.

Figure 5.2. Resin mixtures with clay fillers added and placed in molds, with an actively propagating front, except in the case of Na-bentonite, which would not support a front. The actively propagating front is seen to have a darker color than the uncured resin.

It was found that all clay fillers tested supported a front except Na-bentonite. Compared to a control containing only 5 phr fumed silica, all clays reduced the front velocity of the system shown in Figure 5.3. Calcium carbonate, while not a clay, was used for comparison, and it also reduced the front velocity. These reductions were partially due to heat absorbed by the filler.

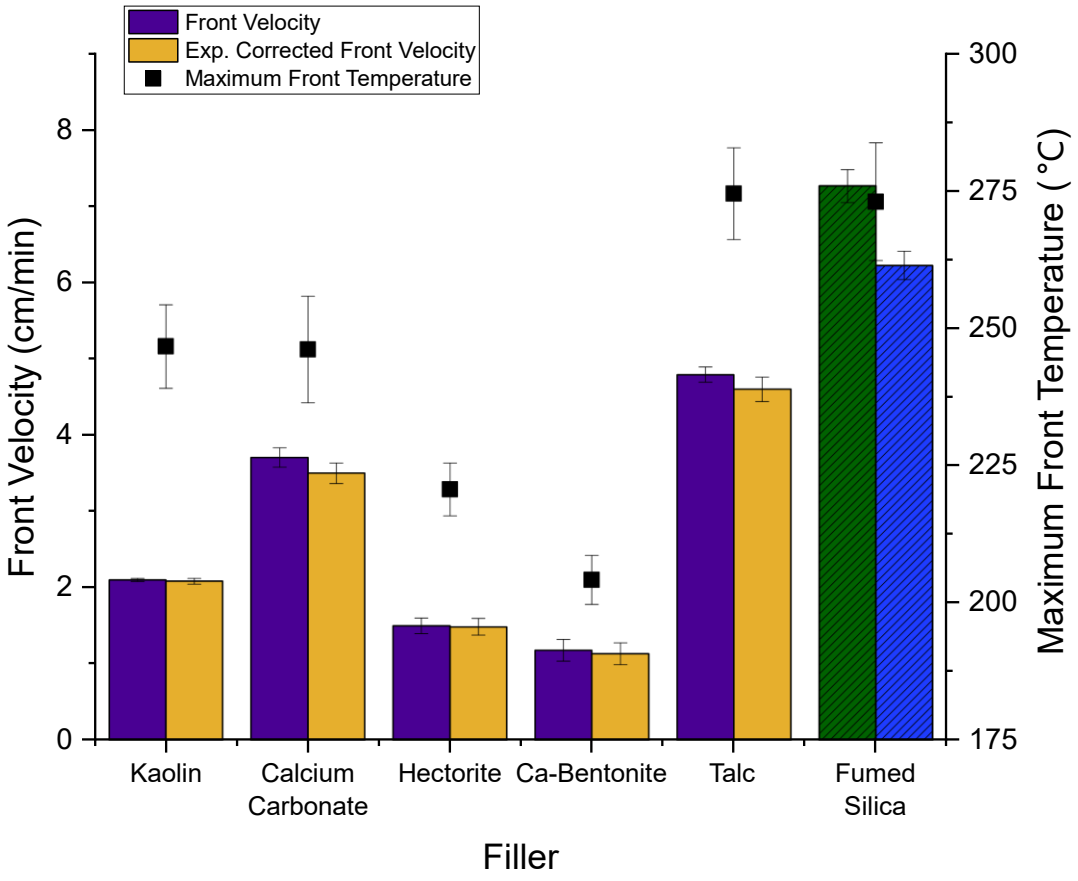

Figure 5.3. Comparison of front velocities and maximum front temperatures for four clays and calcium carbonate tested with RICFP.

The clays all showed differing effects on front velocity. Ca-bentonite was found to reduce the front velocity and front temperature the most, while talc resulted in the least deviation from the control sample for velocity and temperature. Examining talc and kaolin shows a near 230% difference in front velocity, while the thermal diffusivities, heat capacities and thermal conductivities of the two clays are similar as shown in Table 5.1. The thermal properties for hectorite are not available, though it is proposed that they are similar to the thermal properties of bentonite, as both clays are smectites. Likewise, calcium carbonate is known to have a thermal diffusivity an order of magnitude higher than talc or kaolin, yet the front velocity found lies within the values observed for kaolin and talc.

It is likely that the differences in front velocity and temperature among the clays are due to chemical effects, such as interaction of the clays with propagating cations or the superacid, or water content rather than thermal properties. Some clays, such as kaolinites, carry a net negative charge that could be a source of inhibition for RICFP. [107, 108] It has been reported that cationic dyes can adsorb to kaolinites, which supports inhibitory interactions with superacid cations. [109] Adsorption is shown to be related to high cation exchange capacity or surface area. Cationic exchange capacity is a measurement of the number of cations available to exchange with other cationic species in the environment onto a clay's surface. [110] Each clay possesses a different cationic exchange capacity. If protons of the superacid were to exchange with ions present in the structure of the clay or adsorb onto the clay, this could give rise to inhibitory effects. The structures and compositions of most clays are complicated and occur as sheets, but most clays have hydroxyl sites which could also be contributing to chain transfer and front velocity decrease. [110]

Table 5.1. Physical and thermal properties of fillers used in this study.

	Density ($g\ cm^{-3}$)	Heat Capacity ($J\ g^{-1}\ K^{-1}$)	Conductivity ($W\ cm^{-1}\ K^{-1}$)	Thermal Diffusivity ($cm^2\ s^{-1}$)
Kaolin[a, 22]	2.6	0.92	2.0×10^{-2}	8.2×10^{-3}
Calcium carbonate[a, 22]	2.7	0.87	2.5×10^{-2}	1.1×10^{-2}
Talc[a, 22]	2.8	0.87	2.1×10^{-2}	8.6×10^{-3}
Bentonite[a, 22]	2.6	1.30	1.0×10^{-2} 1.3×10^{-2}	3.0×10^{-3} – 3.9×10^{-3}
Wood flour [111]	0.4 – 1.35	1.75	0.25×10^{-2}	3.6×10^{-3} – 1.1×10^{-3}
Milled carbon fiber[a, 22]	1.8	0.60	6.4×10^{-2}	5.9×10^{-2}
Fumed silica[a, 22]	2.2	0.79	1.5×10^{-4}	8.6×10^{-5}

[a]Provided by manufacturer

The results shown in this work are contrary to previous studies of clays added to free-radical FP systems, where calcium carbonate, kaolin, and talc all behaved similarly. Calcium carbonate was initially hypothesized to not support FP due to its basic character. This was proven otherwise and attributed to the calcium carbonate being mixed into the system as a suspension and not dissolved. Therefore, the basic character of the filler was unable to quench the cationic polymerization. It could still inhibit cationic FP, as it has a lower front velocity than talc while having a higher thermal diffusivity. Some clay fillers have also been shown to act as radical scavengers. The mechanism for RICFP dictates a radical-producing step, which could be inhibited by potential radical scavenging by the clay, resulting in a reduction in front velocity.

The effects of adding increasing amounts of talc and hectorite were investigated. It was found that for both talc and hectorite, adding more clay filler resulted in decreasing front velocity and front temperature as shown in Figure 5.4 for talc. A loading of up to 120 phr of talc was

tested, and the front was still viable. However, at only 32 phr hectorite, the front would quench after a few centimeters of propagation as seen in Figure 5.5. Overall, adding hectorite resulted in much lower front velocities than adding talc. The differences in maximum possible loadings and lower front velocities with hectorite are attributed again to water content and chemical effects. Decreasing front temperature and front velocity points to both the water content and the clays acting as heat sinks, leading to decreased reactivity. The trend of decreasing front velocity with increasing filler loadings has been previously reported by Tran et al. for RICFP systems and Scognamillo et al. for a BF_3-amine cured epoxy system. [34, 38]

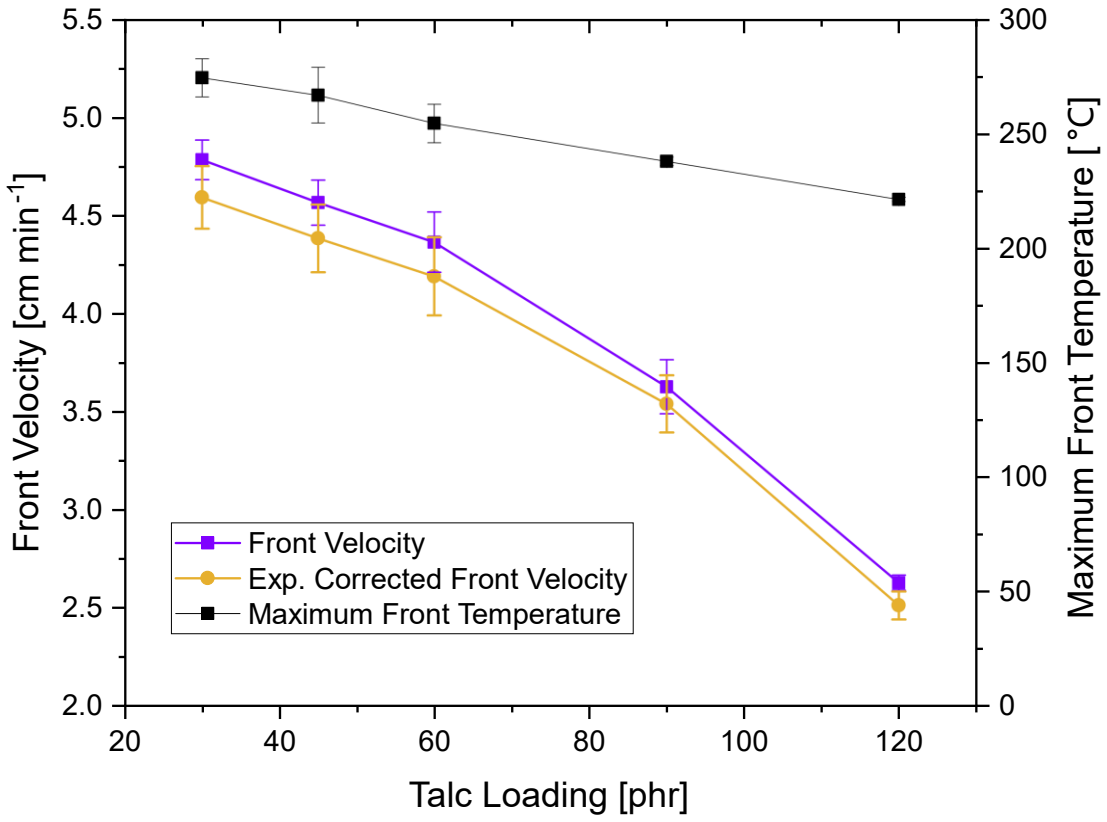

Figure 5.4. Front kinetics and temperature versus talc loading for the resin.

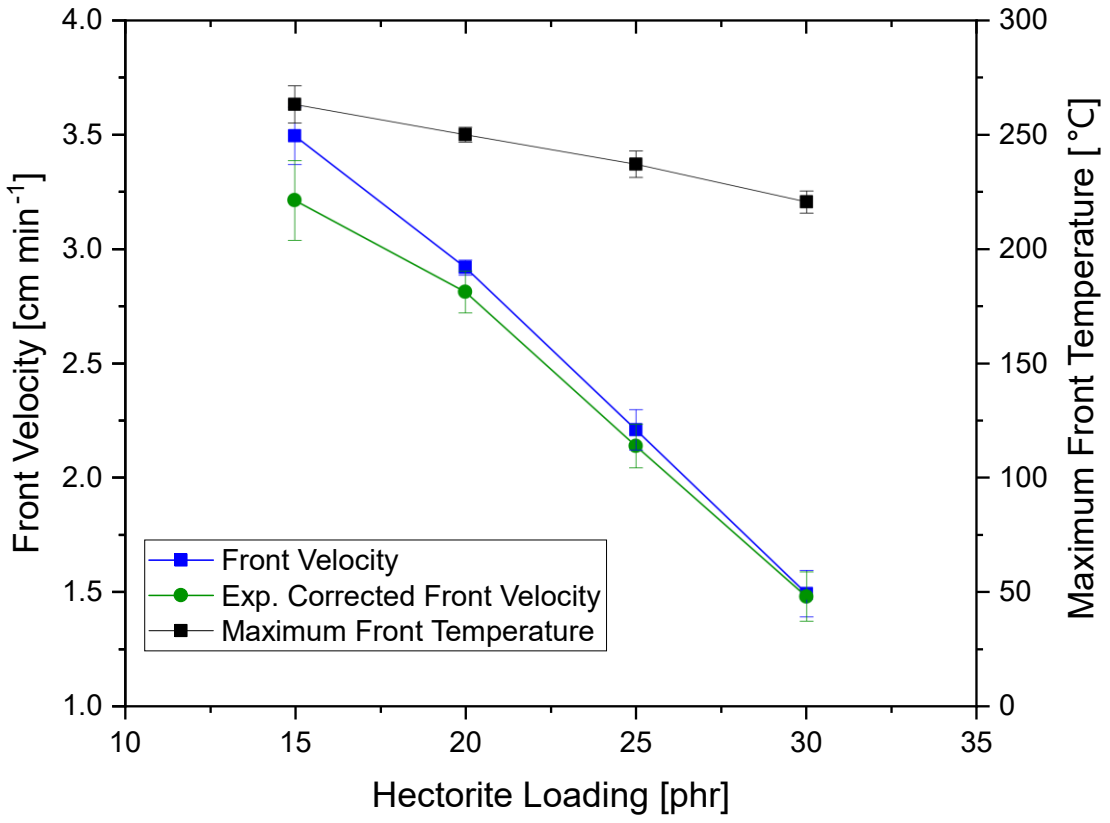

Figure 5.5. Front kinetics and temperature versus hectorite loading for the resin.

5.4. Characterization of Resin and Polymer Composite

SEM-EDS was used to identify the distribution of the filler in the polymer matrix. Analysis of the cured resins by examining characteristic elements with EDS maps showed that dispersion of the fillers varied with the selected filler. EDS allowed for an easier determination of the filler within the polymer composite, compared to just the SEM image. An example SEM image of a 30 phr talc, 5 phr fumed silica composite is shown in Figure 5.6 where the brighter portions are particles of talc.

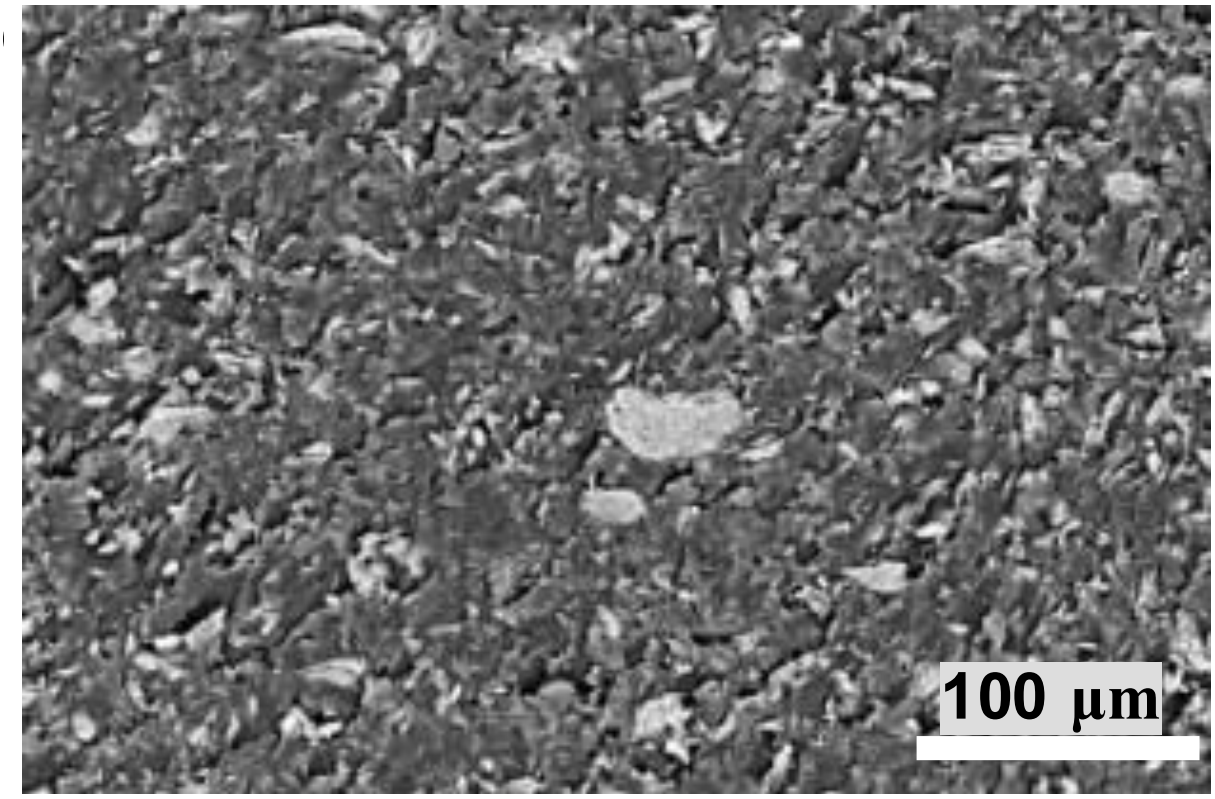

Figure 5.6. SEM image of the composite with 5 phr fumed silica and 30 phr talc.

Ca-bentonite, hectorite, and talc had some larger particles remaining in addition to portions of the unfilled polymer. Calcium carbonate was homogeneously distributed in the system while kaolin appeared to be distributed only in specific sections of the system. The dispersions of 30 phr Ca-bentonite, hectorite, kaolin, and calcium carbonate are shown in Figure 5.7. In addition, increasing talc loading was studied and shown in Figure 5.8. There is an expected increase in the amount of talc seen dispersed in the composite and the particle sizes don't appear to change substantially.

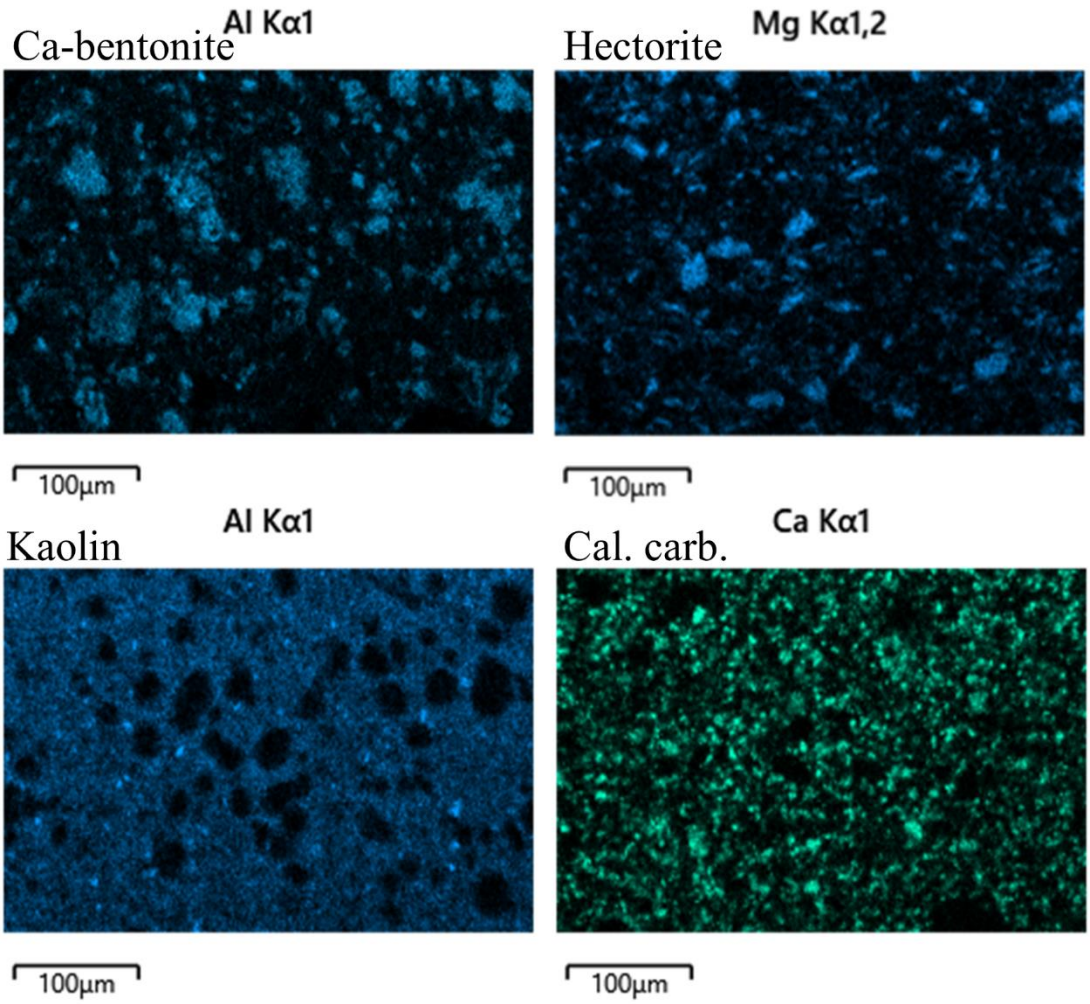

Figure 5.7. EDS map of characteristic elements present in composites containing 5 phr fumed silica and 30 phr of the indicated filler. The elements studied are shown above the EDS map.

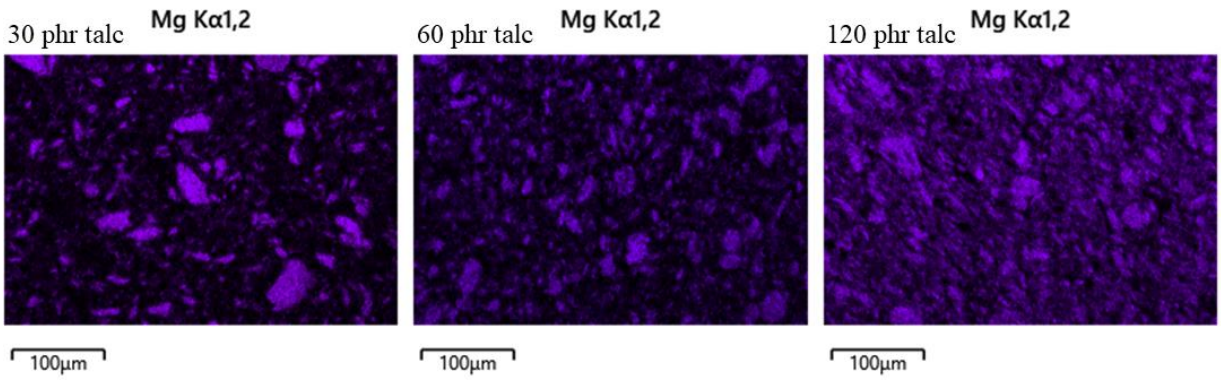

Figure 5.8. EDS map of Mg present in composite filled with increasing loadings of talc in addition to 5 phr fumed silica.

Dispersion of clays has been shown to be affected by the environment of the solution, where increasing pH results in greater dispersion for kaolinites and smectites. [110] Flocculation is also affected, which is the clumping of clays due to attractive forces. Comparing the clay dispersion in Figures 5.7 and 5.8 to the particle sizes of the clays indicated in Table 5.2 shows that there are different degrees of clay flocculation occurring in these composites depending on the filler. The particle sizes are either reported as average or median sizes. Calcium carbonate is dispersed well while kaolin appears to maintain small particle sizes and was not homogeneously dispersed. Ca-bentonite and hectorite have larger particles present than the indicated particle sizes of the fillers, which signals there is some conglomerates of filler happening. For talc, there are much larger particles than the reported particle sizes, therefore there is poor mixing of the aggregated particles and a lack of homogeneity in the composite.

Table 5.2. Average or median particle sizes of clay fillers studied.

	Average Particle Size (μm)	Median Particle Size (μm)
Kaolin (Polygloss 90)[a]	200	400
Calcium carbonate (Hubercarb Q3)[a]	-	3.2
Talc[a, b]	-	5 – 9[b]
Hectorite (Hectalite 200)[a]	95% < 44	-
Ca-bentonite (Bentolite L10)[a]	95% < 44	-
Fumed silica (Aerosil 200)[a]	0.012	-

[a]Provided by manufacturer.
[b]Talc particle size measured by Sedigraph and laser light scattering.

The EDS results above were all gathered from formulations where the filler was speed mixed upon addition. Therefore, the dispersion using a speed mixer versus hand mixing was also analyzed in Figure 5.9 for Ca-bentonite and 5.10 for talc. In the case of 30 phr talc, large aggregated particles remained but the filler appeared more homogeneously distributed throughout the entire system. For all other fillers such as Ca-bentonite as shown, there were insignificant differences in the distribution when speed mixed.

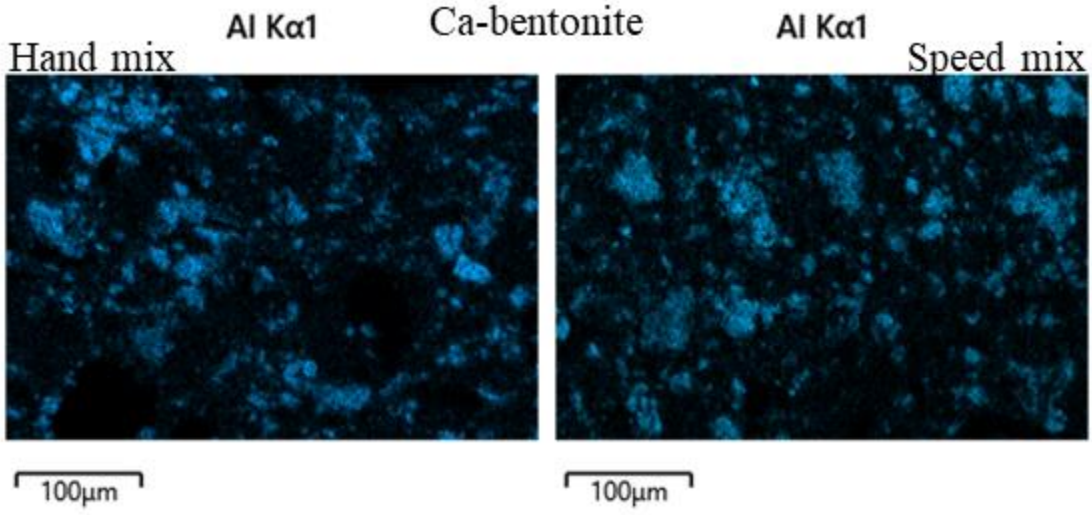

Figure 5.9. Comparison of Ca-bentonite dispersion in the polymer composite through observation of Al using EDS.

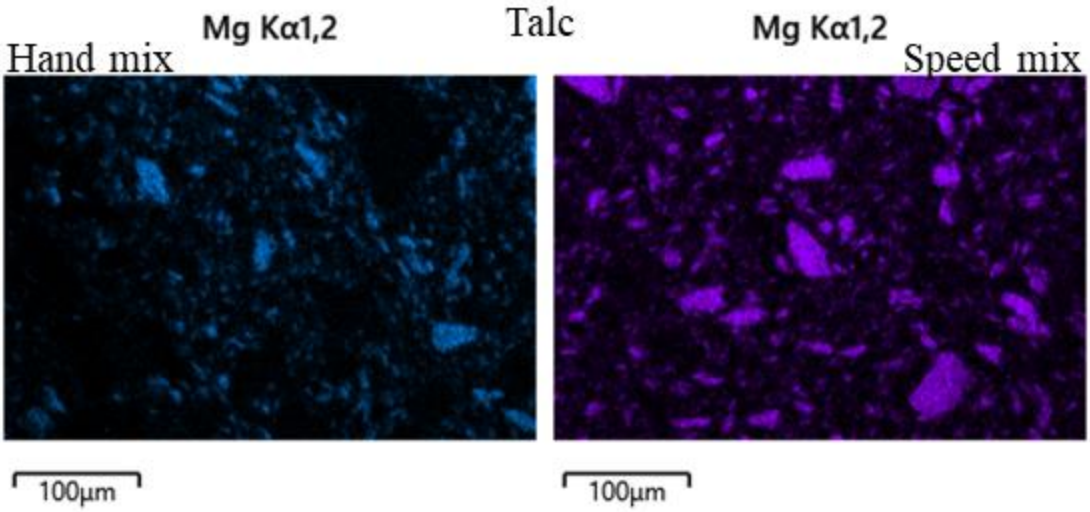

Figure 5.10. Comparison of talc dispersion in the polymer composite containing 30 phr talc through observation of Mg using EDS.

Interestingly, a significant presence of chlorine was also identified through EDS in the polymer region, which is attributed to impurities present from the production of the epoxy monomer that involves the reaction of trimethylolpropane and epichlorohydrin. An example EDS map of a composite containing talc examining Cl and Mg is shown in Figure 5.11. The lack of Cl in the filler can be clearly seen.

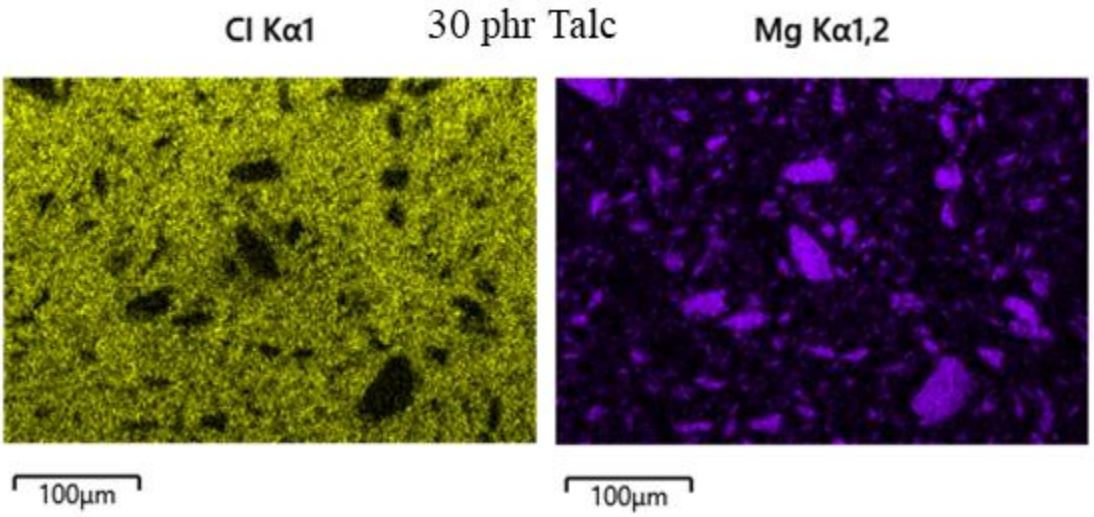

Figure 5.11. EDS maps of Cl and Mg present in the same 30 phr talc, 5 phr fumed silica composite.

While SEM-EDS is a powerful method for analyzing the homogeneity of the filler dispersion in the polymer matrix, SEM alone can be useful for analyzing the void content in the polymer matrix, as seen in Figure 5.12, which is a polymer containing no clays and just 10 phr fumed silica. There are large voids visible in this crossection of the polymer. With a larger area of observation via SEM, void content could be estimated for the entire polymer. The other option to measure the density of voids in composites is ASTM D2734, which uses differences in density to estimate the void content.

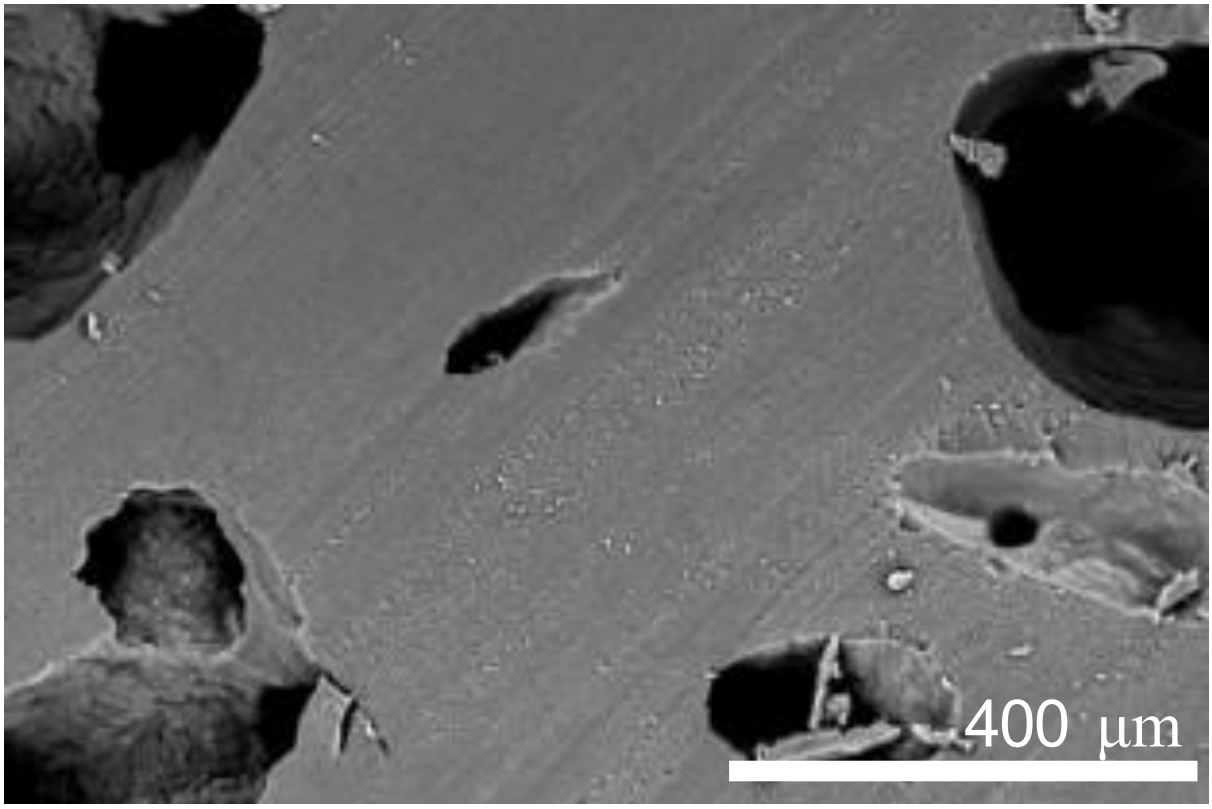

Figure 5.12. SEM image of the polymer with 10 phr fumed silica added, where large voids are visible.

5.5. Effects of Viscosity on Front Velocity

In the initial kinetics studies, there was an observable difference in viscosity with equivalent loadings of clays, due to their different densities and properties. Viscosity can be affected by the

dispersion and flocculation of clay particles, as mentioned in the previous section. The viscosity profile of each clay formulation was evaluated using a rheometer and shown in Figure 5.13. The differences in viscosity based upon which clays are added and hand mixed into the formulation can be quantitatively seen. The viscosity profile is based on a method of low-high-low shear rates over time, to account for the thixotropic and shear thinning behavior of the resin. The drop and recovery in the viscosity moving from low to high and high to low shear rates can be seen which is characteristic of shear thinning.

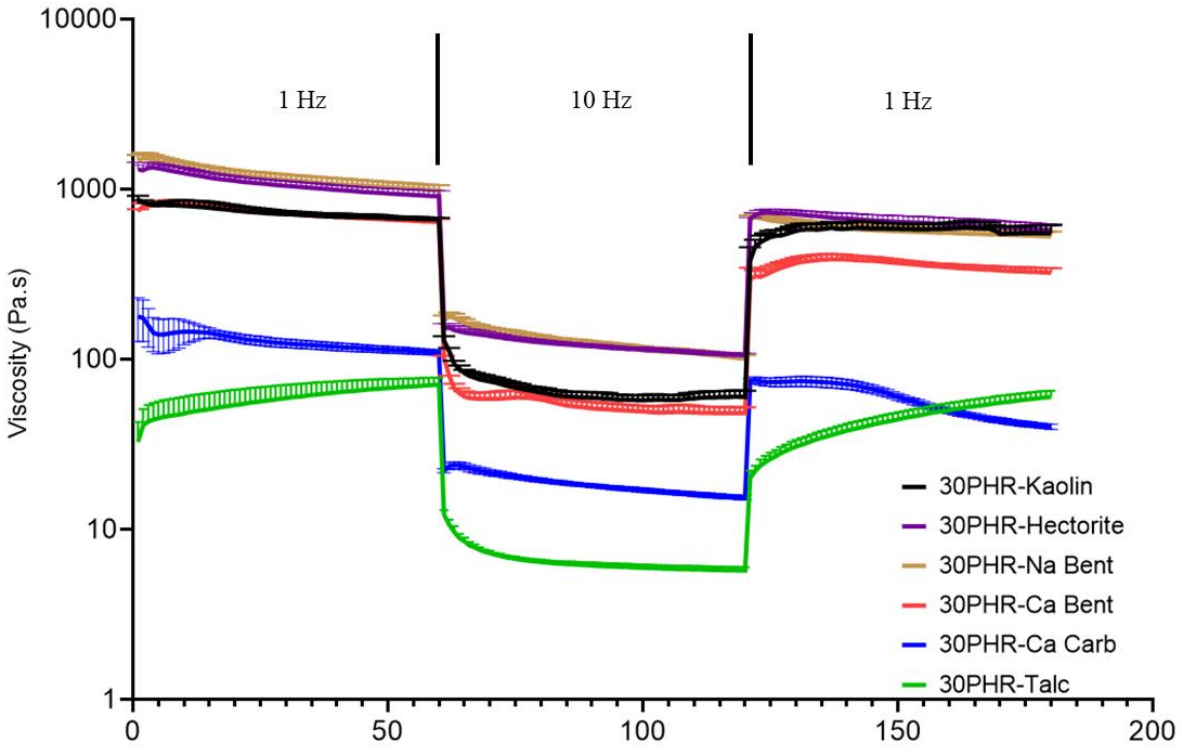

Figure 5.13. Viscosity profiles of formulations containing the resin system, along with 30 phr of the indicated clay with 5 phr fumed silica. The first shear rate was 1 Hz, followed by 10 Hz and 1 Hz, with each shear rate held for 60 s at 25 ℃.

Given that the clays all affected front velocities to different degrees and most of them exhibited varying viscosities upon addition to formulations, to confirm that the differing viscosities were

not the source of the front kinetics results a study with increasing fumed silica was carried out. Increasing talc can give increasing viscosity as shown in Figure 5.14, but the front kinetics may be affected by the talc as shown with the decreasing front velocity with increasing talc. Instead, fumed silica is inert in the system and serves to isolate the effects of viscosity on front velocity. The amount of fumed silica was varied from 5 phr to 15 phr in absence of other fillers, which produces a significant increase in viscosity as shown in Figure 5.15.

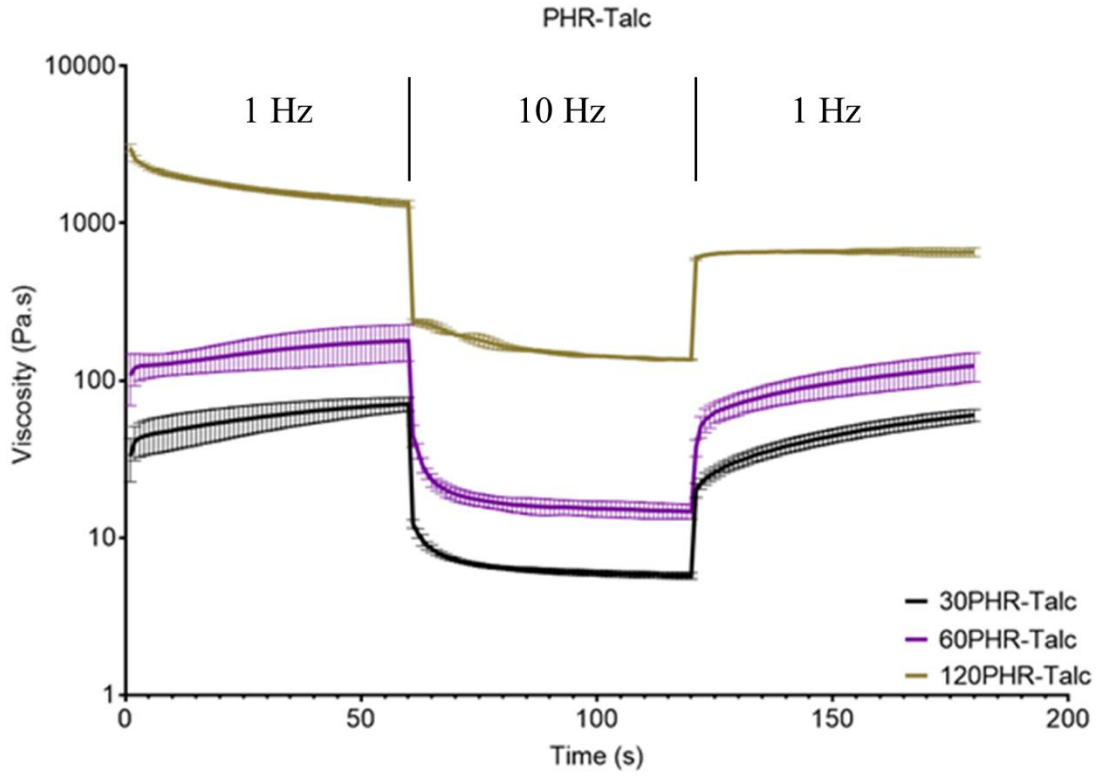

Figure 5.14. Viscosity profile of formulations containing the resin system with 5 phr fumed silica and increasing talc loading. The first shear rate was 1 Hz, followed by 10 Hz and 1 Hz, with each shear rate held for 60 s at 25 ℃.

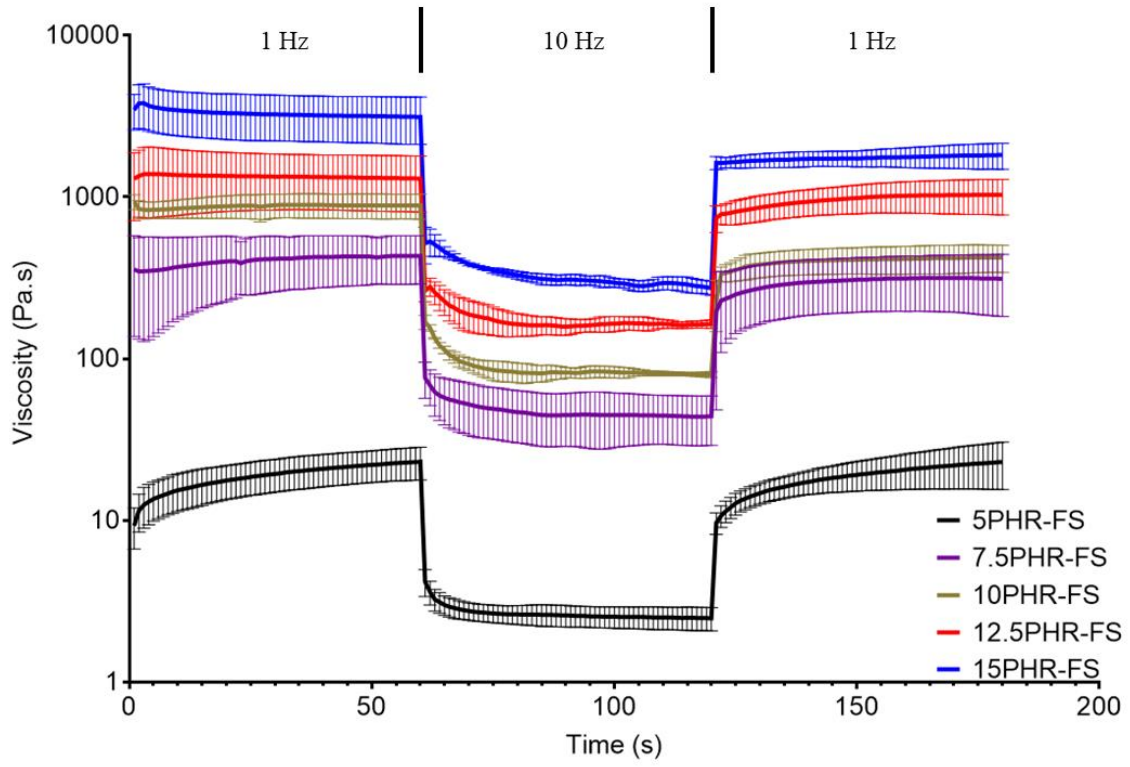

Figure 5.15. Viscosity profile of formulations containing the resin system with increasing fumed silica loading over the low-high-low shear rate method. The first shear rate was 1 Hz, followed by 10 Hz and 1 Hz, with each shear rate held for 60 s at 25 °C.

As shown in Figure 5.16, the front velocity decreased from 7.3 cm min^{-1} with 5 phr fumed silica to 6.1 cm min^{-1} with 7.5 phr fumed silica. The front velocity then remained constant with increasing additions. The higher front velocity with less viscous material is expected with FP, where previous studies have shown that convection could affect front propagation. [19, 95] Correcting for the expansion of the sample as the front propagated gave a weak dependency of front velocity across all fumed silica loadings tested, which was initially expected. The front temperature appeared nearly constant with fumed silica loadings of 10 to 15 phr, and the lower front temperature at 5 and 7 phr loading could be indicative of convection giving rise to heat loss.

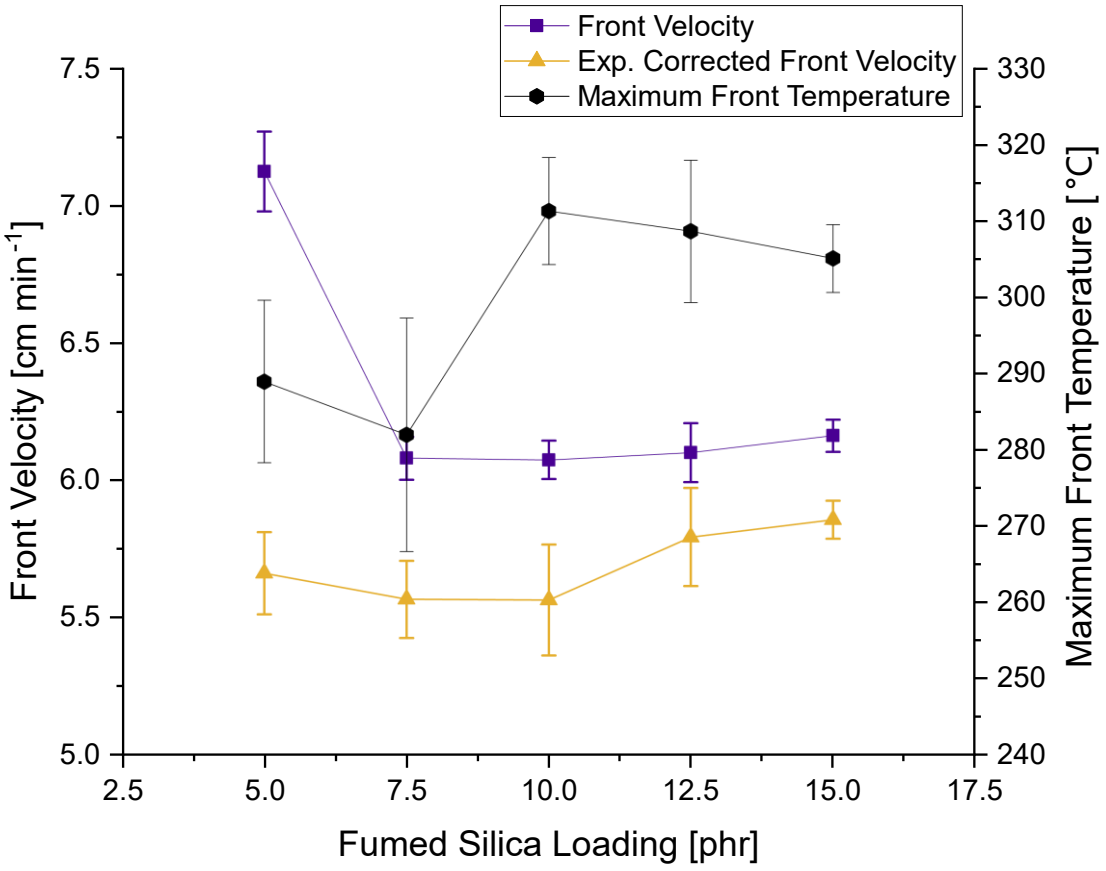

Figure 5.16. Front velocity, front velocity corrected for expansion, and front temperature as a function of fumed silica loading.

A system with 30 phr calcium carbonate while varying the fumed silica loading from 5 phr to 7 phr was also tested. The qualitative increase in viscosity resulted in a statistically insignificant difference in front velocity. 5 phr fumed silica with calcium carbonate gave an expansion-corrected front velocity of 3.49 ± 0.11 cm min^{-1}, while 7 phr fumed silica resulted in 3.43 ± 0.09 cm min^{-1}. Calcium carbonate was chosen because it is not a clay, so there are no chemical effects regarding swelling or acidic sites. With these studies, it was concluded that above a threshold for eliminating buoyancy-driven convection, the viscosity has no significant effect on the front velocity. Therefore, it is concluded that the trends observed with increasing clay loadings are not related to viscosity.

Since samples for characterization with 3 point bending and SEM were made using a speed mixer rather than hand mixing, comparisons in the viscosity profile were also examined. It was found that speed mixed samples containing kaolin and talc have both lower viscosity and more deviation in their viscosities in Figure 5.17. Notably, speed mixed samples with 30 phr talc and 5 phr fumed silica were difficult to work with due to their much lower viscosity. In molds with open ends they would simply flow out of the mold with a high degree of expansion. They also exhibited a unique phenomenon that appeared to be a phase separation of high and low viscosity portions after speed mixing. However, comparing front velocities in Figure 5.18 of hand and speed mixed samples showed that the values overall vary slightly, but the trends remain the same. Therefore, speed mixing could be useful for applications that require shear thinning, lower viscosity, or highly filled systems, but for front velocity measurements it can make measurements more difficult.

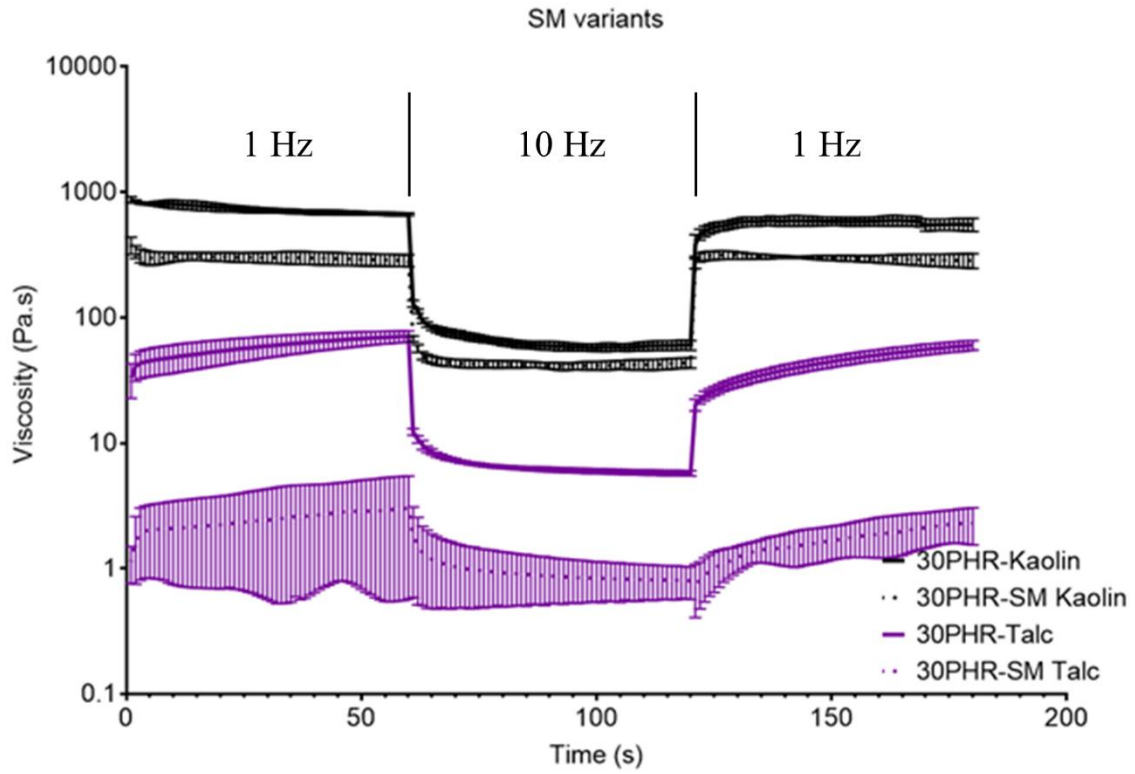

Figure 5.17. Comparisons of the viscosity profile of formulations containing the resin system with 5 phr fumed silica and either 30 phr kaolin or talc, speed mixed (SM) versus hand mixed. The first shear rate was 1 Hz, followed by 10 Hz and 1 Hz, with each shear rate held for 60 s at 25 ℃.

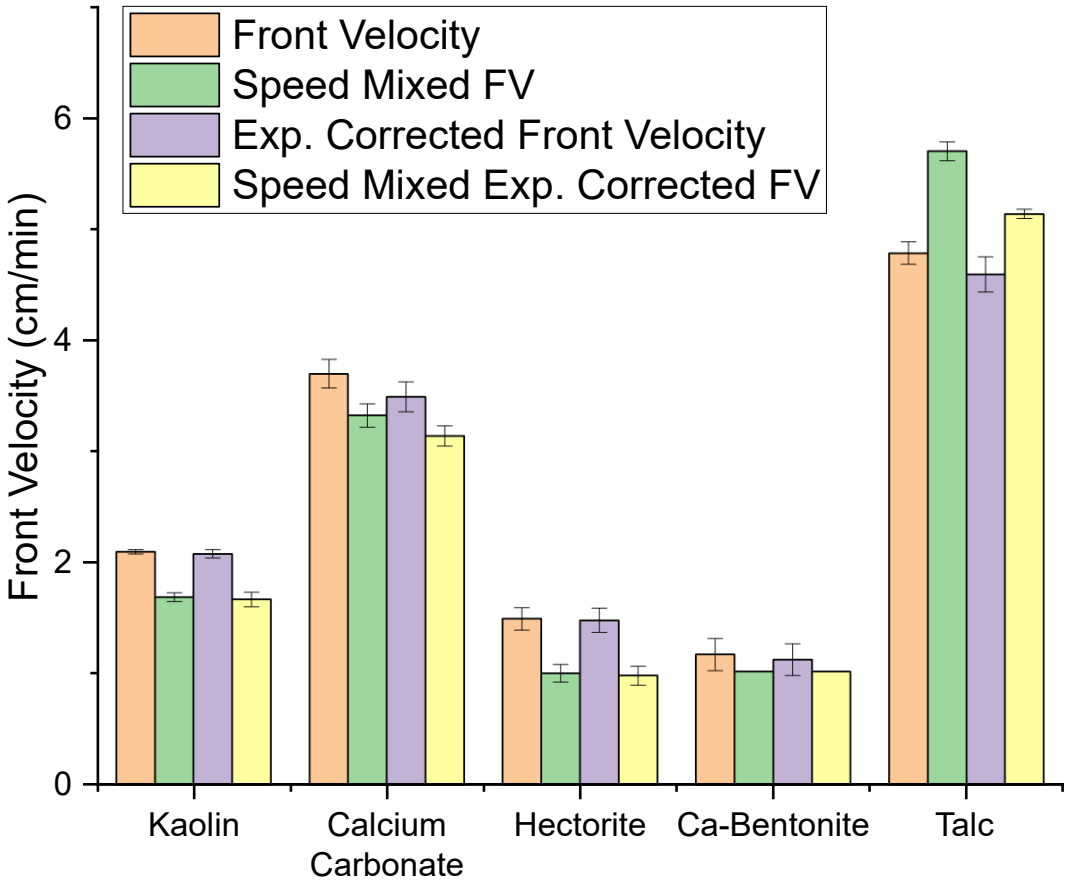

Figure 5.18. Front velocity and expansion corrected front velocity of hand-mixed and speed mixed samples with 5 phr fumed silica and 30 phr of the indicated filler added to the resin system. Ca-bentonite speed mixed measurements are duplicates, not triplicates like other data points.

As mentioned, all the formulations exhibited shear thinning thixotropic behavior with a recovery of viscosity after application of high shear. Recovery of viscosity was calculated, and recovery appears to decrease as the talc loading is increased. The recovery is a measure of the degree to which the viscosity returned to the initial viscosity after a higher shear rate. There is no current explanation for the decreasing recovery. It is important to note that this recovery is on a time scale of 60 seconds. The recovery could be comparable with the increased talc loading to lower loadings, but on a longer timescale.

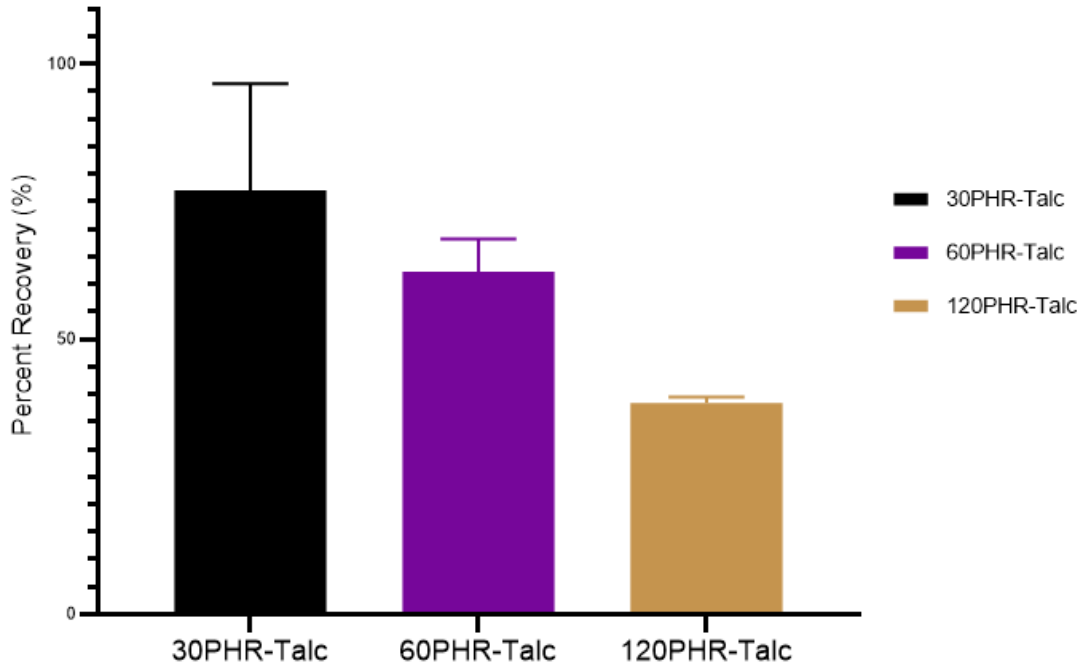

Figure 5.19. Percent recovery of viscosity after high shear of formulations containing the resin system of 25 wt% TEGDVE, 75 wt% TMPTE, 1 phr IOC-8 and 1 phr Luperox® 231 with 5 phr fumed silica and increasing talc loading.

5.6. Effects of Drying Clays

Drying the clays had substantial effects on the front velocity and temperature and produced an overall increase in front velocity and temperature in all cases, as shown in Figure 5.20a, and Figure 5.20b for the smectite clays. The differences are attributed to the water content of the clays, which can be seen as percentage weight change measured gravimetrically and with a thermogravimetric analyzer (TGA), compared with the manufacturer reported moisture content in Table 5.3.

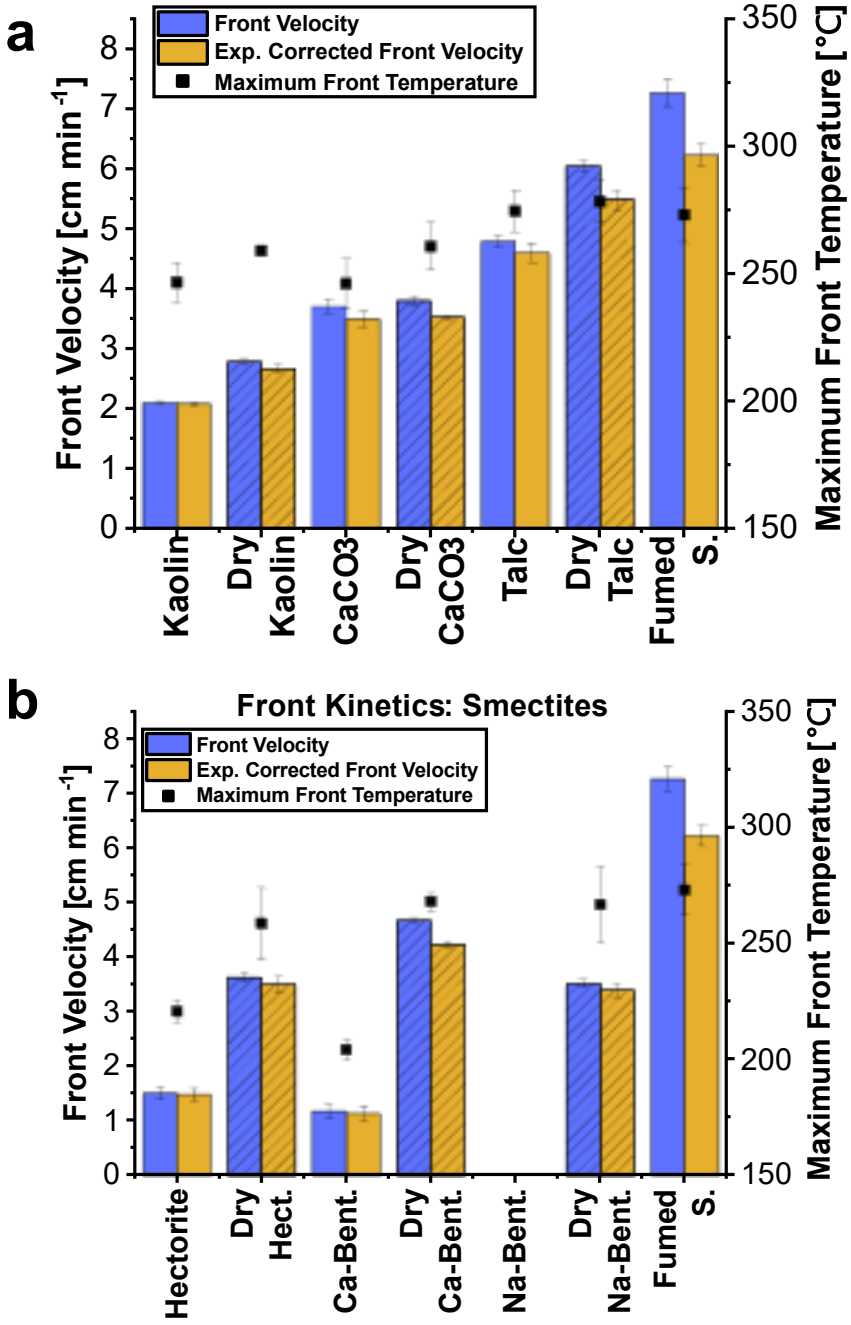

Figure 5.20. Comparison of dried and as-received clays tested for front velocity and front temperature. Samples contained 30 phr clay and 5 phr fumed silica added to a resin system of 25 wt% TEGDVE, 75 wt% TMPTE, 1 phr IOC-8 and 1 phr Luperox® 231. "Fumed S." contained only 5 phr fumed silica added with no clay. Dried fillers are shown with a filled pattern. (a) Front kinetics comparisons with dry and as-received clays and calcium carbonate. (b) Front kinetics comparisons with dry and as-received smectite clays. "Hect." is hectorite and "Bent." is bentonite.

Table 5.3. Water loss after drying measured through gravimetric and thermogravimetric analysis.

	wt% Water Loss	wt% Water Loss (TGA)	Reported Moisture Content (wt%)[a]
Kaolin	1.3	0.74	1.0
Calcium carbonate	0.15	0.32	0.2
Hectorite	8.0	7.1	<12
Ca-bentonite	13.9	11.4	<8.0
Na-bentonite	8.4	7.2	<12
Talc	0.25	0.61	Not provided

[a]From manufacturer technical data sheet

A TA Instruments TGA 550 was used to analyze fillers thermogravimetrically. A Hi-Res™ Ramp 50 °C/min to 600 °C method, Resolution 4, Sensitivity 1 was used for each sample with standard aluminum pans under a nitrogen environment. This ramp method will automatically modify the ramp rate dynamically depending on the observed weight change.

The TGA curves for each clay are shown in Figures 5.21-5.26. The water loss observed with TGA was an average of two runs and analyzed over a range of 25 ℃ to 200 ℃ to best mimic the oven drying process. It was calculated by subtracting the weight at 200 ℃ from the initial weight. Both talc and calcium carbonate saw a sudden weight percent increase of approximately 0.4% and 0.7% from 25 ℃ to 50 ℃, respectively, across two separate runs. Thus, the water loss calculated from the TGA curve for talc and calcium carbonate used the weight percentage from 50 ℃ to 200 ℃ rather than the initial weight percentage at room temperature. The cause of this sudden increase is uncertain and the thermal decomposition of the fillers above the temperatures that fronts would propagate (~300 ℃ maximum) is not particularly of interest.

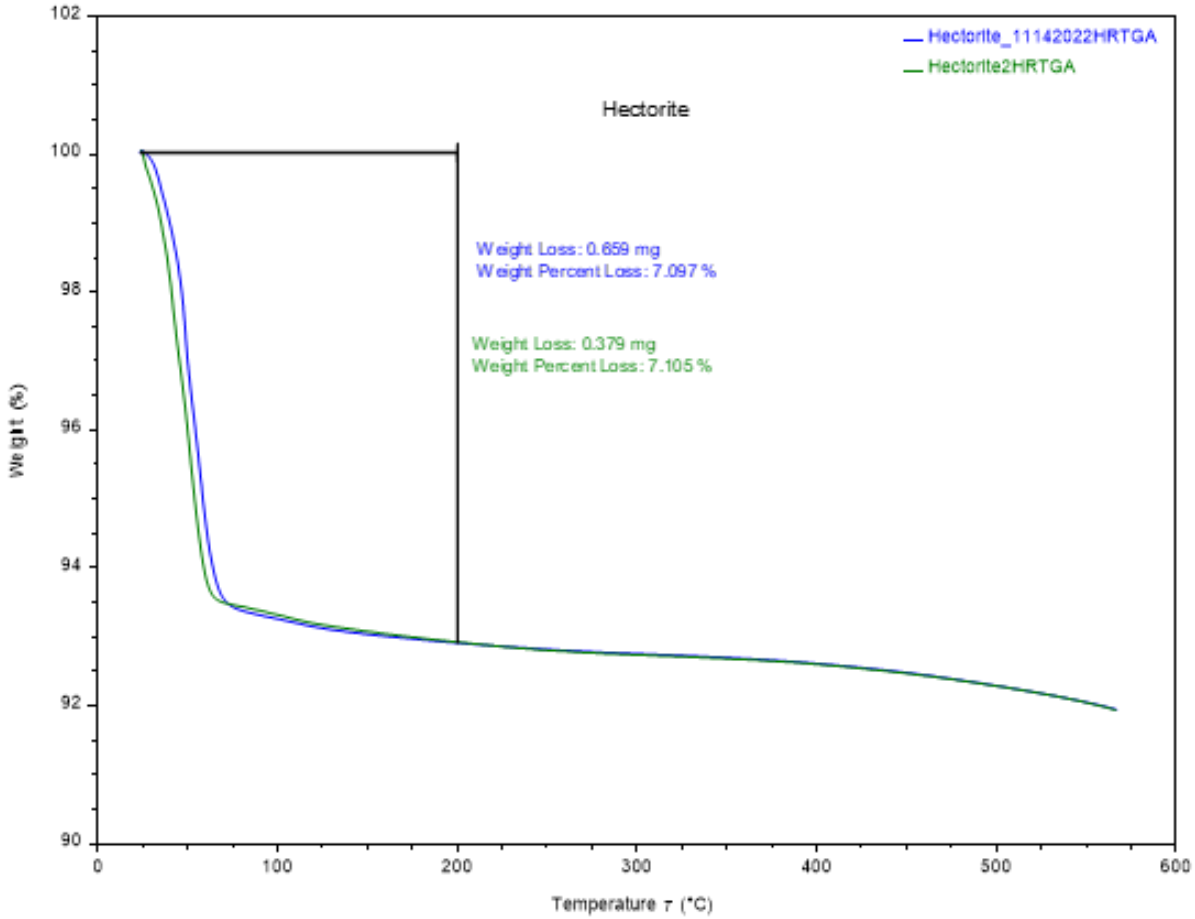

Figure 5.21. Thermogravimetric analysis (TGA) curve of Hectalite® 200 (hectorite) clay. Weight change calculated from starting temperature of approximately 25℃ to 200℃.

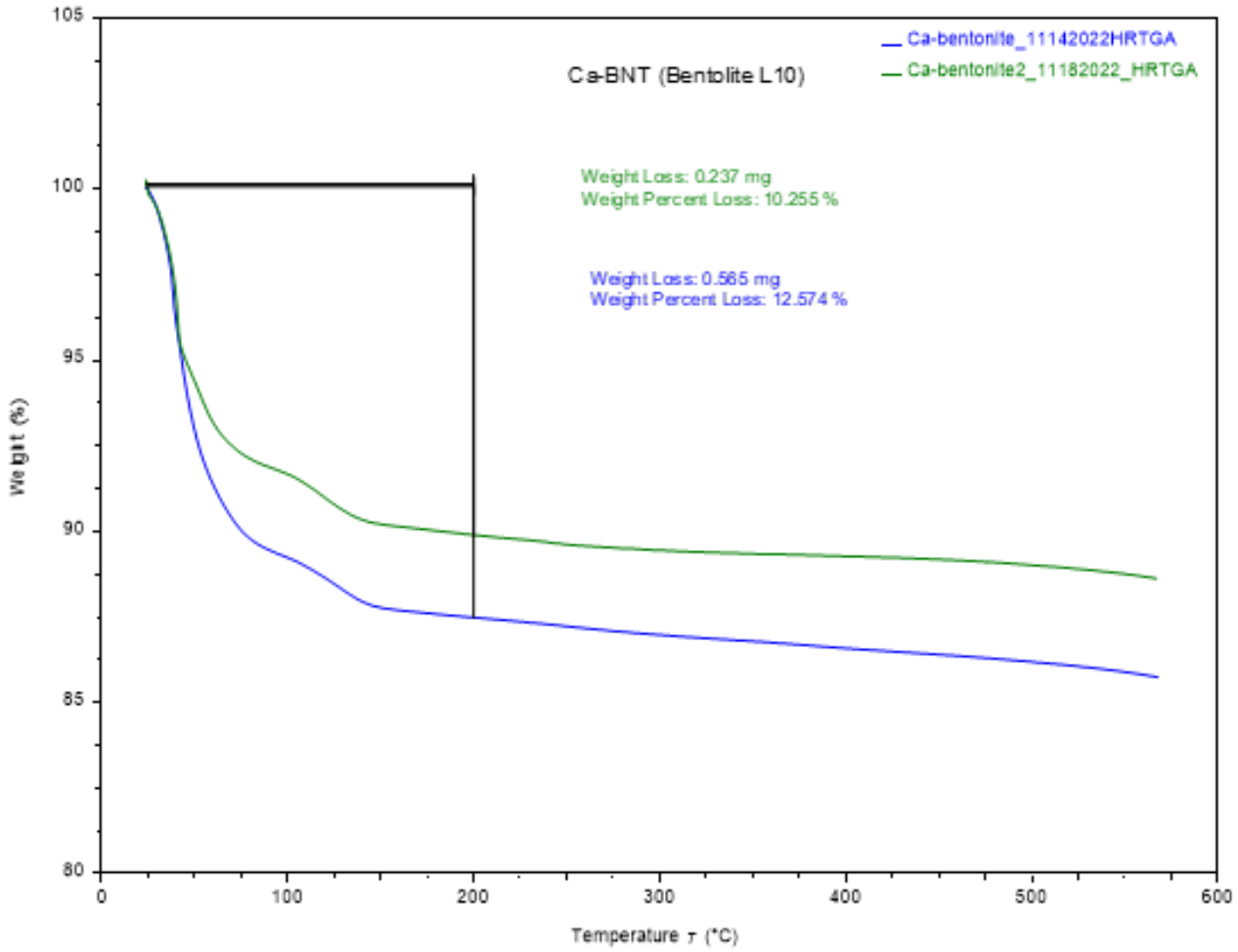

Figure 5.22. Thermogravimetric analysis (TGA) curve of Bentolite L10 (calcium bentonite) clay. Weight change calculated from starting temperature of approximately 25℃ to 200℃.

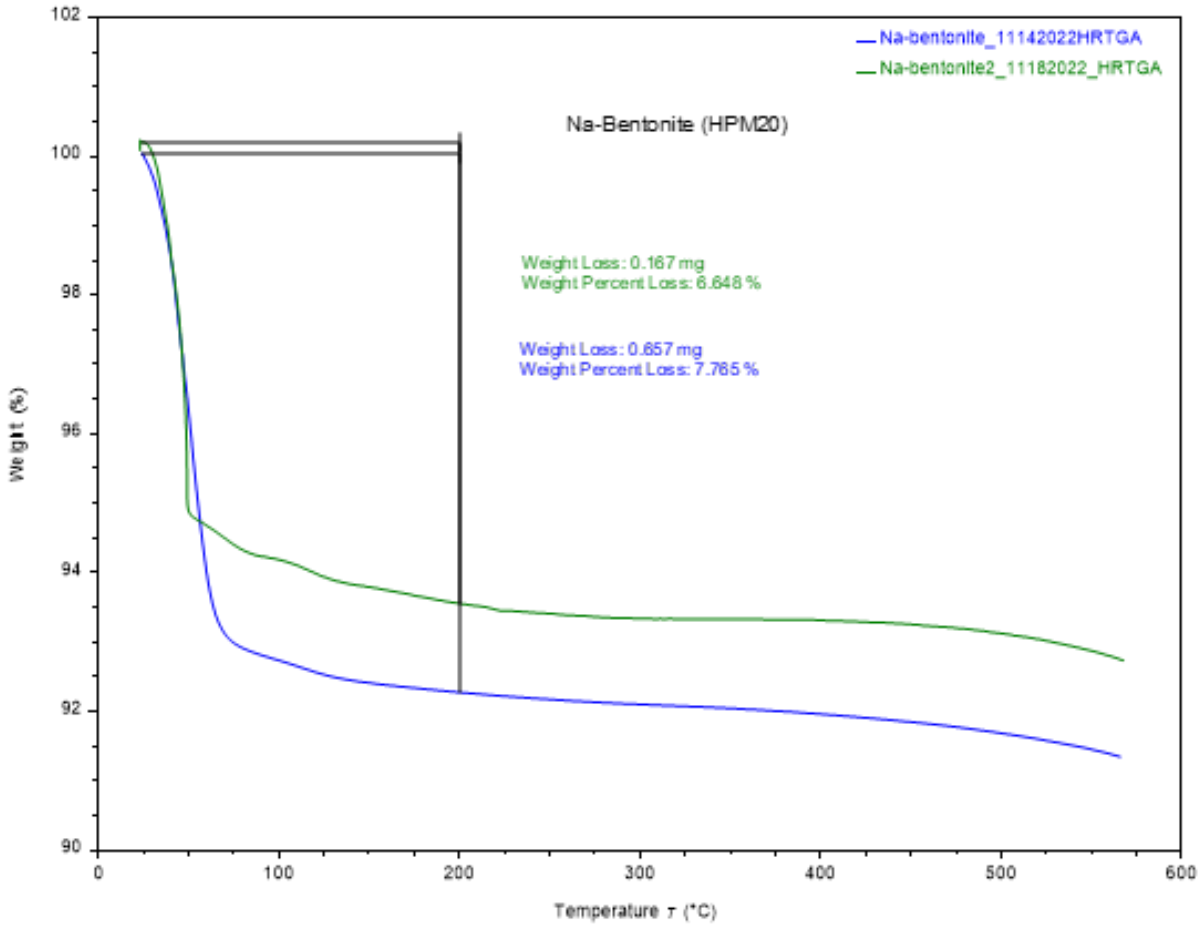

Figure 5.23. Thermogravimetric analysis (TGA) curve of bentonite HPM-20 (sodium bentonite) clay. Weight change calculated from starting temperature of approximately 25℃ to 200℃.

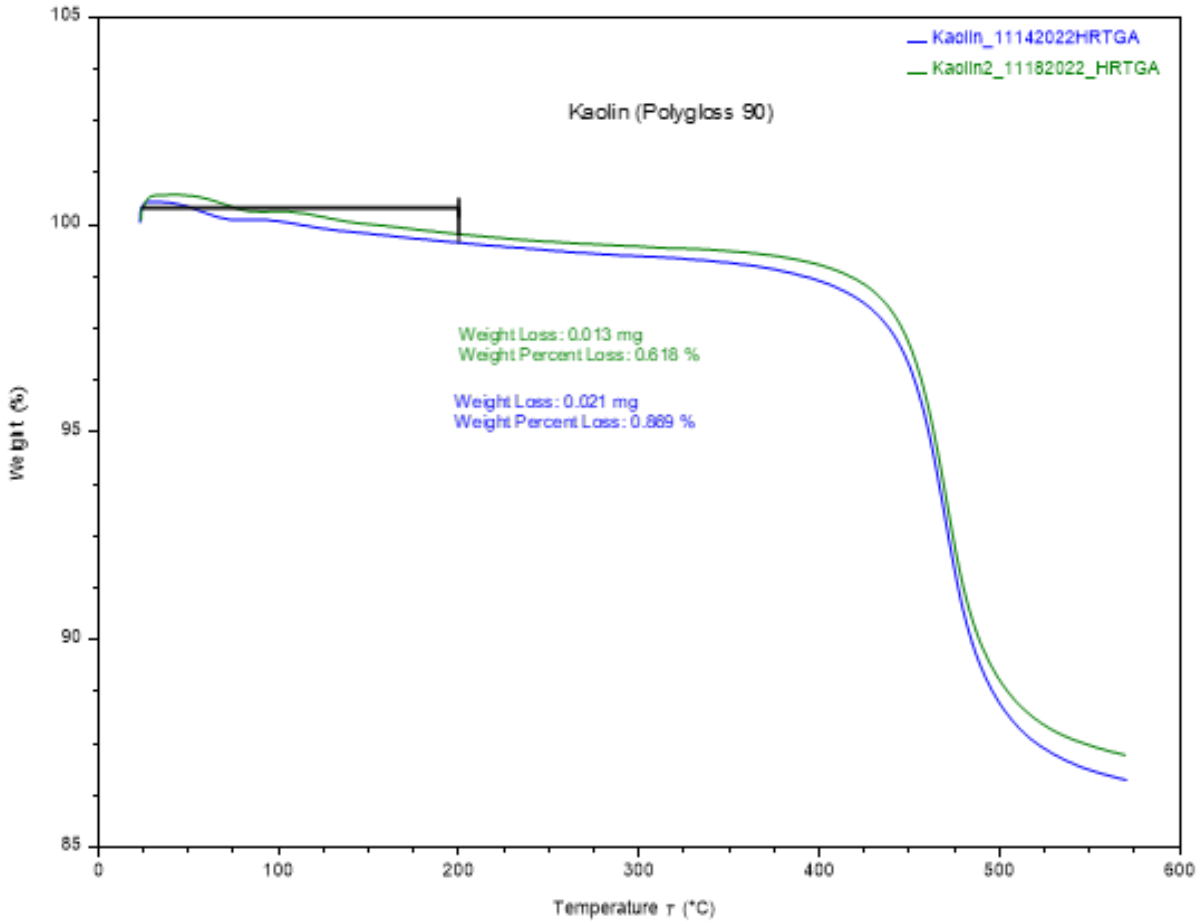

Figure 5.24. Thermogravimetric analysis (TGA) curve of Polygloss® 90 (kaolin) clay. Weight change calculated from starting temperature of approximately 25℃ to 200℃.

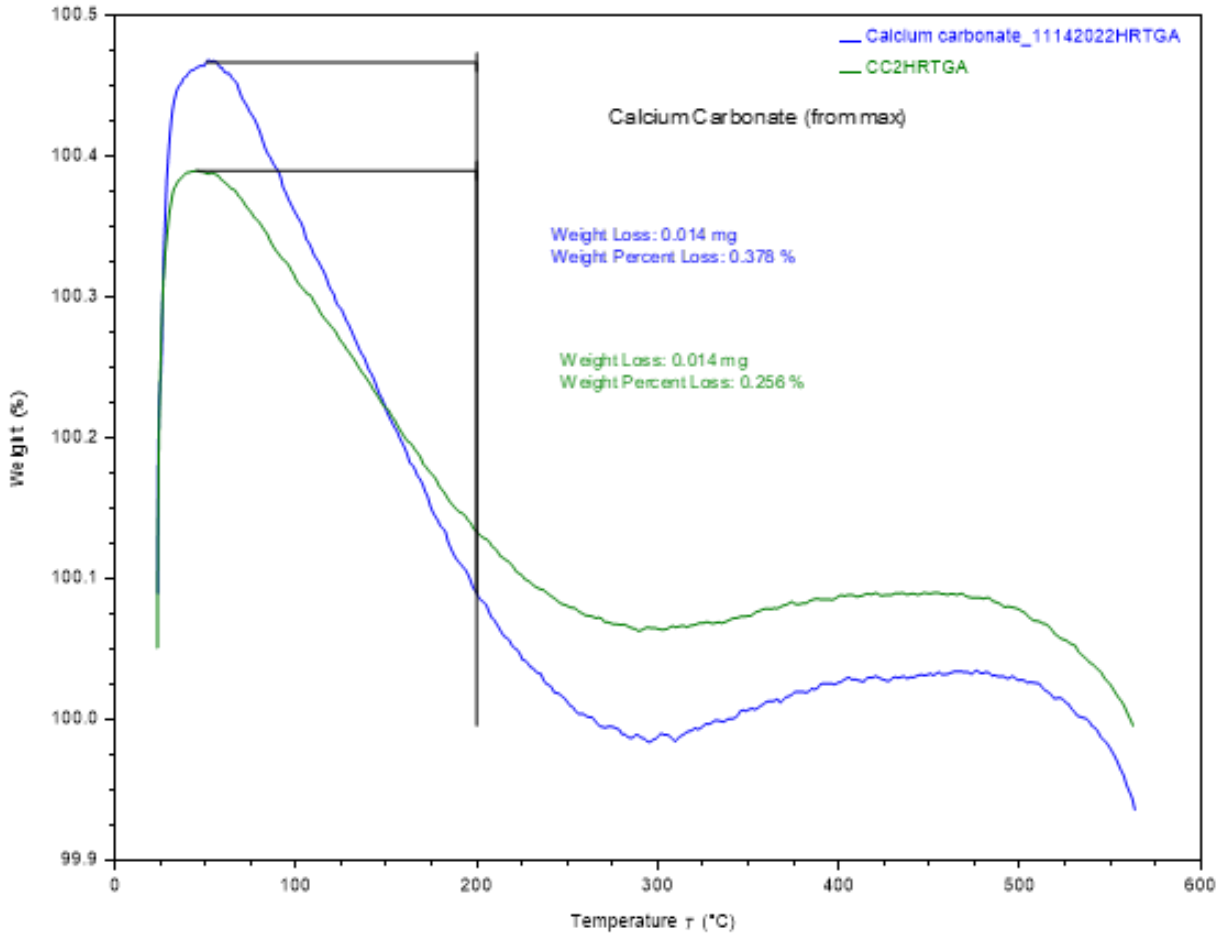

Figure 5.25. Thermogravimetric analysis (TGA) curve of Hubercarb® Q3 (calcium carbonate). Weight change calculated from starting temperature of approximately 50°C to 200°C.

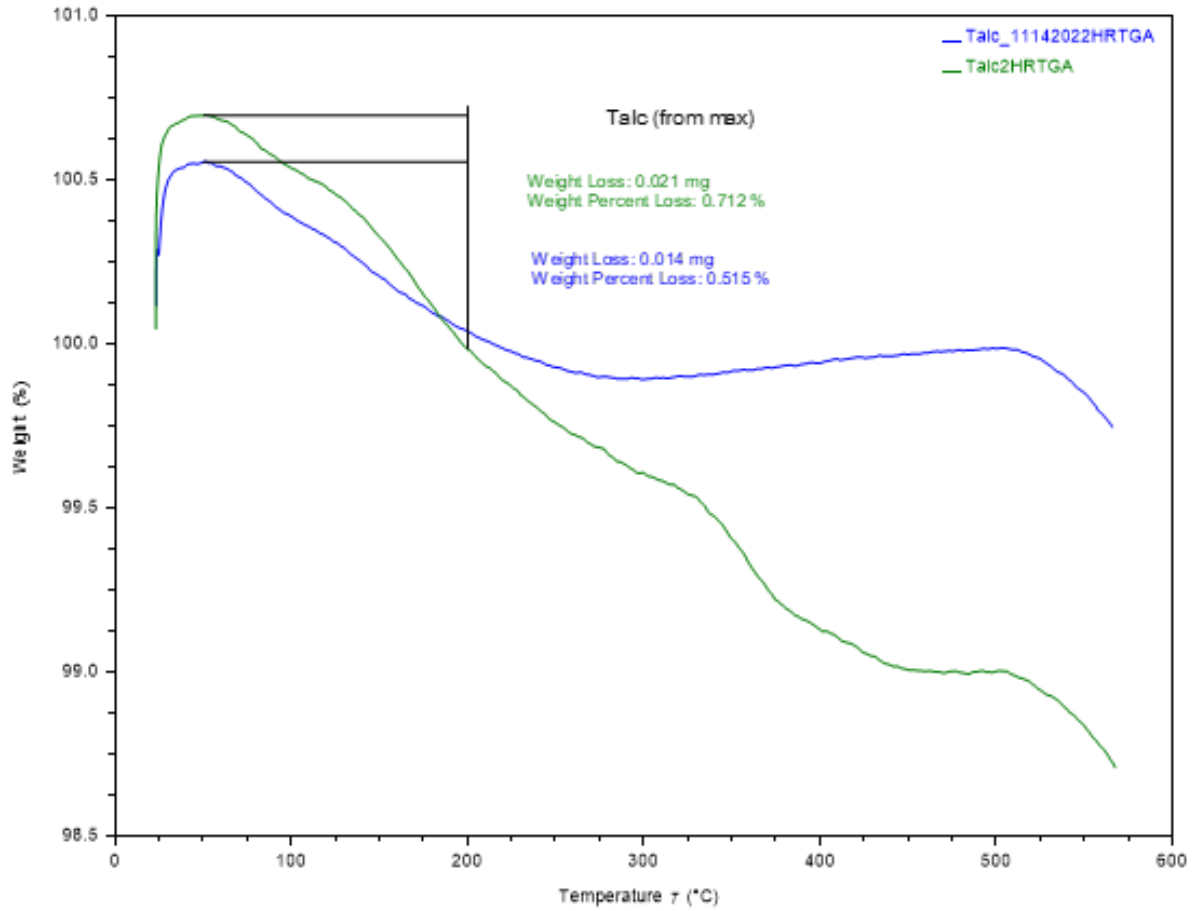

Figure 5.26. Thermogravimetric analysis (TGA) curve of talc. Weight change calculated from starting temperature of approximately 50℃ to 200℃.

Hectorite, sodium bentonite, and calcium bentonite exhibited the highest changes upon drying, which coincides with their much higher water content than the other clays tested and their swelling characteristics. [22, 110] Notably, Na-bentonite would not support a front until dried.

Drying could result in a few possibilities that would both increase the front velocity. First, a higher water content could mean more heat loss in the system due to the vaporization of water. Analyzing the maximum front temperatures reveals that for every clay tested, drying resulted in a temperature almost identical to that of the fumed silica control, while the non-dried clays had much lower front temperatures. This supports the hypothesis that heat loss from vaporization of water is mitigated by drying the clays. Second, drying clays has been associated

with freeing up acidic sites. [102, 103, 112] It is possible that this is catalyzing the RICFP rather than acting as an inhibitor for the process as seen with previous works based on radical FP. Finally, water could inhibit the cationic propagation reaction. The reduction in front velocity with calcium carbonate compared to the fumed silica control can be attributed to potential chemical interaction with propagating cations or the increase in heat capacity of the formulation and heat losses to the calcium carbonate as shown by the reduction in maximum front temperature compared to the fumed silica control. The constant front velocity independent of drying of calcium carbonate is due to a low amount of bound water.

With the clay fillers, the similar front temperatures after drying compared to the control containing no clay imply that the reduction in front velocity is mostly due to chemical effects or the vaporization of water during propagation rather than heat loss to the clay itself. If the heat loss was due to the thermal properties (such as heat capacity) of the fillers themselves rather than water loss, one would expect the front temperature to be significantly lower than the fumed silica, irrespective of drying.

5.7. Material Characterization of Clay Filled Composites

To study the effects of the fillers on final material properties, testing with DSC to determine glass transition temperature (Tg) and flexural testing were undertaken with results in Table 5.4. Composites containing clays of each type, such as kaolinite, calcium carbonate, talc, smectites, were chosen for characterization. An increase of talc loading was examined to show the effects on material properties with increasing filler.

Table 5.4. Mechanical and thermal properties of composites.

	Flexural Strength (MPa)	Flexural Modulus (MPa)	Flexural Strain at Break (mm mm^{-1})	Glass Transition Temperature (°C)
Fumed silica	15.23	1.20	0.110	-3.95
30 phr Talc	8.18	0.55	0.085	-6.16
60 phr Talc	31.20	1.78	0.071	-6.81
120 phr Talc	156.3	4.26	0.035	2.75
Kaolin	43.89	2.73	0.069	-13.05
Calcium carbonate	17.14	0.90	0.062	-12.16
Hectorite	N/A	N/A	N/A	-15.40

It was found that the Tg for all studied clay composites was less than 0 °C, except in the case of 120 phr talc with 5 phr fumed silica, which still had a Tg significantly below room temperature as shown in Table 5.4. The Tg calculation was done in TA Universal Analysis, which finds the midpoint of the tangent line of the slope of the curve. An example is shown in Figure 5.27. There was a notable decrease in Tg after addition of clays compared to a system with only fumed silica. The low Tg values are not unexpected, as the materials are rubbery and flexible in ambient conditions. The water content of the clay could be playing a role in the low Tg, with hectorite having the lowest measured Tg and talc the highest. Additionally, a composite with 30 phr dried talc gave a difference of 4 °C compared to using as-received talc. Calcium carbonate, with the lowest water content of tested fillers does not follow this trend of water content, however. There was an increase in Tg from 30 phr talc to 120 phr talc, likely due to the decreased chain mobility in the system with high filler content. The DSC curves for talc containing composites are shown in Figure 5.28.

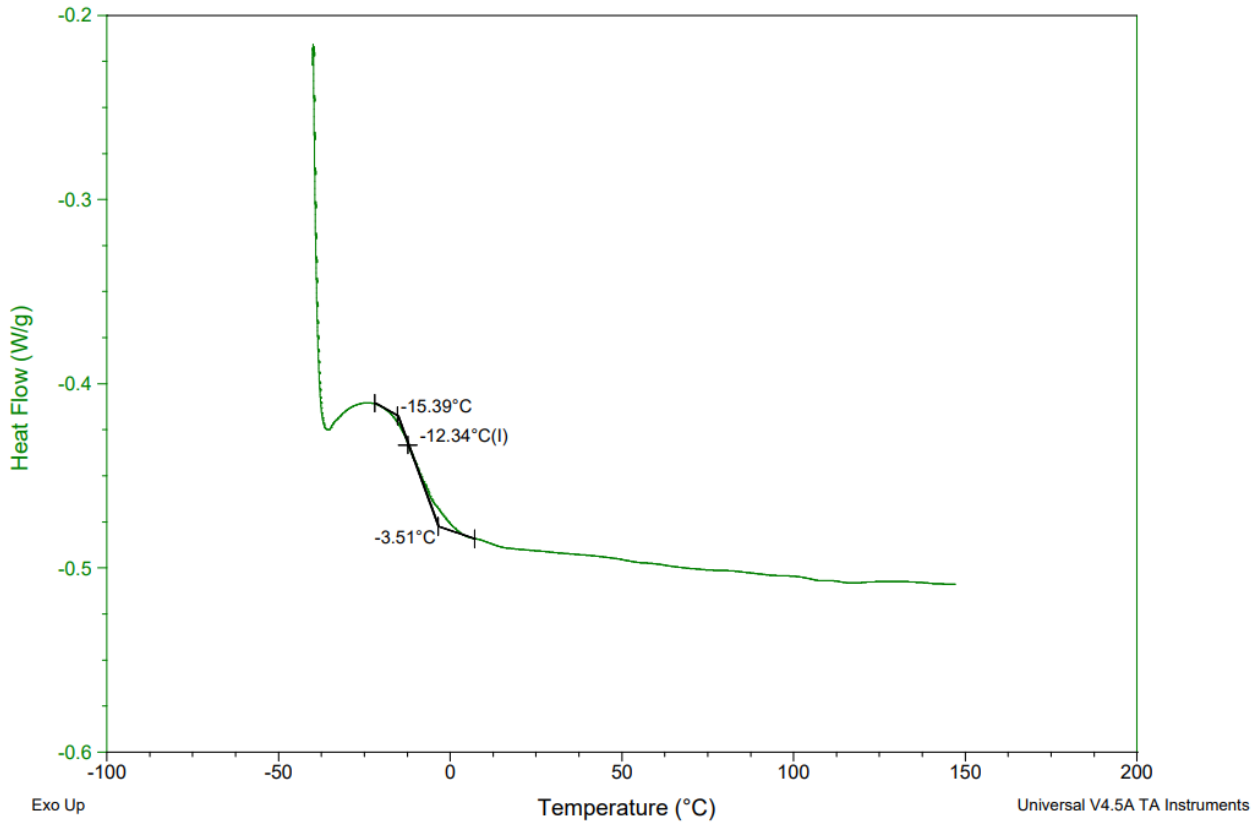

Figure 5.27. Example of the glass transition temperature calculation using TA Universal Analysis software for a composite sample containing calcium carbonate.

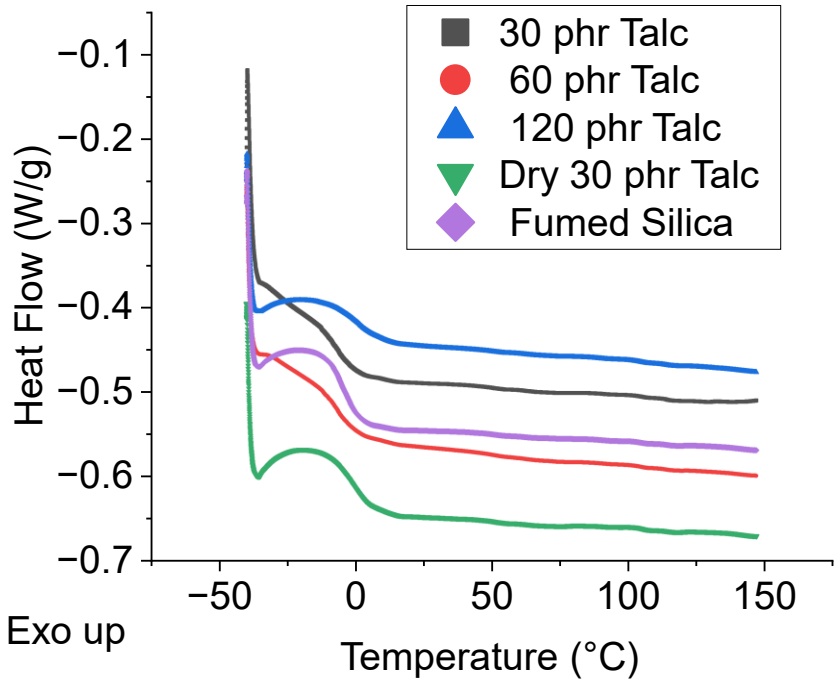

Figure 5.28. DSC curves from -40 ℃ to 150 ℃ of various talc loadings from 30 to 120 phr, 30 phr dried talc and 15 phr fumed silica at a rate of 10 ℃ min^{-1}.

In most DSC curves shown in Figure 5.28, there appears to be a significant exothermic hook from -40 ℃ to -20 ℃, which was examined and found to be due to improper matching of the reference pan weight with the sample pan weight and not related to the thermal properties of the sample. The hook disappears with a reference pan that is similar in weight to the sample, shown with a kaolin composite in Figure 5.29.

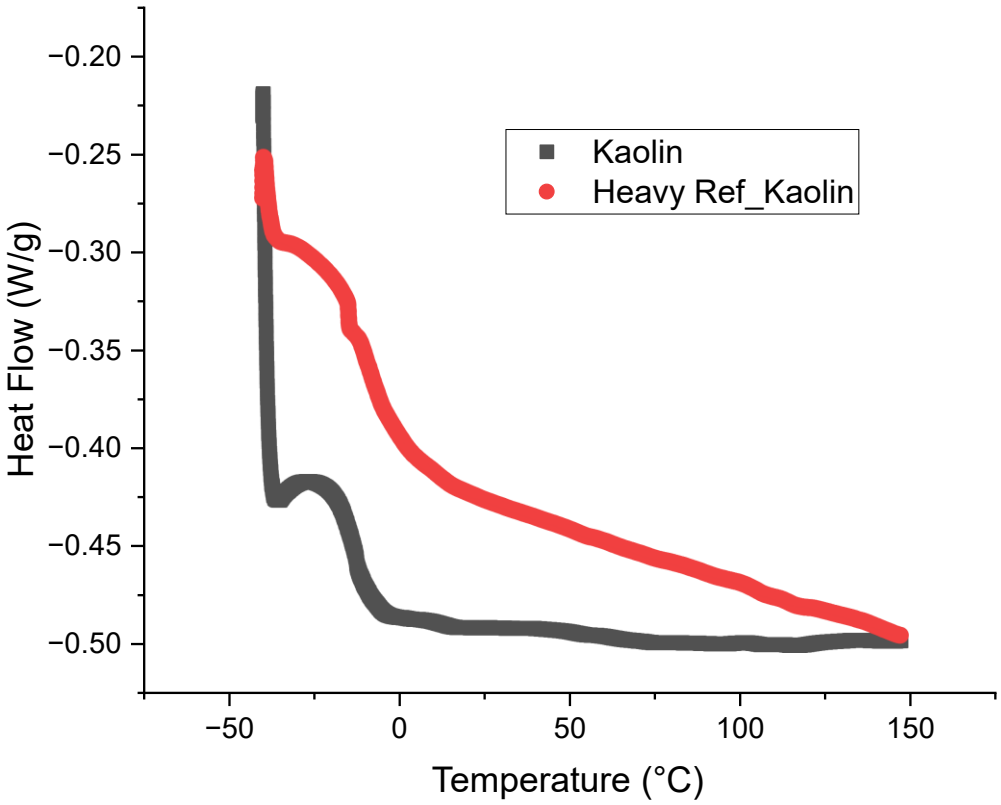

Figure 5.29. Exothermic hook in DSC curves of the same kaolin composite sample disappearing with use of a reference matching the sample weight and evident with a lighter reference pan.

Flexural testing was chosen for mechanical testing due to the inherent homogeneities in these systems with decomposition of the radical initiator generating voids in addition to the flexible nature of the composites. Tensile testing would be difficult due to the possibility of cracks propagating due to voids and the reported strength being much lower than actual. Hectorite was unable to be studied as there were issues with front propagation in thin sheets for sample preparation.

Flexural testing on the Instron universal testing machine initially produces load-extension curves, such as those in Figure 5.30 for various clays. These are converted into flexural stress-

strain curves shown in Figure 5.31 for increasing talc by Equations 5.1 and 5.2 from ASTM D790.

$\sigma = 3PL / 2bd^2$ Equation 5.1

$\varepsilon = 6Dd / L^2$ Equation 5.2

Where: σ is flexural stress (MPa), P is load at a given point (N), L is the support span length (mm), b is the width of the sample (mm), d is the thickness of the sample (mm), D is the deflection or extension (mm), and ε is the flexural strain (mm/mm or %).

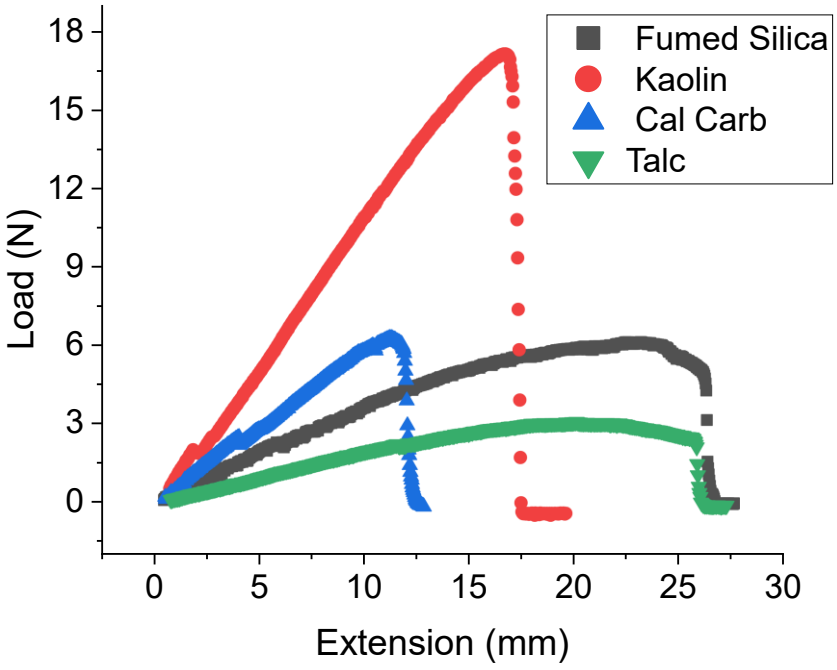

Figure 5.30. Load extension curve produced by the Instron universal testing machine for flexural testing of composites containing 5 phr fumed silica and 30 phr indicated clay, or 15 phr fumed silica.

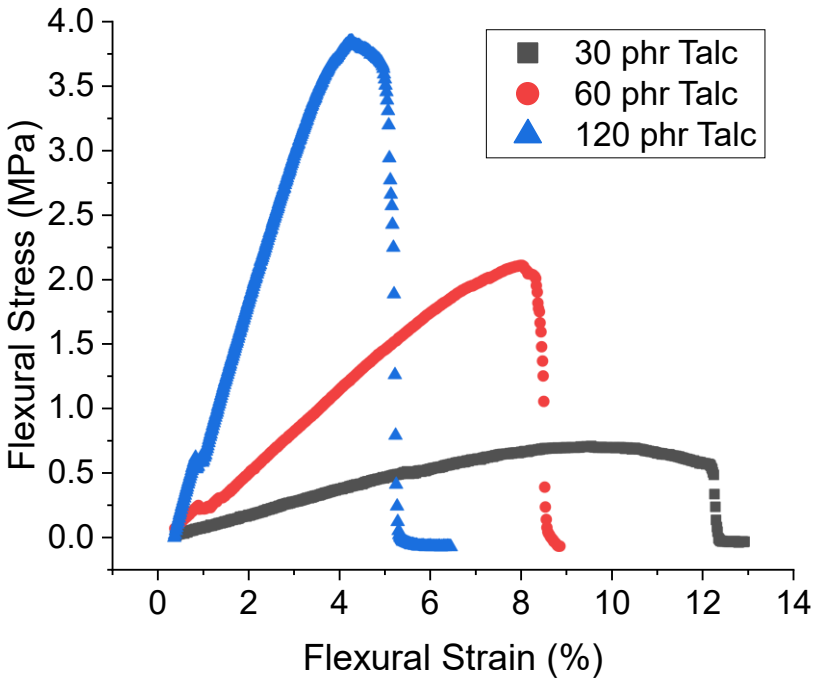

Figure 5.31. Flexural stress-strain curve for composites with 30 to 120 phr talc and 5 phr fumed silica.

It was found that each clay affects the mechanical properties differently, with the highest flexural strength observed with kaolin and the lowest with 30 phr talc. Only in the case of 30 phr talc addition was the flexural strength lower than that of fumed silica alone seen in Figure 5.32. Flexural strength is simply the value of flexural stress at break, or the maximum stress that the material experiences. This is due to the presence of many voids in this composite compared to only fumed silica, which aid in the flexibility of the material but negatively affect its strength. The presence of voids can be seen in Figure 5.33.

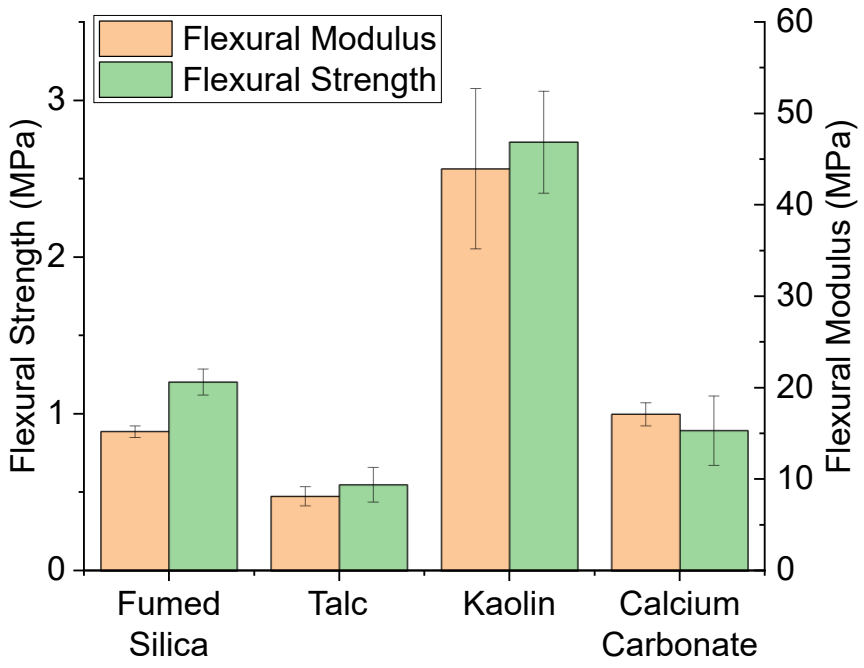

Figure 5.32. Flexural modulus and strength for talc, kaolin, calcium carbonate, and a fumed silica only sample. 30 phr of the clay with 5 phr fumed silica was added or 15 phr fumed silica for the fumed silica sample.

Figure 5.33. Cross section of composite sheets filled with specified filler with noticeable voids in calcium carbonate and talc.

The flexural modulus results in Figure 5.31 show that the addition of 30 phr talc and calcium carbonate reduced the stiffness of the composite, which could be due to more voids present in

these composites compared to the others and fumed silica alone. The flexural modulus was calculated using Equation 5.3 from ASTM D790.

$$E = L^3m / 4bd^3 \qquad \text{Equation 5.3}$$

Where: E is the flexural modulus (MPa), L is the support span (mm), b is the width of the sample (mm), d is the thickness of the sample (mm), and m is the slope of a tangent line for the initial portion of the load-extension curve that occurs as a straight line (N/mm). These straight portions of load-extension curves can be seen in Figure 5.30, where for example the straight line portion for 30 phr talc occurs from 0 to approximately 12.5 extension.

An increase in talc from 30 phr to 120 phr showed significant increases in both the flexural strength and flexural modulus. This was coupled with a decreasing strain at break when increasing the talc loading. The results for increasing talc are shown in Figure 5.34. Increasing filler here results in a stronger material.

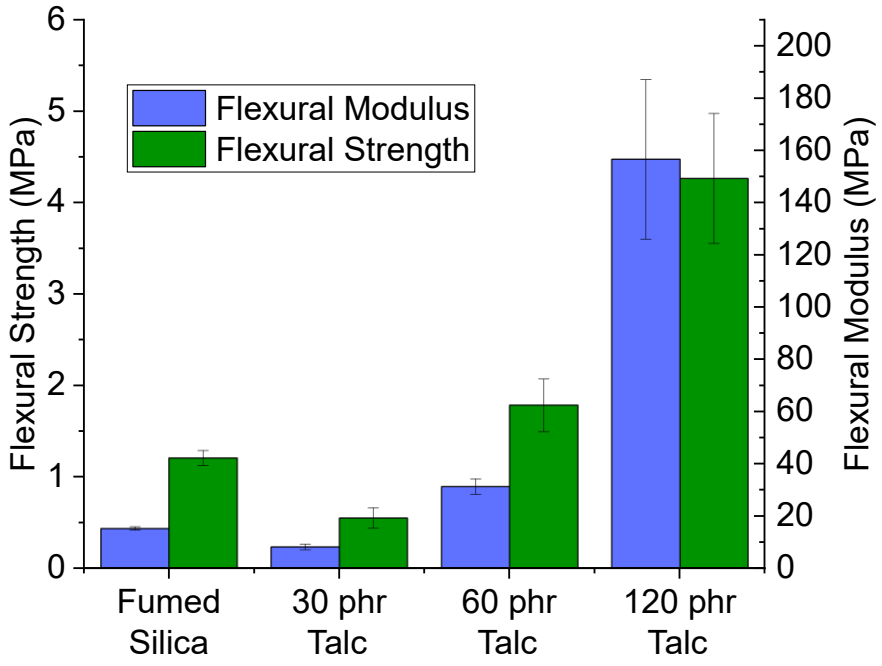

Figure 5.34. Flexural modulus and strength for composites with only fumed silica and composites with 30 to 120 phr talc.

5.8. Addition of Fillers with Differing Thermal Properties

Wood flour and milled carbon fibers were tested to determine the effects of thermal properties on reactivity of the systems. It was found that wood flour, an insulating filler with a higher heat capacity than the clays and milled carbon fibers tested, lowered the front velocity by 100% and front temperature by 26 °C, while the addition of carbon fibers gave an increase in front velocity, as shown in Figure 5.35 with a comparison to the as-received clay fillers studied. It has been reported for FP that adding carbon fibers and other conductive elements will increase front velocities. [9, 22, 113] As seen in Table 5.1, carbon fibers have a thermal diffusivity an order of magnitude higher than wood flour and a higher thermal conductivity. The thermal properties of the carbon fibers aid in the heat diffusion needed to sustain a front, resulting in higher front velocity while maintaining a constant front temperature compared to the fumed silica control. Wood flour's low thermal diffusivity reduces the front velocity and subsequently, the front temperature because the slower front allows for more heat loss.

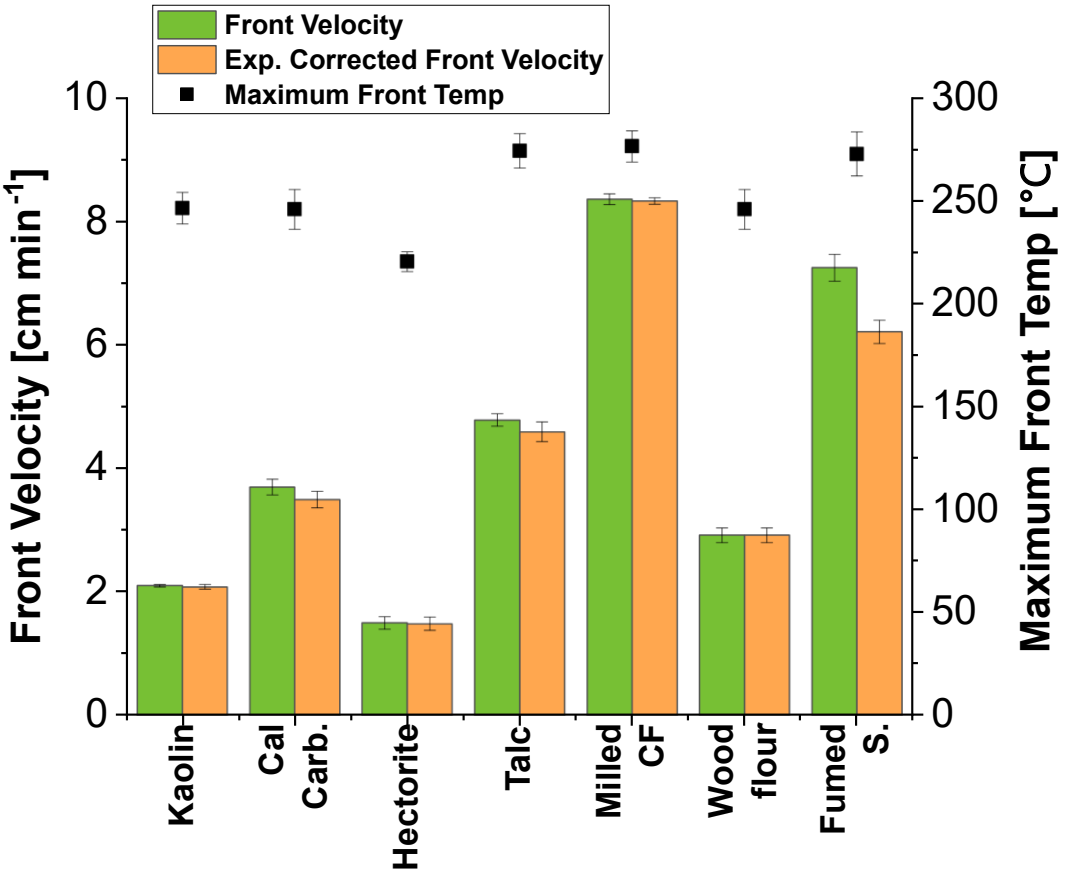

Figure 5.35. Comparison of fillers with differing thermal properties. Samples contained 30 phr shown filler and 5 phr fumed silica added to a resin system of 25 wt% TEGDVE, 75 wt% TMPTE, 1 phr IOC-8 and 1 phr Luperox® 231. "Fumed silica" contained only 5 phr fumed silica added with no other fillers. Front velocities and temperatures are shown. "Milled CF" is milled carbon fiber and "Cal Carb." is calcium carbonate.

5.9. Effect of Filler Dimensions and Sizings

A small study to discern the effects of the aspect ratio and the surface area of fillers was attempted, which is a variable previously indicated worthy of study in frontal polymerization of acrylate formulations with fillers. [22] The aspect ratio is the ratio of length to diameter. Initially, seven fillers were studied: Nyad® G, 10 ES Wollastocoat®, Nyad® 1215 and Fibertec 520S are all produced from wollastonite, a mineral that occurs as needle-like structures. Microglass 7204 and Microglass 9114 are milled e-glass filaments, and FRM is made of mineral wool fibers. The front velocity and temperature results from this study of aspect ratio and surface area are shown

in Figure 5.36 and Figure 5.37. No obvious trend in front velocity or temperature was found with the increasing aspect ratio of these fillers.

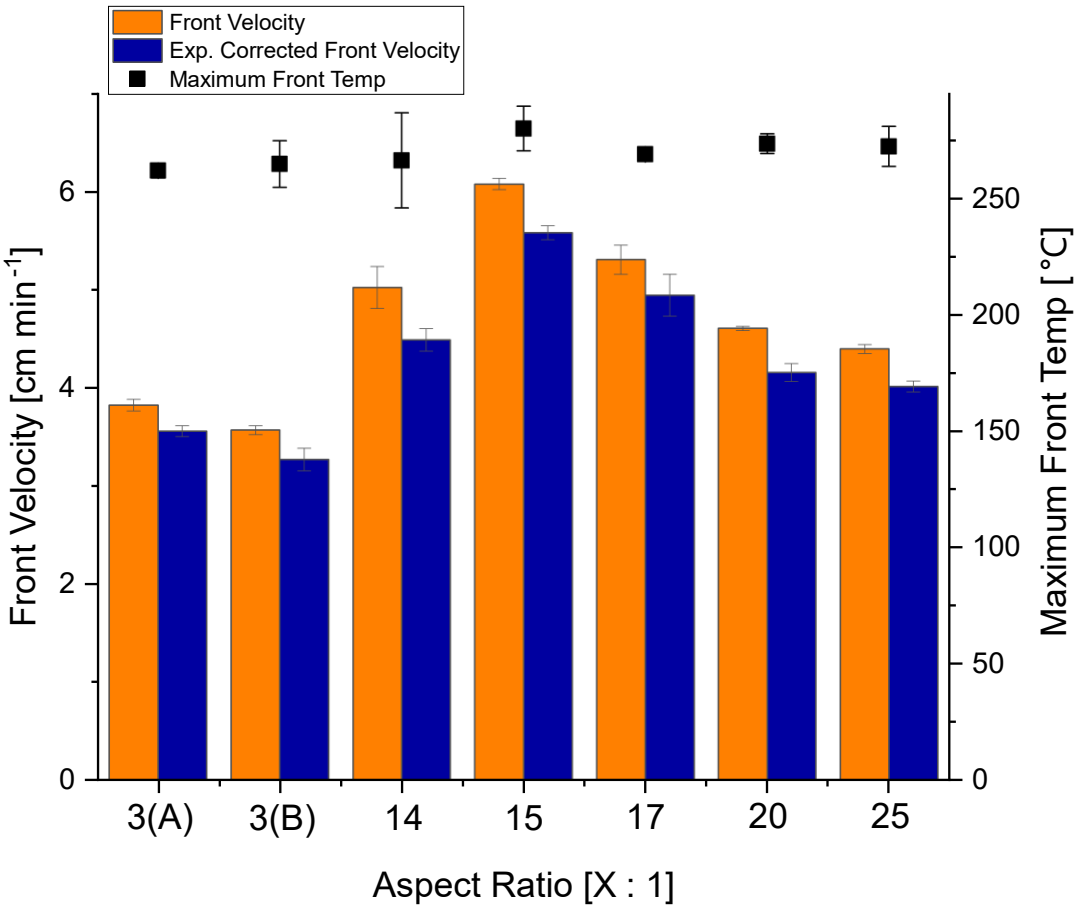

Figure 5.36. Front velocity and temperature as a function of filamentous filler aspect ratios. Resins contained 25 wt% tri(ethylene glycol) divinyl ether and 75 wt% trimethylolpropane triglycidyl ether, with 1 phr (parts per hundred resin) IOC-8 and Luperox® 231. 30 phr of each filamentous filler and 5 phr fumed silica was added (A = Nyad® 1250; B = 10 ES Wollastocoat®).

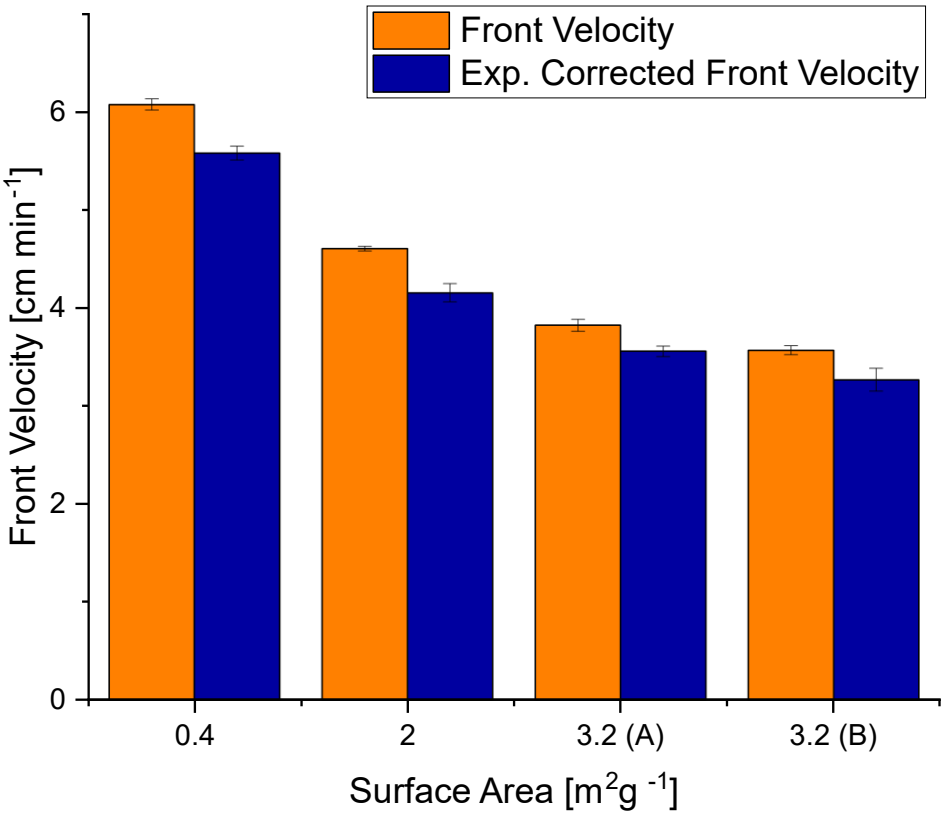

Figure 5.37. Front velocity and temperature as a function of filamentous filler surface area. Resins contained 25 wt% tri(ethylene glycol) divinyl ether and 75 wt% trimethylolpropane triglycidyl ether, with 1 phr (parts per hundred resin) IOC-8 and Luperox® 231. 30 phr of each filamentous filler and 5 phr fumed silica was added (A = Nyad® 1250; B = 10 ES Wollastocoat®).

There are two issues potentially affecting these results. The surface area of every filler is not known, but for the known fillers, surface area may play a greater role than aspect ratio. When arranging the results of fillers with known surface area, it is seen that front velocity decreases as surface area increases. This could be due to the chemistry of the fillers' surfaces inhibiting the cationic polymerization or differences in thermal properties of the filamentous fillers. Many of these filamentous fillers are surface treated, which could be affecting propagation. The chemical composition of many surface treatments or sizings is not provided by the manufacturer and the

fillers with known surface area that were studied have different sizings, as shown in Table 5.5 below which also lists their filamentous physical properties.

Table 5.5. Aspect ratio, surface area and sizing chemistry of filamentous fillers.

	Aspect Ratio (*l*:*d*)	Surface Area (m^2 g^{-1})	Sizing (Coating)
Nyad® G[a]	15:1	0.4	None
Nyad® 1250[a]	3:1	3.2	None
10 ES Wollastocoat®[a]	3:1	3.2	Surface-modified, chemistry NP
Fibertec 520S[a]	20:1	2	Aminosilane
Fibertec Microglass 7204[a]	17:1	Not provided	Cationic
Fibertec Microglass 9114[a]	14:1	Not provided	Aminosilane
Fibertec FRM[a]	25:1	Not provided	None

[a]Provided by manufacturer, some data not provided

Due to the potential issues with chemical treatment of the filamentous fillers, six different fillers were obtained from Imerys S. A. that had no treatment and therefore would not inhibit the cationic polymerization. The samples all had different surface areas and aspect ratios which can be found in Table 5.6. These samples are all wollastonites, but the brand names of each are unknown. The physical properties of the polymers with every wollastonite were similar, however resins with A, B, C, E had a much higher viscosity than resins with D and F added. Additionally, to achieve a similar viscosity to formulations with clays, 10 phr fumed silica was added instead of only 5 phr.

Table 5.6. Aspect ratio and surface area of wollastonite samples tested with RICFP.

Wollastonite Sample	Aspect Ratio (*l*:*d*)	Surface Area (m^2 g^{-1})
A	3:1	3
B	8:1	0.9
C	3:1	2.9
D	15:1	0.4
E	3:2	3.2
F	13:1	1.4

The front velocity and temperature for each formulation with the wollastonite sample added is shown with respect to increasing surface area in Figure 5.38. For surface area, the front velocity decreases as the surface area increases, which is similar to what is seen above for the wollastonites that have chemical sizings. This implies that the surface chemistry of the wollastonite is interfering with the polymerization. There is one report which examined adsorption of poly(methyl methacrylate) and stearic acid onto wollastonite, and found that adsorption of stearic acid was strong which was hypothesized to be due to hydroxyl groups on the surface of the wollastonite. [114] If the hydroxyl groups are present as implied, this could explain the decreasing front velocity due to surface interactions of the growing polymer chain with the hydroxyl groups—as the surface area increases the number of these interactions would be increased and hence the front velocity would be lower as shown with previous results of chain transfer reactions affecting fronts.

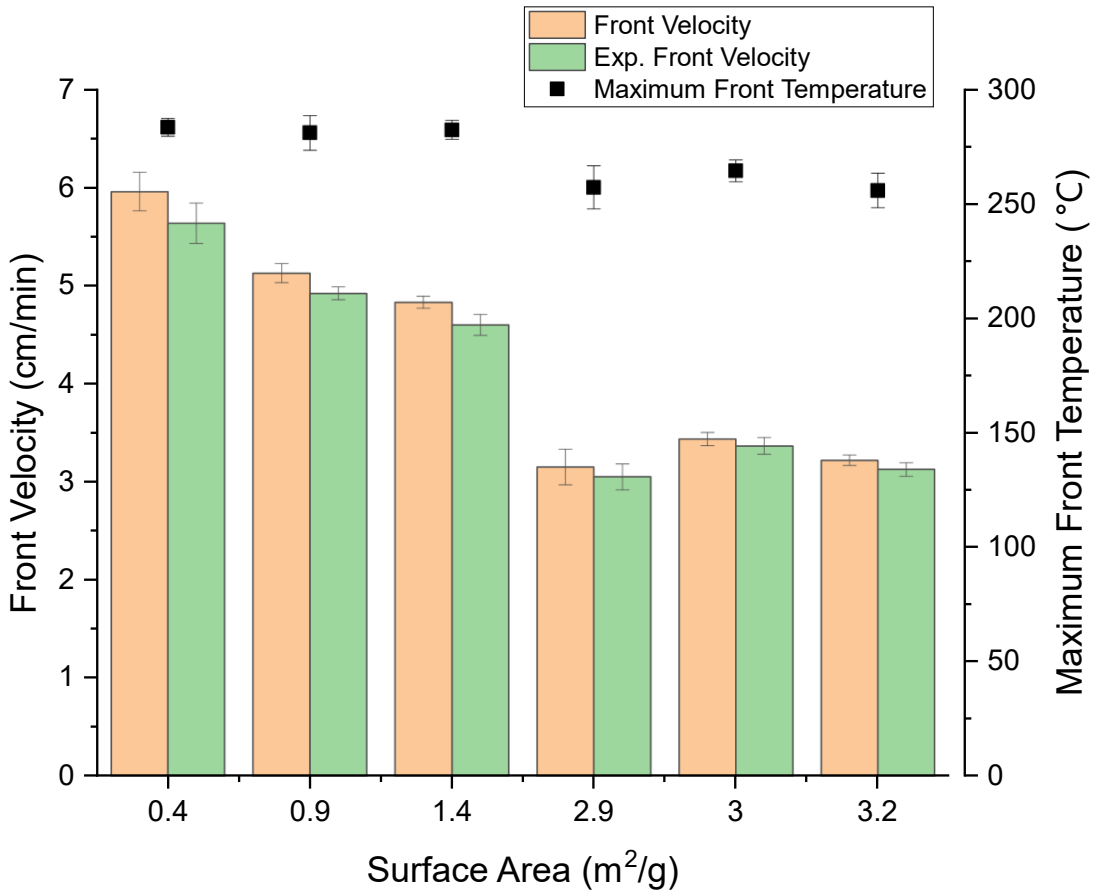

Figure 5.38. Front velocity and temperature as a function of filamentous filler surface area for untreated wollastonite samples. Resins contained 25 wt% tri(ethylene glycol) divinyl ether and 75 wt% trimethylolpropane triglycidyl ether, with 1 phr (parts per hundred resin) IOC-8 and Luperox® 231. 30 phr of each wollastonite and 10 phr fumed silica was added. "Exp. Corrected Front Velocity" is velocity corrected for sample expansion during front propagation.

Regarding the aspect ratio, the front velocity and temperature increased as the aspect ratio increased in Figure 5.39. Within the range of aspect ratios studied, this also follows similar results to the previous tests of treated wollastonites, which saw an increase in front velocity from 3 to 15 and decrease from 15 to 25. One hypothesis of the front velocity increase is that the higher aspect ratio fillers may be large enough to hinder the crosslinked structure and increase the mobility of active chain ends which results in a higher polymerization rate. [81]

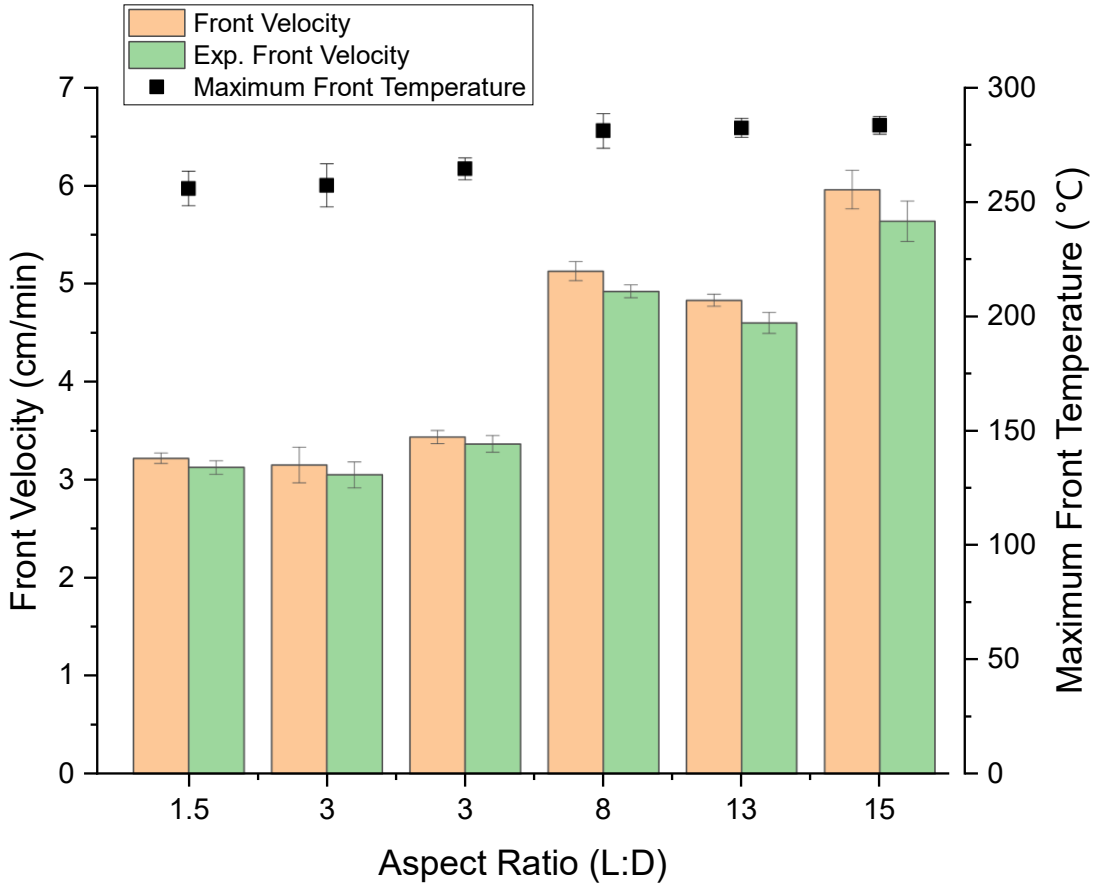

Figure 5.39. Front velocity and temperature as a function of filamentous filler aspect ratio for untreated wollastonite samples. Resins contained 25 wt% tri(ethylene glycol) divinyl ether and 75 wt% trimethylolpropane triglycidyl ether, with 1 phr (parts per hundred resin) IOC-8 and Luperox® 231. 30 phr of each wollastonite and 10 phr fumed silica was added. Samples with aspect ratio of 3 were arranged in increasing surface area.

5.10. Effects of Initiator Concentrations and Vinyl Ether Content

Samples with talc, Ca-bentonite and kaolin were tested with differing amounts of TEGDVE and initiators. Given the ability for clays to show radical-scavenging behavior, [22] it was suspected that increasing initiator concentrations in the presence of clay would result in smaller increases in front velocity than samples with no clay. To study the increases in front velocity, the slope of the linear trendline for front velocity versus Luperox® 231 concentration was determined for samples with and without clays. The compiled data from this study are shown in Table 5.7. From

a graph of front velocity for fumed silica and talc with fumed silica samples with increasing Luperox® 231 concentration from 0.5 phr to 1.5 phr shown in Figure 5.40, it was found that the slope of the linear trendline for the front velocity in fumed silica only samples was 1.94 (cm min^{-1} phr^{-1}), and the slope of expansion corrected front velocity was 1.51 (cm min^{-1} phr^{-1}). For talc samples, the front velocity and expansion corrected front velocities were 1.52 (cm min^{-1} phr^{-1}) and 1.47 (cm min^{-1} phr^{-1}), respectively. The similarity in front velocity after expansion correction implies that radical scavenging is not the primary source of propagation inhibition with talc.

Table 5.7. Slope of trendlines of front velocity and exp. corrected front velocity versus increasing Luperox® 231 concentration for different clays.

	Front Velocity vs Luperox® 231 Concentration (cm min^{-1} phr^{-1})	Exp. Corrected Front Velocity vs Luperox® 231 Concentration (cm min^{-1} phr^{-1})
Fumed silica[a]	1.94	1.51
Fumed silica[b]	2.29	2.51
Ca-bentonite[b]	1.46	1.27
Talc[a]	1.52	1.47
Kaolin[a]	0.81	0.80

[a]Luperox® 231 concentration increased from 0.5 phr to 1.5 phr
[b]Luperox® 231 concentration increased from 1.0 phr to 2.0 phr

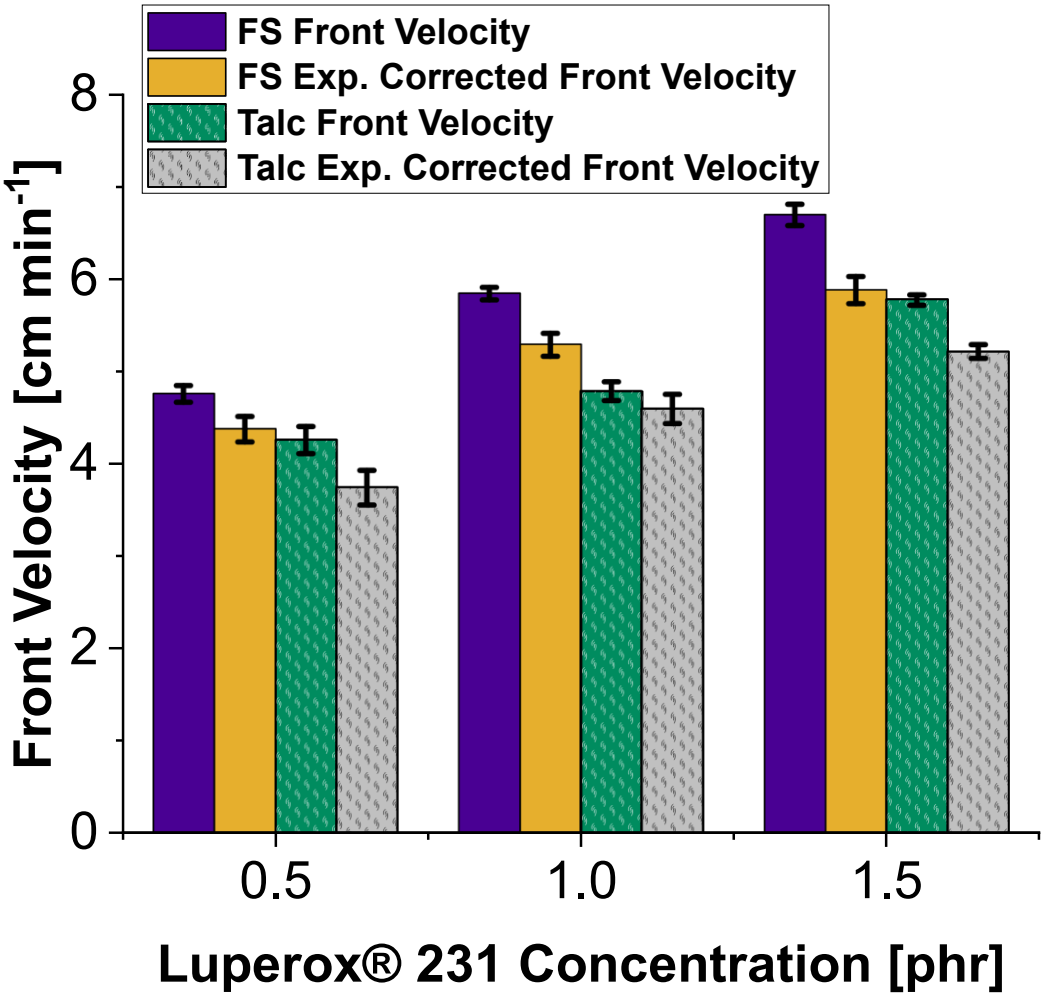

Figure 5.40. Effect of increasing Luperox® 231 concentration on front velocity for formulations containing 25 wt% TEGDVE, 75 wt% TMPTE and 1 phr IOC-8. Samples contained 10 phr fumed silica (FS) or 5 phr fumed silica with 30 phr talc.

In the case of Ca-bentonite and kaolin, the slope of the trendline of increasing front velocity versus Luperox® 231 for these clays is nearly half that of samples with only fumed silica. The graphs of front velocity versus radical initiator concentration are shown in Figures 5.41 and 5.42 for Ca-bentonite and kaolin. Ca-bentonite has been previously shown to affect free-radical FP through potential radical inhibition and low thermal diffusivity. [22] A front after adding Ca-bentonite was not supported with 1.0 phr IOC-8 and 0.5 phr Luperox® 231; therefore, an

increasing Luperox® 231 range of 1.0 phr to 2.0 phr was chosen. The lower slope of Ca-bentonite in this study indicates either radical inhibition or low thermal diffusivity.

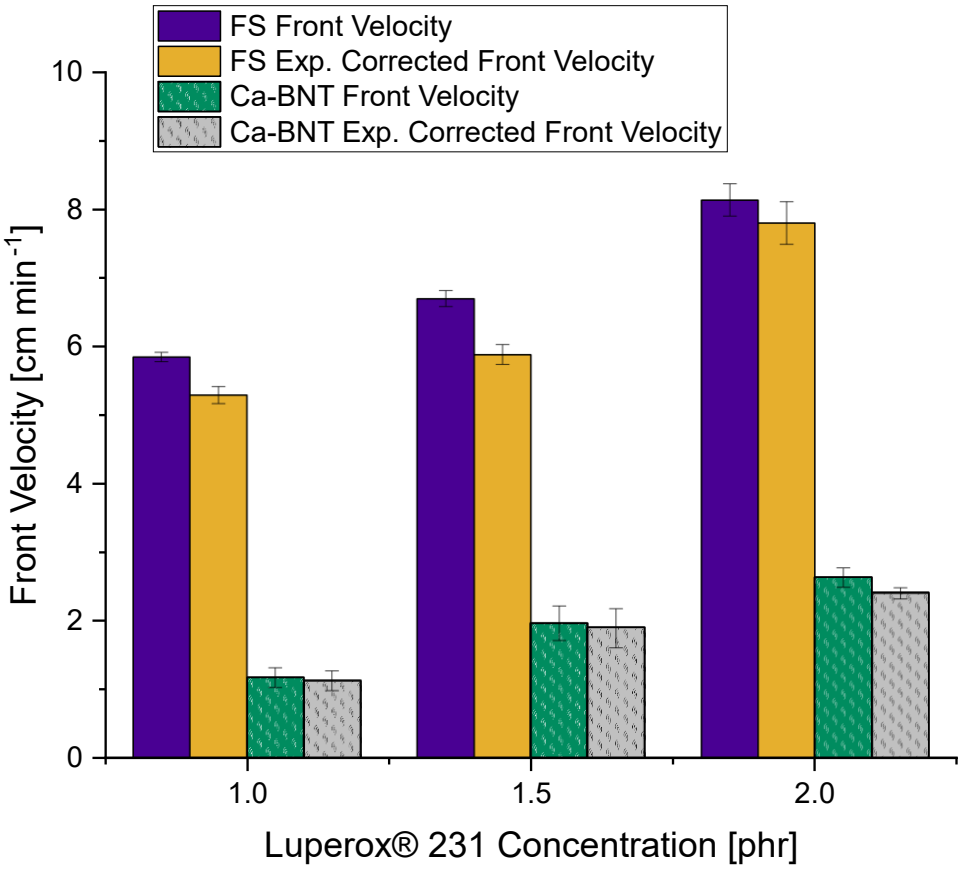

Figure 5.41. Effect of increasing Luperox® 231 concentration on front velocity for formulations containing 25 wt% TEGDVE, 75 wt% TMPTE and 1 phr IOC-8. Samples contained 10 phr fumed silica (FS) or 5 phr fumed silica with 30 phr Ca-bentonite. “Ca-BNT” is Ca-bentonite.

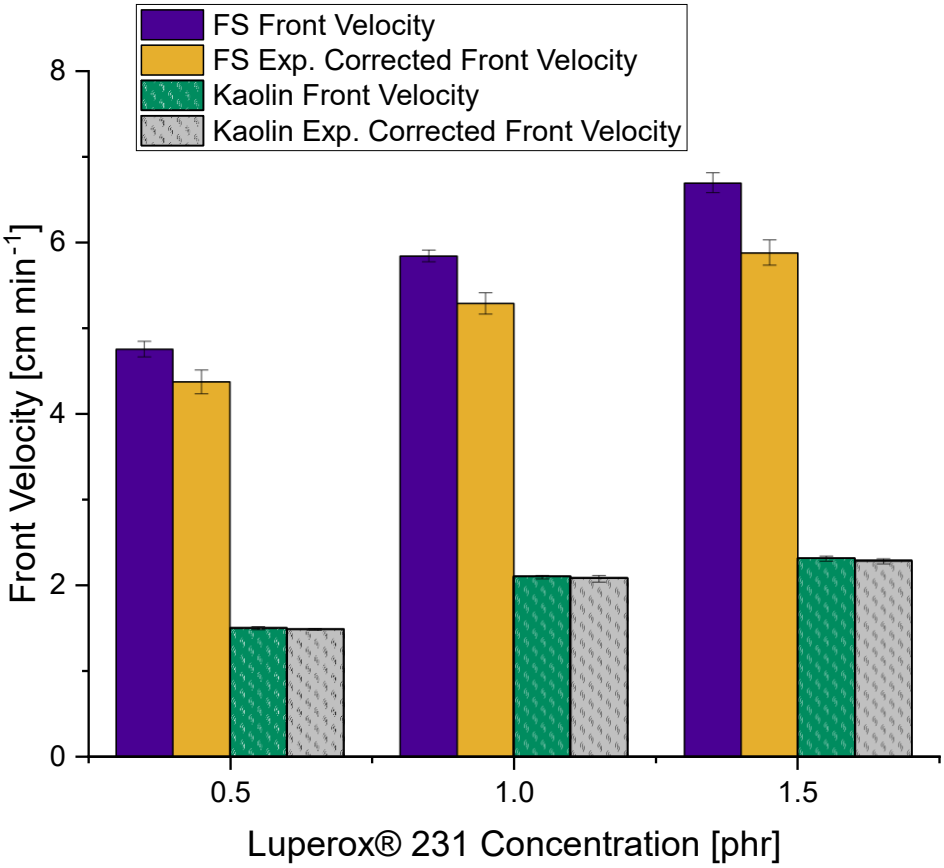

Figure 5.42. Effect of increasing Luperox® 231 concentration on front velocity for formulations containing 25 wt% TEGDVE, 75 wt% TMPTE and 1 phr IOC-8. Samples contained 10 phr fumed silica (FS) or 5 phr fumed silica with 30 phr kaolin.

Kaolin and talc have previously been shown to be inert in free-radical FP systems. [22] The front velocity for kaolin is nearly half that of talc in RICFP systems which, with their similar thermal properties, shows potential chemical inhibition. Although previously shown to be inert in free-radical FP, the slope of the trendline of increasing radical initiator concentration was much less after adding kaolin. This could indicate that the mechanism of inhibition with kaolin is through interaction with free-radicals, contrary to previous work which contrasted kaolin, talc, calcium carbonate and bentonite.

With 0-100% TEGDVE/TMPTE, shown in Figure 5.43, an overall increase in front velocity for samples containing talc was observed with the increasing TEGDVE content, which is an expected trend. [99] At 25% TEGDVE, the front velocity did decrease, which was also observed in previous reports. [99] For samples with hectorite, a front was not supported with 100% TMPTE and no TEGDVE though a localized reaction occurred upon application of heat. This could be attributed to the low reactivity of TMPTE relative to vinyl ether and the low thermal diffusivity of hectorite, in addition to the high water content of hectorite contributing to heat loss and inhibition of the cationic mechanism. Given that talc would support a front with only TMPTE and the initiators, this is suspected to be a result of the unique chemistry of the hectorite.

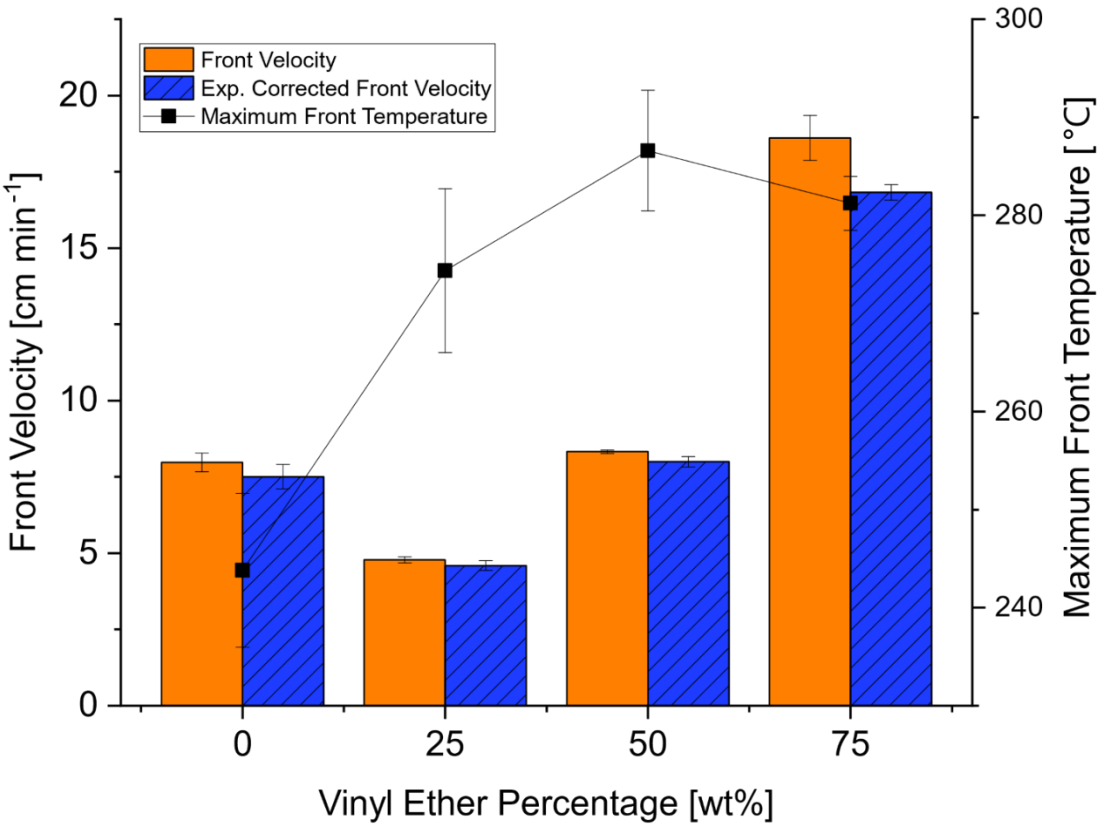

Figure 5.43. Front velocity and temperature as a function of TEGDVE percentage. Resins contained specified wt% TEGDVE and remainder wt% TMPTE, with 1 phr (parts per hundred resin) IOC-8 and Luperox® 231, and 30 phr talc with 5 phr fumed silica.

5.11. Spontaneous Polymerization Induced by Montmorillonite K10

Montmorillonite K10 (MMT K10), an acid-treated bentonite clay, was able to initiate polymerization in the absence of any applied external energy, resulting in many localized fronts in the material in Figure 5.44. The rapid initiation, with a decreasing onset time as MMT K10 loading is increased, is contrary to previous reports of filler addition in free-radical FP. [22] This is attributed to the acidic character of the clay, as it is well known that vinyl ethers and other monomers will polymerize upon addition of acid; [61] acid-treated montmorillonites have also been used as catalysts for cationic polymerizations and organic reactions. [115-117] It was found that a minimum of 10 phr MMT K10 was needed to initiate polymerization. With free-radical FP, MMT K10 and other acid-treated clays were shown to inhibit the FP process or even quench it at high loadings[22], while in this case for cationic monomers, the acidic character is resulting in the initiation of polymerization.

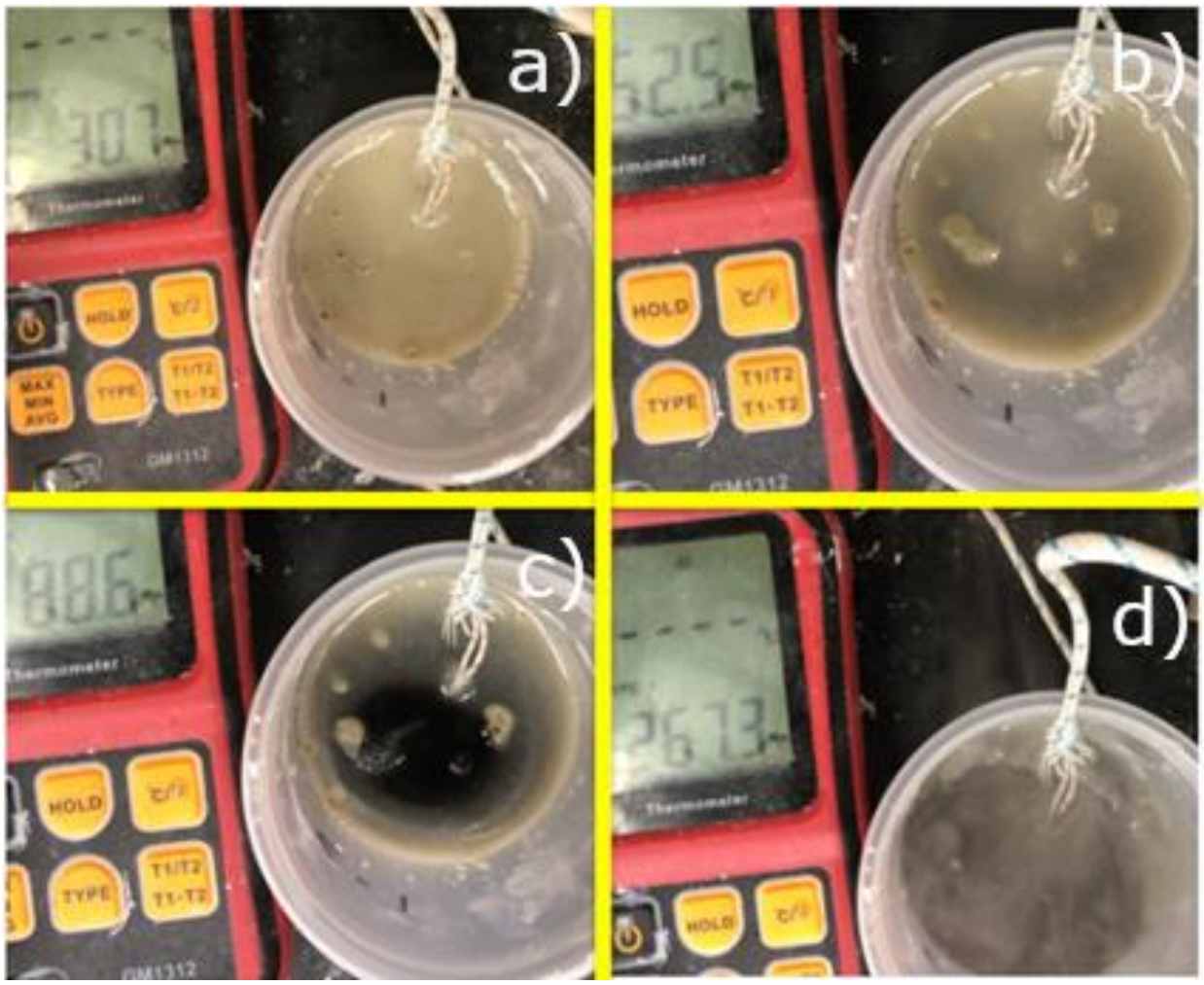

Figure 5.44. Spontaneous polymerization over time of a 25 wt% TEGDVE, 75 wt% TMPTE and 1 phr IOC-8 with 1 phr Luperox® 231 formulation via addition of MMT K10. The time intervals shown are: a) 80 seconds; b) 335 seconds; c) 435 seconds; d) 465 seconds.

Increasing the ratio of talc to MMT K10 resulted in a prolonged initiation time. Drying the clay with the above mentioned procedure did not affect the starting time. A similar result was achieved by Gary et al., who saw that the front velocity of acrylates was unaffected by the drying of Fulcat® 435, another acid-activated clay. [22] The addition of fumed silica also did not significantly affect the pot life. The initiation time based on drying and talc addition is shown in Figure 5.45. Observing the front velocity of high loadings of MMT K10 was unachievable, given

the short pot life until spontaneous polymerization. Likewise, with these formulations it was impossible to predict the starting location of a front, making the propagation difficult to track.

To confirm that this phenomenon is due to acid treatment and not another property of the clay, tests on identical samples were carried out but Fulcat® 435, another acid treated clay, was added. The addition of this clay also resulted in spontaneous polymerization. Additions of other untreated clays did not show spontaneous polymerization.

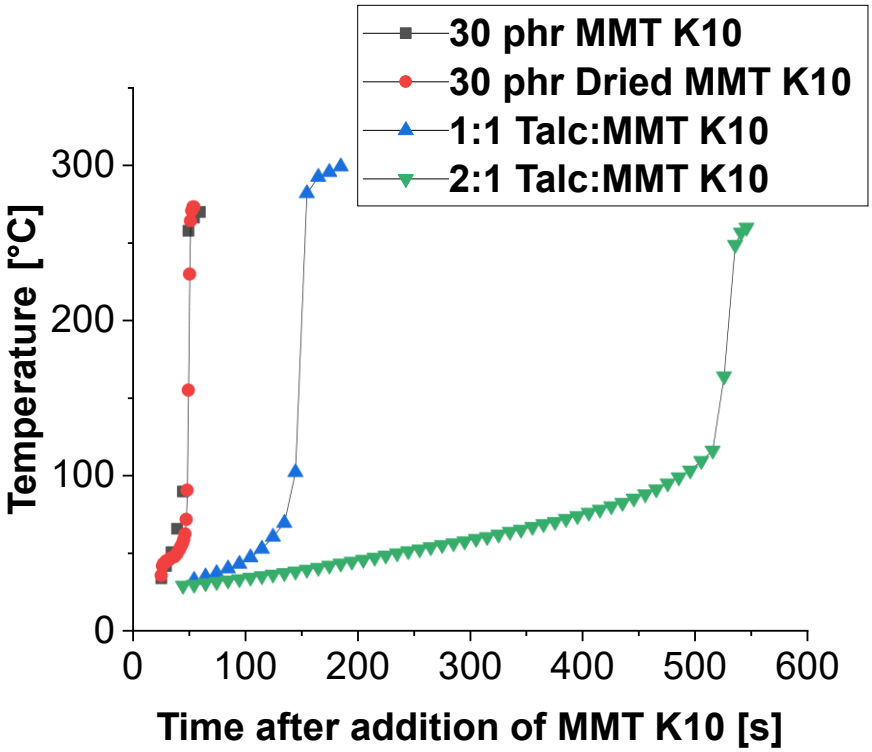

Figure 5.45. Effects of talc and MMT K10 addition along with drying on the pot life of 25 wt% TEGDVE, 75 wt% TMPTE with 1 phr IOC-8 and 1 phr Luperox® 231 formulations.

Formulations containing only TMPTE and MMT K10 did not exhibit spontaneous polymerization within similar timespans. This indicates that interactions between the vinyl ether and MMT K10 are causing the polymerization. The nucleophilic double bonds of vinyl ethers are known to be easily protonated. [60] Like the concept of kick-starting in photopolymerized vinyl

ether-epoxy blends, [72, 76] the vinyl ether reactivity drives the polymerization to occur upon protonation via MMT K10.

5.12. Conclusions and Future Outlook

The effects of adding fillers, with a focus on clay minerals, to a resin system of epoxy (TMPTE) and vinyl ether (TEGDVE), which undergoes RICFP through combination of an iodonium salt (IOC-8) and peroxide-based free-radical thermal initiator (Luperox® 231) were investigated.

Multiple clay minerals were tested for their viability in RICFP and effects on front velocity and temperature. Talc, kaolin, hectorite, and Ca-bentonite all supported fronts for epoxy vinyl ether blends when added in 30 phr amounts (with 5 phr fumed silica as a viscosifier), while Na-bentonite did not support a front. Calcium carbonate was also used, though it is not a clay mineral, because there was an interest in studying its viability as a basic compound in a cationic system. Compared to a control containing only 5 phr fumed silica with the resin, these fillers all reduced the front velocity of the system by different amounts compared to previous studies of clays in free-radical FP. Talc reduced the front velocity the least and Ca-bentonite reduced it the most. The clays have similar thermal properties; therefore, we conclude that the fillers are affecting the polymerization mechanism.

Increasing loadings of talc and hectorite reduced front velocity, which is attributed partially to the fillers acting as heatsinks. It was determined that viscosity has little effect on the front velocity through increasing loading of only fumed silica in the resin system. After correcting for expansion of the material, the front velocity exhibited a weak dependence on fumed silica loading. This also confirms that the differing front velocities with the clays are not due to differing viscosities.

Drying the clay fillers results in a higher front velocity than non-dried clays. This is due to the presence of water absorbing heat and contributing to heat loss in the system, reducing front velocity. Calcium carbonate, which had low measured water content, gave the same velocity after drying, indicating that water content for the other fillers is affecting the front velocity through heat loss. Additionally, drying can free up acid sites in clay minerals which could catalyze the RICFP process.

The effects of adding wood flour and carbon fibers were tested. Carbon fibers are conductors with a thermal diffusivity much higher than wood flour. Carbon fibers increased the front velocity when added, like previously published work for FP, [9, 22] but wood flour decreased the front velocity. This highlights the importance of choosing fillers with thermal properties that benefit front propagation.

It was also found that increasing vinyl ether percentage relative to epoxy would increase the front velocity, as expected. Notably, samples with hectorite would not support a front with only epoxy (TMPTE) and no vinyl ether. Increasing Luperox® 231 concentration was also studied in formulations with and without talc, Ca-bentonite and kaolin. It was expected that if radical scavenging was the main mechanism of decreasing front velocity, the rate of front velocity change over the increasing concentrations would be higher without talc, since it would scavenge radicals. There was a negligible difference in the rate of front velocity change over increasing Luperox® 231 concentration, which implies that radical scavenging is not the main source of suppressed propagation with talc. In the case of Ca-bentonite and kaolin, the rate of front velocity change over the increasing radical initiator concentration was nearly half that of samples without clay. This indicates potential radical inhibition with these two clays, which is expected in the case of Ca-bentonite but not kaolin.

Finally, it was seen that adding montmorillonite K10, an acid-treated bentonite clay, would cause formulations to spontaneously polymerize and show small, localized fronts. This only occurred if vinyl ether was present in the system, which is attributed to the acid character of the clay reacting with the highly nucleophilic vinyl ether. Neither drying the clay nor adding fumed silica influenced the start time of this polymerization.

Knowledge of the effects of different fillers on FP is important for the development of composite materials using epoxy or vinyl ether resins. Fillers can have different effects upon RICFP rather than free-radical FP. It was shown that choosing the correct filler entails a balance of thermal properties, chemical effects and water content. Some fillers are surface treated which could interfere with propagation, such as filamentous fillers with sizings. Care must be taken to ensure that there are no modifications to the fillers to adversely affect the pot life and kinetics of RICFP systems. The chemistry of clays is complicated and more detailed studies of the differences between clays in terms of structure could provide more insight into optimization of frontal polymerization of filled resins.

CHAPTER 6. CATIONIC FRONTAL POLYMERIZATION WITH NO PRIMARY RADICAL SOURCE

6.1. Introduction to the Role of Onium salts in RICFP

Most notably, RICFP has been used for the polymerization of epoxy resins, which are ubiquitous in practical applications. [37] The addition of vinyl ethers to epoxies has been shown to increase the front velocity, [99] following similar results for bulk photopolymerizations. [48, 76]

There is minimal literature describing FP of cationically-cured monomers through procedures that do not employ RICFP. Scognamillo et al. [21, 34] studied the frontal curing of epoxides with BF_3-amine complexes, Chekanov et al. [35] observed FP of epoxies using an aliphatic amine curing agent, and Pojman et al. [74, 75] used a BCl_3-amine complex with the aliphatic amine curing agent in hybrid systems of epoxy and acrylates. Lecompère et al. [72] published that FP of epoxies is viable through thermal or UV initiation in the presence of a pyrylium salt/vinyl ether coinitiator mixture. They saw small additions of vinyl ether have a "kick-starting effect" raising the reaction rate of the less reactive cycloaliphatic epoxy monomer. In addition, the group studied the effects of pyridine delaying premature reactions in solutions containing only pyrylium salts and epoxides. [118] In studies by Crivello, [50, 119, 120] thermally-initiated FP of oxetanes and alkyl glycidyl ethers was possible with iodonium antimonate salts, but the FP would only propagate in areas that were previously irradiated by UV, and the front would stop at the boundary of these areas.

In their initial discovery of RICFP, Mariani et al. [36] demonstrated that front propagation was possible using an iodonium hexafluoroantimonate salt with dibenzoyl peroxide, but not with

---

This chapter was previously published as B. R. Groce, M. M. Ferguson, J. A. Pojman. Thermally Initiated Cationic Frontal Polymerization of Epoxies and Vinyl Ethers Through a Lone Iodonium Salt. Journal of Polymer Science, 2023, 1. Reprinted with permission from Wiley.

the iodonium salt alone. Therefore, in most cases in the literature it is generally reported that photoacid generating salts and TRIs are required for FP; there are no studies showing that FP is possible through addition of only iodonium salts without prior irradiation. With the specificity needed for TRI selection and the potential for gas production during polymerization with peroxides, a system that does not require a TRI would be advantageous to future developments in cationic FP.

There is a report from 1996 that found that superacid is generated upon decomposition of a diaryliodonium salt with tetrafluoroborate and hexafluorophosphate counterions. [121] They measured acid generation by pyrolysis of the salts at 250 ℃ for 20 minutes and titration of the resulting product with NaOH. It was found that an average 1.97 equivalents superacid was formed from the diaryliodonium hexafluorophosphate and 1.36 equivalents superacid from the diaryliodonium tetrafluoroborate salt. They also heated the salt at 239 ℃ for 15 minutes and analyzed the composition of the solution with gas chromatography mass spectrometry. The two major products by percent composition were iodobenzene and fluorobenzene, though they identified many more products and explained their formation with Figure 6.1 below adapted from their work.

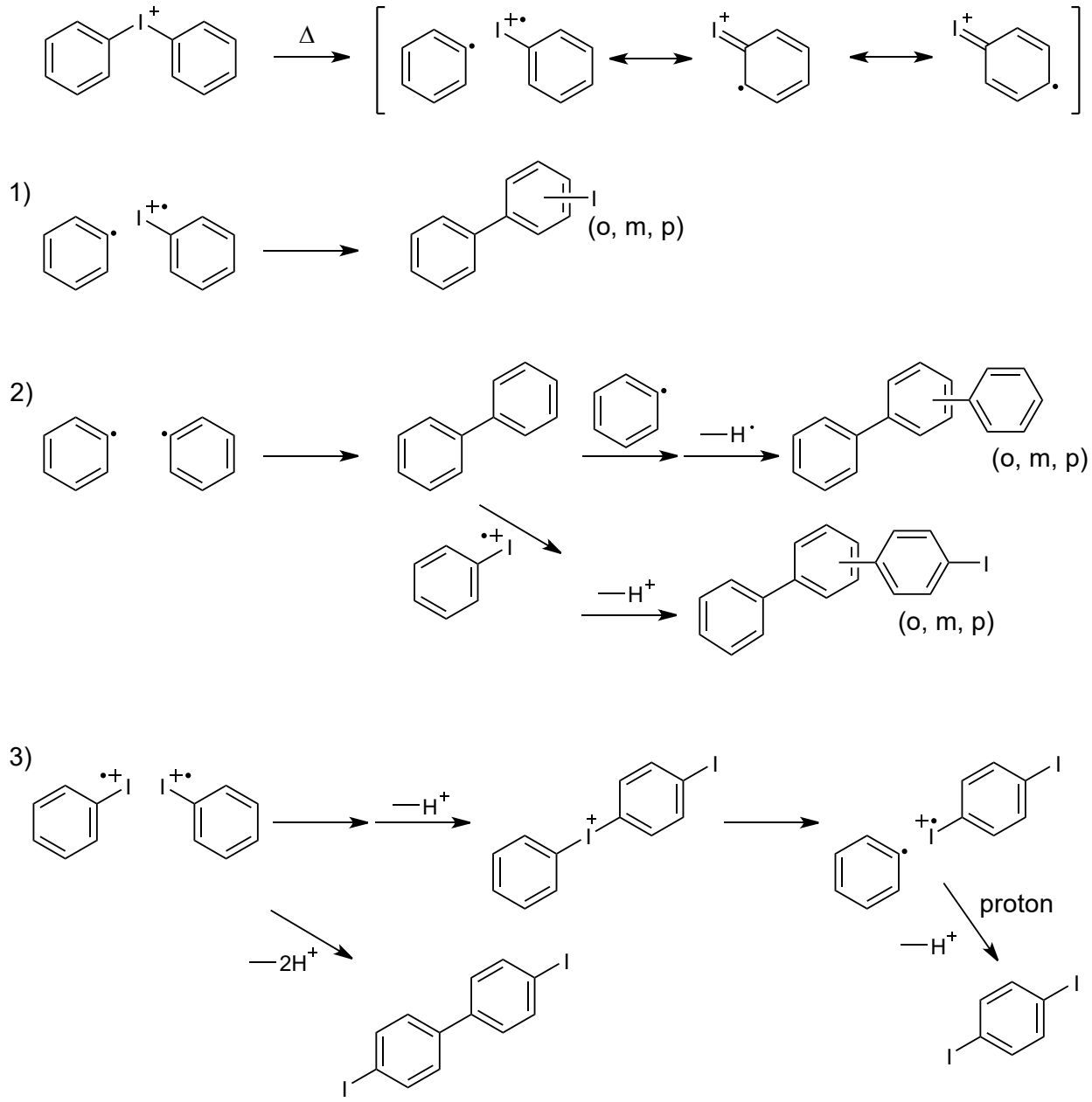

Figure 6.1. Proposed mechanism of diaryliodonium salt thermal decomposition adapted from McEwen et al. (1996).

In the Figure 6.2, which is also adapted from their work, they explain the formation of the fluorobenzene, which is shown from a hexafluoroantimonate source to better fit the work in this dissertation. This is thought to happen as a nucleophilic aromatic subsitution that competes with

the initial homolytic cleavage of the salt, and a fluoride ion from the counterion attacks the diaryliodonium ion to generate fluorobenzene.

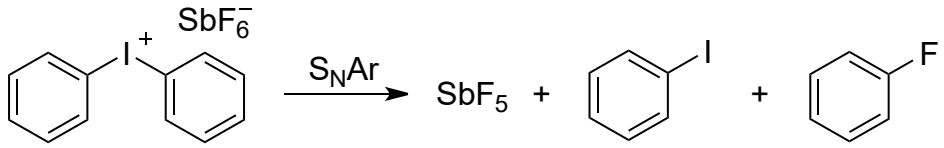

Figure 6.2. Formation of fluorobenzene in thermal decomposition of a diaryliodonium hexafluoroantimonate salt proposed by McEwen et al. (1996).

The acid generation of the diaryliodonium salts at 250 ℃ follows a result shown in a thesis by Taschner in 2023. [122] In the thesis, a DSC scan from 25 ℃ to 350 ℃ at a rate of 10 K min^{-1} of a resin consisting of 80 mol% BADGE and 20 mol% 1,6-hexanediol diglycidyl ether with 1 mol% IOC-8 was conducted. The onset temperature of the exothermic polymerization reaction was gathered by the DSC thermocouple and determined to be 217 ℃. This polymerization would only be possible if the IOC-8 was decomposing to form the superacid initiating species. Regarding the ~30 ℃ difference, it could be that decomposition of the diaryliodonium hexafluorophosphate and tetrafluoroborate studied by McEwen et al. [121] occurs at a higher temperature, or was occurring in a range rather than specifically at 250 ℃ that was studied.

With the evidence that superacid can be generated by heat, this chapter seeks to determine if a front can be initiated and sustained with thermal decomposition of IOC-8 at the front temperature. The IOC-8 concentration and composition of formulations was studied, along with front viability of different epoxies and vinyl ethers. To give some insight into the mechanism behind decomposition of IOC-8 and confirm that the radical and radical-cation species described by McEwen et al. [121] are formed, a free-radical inhibitor (MeHQ) was added to see the effects on the front kinetics.

6.2. Materials and Methods of Cationic Frontal Polymerization with No Radical Source

In this chapter, many different epoxies and vinyl ethers were studied. The epoxies used were trimethylolpropane triglycidyl ether (TMPTE), neopentyl glycol diglycidyl ether (NPDGE), bisphenol-A diglycidyl ether (BADGE), and 3,4-epoxycyclohexylmethyl-3’,4’-epoxycyclohexane carboxylate (CE). Tri(ethylene glycol) divinyl ether (TEGDVE) and 1,4-cyclohexanedimethanol divinyl ether (DVE-1,4) were tested as vinyl ethers. p-(octyloxyphenyl)phenyliodonium hexafluoroantimonate (IOC-8) was the superacid generator used. For comparison with systems that employ thermal radical initiators, benzopinacol (TPED) and 1,1-bis(tert-butylperoxy)-3,3,5-trimethylcyclohexane (Luperox 231, L231) were used. Aerosil E805 fumed silica was used as a viscosity enhancer. Dodecanol and 4-methoxyphenol (MeHQ) were used in the study of radical inhibitors. All chemicals were used as received with no purification. Chemical structures of the monomers and initiators used are shown in Figure 6.3.

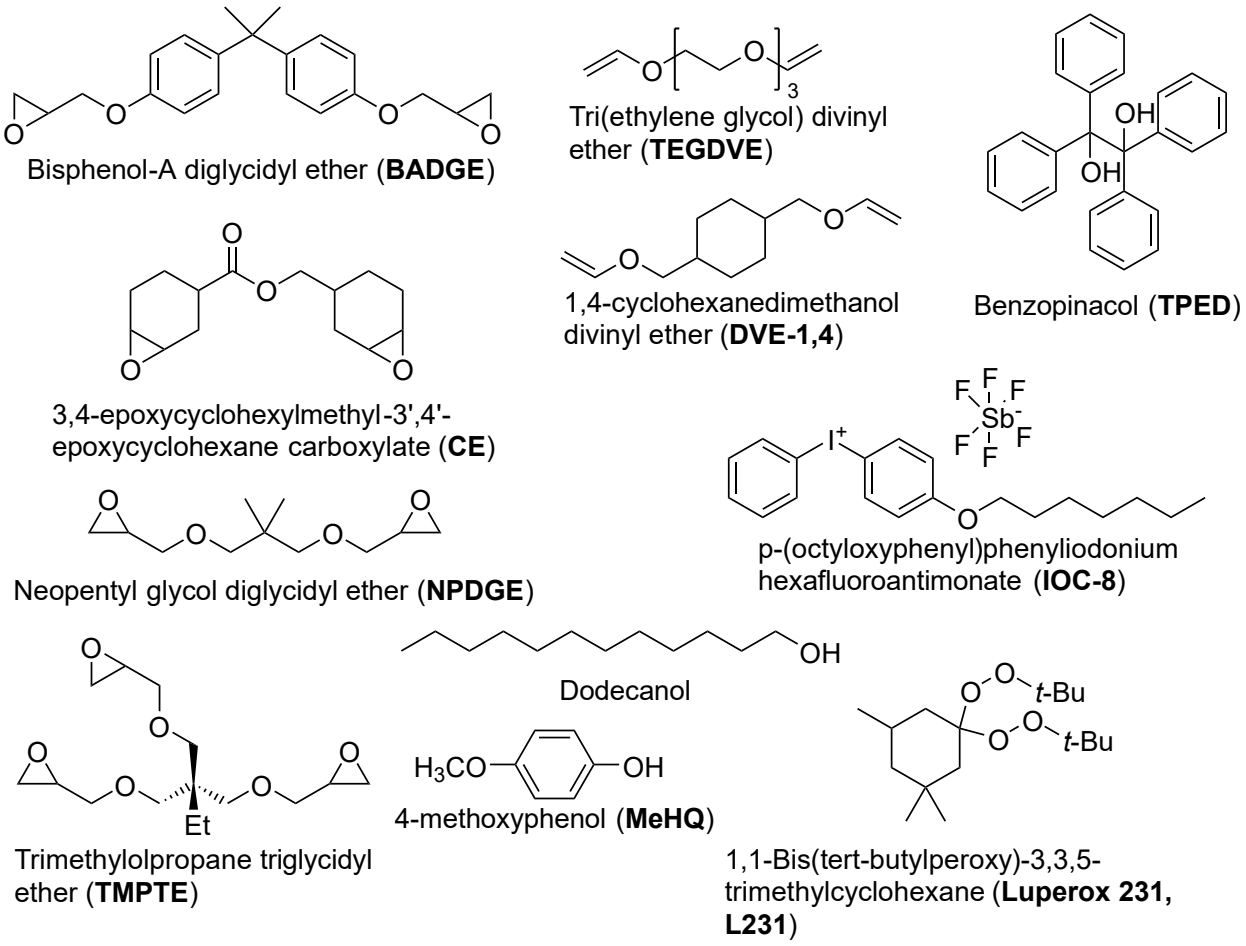

Figure 6.3. Structures and abbreviations of chemicals used in this chapter.

6.2.1 Formulation Preparation and Frontal Polymerization

Each formulation was made containing the specified epoxy, glycidyl ether, or vinyl ether with varying concentrations of IOC-8 in parts per hundred resin (phr). Parts per hundred resin is a unit meaning 1 gram of material for every 100 g of resin. For the epoxy and glycidyl ethers, IOC-8 was first dissolved in the monomer using a heated sonicator bath at 40 °C for approximately 15 to 30 minutes, depending on concentration. For the vinyl ethers, IOC-8 was dissolved in propylene carbonate in a 1:1 weight ratio before adding the monomer. The formulation was shaken in either case with a vortex mixer for a minute to ensure homogeneity. To increase viscosity, 10 wt% fumed silica was added to the formulations and hand mixed. Aerosil E805 was

used in lieu of previously used Aerosil 200 as it is marketed as easy-to-disperse. Aerosil 200 and TMPTE was experiencing issues with viscosity, whereas the Aerosil E805 had a higher viscosity.

Similar to previous chapters, the moldable resin putty was loaded into a wooden mold (13.5 cm × 2 cm × 0.6 cm) lined with wax paper for easy removal. To initiate the front, a soldering iron was heated to 330 ℃ for epoxy and glycidyl ethers or 200 ℃ for vinyl ethers and contact with the putty was maintained until the front began to propagate approximately 0.5 cm, then the soldering iron was removed. A Seek Thermal CompactPRO FF infrared camera was used to observe the evolving thermal field as the front propagated. The mold was cooled to room temperature prior to subsequent experiments. Triplicate experiments were performed by running three trials from the same solution.

For front velocity, the fronts were tracked using a video camera placed directly above the sample. Front velocity was calculated from the slope of the graph of front position versus time. Expansion-corrected front velocity was calculated by taking a ratio of initial material length to cured material length and multiplying this factor by the raw front velocity. The expansion only accounts for the expansion in the direction parallel to the front propagation.

For UV-initiation, samples were loaded into the same wooden mold used for thermal initiation with a video camera and Seek Thermal CompactPRO FF infrared camera to record front position and temperature, respectively. Above the end of the mold, a ThorLabs M365LP1 365 nm light was fixed at a distance of 7 cm with an intensity of approximately 48 mW cm^{-2}, which was measured with a ThorLabs S302C sensor. About 8 to 10 mm of the resin was exposed to the light. Once the front had begun to propagate, the light was immediately turned off.

Uncured resins in molds ranged from 8 to 10 cm prior to polymerization, much longer than the exposure radius.

6.3. Iodonium Salt Dependencies of Epoxy Monomers in Frontal Polymerization

The effects of varying IOC-8 concentration were first analyzed with epoxies initiated thermally. It was found, like in previous literature using RICFP, [54, 99] that the front velocity greatly depended on IOC-8 concentration. Increasing amounts of IOC-8 were shown to increase the front velocity. The plot in Figure 6.4 shows the dependence of the front velocity on the IOC-8 concentration with TMPTE as the monomer. For comparison of phr with other units of concentration, note that 1 phr IOC-8 is equivalent to 0.016 molal, 2.5 phr IOC-8 is 0.039 molal, 5 phr IOC-8 is 0.078 molal, and 7.5 phr IOC-8 is 0.12 molal.

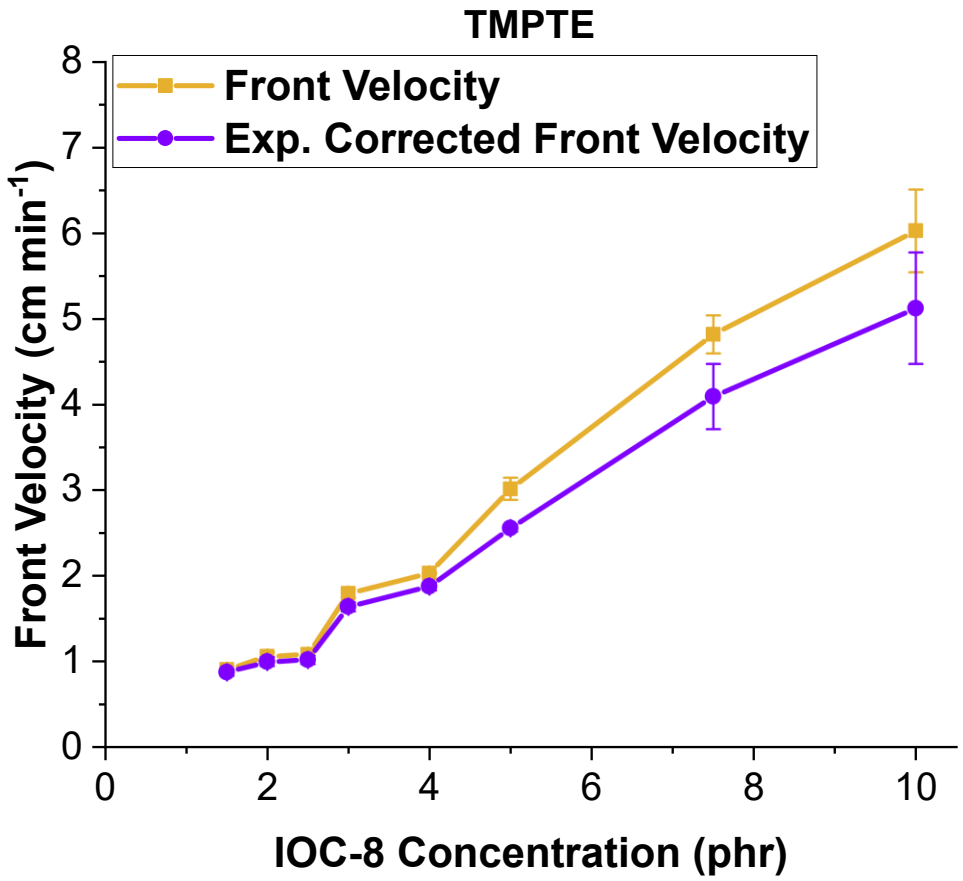

Figure 6.4. Front velocity and expansion corrected front velocity versus IOC-8 concentration for TMPTE samples with 10 wt% fumed silica added. “Exp. Corrected Front Velocity” is front velocity corrected for material expansion.

The same trend of increasing front velocity with increasing IOC-8 concentration is seen with NPDGE in Figure 6.5. NPDGE experienced significant material expansion at higher concentrations of IOC-8. CE would partially support a front with 2 phr IOC-8 before quenching. With all concentrations of IOC-8, CE had substantial expansion vertically in addition to expansion horizontally. The expansion is due to the creation of bubbles, which is likely from the decarboxylation of the monomer. [123] The monomer has a boiling point of 363 °C according to the manufacturer. The vertical expansion of CE can be seen in Figure 6.6 with an actively propagating front through the uncured resin, along with the fumes visible during propagation that led to the formation of many voids, including hollow, transparent bubbles. The high expansion in

the direction of the propagating front gave a large difference between the expansion-corrected front velocity and the raw front velocity. This expansion-corrected front velocity only accounts for the expansion in the horizontal direction and does not include the vertical expansion. It was seen that an increase in front velocity occurred from 4 phr to 12 phr IOC-8 with a drop at 10 phr IOC-8 in Figure 6.7. The 10 phr IOC-8 concentration was tested multiple times to confirm the drop in front velocity is reproducible. There is no current hypothesis why this is occurring.

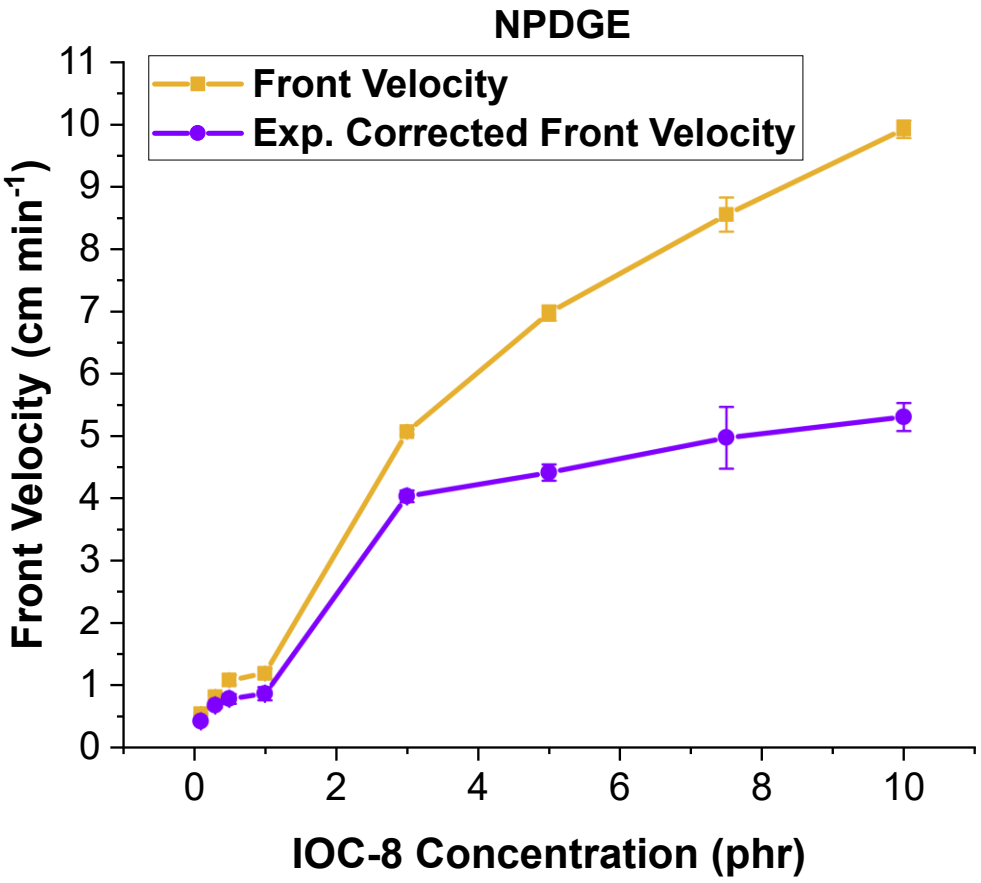

Figure 6.5. Front velocity and expansion corrected front velocity versus IOC-8 concentration for NPDGE samples with 10 wt% fumed silica added. “Exp. Corrected Front Velocity” is front velocity corrected for material expansion.

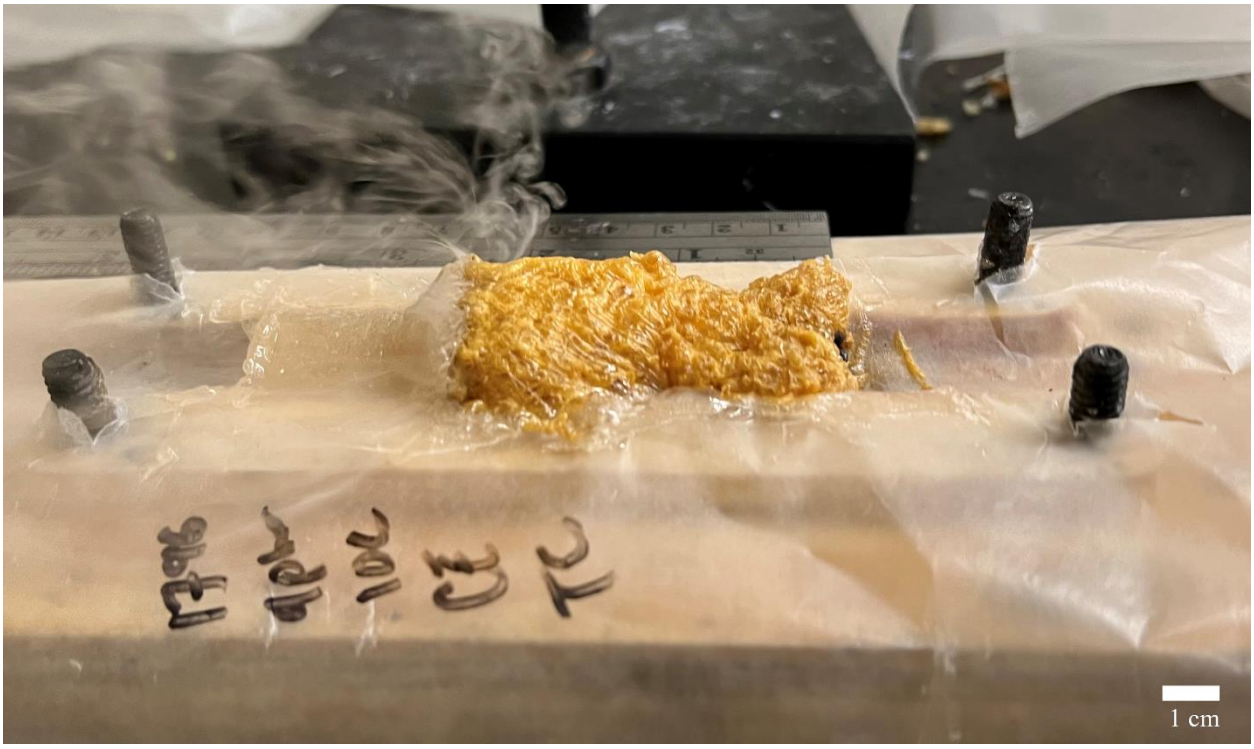

Figure 6.6. Vertical expansion of a system of 9 phr IOC-8 in CE, with 10 wt% fumed silica added.

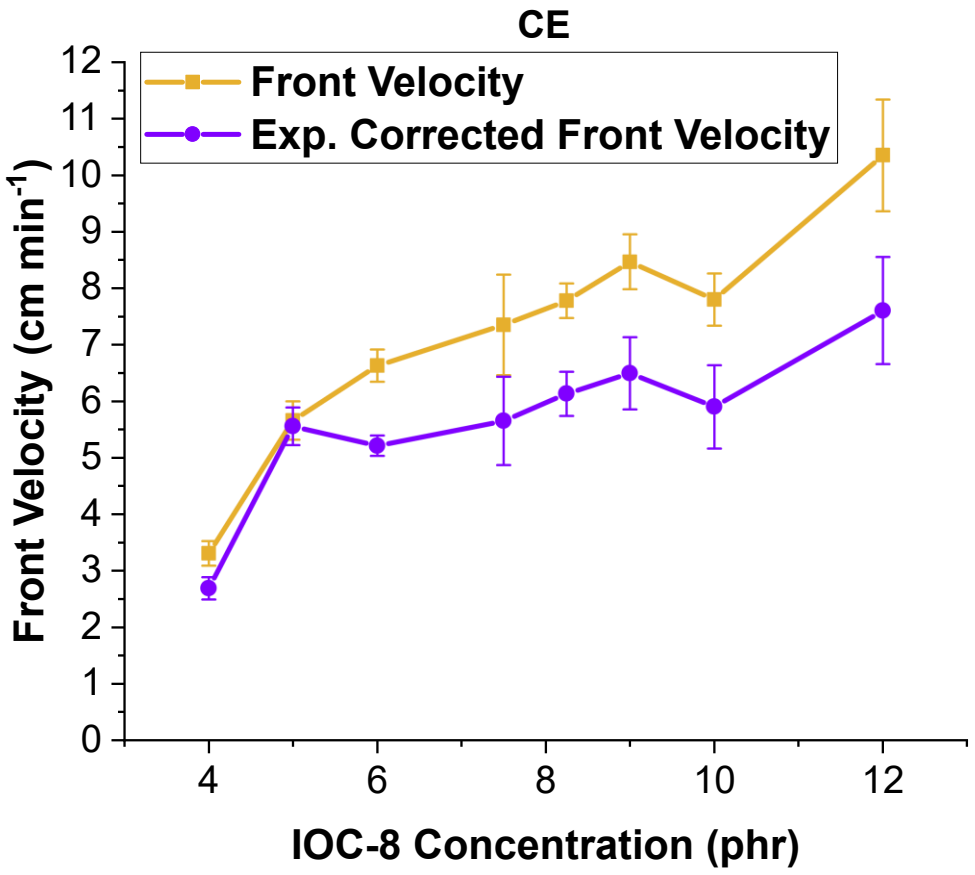

Figure 6.7. Front velocity and expansion corrected front velocity versus IOC-8 concentration for CE samples with 10 wt% fumed silica added. “Exp. Corrected Front Velocity” is front velocity corrected for material expansion. Results for 7.5 phr IOC-8, 9 phr IOC-8, and 10 phr IOC-8 are averaged over 2 sets of triplicates.

The polymers produced by TMPTE, CE, and NPDGE presented many voids. This could either be due to bubbles introduced during mixing, formation of volatile compounds from decomposition of IOC-8, or impurities present in the monomer. Based on the previously reported analysis of iodonium salt thermal decomposition, there are many volatile byproducts released. [121] TMPTE was soft, somewhat flexible, and appeared to have the least amount of voids. CE had a large amount of voids and was very brittle and inflexible, while NPDGE was flexible and had streaking bubbles through the material parallel to the front direction at low IOC-8 concentrations, which has previously been documented. [124] [125] The color of the three polymers also varied, with

TMPTE being brown, CE was yellow, and NPDGE was off-white. Increasing the IOC-8 concentration shifted the colors of the polymers darker. [99]

Results for expansion-corrected front velocity with each monomer at the minimum IOC-8 concentration, 5 phr IOC-8, and 10 phr IOC-8 are shown in Table 6.1. In the studied IOC-8 concentration range for all epoxies from 0 – 10 phr after expansion correction, CE yields the highest front velocities at 9 phr IOC-8. Ring strain in the CE epoxide due to the attachment to the cyclohexane ring results in higher reactivity for the epoxy ring opening polymerization mechanism, [59] which potentially explains these results. However, the higher minimum IOC-8 concentration needed for CE compared to TMPTE and NPDGE could be related to the higher molecular weight per functional group resulting in lower relative heat production, or the bubbles that are formed from gas production contributing to heat loss. The molecular weight per functional group of CE is 126.2 g mol^{-1}, while for TMPTE it is 100.8 g mol^{-1} and NPDGE is 108.1 g mol^{-1}.

For all monomers, front temperatures were approximately 230 ℃. Formulations with pure BADGE were attempted, but it was found that BADGE could only support a front when TEGDVE was added. There is a minimum of 3 phr IOC-8 and 1:4 weight ratio of TEGDVE:BADGE needed. The front from this formulation is much slower than other monomers with comparable IOC-8 concentrations. BADGE formulations with concentrations of up to 5 phr IOC-8 with 0 to 20 wt% TEGDVE did not support fronts, along with attempts at up to 10 phr IOC-8 with no vinyl ether added. Due to these limitations, only the front velocity at minimum IOC-8 concentration for BADGE was studied.

Table 6.1. Observed minimum IOC-8 concentration and range of front velocities and expansion-corrected front velocities for epoxy and glycidyl ether monomers up to 10 phr IOC-8.

	Minimum IOC-8 Concentration (phr)	Expansion-corrected front velocity at minimum IOC-8 concentration (cm min^{-1})	Expansion-corrected front velocity at 5 phr IOC-8 (cm min^{-1})	Expansion-corrected front velocity at 10 phr IOC-8 (cm min^{-1})
TMPTE	1.5	0.9	4.1	5.1
CE	4.0	3.3	5.6	6.6
BADGE	3[a]	1.0	-	-
NPDGE	0.1	0.6	4.4	5.3

[a]Formulation consisted of 25 wt% TEGDVE and 75 wt% BADGE.

6.4. Iodonium Salt Dependencies for Vinyl Ethers

Vinyl ether monomers, like epoxies and glycidyl ethers, were also able to undergo cationic FP through only addition of IOC-8. Both TEGDVE and DVE-1,4 were tested and found to support fronts with much lower concentrations of IOC-8 than epoxies and at an initiation temperature of 200 ℃ as opposed to 330 ℃ with epoxies due to higher reactivity of vinyl ethers. In addition, TEGDVE resulted in overall much faster fronts than the epoxies. The front velocity dependency on IOC-8 concentration for TEGDVE is found in Figure 6.8.

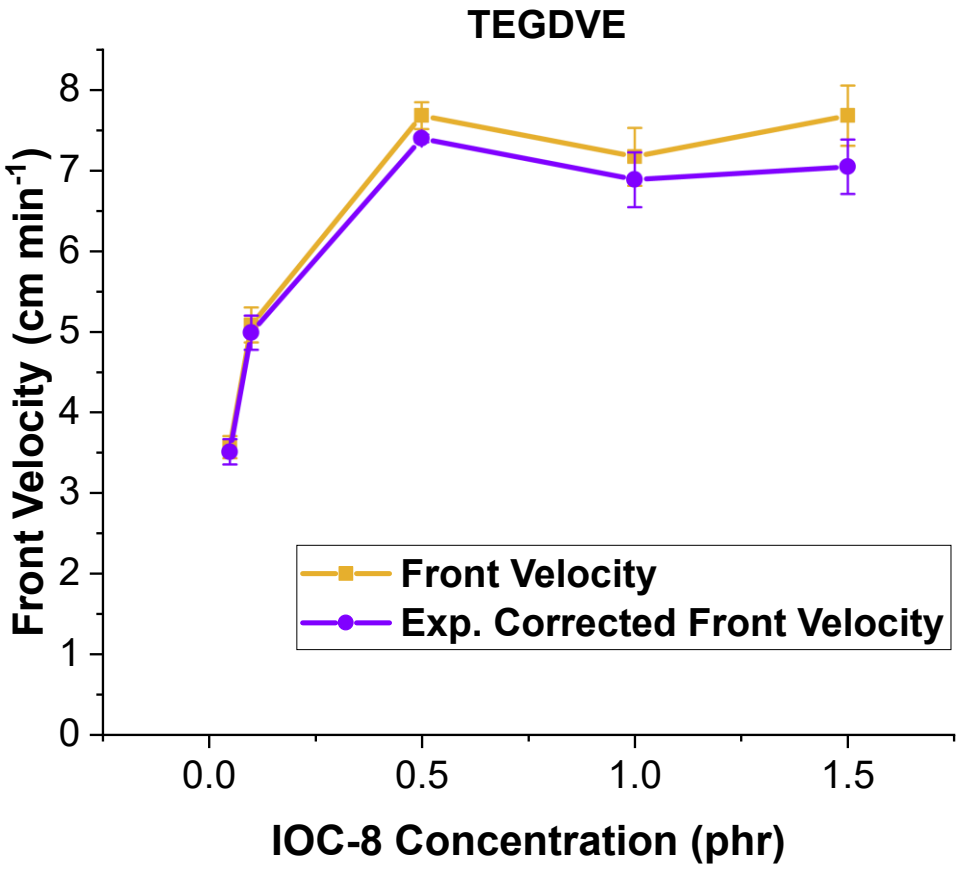

Figure 6.8. Front velocity and expansion corrected front velocity versus IOC-8 concentration for TEGDVE samples with 10 wt% fumed silica added. Data for 1.5 phr IOC-8 is calculated over 3 separate sets of triplicates. "Exp. Corrected Front Velocity" is front velocity corrected for material expansion.

With TEGDVE, there appeared to be a plateau of front velocity after reaching 0.5 phr IOC-8 after initial increases in front velocity from 0.01 phr to 0.5 phr. Similar to the drop in front velocity of CE at 10 phr IOC-8, the cause of the small drop in front velocity at 1.0 phr IOC-8 is uncertain. Interestingly, there appeared to be bubbles and fingering at the interface of the front, a phenomenon previously observed in thermally unstable FP. [19] The overall kinetics of increasing IOC-8 concentration with DVE-1,4 were not studied, as the material was very brittle and encountered substantial expansion as the front progressed which made it impossible to determine

the position of the front. DVE-1,4 required a similar minimum concentration of IOC-8 as TEGDVE. Both pure TEGDVE and DVE-1,4 had noticeable disadvantages in material quality. TEGDVE resulted in brown polymers that were easily broken, but flexible and remained in once piece, while DVE-1,4 gave yellow polymers that were very brittle and would crack into pieces upon polymerization. The loading of fumed silica had to be increased from 10 wt% to 15 wt% for DVE-1,4 to achieve a qualitatively similar viscosity to TEGDVE. A comparison of both materials is seen in Figure 6.9. A range of front velocities possible for studied epoxy and vinyl ether monomers is shown in Figure 6.10.

Figure 6.9. Example of material produced with pure TEGDVE (top) and DVE-1,4 (bottom), both containing 0.1 phr IOC-8.

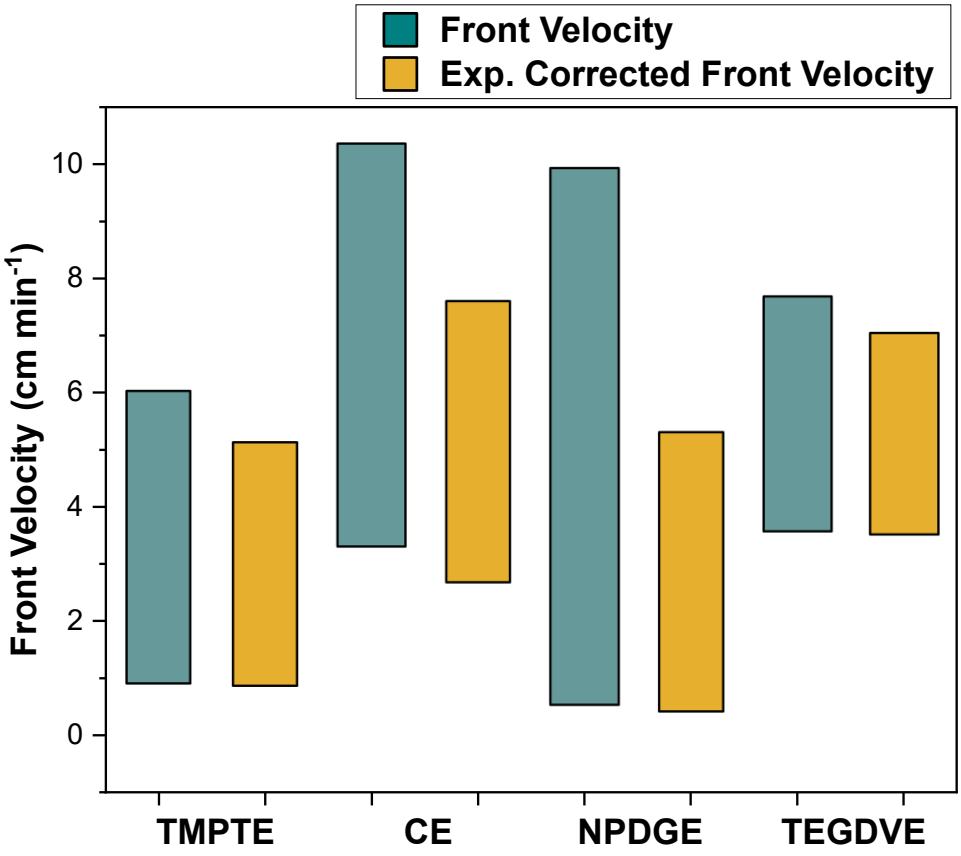

Figure 6.10. Comparison of front velocity ranges with monomers studied. IOC-8 concentrations varied depending on monomer. TMPTE (1.5—10 phr IOC-8); CE (4—12 phr IOC-8); NPDGE (0.1—10 phr IOC-8); TEGDVE (0.05—1.5 phr IOC-8).

6.5. UV Initiation of Epoxies and Vinyl Ethers

Fronts were also initiated using a 365 nm UV light at a measured intensity of approximately 50 mW cm^{-2} for formulations containing TMPTE, NPDGE, CE, and TEGDVE. The setup is shown in Figure 6.11. The samples were made to be longer than the cone of UV light contacting the sample to ensure that propagation was not only due to irradiation of the sample ahead of the front as described in literature. [50]

Figure 6.11. Setup of frontal polymerization initiation via UV-initiation.

In every system, there was an obvious difference in the cured material properties in the UV exposed region versus the region that cured via thermal front propagation as shown with the CE system in Figures 6.12a and 6.12b. The region that was exposed to UV light was harder, darker in color, did not have voids, and did not expand. This could be due to higher conversion in the light cured region. This phenomenon warrants further investigation.

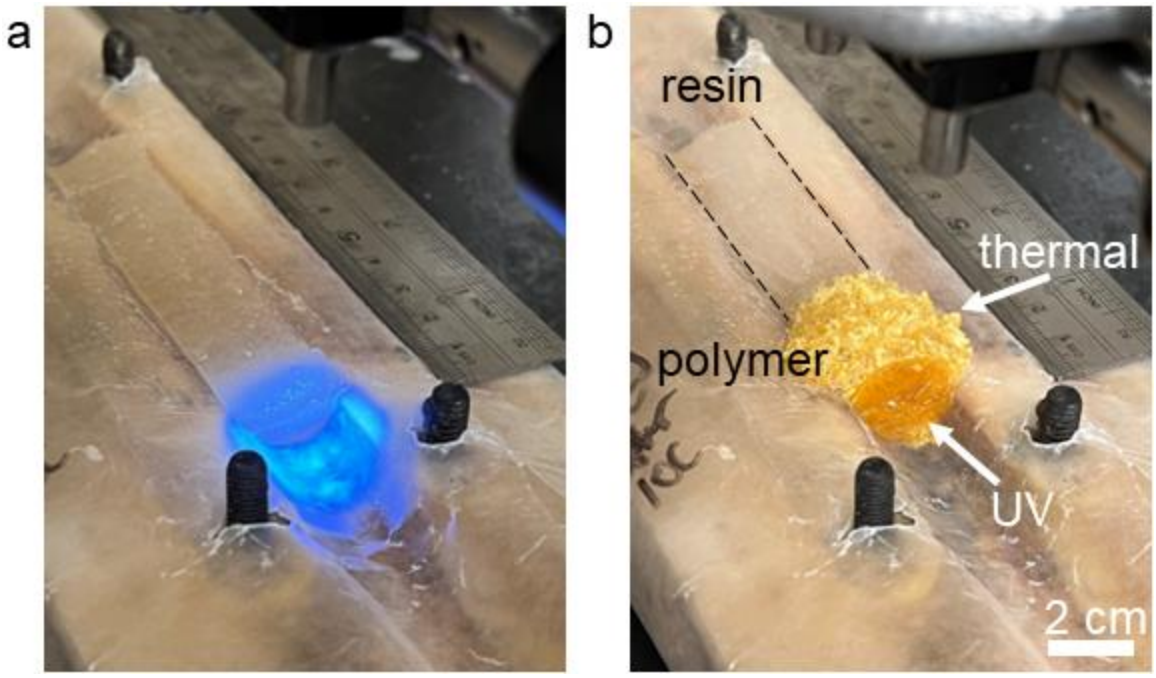

Figure 6.12. UV initiated frontal polymerization. a) uncured CE resin being irradiated with UV light; b) propagating front of CE resin after initiation, where the polymer is a different color from the resin and labelled, and the extent of the resin is labelled and outlined with dashed lines. “UV” is the portion of the polymer irradiated with UV light, and “thermal” is the polymer that was cured by the thermal propagation of the front.

The front velocities of the resins initiated with heat or UV were similar across both methods with consideration of standard deviation. Two concentrations of IOC-8 were chosen for these studies: the minimum concentration needed to support a front thermally, and one concentration which lain within the studied ranges. Front kinetic results with comparisons are shown for both the minimum and mid-range IOC-8 concentration in Figure 6.13 and 6.14, respectively. Regardless of initiation method, front velocity should be constant for equivalent formulations if the front has reached a steady state, given that the propagation occurs with the heat generation of the reaction. More experiments are needed to confirm the constant front velocities; longer samples may be needed to ensure that the front reached a steady state.

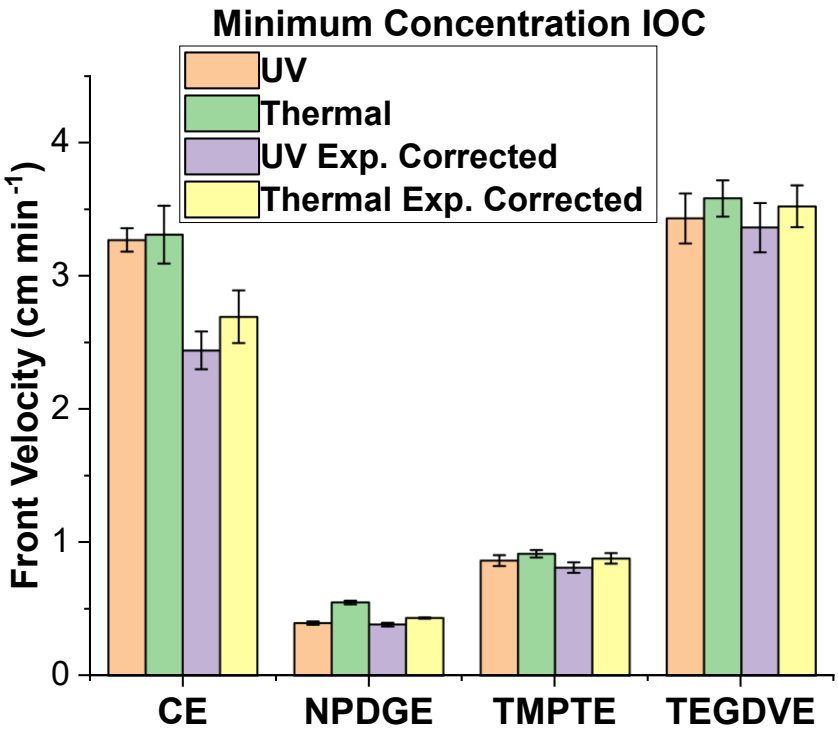

Figure 6.13. Front velocity at minimum concentrations of IOC-8 for three epoxies and a divinyl ether with comparisons between thermal and UV initiation methods. IOC-8 concentrations: CE 4 phr IOC-8; NPDGE 0.1 phr IOC-8; TMPTE 1.5 phr IOC-8; TEGDVE 0.05 phr IOC-8.

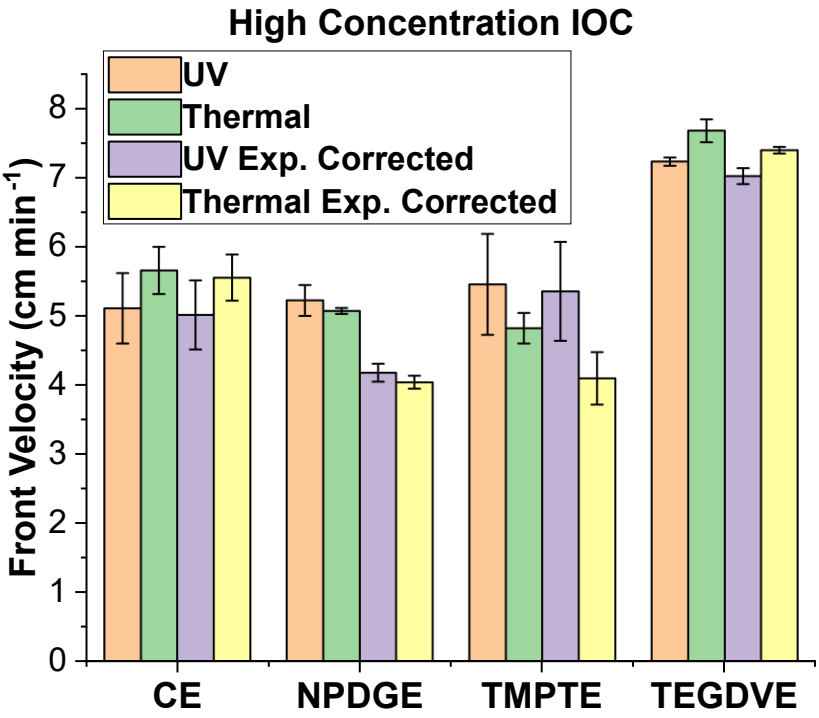

Figure 6.14. Front velocity at midrange concentrations of IOC-8 for three epoxies and a divinyl ether with comparisons between thermal and UV initiation methods. IOC-8 concentrations: CE 5 phr IOC-8; NPDGE 3 phr IOC-8; TMPTE 7.5 phr IOC-8; TEGDVE 0.5 phr IOC-8.

With 0.1 phr IOC-8 in NPDGE, fronts were extremely slow, and initiation time was over 10 minutes. The front temperature for this formulation was also low at 130 ℃, compared to other formulations that had front temperatures of approximately 200 – 230 ℃. Figure 6.15 shows the front velocity increase with increasing IOC-8 concentration for NPDGE.

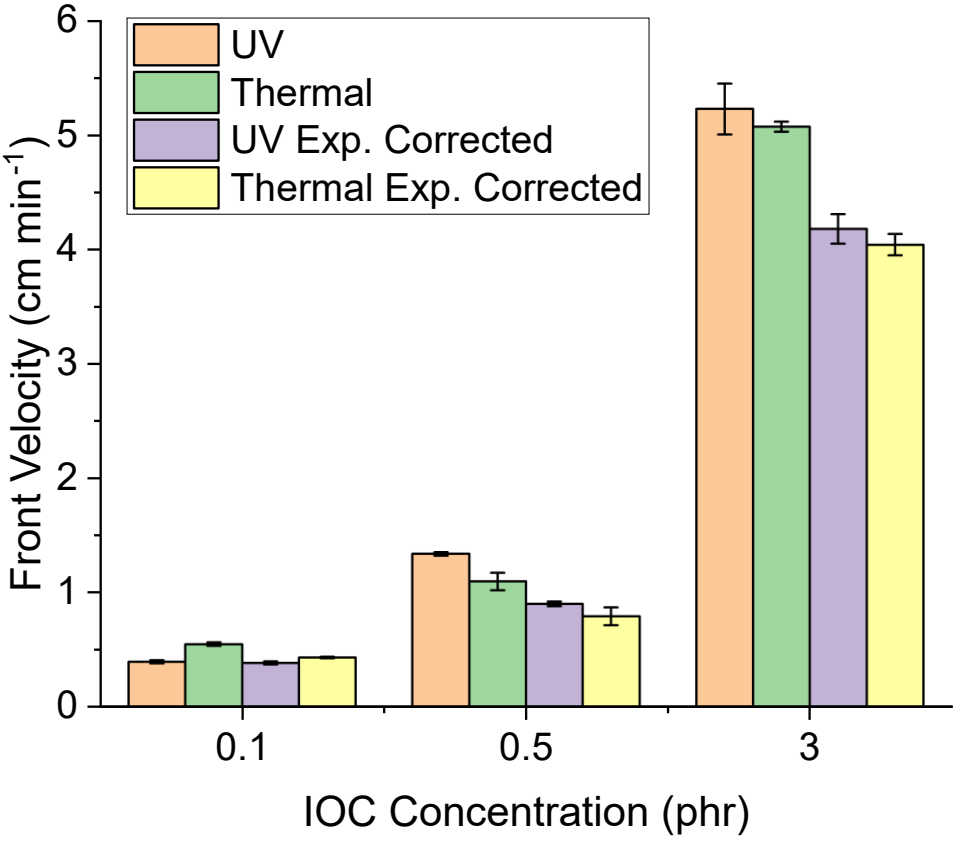

Figure 6.15. Front velocity versus IOC-8 concentration for NPDGE, with comparisons of UV and thermal initiation.

Nonetheless, these results once again affirm that the heat of the polymerization reaction is sufficient to thermally decompose the iodonium salt and generate superacid for the cationic FP of these monomers, regardless of initiation method. [121]

6.6. Effects of Vinyl Ether Addition to Epoxies

Increasing additions of TEGDVE to TMPTE with 1.5 phr IOC-8 were found to increase the front velocity, as expected from previous work. [99] The results are shown in Figure 6.16 for the front velocity and Figure 6.17 for the expansion corrected front velocity. The front velocities are low compared to systems that also contain thermal radical initiators, Luperox 231 or benzopinacol.

The front also initiates at lower temperatures with increasing TEGDVE ratio, from 300 ℃ with 100 wt% TMPTE to 200℃ with 75 wt% TEGDVE and 25 wt% TMPTE and down to 150 ℃ for pure TEGDVE. The cause of the increases in front velocity could be due to the high reactivity of vinyl ether or redox reactions occurring between IOC-8 and vinyl ether. Formulations of only DVE-1,4 and IOC-8 will react within hours at ambient conditions, suggesting that there are redox interactions of the vinyl ether and iodonium salt. Further, samples of pure TMPTE with 1.5 phr IOC-8 show a slow front velocity (0.92 cm min^{-1}) and long pot lives of months at room temperature. These observations suggest that epoxies do not undergo any redox interactions with IOC-8 but cationic polymerization of TMPTE occurs due to thermal decomposition of IOC-8 generating superacid. [121] Interestingly, formulations containing only TEGDVE and IOC-8 have much longer pot lives than DVE-1,4. Samples have been observed to remain unreacted for months. There is no explanation why TEGDVE formulations are more stable than DVE-1,4 in ambient conditions while still being reactive once initiated. Perhaps the DVE-1,4 is inherently more reactive than the TEGDVE.

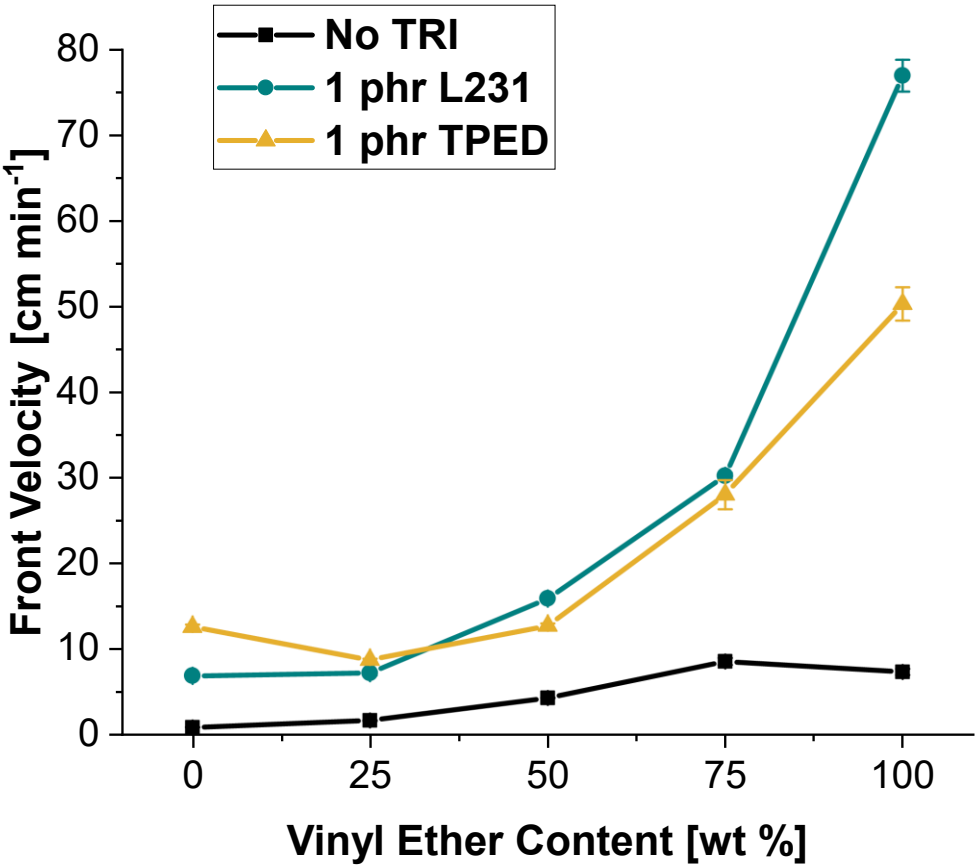

Figure 6.16. Effect of increasing vinyl ether content on the raw front velocity of systems containing TMPTE and specified wt % TEGDVE, with 1.5 phr IOC-8 and either no L231, 1 phr L231, or 1 phr TPED.

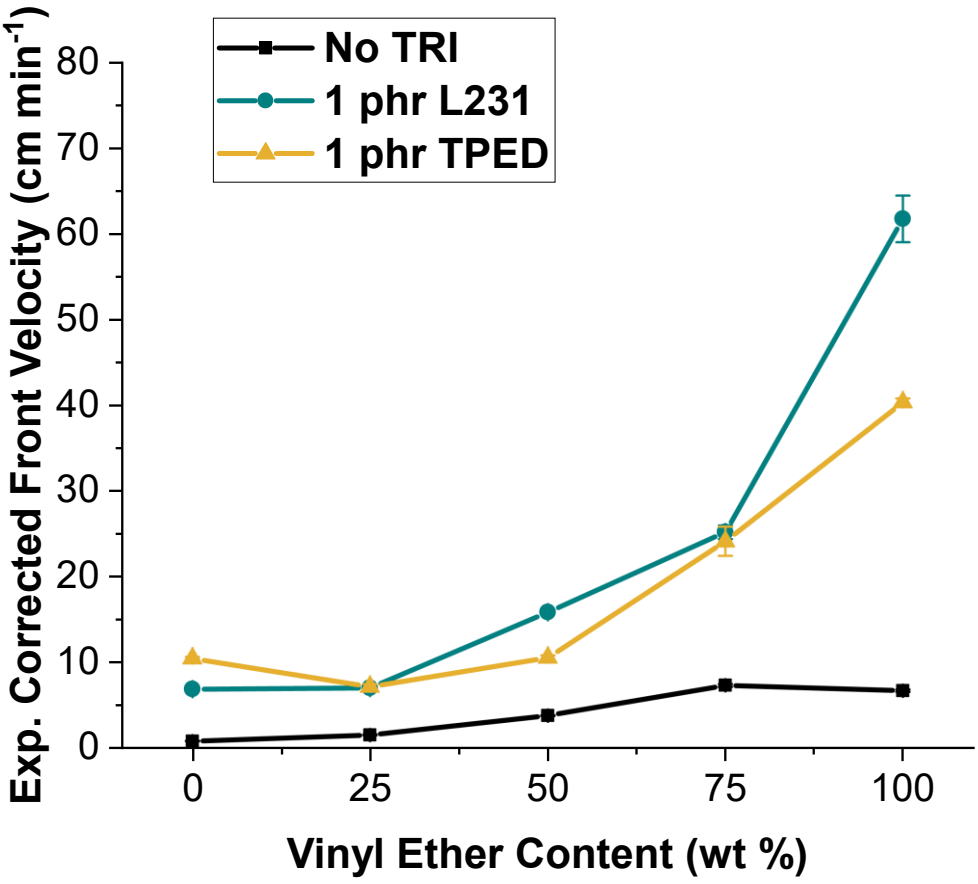

Figure 6.17. Effect of increasing vinyl ether content on the expansion-corrected front velocity of systems containing TMPTE and specified wt % TEGDVE, with 1.5 phr IOC-8 and either no L231, 1 phr L231, or 1 phr TPED.

The interactions of vinyl ethers with onium salts are reported in the literature. Lecompère et al. [72, 126] reported only 0.7 wt% isobutyl vinyl ether added to a formulation of 3 wt% triphenyl pyrylium salt and cycloaliphatic epoxides reduced the gel time from 3-4 hours to only 20 min. They suggest the 'kick-starting effect' of vinyl ether reactivity boosting epoxide reactivity occurs from a nucleophilic attack of the vinyl ether onto the pyrylium salt, where the vinyl ether can be resonance stabilized. A mechanism proposed by Rajaraman et al. [48] and adapted from their work in Figure 6.18 for the evidence of polymerization rates increasing in bulk epoxy photopolymerization with vinyl ethers shows interaction of vinyl ether with radical species

formed from diaryliodonium salts. The interaction eventually forms carbenium ions which will initiate cationic polymerization. The process is a chain reaction formation of radical and carbenium ions. This is expected to occur in addition to the initiation of vinyl ethers with superacid. It is uncertain whether a similar process occurs for epoxies, but their lower front velocities imply that only acid generation during thermal decomposition of IOC-8 is the only process contributing to initiation.

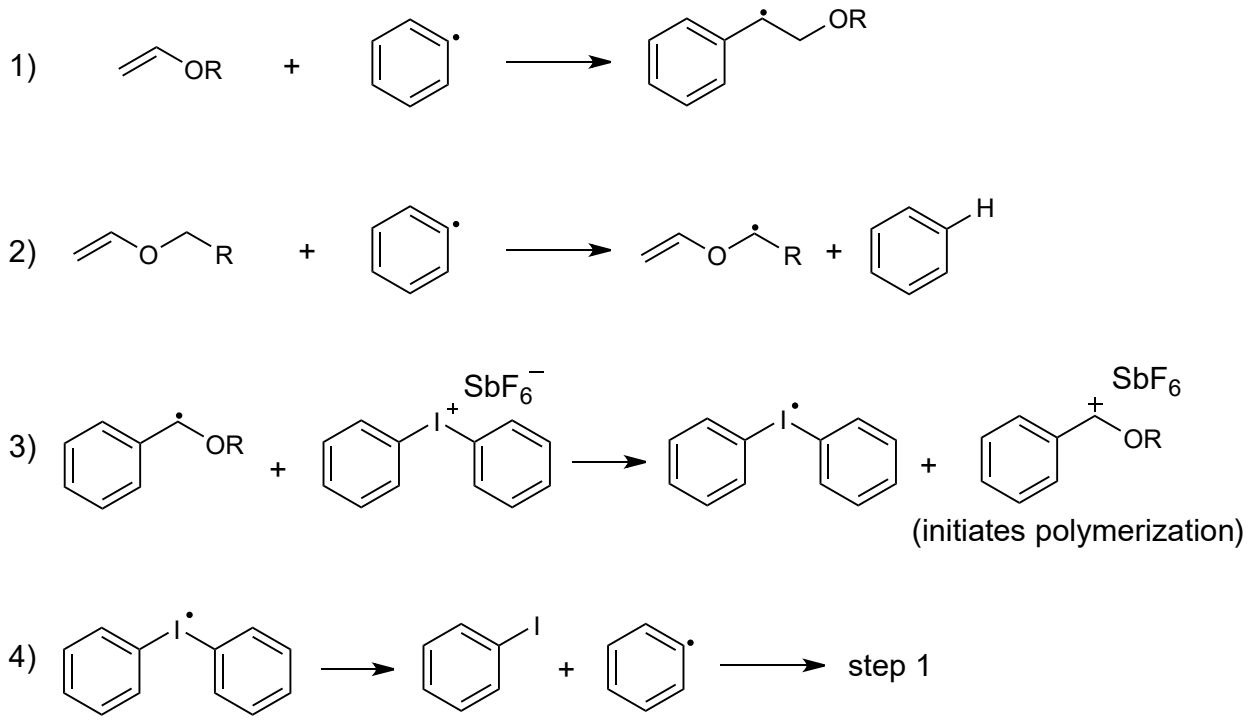

Figure 6.18. Redox interaction of vinyl ethers with radical species formed during IOC-8 decomposition to produce initiating species and a chain radical formation, adapted from Rajaraman et al. (1999).

6.7. Effect of Radical Inhibitor Addition

To test if radicals are generated that are promoting the decomposition of IOC-8 in the system with an absence of a primary radical initiator, MeHQ was added. MeHQ is a commonly used radical inhibitor. The concentrations of IOC-8 were chosen because they are guaranteed to support FP under typical conditions.

It was found that increasing amounts of MeHQ decreased the front velocity in formulations overall, shown in Figure 6.19 and Figure 6.20 for the front velocity and front velocity after expansion correction, respectively. For TMPTE, there was a decrease in front velocity as the concentration of inhibitor increased. Notably, TMPTE with 3 phr IOC-8 would not produce a front with 0.1 phr or more MeHQ added. With TEGDVE, there appeared to be a substantial decrease with MeHQ addition followed by a plateau. CE also showed a decrease in front velocity after addition before plateauing at higher concentrations of MeHQ, only visible in the expansion corrected front velocity. It is believed that this trend only appeared in the expansion-corrected velocity due to the substantial expansion present in CE systems. NPDGE did not follow the same trend as the other epoxies. In both raw and expansion-corrected front velocities, there appeared to be two peaks at 0.1 phr and 0.5 phr MeHQ. However, upon addition of 1.5 phr MeHQ, a front was not supported, which indicates that IOC-8 with NPDGE can still be inhibited by radical inhibitors.

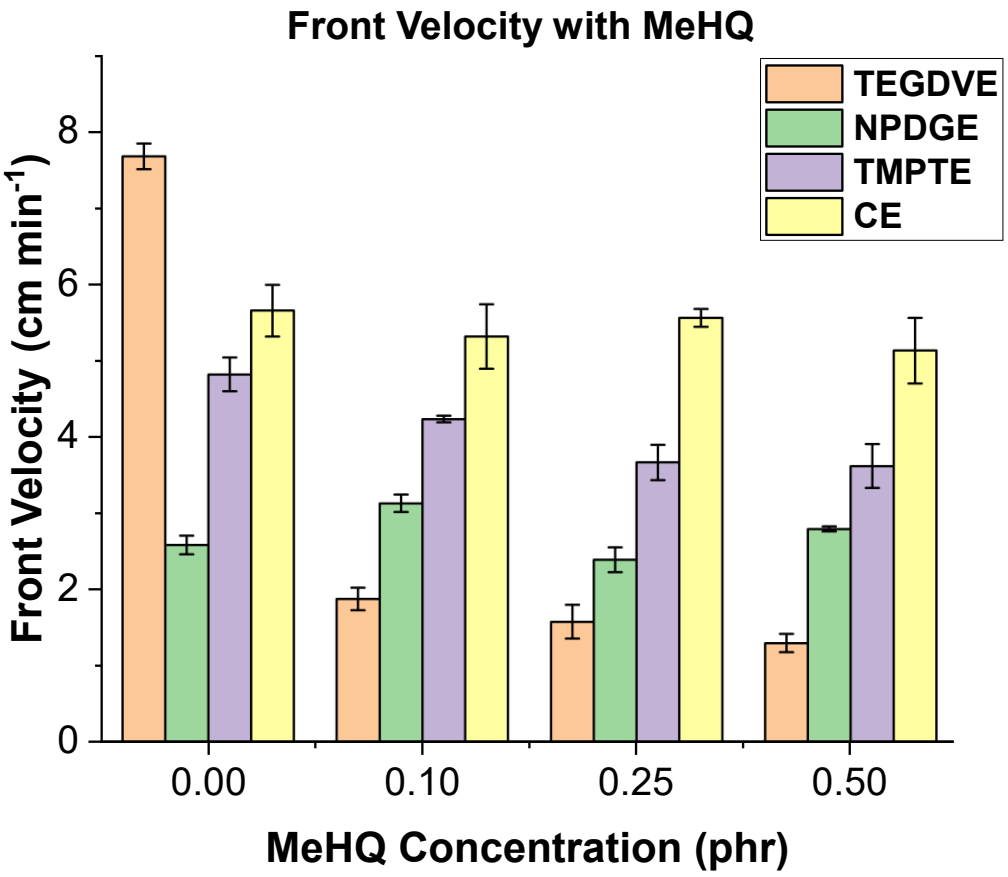

Figure 6.19. Effect of increasing MeHQ concentration on the uncorrected front velocity for epoxy and vinyl ether monomers. The concentration of IOC-8 in each formulation was as follows: TMPTE 7.5 phr IOC-8, NPDGE 3 phr IOC-8, CE 5 phr IOC-8, TEGDVE 0.5 phr IOC-8.

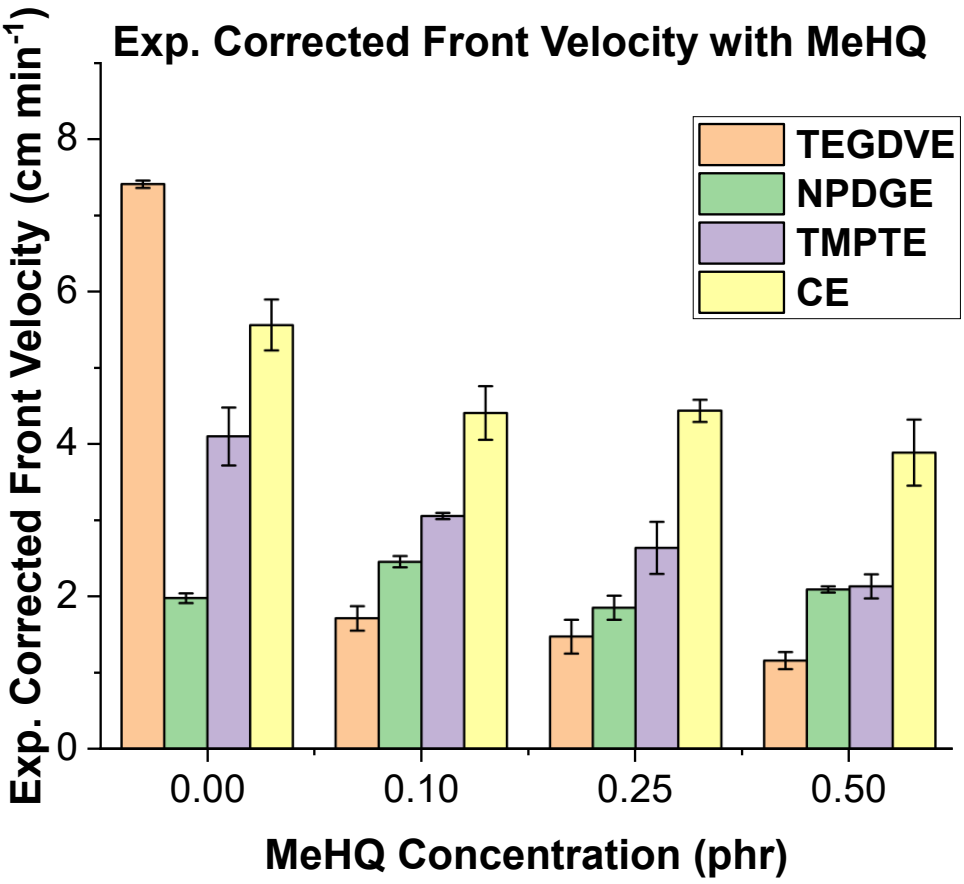

Figure 6.20. Effect of increasing MeHQ concentration on the expansion corrected front velocity for epoxy and vinyl ether monomers. The concentration of IOC-8 in each formulation was as follows: TMPTE 7.5 phr IOC-8, NPDGE 3 phr IOC-8, CE 5 phr IOC-8, TEGDVE 0.5 phr IOC-8.

Chain transfer to hydroxyl-containing compounds can occur with cationic polymerization, and there is evidence that it can cause a drop in front velocity. [60, 99] To test that the reduction of front velocity was due to radical quenching and not chain transfer to the hydroxyl of MeHQ, MeHQ in a TMPTE and 7.5 phr IOC-8 system was substituted with an equimolar amount of dodecanol by molality. Because of the difference in molecular weight, the concentration in phr of MeHQ and dodecanol are different while the molality is equal. The high boiling point of dodecanol (259 °C) ensured that significant heat loss to vaporization was not occurring. With addition of dodecanol,

there is a slight increase in front velocity followed by a small decrease at 0.0081 molal and 0.039 molal shown in Figure 6.21. The front velocity then decreases at 0.24 molal. This is the opposite trend of MeHQ addition, which saw an overall decrease in front velocity. With the divergence in these results, it is concluded that MeHQ is indeed scavenging radicals. Therefore, the system operates similar to RICFP, but with the acid generator alone producing radicals and superacid species.

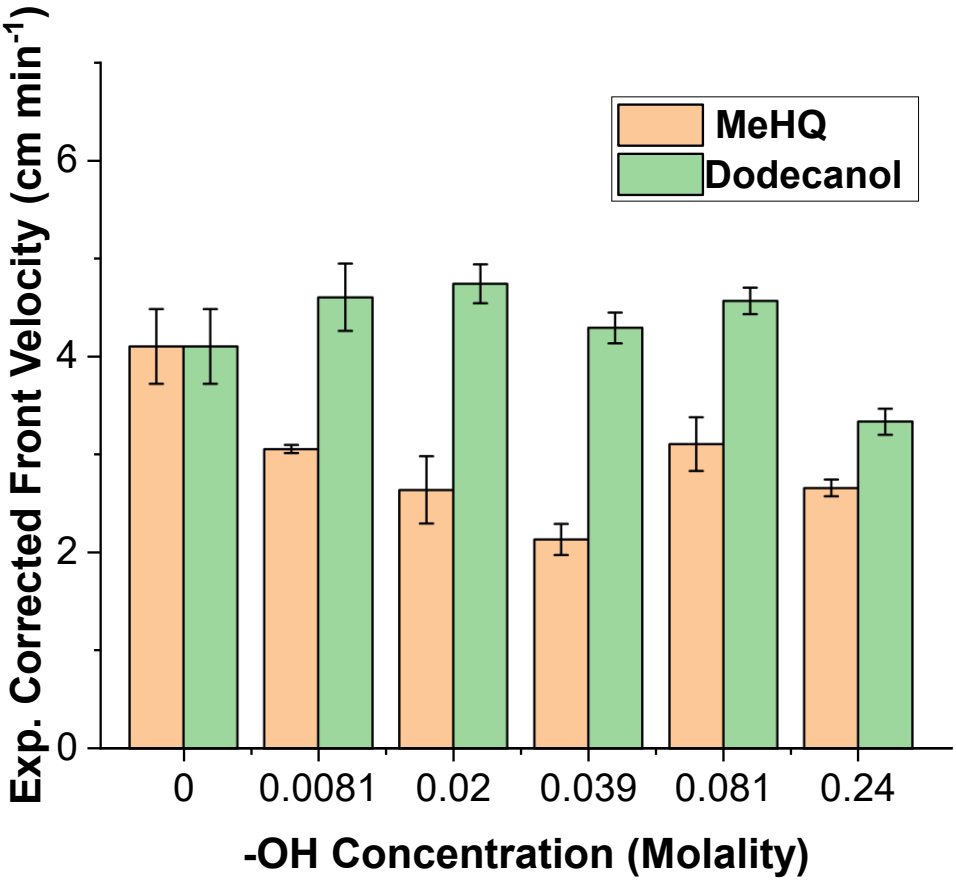

Figure 6.21. Expansion-corrected front velocity as a function of mol of MeHQ or dodecanol added for a resin containing 7.5 phr IOC-8 in TMPTE with 10 wt% fumed silica. The concentrations for dodecanol and MeHQ in phr were as follows: 0.008 molal = (0.1 phr MeHQ, 0.1 phr dodecanol); 0.02 molal = (0.25 phr MeHQ, 0.38 phr dodecanol); 0.039 molal = (0.5 phr MeHQ, 0.73 phr dodecanol); 0.081 molal = (1 phr MeHQ, 1.5 phr dodecanol); 0.24 molal = (3 phr MeHQ, 4.5 phr dodecanol).

6.8. Conclusions and Future Outlooks

It was shown that frontal polymerization of epoxies and/or vinyl ethers is possible through the addition of iodonium salts in absence of any primary thermal radical initiator or pre-curing UV irradiation. This technique presents a modification of radical-induced cationic frontal polymerization where both the thermal radical initiator and an acid generating salt are required. It was found that vinyl ethers were highly reactive and required much less IOC-8 to support a front than epoxies. Addition of vinyl ether to epoxy systems with no standalone radical initiator decreases the initiation temperature and increases the front velocity. Initiation with 365 nm UV irradiation and subsequent frontal polymerizations of these systems was possible.
Addition of radical inhibitor indicated that the IOC-8 acts as both an acid generator and generator of radicals. It was shown that not every epoxy will support FP through this method, such as the case with BADGE which required addition of vinyl ether to enhance reactivity. With no standalone radical initiator, fronts are slower than systems with radical initiator and more IOC-8 is required to sustain a front.

By preparing a solution of iodonium salt in propylene carbonate, formulations that support frontal polymerization with only liquid components can be made rapidly. The absence of a thermal radical initiator simplifies the preparation of formulations that support frontal polymerization in addition to simplifying the kinetics. There are many onium salts available commercially and some that can be synthesized and the study of these salts with a lack of radical initiator could find optimal salts to add to achieve high reactivity through this method. A remaining challenge is to develop salts that would not release so many volatile byproducts so that there are less bubbles produced.

CHAPTER 7. APPLICATIONS OF CATIONIC FRONTAL POLYMERIZATION

7.1. State of the Art

Reports of the applications of cationic FP have been limited mostly to composites, whereas free-radical FP and FROMP have been shown to be useful for coatings, [28, 127, 128] composites, [86] hydrogels, [129-133] and 3D printing. [9, 134, 135] Initial papers of BF_3-amine complex cured epoxies via FP were concerned with the system's use as a means of making materials filled with fumed silica, kaolin, and expanding compounds for foams. [21, 34] With RICFP, there have been multiple reports of developing composites with many different materials such as carbon and glass fibers, clays, and other minerals, [38, 41, 54, 69, 70, 136, 137] including the work shown in this dissertation. Only a few reports have been concerned with other applications. The following sections intend to show different potential avenues for application of cationic FP and work that has been reported and undertaken thus far.

7.2. Additive Manufacturing

3D printing or additive manufacturing is undoubtedly a quickly growing field with the unique advantages of generating parts much faster and with less energy than traditional methods of autoclave curing or injection molding.

There are currently four reports of epoxies cured by RICFP used in additive manufacturing from a group at Texas A&M. [138-140] In all reports, they looked at the effects of adding carbon nanotubes (CNTs), carbon fibers, and graphene oxide on the printing process. The first paper by Zhang et al. examined successful 3D printing of continuous carbon fiber tows which were coated while extruded with a resin of BADGE and an iodonium aluminate salt and TPED. [139] A subsequent report showed addition of 1 wt% CNTs catalyzed the polymerization of the same continuous carbon fiber printing process with the same resin. [140] They completed a

more detailed report of different carbon-based fillers, this time printing without the continuous carbon fiber. [138] In this paper, using the same resin as above, they found 1 wt% of discontinuous carbon fibers or CNTs afforded slight increases in front velocity over neat resins. 1 wt% graphene oxide reduced the front velocity. Additionally, increasing the wt% of CNTs from 0 to 1 wt% reduced the front temperature while the front velocity remained constant. They encountered issues with higher loadings of CNTs due to difficulties obtained good dispersion. In the above cases, the front was initiated by printing onto a heat bed set to 120 ℃. Finally, they printed a viscous novolac epoxy resin mixed with discontinuous carbon fibers and phenolic microballoons while simultaneously spraying an iodonium aluminate and benzopinacol solution with an atomizer as the material was extruded. [141] The front velocity was found to depend on the atomizer parameters and layer thickness.

The benefit to doing 3D printing with RICFP systems is typically much longer pot lives than FROMP resins and availability and pricing of the components of the epoxy resin, in addition to typically higher strength than acrylate-based FP systems. The idea behind FP-enabled 3D printing is that the front will very closely follow the extrusion of material, demonstrated in Figure 7.1. 3D printing has been demonstrated many times with FROMP systems. [9, 134, 142]

Figure 7.1. 3D printing using manual extrusion of an epoxy-vinyl ether resin from a syringe, with a visible front. The dark material is polymer while the colorless material is uncured resin.

To this aim, the Pojman lab has worked with groups in engineering to uncover potential use for our systems in 3D printing. One such project in collaboration with the Palardy group at LSU is examining the use of a resin system of BADGE, CE, TEGDVE, IOC-8 and Luperox 231 to print free-standing structures which do not require printed supports and can be printed in any axis. BADGE provides strength, while CE lowers viscosity and TEGDVE increases the front speed. The front velocity dependence on the loading of the fumed silica and carbon nanofibers (CNFs) used as fillers in this system is shown in Figure 7.2. Fumed silica is added to control the rheology of the resin. CNFs were chosen as they can increase the front velocity with their high thermal diffusion, while remaining cheaper than CNTs. CNFs have a diameter of approximately 100 nm versus 10000 nm or more for carbon fibers. [143, 144] This results in an increase of specific surface area which may help with physical properties. CNFs are larger than CNTs and differ from CNTs in structure, where CNFs are cylinders composed of layers stacked onto one another, and CNTs are hollow cylinders. CNFs are also less thermally conductive and have a lower resistivity than CNTs. [144] Controlling parameters of extrusion lies more within the scope of engineering, but choosing the correct resin to balance pot life and front speed of the extruder involves the

optimization of formulations including monomer ratios and initiator concentration. To print free-standing structures the viscosity of the resin must be high enough to not sag while extruding. The system has shown promise in preliminary testing of additive manufacturing via thermally-initiated frontal polymerization.

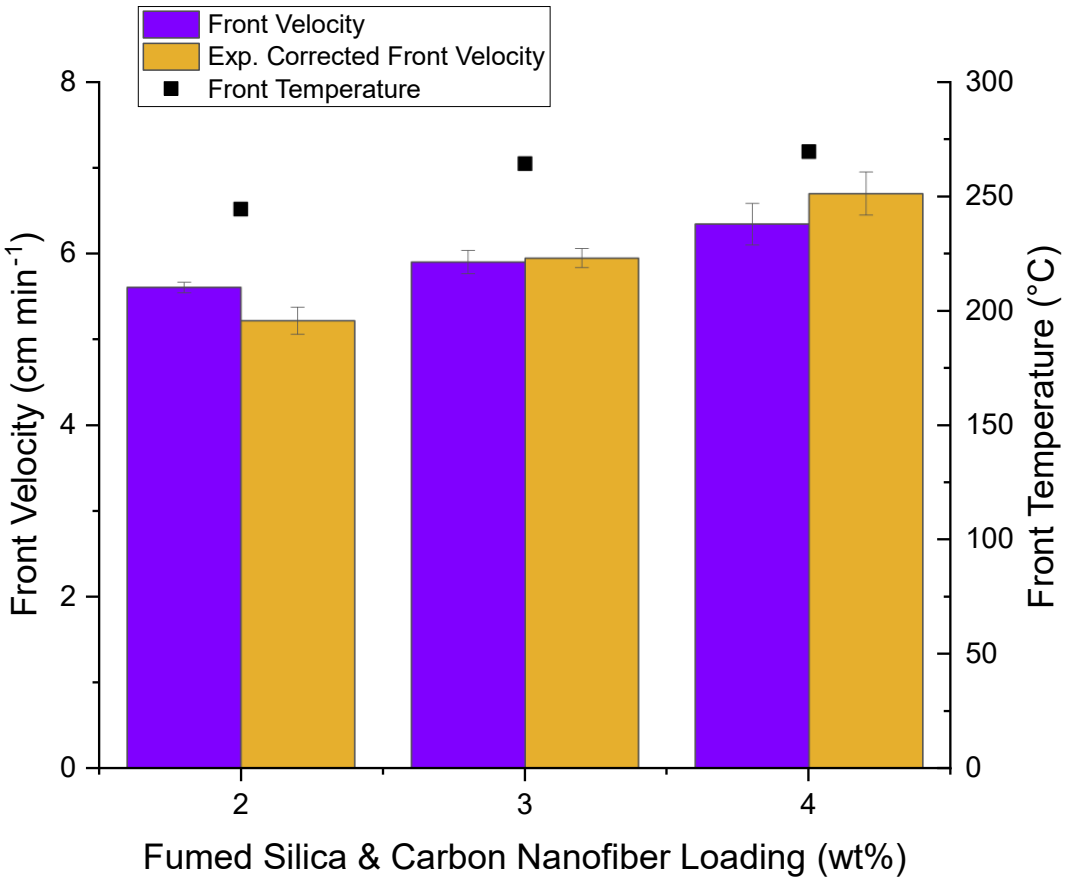

Figure 7.2. Front velocity and temperature versus fumed silica and carbon nanofiber loading for resin system of 60 wt% BADGE, 20 wt% CE, 20 wt% TEGDVE, 1 phr IOC-8 and 1 phr Luperox 231 meant for additive manufacturing.

7.3. Coatings using RICFP

Coatings are a large field in the chemical industry. The biggest challenge to developing a coating formulation for curing with FP is heat loss to the surroundings. The surface to volume ratio of a thin layer is much larger than a typical polymer, which lends itself to the heat generation in a

system being overcome by heat loss. Nonetheless, thin layers including coatings and adhesives have been reported for RICFP. The Liska group have shown that increasing onium salt or thermal radical initiator concentration lowers the minimum layer thickness required for sustaining FP. [56] Likewise, the Sangermano group showed that an adhesive, which can be thought of as a thin layer between two substrates, was supported at 500 μm thicknesses but not 250 μm. [145] Adjusting the ratio of a more reactive epoxy to BADGE also affected their generated heat for sustaining FP and strength of the adhesive.

With the existing literature in mind, there was an effort to examine more of the parameters required for FP of thin layers and coatings. As mentioned earlier, there must be a minimum viscosity of formulations for FP that are polymerized horizontally outside of test tubes so that buoyancy-driven convection is suppressed. It was found that application using a drawdown bar at a thickness of 1000 μm, a minimum fumed silica loading of 5 wt% is needed with 50/50 TMPTE/TEGDVE and 1 phr IOC-8 and 1 phr Luperox 231 resins. Increasing the amount of fumed silica, which in turn increases viscosity, showed that front velocity will not increase substantially in Figure 7.3. However, 7.5 wt% and 10 wt% FS gave a poorer material with many areas that had no polymer. This is attributed to the difficulty in applying a homogeneous layer using the drawdown bar with very viscous material. Resins with only 5 wt% FS were much less viscous and always resulted in a homogeneous layer.

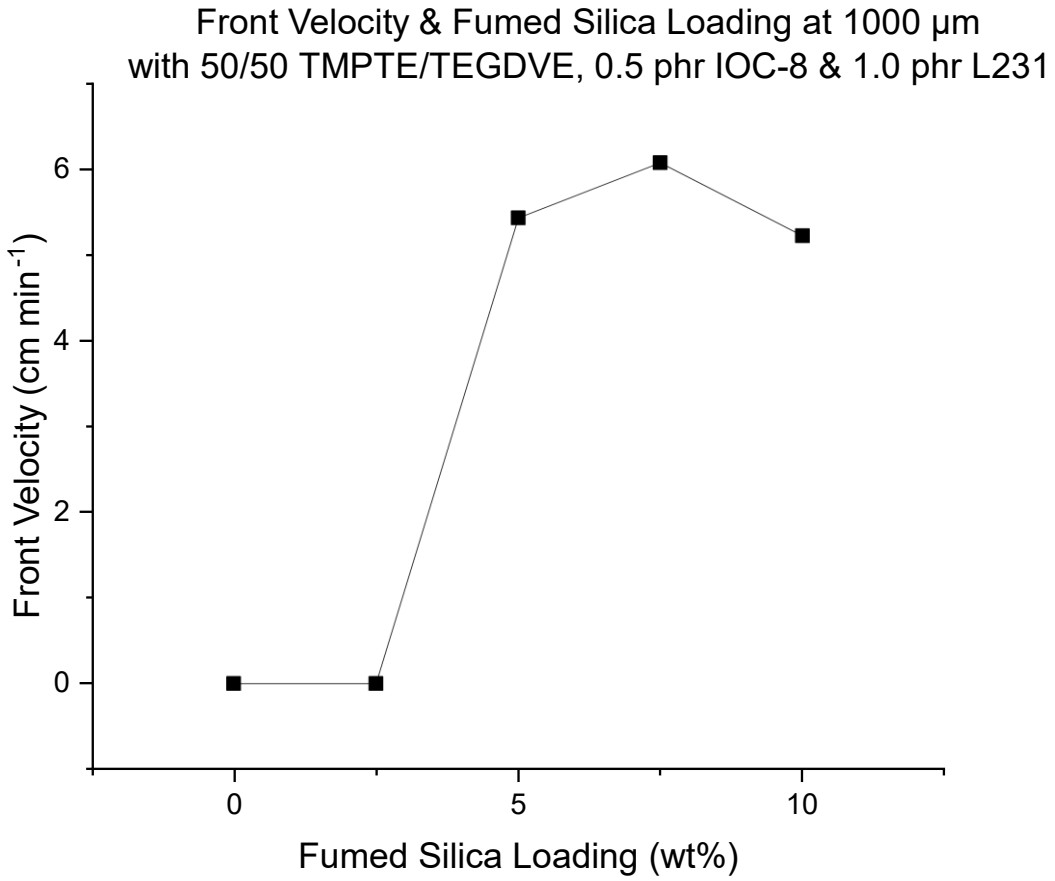

Figure 7.3. Front velocity as a function of increase of fumed silica with a 1:1 TMPTE:TEGDVE and 1 phr IOC-8, 1 phr Luperox 231 system in a 1000 µm layer.

The other parameter that must be controlled when considering thin layers is the thickness of the coating. With the established minimum of 5 wt% fumed silica, the layer thickness was increased from 250 µm to 4000 µm using a drawdown bar. Using the same 1:1 ratio of TMPTE:TEGDVE, for two concentrations of IOC-8 it was found that the front velocity increased as the layer thickness increased as shown in Figure 7.4. This is due to the decrease of the surface area to volume ratio as the thickness of the layer increased and a decrease in heat loss overall. No front was supported for either initiator concentration at 250 µm thickness. Additionally, 500 µm thick layers did not propagate throughout the entire layer. Thick layers of more than 1000 µm would experience more cracking than the thinner layers.

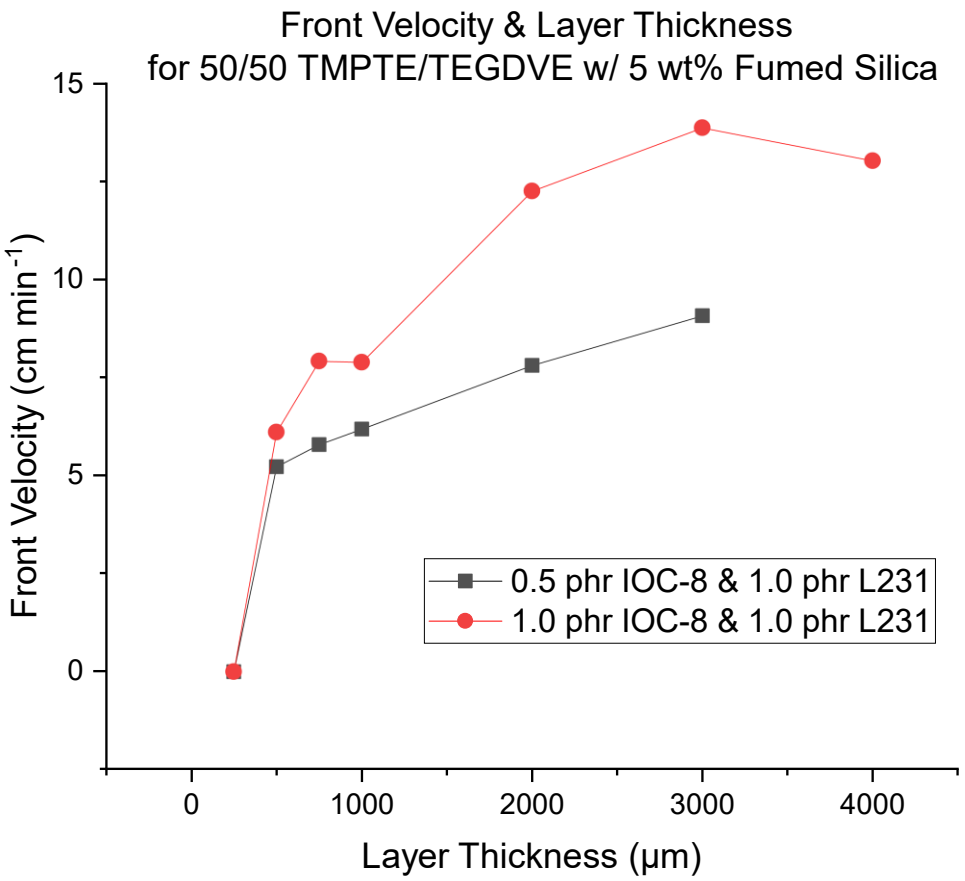

Figure 7.4. Effect of layer thickness on front velocity for systems of 1:1 TMPTE:TEGDVE and 5 wt% fumed silica added with both 1 phr IOC-8 and 1 phr Luperox 231 or 0.5 phr IOC-8 and 1 phr Luperox 231.

One other aspect to consider is the substrate to which the coating is applied. The preceding experiments were carried out on planks of pine wood. Interestingly, likely due to the different thermal properties of the grain in pine, the front would not propagate along the separations of the grain as shown in Figures 7.5 and 7.6. There is evidence that thermal conductivity will differ based on the direction of grains for different species of wood. [146] Based on these figures, it also appears that the layer thickness affects the propensity for the front to follow the grain pattern. Thicker samples will propagate completely regardless of the grain. Wood is chosen for most FP molds since due to cost. Attempts with the resin on glass will support fronts, but the material did

not adhere due to the lack of surface -OH bonds for the polymer to hydrogen bond to, unlike wood. Primed steel did not support a front, but only locally polymerized upon heat. This is because metal is a good conductor of heat and acts as a heat sink, contributing to heat loss. While the material is primed and can adhere, the thermal properties of metal inhibit the FP. Aluminum strips substrates also would not support fronts.

Figure 7.5. Sample of 50/50 TMPTE/TEGDVE with 0.5 phr IOC-8, 1 phr Luperox 231, and 5 wt% fumed silica in a 500 μm layer on pine wood. The resin with exposed grain is shown on the left with the cured polymer after FP on the right.

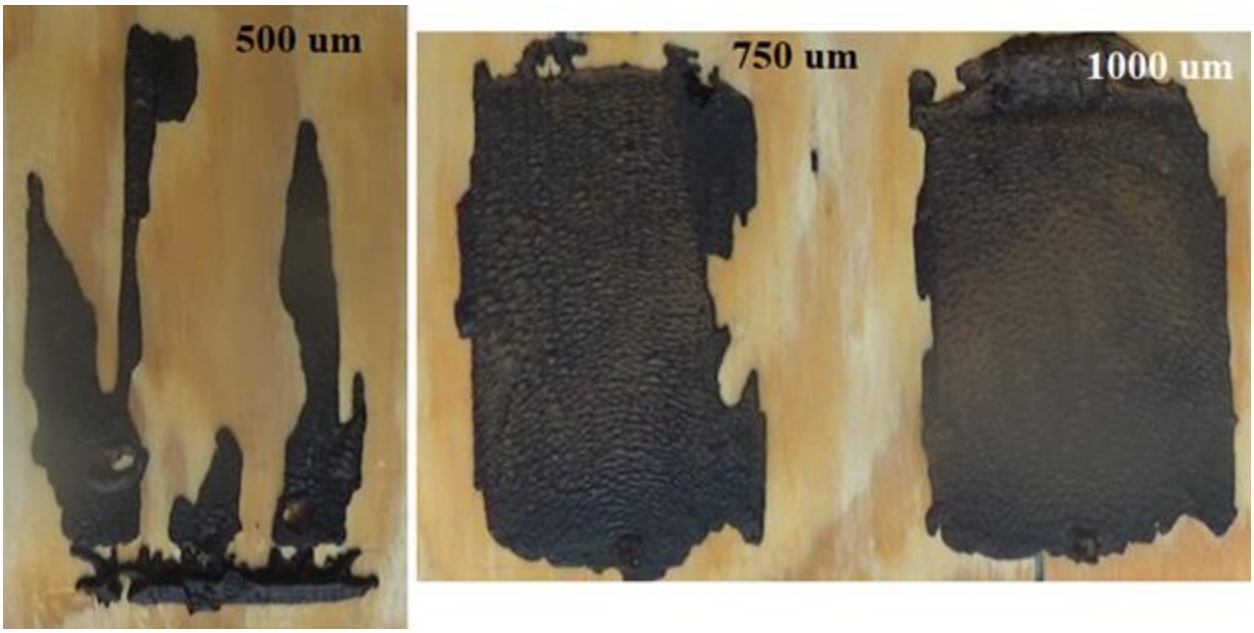

Figure 7.6. Polymerized samples of 50/50 TMPTE/TEGDVE with 1 phr IOC-8, 1 phr Luperox 231, and 5 wt% fumed silica in layers from 500 to 1000 μm pine wood (um = μm).

7.4. Utilization of Fpoxy-functionalized Bio-derived Monomers

There are many recent attempts to utilize epoxidized bio-based compounds, such as vegetable oils. While the advantages and disadvantages of using compounds derived from food feedstocks are under debate, it has been shown that vanillin-derived monomers are reactive in RICFP. [136] Other common bio-based epoxies are soybean and linseed oils. RICFP is possible using these epoxidized soybean and linseed oils. Vikoflex 7190 (V7190), an epoxidized linseed oil, and epoxidized sucrose soyate (ESS) provided by collaborators at North Dakota State University

were tested. The structures of V7190 and ESS are shown below in Figure 7.7.

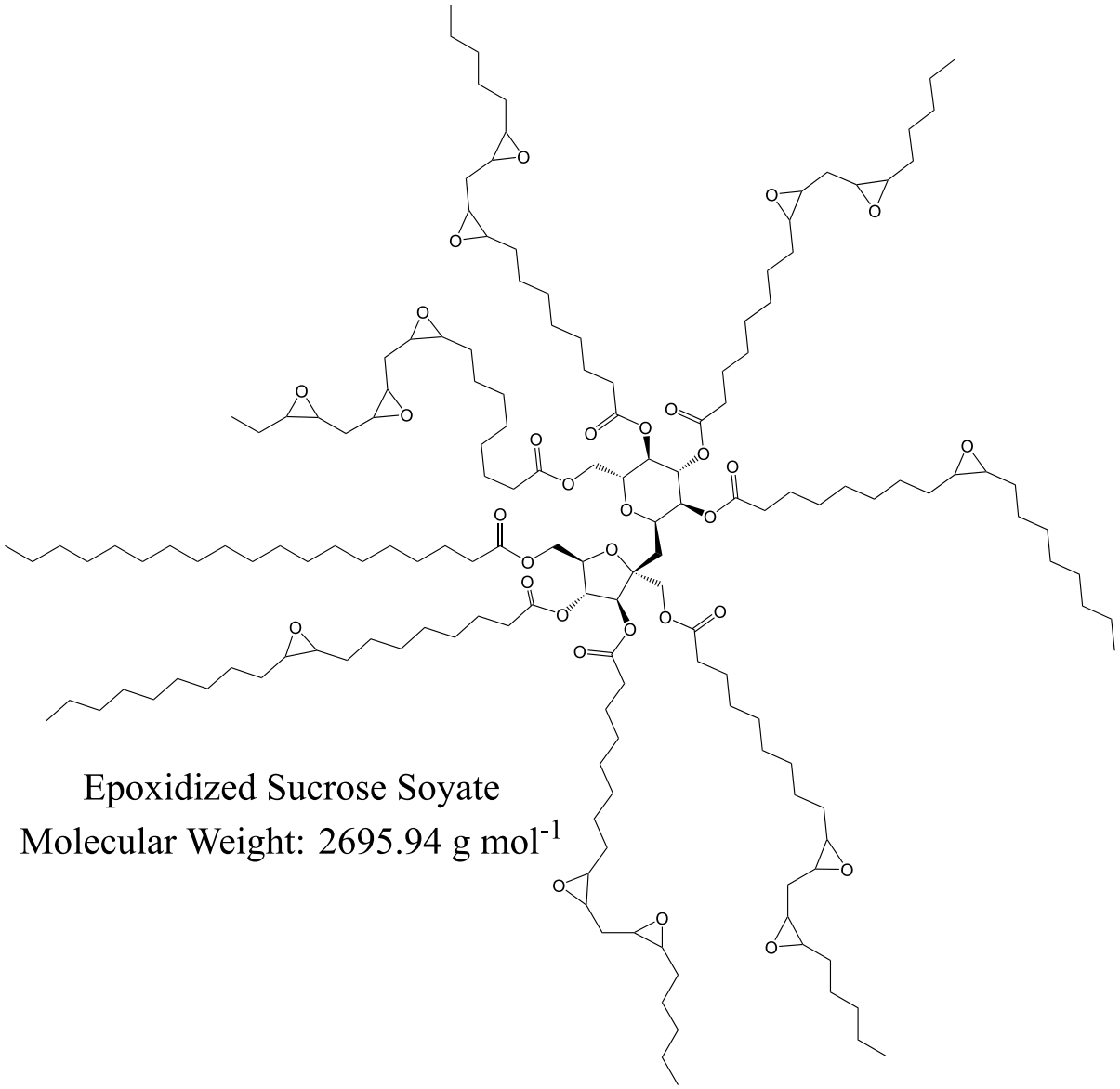

Figure 7.7. Structures of epoxidized sucrose soyate (ESS) and Vikoflex 7190 (V7190) epoxidized linseed oil.

The two oil-based epoxies and TMPTE were compared with 1 phr IOC-8 and 1 phr Luperox® 231 in Figure 7.8 below. It is seen that ESS has a very slow front velocity and V7190 is faster, though still much slower than TMPTE. The three epoxies were also compared with either no TEGDVE or 5 wt% TEGDVE added. The addition of even small amounts of vinyl ether, 5 wt% in this case, resulted in nearly double the front velocity in all cases. It was found that ESS would not support a front without TEGDVE added, unlike V7190 and TMPTE.

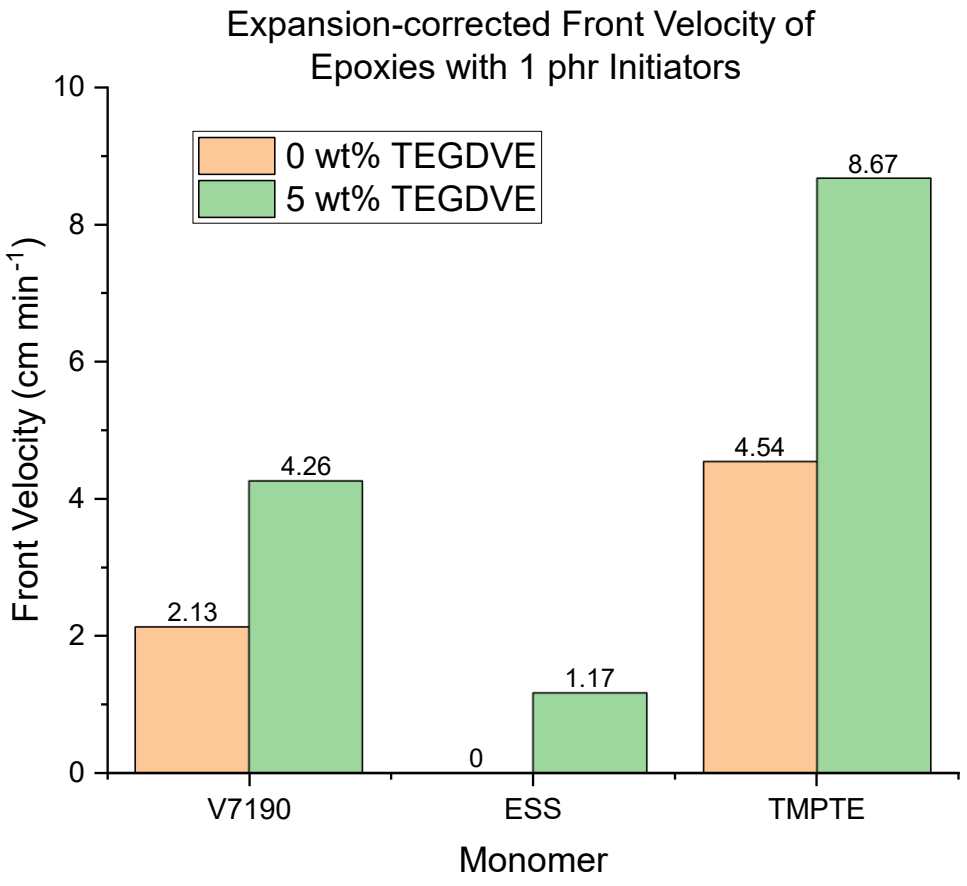

Figure 7.8. Comparison of expansion-corrected front velocities for epoxidized linseed oil (V7190), epoxidized sucrose soyate (ESS), and TMPTE with 1 phr IOC-8, 1 phr Luperox 231, and 10 wt% fumed silica with either 0 wt% TEGDVE or 5 wt% TEGDVE added.

The front velocity of the three monomers was also shown to increase with increasing initiator concentration much like previous RICFP work. Figure 7.9 shows the front velocity versus

initiator concentration for each monomer. The change was most drastic for TMPTE, which nearly doubled with doubled initiator concentration. The effect of each initiator separately was not studied.

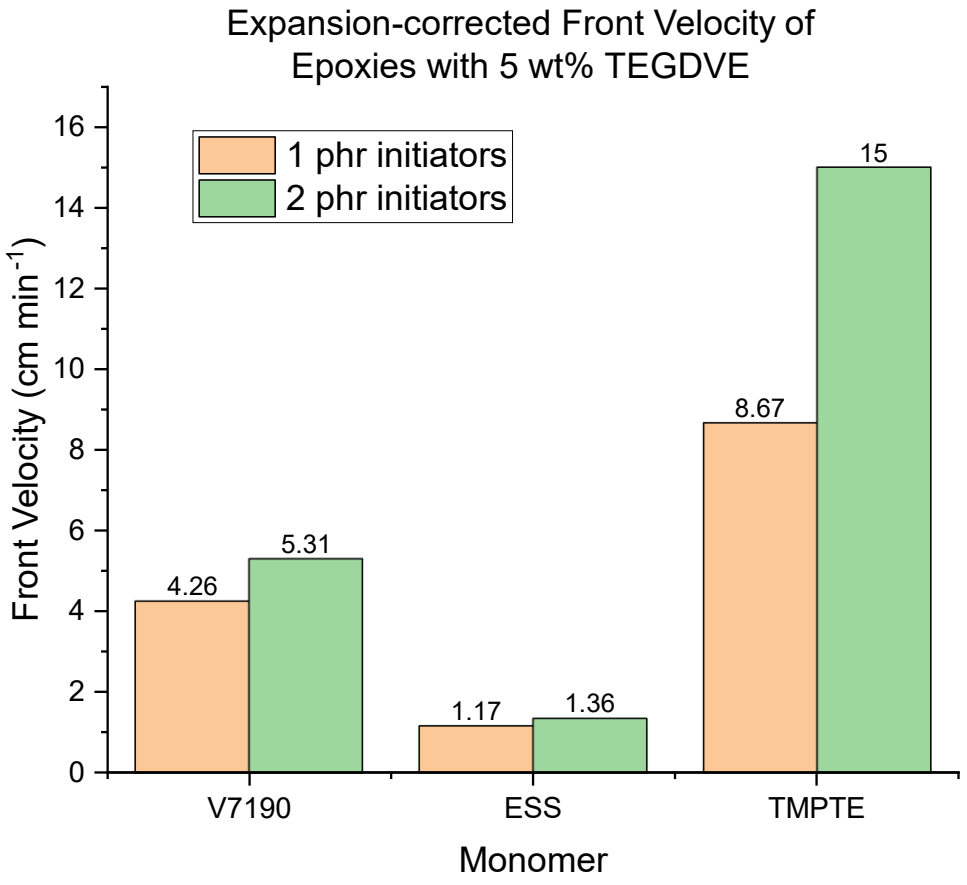

Figure 7.9. Comparison of expansion-corrected front velocities for epoxidized linseed oil (V7190), epoxidized sucrose soyate (ESS), and TMPTE with 10 wt% fumed silica and 5 wt% TEGDVE added and either 1 phr IOC-8 and 1 phr Luperox 231 or 2 phr IOC-8 and 2 phr Luperox 231.

The low front velocity of ESS and V7190 compared to TMPTE can be mostly attributed to the low MW/epoxy group ratio as displayed in Table 7.1, which results in lower heat generated per unit of monomer. Across all monomers the front velocity is inversely proportional to the molecular weight per epoxy group. Overall, bio-based epoxy resins can be useful to RICFP

through imparting different material properties, but for large scale implementation, care must be taken to choose materials that are coming from renewable feedstocks—waste products that would otherwise serve no purpose are particularly promising for this case.

Table 7.1. Comparison of molecular weights and molecular weight per epoxy group for two bio-based epoxies and TMPTE.

	Molecular weight (g mol^{-1})	Molecular weight per epoxy group
TMPTE	302.4	100.8
V7190	891.2	148.5
ESS	2695.9	207.4

7.5. Conclusions and Outlook for Applications

Many potential applications for frontal polymerization have been shown in the literature, including composites, coatings, adhesives, hydrogels, and additive manufacturing. Most of this published work uses free-radical frontal polymerization or frontal ring-opening metathesis polymerization. The use of radical-induced cationic frontal polymerization for applications widens the potential monomers capable of producing practical, functional materials. Bio-based epoxy monomers are among the potential useful monomers that can be used, which have low front velocity due to their high molecular weight to epoxy group ratio but could have interesting material properties with their large structures. It was shown that RICFP is promising for additive manufacturing and coatings, as well as the production of composites as shown in previous chapters of this dissertation. A consistent issue among both additive manufacturing and coatings is heat loss becoming dominant and quenching fronts because the surface area to volume ratio is small in these systems. Promising systems using vinyl ethers for additive manufacturing were used, which had high reactivity, and with carbon nanofibers added to promote heat diffusion. These systems were successful in preliminary studies of printing of free-standing structures. It was found that minimum layer thicknesses to overcome heat loss and filler loading to overcome

buoyancy-induced convection exist for coatings. Optimizing formulations to obtain the desired material properties will continue in RICFP. With epoxies being an abundant class of monomers in industry, there are many options to formulate resins for a given application, and addition of vinyl ethers or other filler additives can enhance reactivity or add other interesting material properties.

CHAPTER 8. SUMMARY AND OUTLOOK

Frontal polymerization as a technique has many unique advantages compared to typical curing methods for materials. FP formulations are one-pot, cure on-demand resins which cure quickly and have lower energy requirements than autoclave curing. By broadening the possible monomer selection from free-radically polymerizable acrylates to epoxies and vinyl ethers using cationic FP, comparable materials to existing two-part epoxies can be produced. RICFP is a growing method to produce epoxy materials through FP and using an onium salt superacid generator coupled with a thermal radical initiator.

It was shown that adding divinyl ethers to epoxies using RICFP increases the front speed. Hydroxy-functionalized monovinyl ethers tested were shown to reduce front velocity as the ratio of their addition increased. This is likely due to chain transfer effects, or low boiling point. With accelerated pot life studies, the front velocity decreases over time due to decomposition of the thermal radical initiator and increasing vinyl ether ratio lowered the pot life. The pot life can be lengthened through addition of free-radical inhibitors. Analysis of the epoxy-vinyl ether polymers using IR spectroscopy showed a decrease in conversion of the epoxy when mixed 1:1, along with an increase in vinyl ether conversion. Based on previous photopolymerization publications, the reduction in epoxy conversion indicates no copolymerization of the two monomers, but the increase in vinyl ether conversion instead suggests that there is some catalytic process arising from the interaction of the two monomers which would suggest copolymerization. More detailed study into determining if copolymerization is occurring between epoxy and vinyl ether monomers in these RICFP systems is needed.

Development of new vinyl ethers for FP with desirable structures and high functionality could allow for better control over structure-property relationships of high reactivity systems.

Attempts at synthesizing new vinyl ethers included solid urethane-based vinyl ethers using diisocyanates and hydroxy-functionalized vinyl ethers, which would not support fronts due to the urea group inhibiting the cationic polymerization. Vinyl ethers with high boiling points based on fatty acids were synthesized but did also not support fronts likely because of low yield of the product or low relative heat production because of the high molecular weight of the vinyl ether. Finally, in a collaboration with the García-López group at LSU, synthesis of high functionality vinyl ethers based on glycerol and pentaerythritol using calcium carbide was carried out, but purification of the product is difficult due to its low boiling point.

The well-studied free-radical FP of acrylates with minimal fillers produces polymers with poor properties and can experience oxygen inhibition along with shrinkage during polymerization. To mitigate these issues, hybrid systems of acrylate with epoxy and vinyl ether using RICFP were studied. In both acrylate/epoxy and acrylate/vinyl ether mixtures, a concave dependence of the front velocity on monomer ratio was found, which indicates no copolymerization between the two monomers.

To generate practical materials, fillers are useful to reduce overall cost through a reduction of resin needed, while also enhancing material properties of the composite produced. In this work, addition of different fillers to RICFP was studied, where it was found that clays do not follow the same trends seen previously with free-radical FP. [22] Clays have unique chemistries and affect the mechanical and rheological properties of materials. Overall, the addition of clays reduces the front velocity by different values depending on which clay is used. For one, the clays contribute to heat loss. As an example, analysis of the addition of conductive carbon fibers and insulative wood flour showed that carbon fibers increase front velocity by aiding in heat transfer, while the wood flour decreases front velocity. Clays also inherently swell with water and after

drying the clays, an increase in front velocity and front temperature can be seen. The possible inhibition of radicals by clays was also studied, where it was found that talc likely does not inhibit radicals, while kaolin and Ca-bentonite do. The viscosity of the uncured formulations was found to be vary from clay to clay, but this was found to not affect the front velocity.

Regarding the mechanical properties of RICFP composites with clays, through flexural testing it was found that an increase of talc loading will increase the flexural strength and modulus. The clays studied all resulted in differing flexural strength and moduli, which is attributed to the composites having varying void content. The glass transition temperatures of the flexible composites were lower than room temperature and found to increase with increasing clay loading due to decreased chain mobility and decrease with clays containing more water. Dispersion of the clays in the polymer matrix was studied using SEM-EDS and found to vary for every clay composite. Using untreated wollastonites, increasing surface area of fillers was found to decrease front velocity, while increasing aspect ratio increased front velocity. The surface area results are likely due to increased interaction of the clay with the monomers, while the aspect ratio may be disrupting the crosslinked structure and enhancing active end mobility. Finally, montmorillonite K 10, an acid-treated bentonite clay, was found to cause spontaneous polymerization upon addition due to the acidity initiating cationic polymerization.

RICFP normally requires the use of both a superacid generator and thermal radical initiator. It was found that FP of epoxies and vinyl ethers is still possible through only addition of a superacid generator, which thermally decomposes to generate superacid. This should result in a polymer containing fewer voids due to the lack of volatile materials produced by the free-radical initiator, but it also simplifies the formulating process and any assumptions of FP mechanisms with only two components required (monomer and initiator). With both epoxy and vinyl ether,

front velocity increased as the concentration of IOC-8 was increased. The minimum IOC-8 concentration varied depending on the monomer, with vinyl ethers requiring much less IOC-8 and having higher front velocities. The fronts with only IOC-8 were initiated with UV light and heating. Adding radical inhibitor to the system resulted in a decrease in front velocity, indicating that the superacid generator is generating radical species that aid in decomposition of IOC-8.

Applications of the RICFP systems were investigated as well. There have been many applications of free-radical FP and FROMP, such as coatings, adhesives, and additive manufacturing. With additive manufacturing of RICFP systems, a resin was developed based on two epoxies and a vinyl ether to have high reactivity, and with addition of carbon nanofibers and fumed silica the viscosity was high enough to print free-standing structures. Thin layers using RICFP of epoxy/vinyl ether systems were also studied, where a minimum layer thickness to support a front was found. Increasing layer thickness increased the front velocity. There was also a minimum viscosity indicated by fumed silica loading needed to support a front. Bio-based epoxy monomers were also studied, which could affect the properties of polymers.

Overall, there is a lot of promise for useful applications of RICFP, which is still a young and relatively unexplored field, relative to other methods of FP. For one, additive manufacturing is shown to be possible and needs more study, but it could be a faster method to 3D print compared to traditional deposition using polylactic acid. More study is needed to understand the fundamentals of RICFP as well as photopolymerization of similar systems has been studied. Detailed analysis of polymers produced with epoxy/vinyl ether systems to determine how monomer selection affects conversion and incidence of copolymerization could be useful. This also echoes for hybrid systems containing acrylate, where IR spectroscopy studies are found to be more difficult and could provide useful information about the extent of the FP. Synthesis of

novel vinyl ethers remains a problem but with success could give highly reactive resins with polymers possessing desirable qualities.

APPENDIX A. CHAPTER 2 COPYRIGHT PERMISSIONS

JOHN WILEY AND SONS LICENSE
TERMS AND CONDITIONS
Sep 25, 2023

This Agreement between Brecklyn Groce ("You") and John Wiley and Sons ("John Wiley and Sons") consists of your license details and the terms and conditions provided by John Wiley and Sons and Copyright Clearance Center.

License Number	5636141355486
License date	Sep 25, 2023
Licensed Content Publisher	John Wiley and Sons
Licensed Content Publication	Journal of Polymer Science
Licensed Content Title	Front velocity dependence on vinyl ether and initiator concentration in radical-induced cationic frontal polymerization of epoxies
Licensed Content Author	Brecklyn R. Groce, Daniel P. Gary, Joseph K. Cantrell, et al
Licensed Content Date	May 31, 2021
Licensed Content Volume	59
Licensed Content Issue	15
Licensed Content Pages	8
Type of use	Dissertation/Thesis
Requestor type	Author of this Wiley article
Format	Print and electronic
Portion	Full article
Will you be translating?	No
Title	CATIONIC FRONTAL POLYMERIZATION: FRONT KINETICS, EFFECTS OF ADDITIVES, AND APPLICATIONS
Institution name	Louisiana State University
Expected presentation date	Oct 2023

	Brecklyn Groce
Requestor Location	Baton Rouge, LA 70808 United States Attn: Brecklyn Groce
Publisher Tax ID	EU826007151
Total	0.00 USD

Terms and Conditions

TERMS AND CONDITIONS

This copyrighted material is owned by or exclusively licensed to John Wiley & Sons, Inc. or one of its group companies (each a"Wiley Company") or handled on behalf of a society with which a Wiley Company has exclusive publishing rights in relation to a particular work (collectively "WILEY"). By clicking "accept" in connection with completing this licensing transaction, you agree that the following terms and conditions apply to this transaction (along with the billing and payment terms and conditions established by the Copyright Clearance Center Inc., ("CCC's Billing and Payment terms and conditions"), at the time that you opened your RightsLink account (these are available at any time at http://myaccount.copyright.com).

Terms and Conditions

- The materials you have requested permission to reproduce or reuse (the "Wiley Materials") are protected by copyright.

- You are hereby granted a personal, non-exclusive, non-sub licensable (on a stand-alone basis), non-transferable, worldwide, limited license to reproduce the Wiley Materials for the purpose specified in the licensing process. This license, **and any CONTENT (PDF or image file) purchased as part of your order,** is for a one-time use only and limited to any maximum distribution number specified in the license. The first instance of republication or reuse granted by this license must be completed within two years of the date of the grant of this license (although copies prepared before the end date may be distributed thereafter). The Wiley Materials shall not be used in any other manner or for any other purpose, beyond what is granted in the license. Permission is granted subject to an appropriate acknowledgement given to the author, title of the material/book/journal and the publisher. You shall also duplicate the copyright notice that appears in the Wiley publication in your use of the Wiley Material. Permission is also granted on the understanding that nowhere in the text is a previously published source acknowledged for all or part of this Wiley Material. Any third party content is expressly excluded from this permission.

- With respect to the Wiley Materials, all rights are reserved. Except as expressly granted by the terms of the license, no part of the Wiley Materials may be copied,

modified, adapted (except for minor reformatting required by the new Publication), translated, reproduced, transferred or distributed, in any form or by any means, and no derivative works may be made based on the Wiley Materials without the prior permission of the respective copyright owner.**For STM Signatory Publishers clearing permission under the terms of the STM Permissions Guidelines only, the terms of the license are extended to include subsequent editions and for editions in other languages, provided such editions are for the work as a whole in situ and does not involve the separate exploitation of the permitted figures or extracts,** You may not alter, remove or suppress in any manner any copyright, trademark or other notices displayed by the Wiley Materials. You may not license, rent, sell, loan, lease, pledge, offer as security, transfer or assign the Wiley Materials on a stand-alone basis, or any of the rights granted to you hereunder to any other person.

- The Wiley Materials and all of the intellectual property rights therein shall at all times remain the exclusive property of John Wiley & Sons Inc, the Wiley Companies, or their respective licensors, and your interest therein is only that of having possession of and the right to reproduce the Wiley Materials pursuant to Section 2 herein during the continuance of this Agreement. You agree that you own no right, title or interest in or to the Wiley Materials or any of the intellectual property rights therein. You shall have no rights hereunder other than the license as provided for above in Section 2. No right, license or interest to any trademark, trade name, service mark or other branding ("Marks") of WILEY or its licensors is granted hereunder, and you agree that you shall not assert any such right, license or interest with respect thereto

- NEITHER WILEY NOR ITS LICENSORS MAKES ANY WARRANTY OR REPRESENTATION OF ANY KIND TO YOU OR ANY THIRD PARTY, EXPRESS, IMPLIED OR STATUTORY, WITH RESPECT TO THE MATERIALS OR THE ACCURACY OF ANY INFORMATION CONTAINED IN THE MATERIALS, INCLUDING, WITHOUT LIMITATION, ANY IMPLIED WARRANTY OF MERCHANTABILITY, ACCURACY, SATISFACTORY QUALITY, FITNESS FOR A PARTICULAR PURPOSE, USABILITY, INTEGRATION OR NON-INFRINGEMENT AND ALL SUCH WARRANTIES ARE HEREBY EXCLUDED BY WILEY AND ITS LICENSORS AND WAIVED BY YOU.

- WILEY shall have the right to terminate this Agreement immediately upon breach of this Agreement by you.

- You shall indemnify, defend and hold harmless WILEY, its Licensors and their respective directors, officers, agents and employees, from and against any actual or threatened claims, demands, causes of action or proceedings arising from any breach of this Agreement by you.

- IN NO EVENT SHALL WILEY OR ITS LICENSORS BE LIABLE TO YOU OR ANY OTHER PARTY OR ANY OTHER PERSON OR ENTITY FOR ANY SPECIAL, CONSEQUENTIAL, INCIDENTAL, INDIRECT, EXEMPLARY OR PUNITIVE DAMAGES, HOWEVER CAUSED, ARISING OUT OF OR IN CONNECTION WITH THE DOWNLOADING, PROVISIONING, VIEWING OR USE OF THE MATERIALS REGARDLESS OF THE FORM OF ACTION, WHETHER FOR BREACH OF CONTRACT, BREACH OF WARRANTY, TORT, NEGLIGENCE, INFRINGEMENT OR OTHERWISE (INCLUDING, WITHOUT LIMITATION, DAMAGES BASED ON LOSS OF PROFITS, DATA, FILES, USE, BUSINESS OPPORTUNITY OR CLAIMS OF THIRD PARTIES), AND WHETHER OR NOT THE PARTY HAS BEEN ADVISED OF THE POSSIBILITY OF SUCH DAMAGES. THIS LIMITATION SHALL APPLY NOTWITHSTANDING ANY FAILURE OF ESSENTIAL PURPOSE OF ANY LIMITED REMEDY PROVIDED HEREIN.

- Should any provision of this Agreement be held by a court of competent jurisdiction to be illegal, invalid, or unenforceable, that provision shall be deemed amended to achieve as nearly as possible the same economic effect as the original provision, and the legality, validity and enforceability of the remaining provisions of this Agreement shall not be affected or impaired thereby.

- The failure of either party to enforce any term or condition of this Agreement shall not constitute a waiver of either party's right to enforce each and every term and condition of this Agreement. No breach under this agreement shall be deemed waived or excused by either party unless such waiver or consent is in writing signed by the party granting such waiver or consent. The waiver by or consent of a party to a breach of any provision of this Agreement shall not operate or be construed as a waiver of or consent to any other or subsequent breach by such other party.

- This Agreement may not be assigned (including by operation of law or otherwise) by you without WILEY's prior written consent.

- Any fee required for this permission shall be non-refundable after thirty (30) days from receipt by the CCC.

- These terms and conditions together with CCC's Billing and Payment terms and conditions (which are incorporated herein) form the entire agreement between you and WILEY concerning this licensing transaction and (in the absence of fraud) supersedes all prior agreements and representations of the parties, oral or written. This Agreement may not be amended except in writing signed by both parties. This Agreement shall be binding upon and inure to the benefit of the parties' successors, legal representatives, and authorized assigns.

- In the event of any conflict between your obligations established by these terms and conditions and those established by CCC's Billing and Payment terms and conditions, these terms and conditions shall prevail.

- WILEY expressly reserves all rights not specifically granted in the combination of (i) the license details provided by you and accepted in the course of this licensing transaction, (ii) these terms and conditions and (iii) CCC's Billing and Payment terms and conditions.

- This Agreement will be void if the Type of Use, Format, Circulation, or Requestor Type was misrepresented during the licensing process.

- This Agreement shall be governed by and construed in accordance with the laws of the State of New York, USA, without regards to such state's conflict of law rules. Any legal action, suit or proceeding arising out of or relating to these Terms and Conditions or the breach thereof shall be instituted in a court of competent jurisdiction in New York County in the State of New York in the United States of America and each party hereby consents and submits to the personal jurisdiction of such court, waives any objection to venue in such court and consents to service of process by registered or certified mail, return receipt requested, at the last known address of such party.

WILEY OPEN ACCESS TERMS AND CONDITIONS

Wiley Publishes Open Access Articles in fully Open Access Journals and in Subscription journals offering Online Open. Although most of the fully Open Access journals publish open access articles under the terms of the Creative Commons Attribution (CC BY) License only, the subscription journals and a few of the Open Access Journals offer a choice of Creative Commons Licenses. The license type is clearly identified on the article.

The Creative Commons Attribution License

The Creative Commons Attribution License (CC-BY) allows users to copy, distribute and transmit an article, adapt the article and make commercial use of the article. The CC-BY license permits commercial and non-

Creative Commons Attribution Non-Commercial License

The Creative Commons Attribution Non-Commercial (CC-BY-NC)License permits use, distribution and reproduction in any medium, provided the original work is properly cited and is not used for commercial purposes.(see below)

Creative Commons Attribution-Non-Commercial-NoDerivs License

The Creative Commons Attribution Non-Commercial-NoDerivs License (CC-BY-NC-ND) permits use, distribution and reproduction in any medium, provided the original work

---

APPENDIX B. CHAPTER 5 COPYRIGHT PERMISSIONS

ACS APPLIED MATERIALS & INTERFACES

www.acsami.org Research Article

Kinetic and Chemical Effects of Clays and Other Fillers in the Preparation of Epoxy–Vinyl Ether Composites Using Radical-Induced Cationic Frontal Polymerization

Brecklyn R. Groce, Emma E. Lane, Daniel P. Gary, Douglas T. Ngo, Dylan T. Ngo, Fahima Shaon, Jorge A. Belgodere, and John A. Pojman*

Cite This: *ACS Appl. Mater. Interfaces* 2023, 15, 19403–19413 Read Online

APPENDIX C. CHAPTER 6 COPYRIGHT PERMISSIONS

JOHN WILEY AND SONS LICENSE
TERMS AND CONDITIONS
Sep 25, 2023

This Agreement between Brecklyn Groce ("You") and John Wiley and Sons ("John Wiley and Sons") consists of your license details and the terms and conditions provided by John Wiley and Sons and Copyright Clearance Center.

License Number	5636141183448
License date	Sep 25, 2023
Licensed Content Publisher	John Wiley and Sons
Licensed Content Publication	Journal of Polymer Science
Licensed Content Title	Thermally initiated cationic frontal polymerization of epoxies and vinyl ethers through a lone onium salt
Licensed Content Author	Brecklyn R. Groce, Madison M. Ferguson, John A. Pojman
Licensed Content Date	Sep 23, 2023
Licensed Content Volume	0
Licensed Content Issue	0
Licensed Content Pages	10
Type of use	Dissertation/Thesis
Requestor type	Author of this Wiley article
Format	Print and electronic
Portion	Full article
Will you be translating?	No
Title	CATIONIC FRONTAL POLYMERIZATION: FRONT KINETICS, EFFECTS OF ADDITIVES, AND APPLICATIONS
Institution name	Louisiana State University
Expected presentation date	Oct 2023
Requestor Location	Brecklyn Groce

	Baton Rouge, LA 70808 United States Attn: Brecklyn Groce
Publisher Tax ID	EU826007151
Total	0.00 USD

Terms and Conditions

TERMS AND CONDITIONS

This copyrighted material is owned by or exclusively licensed to John Wiley & Sons, Inc. or one of its group companies (each a"Wiley Company") or handled on behalf of a society with which a Wiley Company has exclusive publishing rights in relation to a particular work (collectively "WILEY"). By clicking "accept" in connection with completing this licensing transaction, you agree that the following terms and conditions apply to this transaction (along with the billing and payment terms and conditions established by the Copyright Clearance Center Inc., ("CCC's Billing and Payment terms and conditions"), at the time that you opened your RightsLink account (these are available at any time at http://myaccount.copyright.com).

Terms and Conditions

- The materials you have requested permission to reproduce or reuse (the "Wiley Materials") are protected by copyright.

- You are hereby granted a personal, non-exclusive, non-sub licensable (on a stand-alone basis), non-transferable, worldwide, limited license to reproduce the Wiley Materials for the purpose specified in the licensing process. This license, **and any CONTENT (PDF or image file) purchased as part of your order,** is for a one-time use only and limited to any maximum distribution number specified in the license. The first instance of republication or reuse granted by this license must be completed within two years of the date of the grant of this license (although copies prepared before the end date may be distributed thereafter). The Wiley Materials shall not be used in any other manner or for any other purpose, beyond what is granted in the license. Permission is granted subject to an appropriate acknowledgement given to the author, title of the material/book/journal and the publisher. You shall also duplicate the copyright notice that appears in the Wiley publication in your use of the Wiley Material. Permission is also granted on the understanding that nowhere in the text is a previously published source acknowledged for all or part of this Wiley Material. Any third party content is expressly excluded from this permission.

- With respect to the Wiley Materials, all rights are reserved. Except as expressly granted by the terms of the license, no part of the Wiley Materials may be copied, modified, adapted (except for minor reformatting required by the new

Publication), translated, reproduced, transferred or distributed, in any form or by any means, and no derivative works may be made based on the Wiley Materials without the prior permission of the respective copyright owner.**For STM Signatory Publishers clearing permission under the terms of the STM Permissions Guidelines only, the terms of the license are extended to include subsequent editions and for editions in other languages, provided such editions are for the work as a whole in situ and does not involve the separate exploitation of the permitted figures or extracts,** You may not alter, remove or suppress in any manner any copyright, trademark or other notices displayed by the Wiley Materials. You may not license, rent, sell, loan, lease, pledge, offer as security, transfer or assign the Wiley Materials on a stand-alone basis, or any of the rights granted to you hereunder to any other person.

- The Wiley Materials and all of the intellectual property rights therein shall at all times remain the exclusive property of John Wiley & Sons Inc, the Wiley Companies, or their respective licensors, and your interest therein is only that of having possession of and the right to reproduce the Wiley Materials pursuant to Section 2 herein during the continuance of this Agreement. You agree that you own no right, title or interest in or to the Wiley Materials or any of the intellectual property rights therein. You shall have no rights hereunder other than the license as provided for above in Section 2. No right, license or interest to any trademark, trade name, service mark or other branding ("Marks") of WILEY or its licensors is granted hereunder, and you agree that you shall not assert any such right, license or interest with respect thereto

- NEITHER WILEY NOR ITS LICENSORS MAKES ANY WARRANTY OR REPRESENTATION OF ANY KIND TO YOU OR ANY THIRD PARTY, EXPRESS, IMPLIED OR STATUTORY, WITH RESPECT TO THE MATERIALS OR THE ACCURACY OF ANY INFORMATION CONTAINED IN THE MATERIALS, INCLUDING, WITHOUT LIMITATION, ANY IMPLIED WARRANTY OF MERCHANTABILITY, ACCURACY, SATISFACTORY QUALITY, FITNESS FOR A PARTICULAR PURPOSE, USABILITY, INTEGRATION OR NON-INFRINGEMENT AND ALL SUCH WARRANTIES ARE HEREBY EXCLUDED BY WILEY AND ITS LICENSORS AND WAIVED BY YOU.

- WILEY shall have the right to terminate this Agreement immediately upon breach of this Agreement by you.

- You shall indemnify, defend and hold harmless WILEY, its Licensors and their respective directors, officers, agents and employees, from and against any actual or threatened claims, demands, causes of action or proceedings arising from any breach of this Agreement by you.

- IN NO EVENT SHALL WILEY OR ITS LICENSORS BE LIABLE TO YOU OR ANY OTHER PARTY OR ANY OTHER PERSON OR ENTITY FOR ANY

SPECIAL, CONSEQUENTIAL, INCIDENTAL, INDIRECT, EXEMPLARY OR PUNITIVE DAMAGES, HOWEVER CAUSED, ARISING OUT OF OR IN CONNECTION WITH THE DOWNLOADING, PROVISIONING, VIEWING OR USE OF THE MATERIALS REGARDLESS OF THE FORM OF ACTION, WHETHER FOR BREACH OF CONTRACT, BREACH OF WARRANTY, TORT, NEGLIGENCE, INFRINGEMENT OR OTHERWISE (INCLUDING, WITHOUT LIMITATION, DAMAGES BASED ON LOSS OF PROFITS, DATA, FILES, USE, BUSINESS OPPORTUNITY OR CLAIMS OF THIRD PARTIES), AND WHETHER OR NOT THE PARTY HAS BEEN ADVISED OF THE POSSIBILITY OF SUCH DAMAGES. THIS LIMITATION SHALL APPLY NOTWITHSTANDING ANY FAILURE OF ESSENTIAL PURPOSE OF ANY LIMITED REMEDY PROVIDED HEREIN.

- Should any provision of this Agreement be held by a court of competent jurisdiction to be illegal, invalid, or unenforceable, that provision shall be deemed amended to achieve as nearly as possible the same economic effect as the original provision, and the legality, validity and enforceability of the remaining provisions of this Agreement shall not be affected or impaired thereby.

- The failure of either party to enforce any term or condition of this Agreement shall not constitute a waiver of either party's right to enforce each and every term and condition of this Agreement. No breach under this agreement shall be deemed waived or excused by either party unless such waiver or consent is in writing signed by the party granting such waiver or consent. The waiver by or consent of a party to a breach of any provision of this Agreement shall not operate or be construed as a waiver of or consent to any other or subsequent breach by such other party.

- This Agreement may not be assigned (including by operation of law or otherwise) by you without WILEY's prior written consent.

- Any fee required for this permission shall be non-refundable after thirty (30) days from receipt by the CCC.

- These terms and conditions together with CCC's Billing and Payment terms and conditions (which are incorporated herein) form the entire agreement between you and WILEY concerning this licensing transaction and (in the absence of fraud) supersedes all prior agreements and representations of the parties, oral or written. This Agreement may not be amended except in writing signed by both parties. This Agreement shall be binding upon and inure to the benefit of the parties' successors, legal representatives, and authorized assigns.

- In the event of any conflict between your obligations established by these terms and conditions and those established by CCC's Billing and Payment terms and conditions, these terms and conditions shall prevail.

- WILEY expressly reserves all rights not specifically granted in the combination of (i) the license details provided by you and accepted in the course of this licensing transaction, (ii) these terms and conditions and (iii) CCC's Billing and Payment terms and conditions.

- This Agreement will be void if the Type of Use, Format, Circulation, or Requestor Type was misrepresented during the licensing process.

- This Agreement shall be governed by and construed in accordance with the laws of the State of New York, USA, without regards to such state's conflict of law rules. Any legal action, suit or proceeding arising out of or relating to these Terms and Conditions or the breach thereof shall be instituted in a court of competent jurisdiction in New York County in the State of New York in the United States of America and each party hereby consents and submits to the personal jurisdiction of such court, waives any objection to venue in such court and consents to service of process by registered or certified mail, return receipt requested, at the last known address of such party.

WILEY OPEN ACCESS TERMS AND CONDITIONS

Wiley Publishes Open Access Articles in fully Open Access Journals and in Subscription journals offering Online Open. Although most of the fully Open Access journals publish open access articles under the terms of the Creative Commons Attribution (CC BY) License only, the subscription journals and a few of the Open Access Journals offer a choice of Creative Commons Licenses. The license type is clearly identified on the article.

The Creative Commons Attribution License

The Creative Commons Attribution License (CC-BY) allows users to copy, distribute and transmit an article, adapt the article and make commercial use of the article. The CC-BY license permits commercial and non-

Creative Commons Attribution Non-Commercial License

The Creative Commons Attribution Non-Commercial (CC-BY-NC)License permits use, distribution and reproduction in any medium, provided the original work is properly cited and is not used for commercial purposes.(see below)

Creative Commons Attribution-Non-Commercial-NoDerivs License

The Creative Commons Attribution Non-Commercial-NoDerivs License (CC-BY-NC-ND) permits use, distribution and reproduction in any medium, provided the original work is properly cited, is not used for commercial purposes and no modifications or adaptations are made. (see below)

Use by commercial "for-profit" organizations

Use of Wiley Open Access articles for commercial, promotional, or marketing purposes requires further explicit permission from Wiley and will be subject to a fee.

Further details can be found on Wiley Online Library http://olabout.wiley.com/WileyCDA/Section/id-410895.html

Other Terms and Conditions:

v1.10 Last updated September 2015

Questions? customercare@copyright.com.

REFERENCES

(1) Chechilo, N. M.; Khvilivitskii, R. J.; Enikolopyan, N. S. On the Phenomenon of Polymerization Reaction Spreading. *Dokl. Akad. Nauk SSSR* **1972**, *204* (N5), 1180-1181.

(2) Begishev, V. P.; Volpert, V. A.; Davtyan, S. P.; Malkin, A. Y. On some Features of the Anionic Activated e-Caprolactam Polymerization Process under Wave Propagation Conditions. *Dokl. Phys. Chem.* **1985**, *279* (N4), 1075-1077.

(3) Volpert, V. A.; Mergabova, I. N.; Davtyan, S. P.; Begishev, V. P. Propagation of the Caprolactam Polymerization Wave. *Combust. Explos. Shock Waves* **1986**, *21*, 443-447.

(4) Arutiunian, K. A.; Davtyan, S. P.; Rozenberg, B. A.; Enikolopyan, N. S. Curing of epoxy resins of bis-phenol A by amines under conditions of reaction front propagation. *Dokl. Akad. Nauk SSSR* **1975**, *223* (3), 657-660.

(5) Surkov, N. F.; Davtyan, S. P.; Rozenberg, B. A.; Enikolopyan, N. S. Calculation of the Steady Velocity of the Reaction Front during Hardening of Epoxy Oligomers by Diamines. *Dokl. Phys. Chem.* **1976**, *228* (1), 435-438.

(6) Pojman, J. A. Traveling Fronts of Methacrylic Acid Polymerization. *J. Am. Chem. Soc.* **1991**, *113*, 6284-6286. DOI: 10.1021/ja00016a063.

(7) Pojman, J. A.; Willis, J.; Fortenberry, D.; Ilyashenko, V.; Khan, A. Factors Affecting Propagating Fronts of Addition Polymerization: Velocity, Front Curvature, Temperature Profile, Conversion and Molecular Weight Distribution. *J. Polym. Sci. Part A: Polym Chem.* **1995**, *33*, 643-652.

(8) Pojman, J. A.; Ilyashenko, V. M.; Khan, A. M. Free-radical frontal polymerization: self-propagating thermal reaction waves. *J. Chem. Soc., Faraday Trans.* **1996**, *92* (16), 2825-2837. DOI: 10.1039/FT9969202825.

(9) Robertson, I. D.; Yourdkhani, M.; Centellas, P. J.; Aw, J. E.; Ivanoff, D. G.; Goli, E.; Lloyd, E. M.; Dean, L. M.; Sottos, N. R.; Geubelle, P. H.; et al. Rapid energy-efficient manufacturing of polymers and composites via frontal polymerization. *Nature* **2018**, *557* (7704), 223-227. DOI: 10.1038/s41586-018-0054-x.

(10) Totaro, N. P.; Murphy, Z. D.; Burcham, A. E.; King, C. T.; Scherr, T. F.; Bounds, C. O.; Dasa, V.; Pojman, J. A.; Hayes, D. J. In vitro evaluation of thermal frontally polymerized thiol-ene composites as bone augments. *J. Biomed. Mater. Res. Part A: Appl. Biomater.* **2016**, *104*, 1152–1160. DOI: 10.1002/jbm.b.33466.

(11) Pojman, J. A. Cure-on Demand Materials Based on Frontal Polymerization. *CSJ (Chem. Soc. Jpn.) Current Review* **2020**, *35*, 163 -169.

(12) Holt, T.; Fazende, K.; Jee, E.; Wu, Q.; Pojman, J. A. Cure-on-demand wood adhesive based on the frontal polymerization of acrylates. *J. Appl. Polym. Sci.* **2016**, *133* (40), 44064. DOI: 10.1002/app.44064.

(13) Mota-Morales, J. D.; Gutiérrez, M. C.; Ferrer, M. L.; Sanchez, I. C.; Elizalde-Peña, E. A.; Pojman, J. A.; Monte, F. D.; Luna-Bárcenas, G. Deep eutectic solvents as both active fillers and monomers for frontal polymerization. *J. Polym. Sci. Part A: Polym. Chem.* **2013**, *51*, 1767–1773. DOI: 10.1002/pola.26555.

(14) Yu, C.; Wang, C.-F.; Chen, S. Robust Self-Healing Host–Guest Gels from Magnetocaloric Radical Polymerization. *Adv. Funct. Mater.* **2014**, *24*, 1235-1242.

(15) Liu, J.-D.; Du, X.-Y.; Wang, C.-F.; Li, Q.; Chen, S. Construction of triple non-covalent interaction-based ultra-strong self-healing polymeric gels via frontal polymerization. *Journal of Materials Chemistry C* **2020**, *8* (40), 14083-14091. DOI: 10.1039/d0tc02986f.

(16) Su, J.; Yang, Y.; Chen, Z.; Zhou, J.; Liu, X.; Fang, Y.; Cui, Y. Preparation and performance of thermosensitive poly(N-isopropylacrylamide) hydrogels by frontal photopolymerization. *Polymer International* **2019**, *68* (10), 1673-1680. DOI: 10.1002/pi.5868.

(17) Tonoyan, A. O.; Varderesyan, A. Z.; Ketyan, A. G.; Minasyan, A. H.; Hovnanyan, K. O.; Davtyan, S. P. Continuous reactors of frontal polymerization in flow for the synthesis of polyacrylamide hydrogels with prescribed properties. *Journal of Polymer Engineering* **2020**, *40* (7), 601. DOI: 10.1515/polyeng-2019-0369.

(18) Caria, G.; Alzari, V.; Monticelli, O.; Nuvoli, D.; Kenny, J. M.; Mariani, A.; Bidali, S.; Fiori, S.; Sangermano, M.; Malucelli, G.; et al. Poly(N,N-dimethylacrylamide) hydrogels obtained by frontal polymerization. *J. Polym. Sci. Part A Polym. Chem.* **2009**, *47*, 1422-1428.

(19) Pojman, J. A. Frontal Polymerization. In *Polymer Science: A Comprehensive Reference*, Matyjaszewski, K., Möller, M. Eds.; Vol. 4; Elsevier BV, 2012; pp 957–980.

(20) Suslick, B. A.; Hemmer, J.; Groce, B. R.; Stawiasz, K. J.; Geubelle, P. H.; Malucelli, G.; Mariani, A.; Moore, J. S.; Pojman, J. A.; Sottos, N. R. Frontal Polymerizations: From Chemical Perspectives to Macroscopic Properties and Applications. *Chemical Reviews* **2023**, *123* (6), 3237-3298. DOI: 10.1021/acs.chemrev.2c00686.

(21) Scognamillo, S.; Bounds, C.; Thakuri, S.; Mariani, A.; Wu, Q.; Pojman, J. A. Frontal Cationic Curing of Epoxy Resins in the Presence of Defoaming or Expanding Compounds. *J. Appl. Polym. Sci.* **2014**, *131*, 40339-40349.

(22) Gary, D. P.; Bynum, S.; Thompson, B. D.; Groce, B. R.; Sagona, A.; Hoffman, I. M.; Morejon-Garcia, C.; Weber, C.; Pojman, J. A. Thermal transport and chemical effects of fillers on free-radical frontal polymerization. *J. Polym. Sci.* **2020**, *58* (16), 2267-2277. DOI: 10.1002/pol.20200323.

(23) McCaughey, B.; Pojman, J. A.; Simmons, C.; Volpert, V. A. The Effect of Convection on a Propagating Front with a Liquid Product: Comparison of Theory and Experiments. *Chaos* **1998**, *8*, 520-529.

(24) Zhou, J.; Jia, S.; Fu, W.; Liu, Z.; Tan, Z. Fast curing of thick components of epoxy via modified UV-triggered frontal polymerization propagating horizontally. *Materials Letters* **2016**, *176*, 228-231. DOI: 10.1016/j.matlet.2016.04.103.

(25) Pojman, J. A.; Khan, A., M.; West, W. Traveling Fronts Of Addition Polymerization: A Possible New Method Of Materials Synthesis. *Polymer Preprints* **1992**, *33*, 1188-1189.

(26) Pojman, J. A.; Craven, R.; Khan, A.; West, W. Convective Instabilities In Traveling Fronts of Addition Polymerization. *J. Phys. Chem.* **1992**, *96*, 7466-7472.

(27) Bynum, S.; Tullier, M.; Morejon-Garcia, C.; Guidry, J.; Runnoe, E.; Pojman, J. A. The effect of acrylate functionality on frontal polymerization velocity and temperature. *J. Poly. Sci: Part A: Pol. Chem.* **2019**, *57* (9), 982-988. DOI: 10.1002/pola.29352.

(28) Bansal, K.; Pojman, J. A.; Webster, D.; Quadir, M. Frontal Polymerization of a Thin Film on a Wood Substrate. *ACS Macro Lett.* **2020**, *9*, 169-173. DOI: 10.1021/acsmacrolett.9b00887.
(29) Chechilo, N. M.; Enikolopyan, N. S. Effect of the Concentration and Nature of Initiators on the Propagation Process in Polymerization. *Dokl. Phys. Chem.* **1975**, *221* (5), 392-394.

(30) Mariani, A.; Fiori, S.; Chekanov, Y.; Pojman, J. A. Frontal Ring-Opening Metathesis Polymerization of Dicyclopentadiene. *Macromolecules* **2001**, *34*, 6539-6541.

(31) Robertson, I. D.; Pruitt, E. L.; Moore, J. S. Frontal Ring-Opening Metathesis Polymerization of Exo-Dicyclopentadiene for Low Catalyst Loadings. *ACS Macro Lett.* **2016**, *5* (5), 593-596. DOI: 10.1021/acsmacrolett.6b00227.

(32) Ruiu, A.; Sanna, D.; Alzari, V.; Nuvoli, D.; Mariani, A. Advances in the frontal ring opening metathesis polymerization of dicyclopentadiene. *J. Poly. Sci. Part A. Poly. Chem.* **2014**, *52* (19), 2776-2780. DOI: 10.1002/pola.27301.

(33) Robertson, I. D.; Dean, L. M.; Rudebusch, G. E.; Sottos, N. R.; White, S. R.; Moore, J. S. Alkyl Phosphite Inhibitors for Frontal Ring-Opening Metathesis Polymerization Greatly Increase Pot Life. *ACS Macro Letters* **2017**, *6* (6), 609-612. DOI: 10.1021/acsmacrolett.7b00270.

(34) Scognamillo, S.; Bounds, C.; Luger, M.; Mariani, A.; Pojman, J. A. Frontal cationic curing of epoxy resins. *J. Polym. Sci. Part A: Polym. Chem.* **2010**, *48* (9), 2000-2005. DOI: 10.1002/pola.23967.

(35) Chekanov, Y.; Arrington, D.; Brust, G.; Pojman, J. A. Frontal Curing of Epoxy Resin: Comparison of Mechanical and Thermal Properties to Batch Cured Materials. *J. Appl. Polym. Sci.* **1997**, *66*, 1209-1216. DOI: 10.1002/(SICI)1097-4628(19971107)66:6<1209::AID-APP20>3.0.CO;2-V.

(36) Mariani, A.; Bidali, S.; Fiori, S.; Sangermano, M.; Malucelli, G.; Bongiovanni, R.; Priola, A. UV-Ignited Frontal Polymerization of an Epoxy Resin. *J. Poly. Sci. Part A. Polym. Chem.* **2004**, *42*, 2066-2072. DOI: 10.1002/pola.20051.

(37) Malik, M. S.; Schlogl, S.; Wolfahrt, M.; Sangermano, M. Review on UV-Induced Cationic Frontal Polymerization of Epoxy Monomers. *Polym.* **2020**, *12* (9), 2146. DOI: 10.3390/polym12092146.

(38) Tran, A. D.; Koch, T.; Knaack, P.; Liska, R. Radical induced cationic frontal polymerization for preparation of epoxy composites. *Composites Part A: Applied Science and Manufacturing* **2020**, *132*, 105855. DOI: 10.1016/j.compositesa.2020.105855.

(39) Švajdlenková, H.; Kleinová, A.; Šauša, O.; Rusnák, J.; Dung, T. A.; Koch, T.; Knaack, P. Microstructural study of epoxy-based thermosets prepared by "classical" and cationic frontal polymerization. *RSC Advances* **2020**, *10* (67), 41098-41109. DOI: 10.1039/d0ra08298h.

(40) Birkner, M.; Seifert, A.; Spange, S. Radical induced cationic frontal twin polymerization of Si-spiro compound in combination with bisphenol-A-diglycidylether. *Polymer* **2019**, *160*, 19-23. DOI: 10.1016/j.polymer.2018.11.037.

(41) Sangermano, M.; D'Anna, A.; Marro, C.; Klikovits, N.; Liska, R. UV-activated frontal polymerization of glass fibre reinforced epoxy composites. *Composites Part B: Engineering* **2018**, *143*, 168-171. DOI: 10.1016/j.compositesb.2018.02.014.

(42) Bomze, D.; Knaack, P.; Liska, R. Successful radical induced cationic frontal polymerization of epoxy-based monomers by C-C labile compounds. *Polym. Chem.* **2015**, *6*, 8161-8167. DOI: 10.1039/C5PY01451D.

(43) Crivello, J. V.; Lam, J. H. W. Diaryliodonium Salts. A New Class of Photoinitiators for Cationic Polymerization. *Macromolecules* **1977**, *10* (6), 1307-1315. DOI: 10.1021/ma60060a028.

(44) Crivello, J. V.; Lee, J. L. The synthesis, characterization, and photoinitiated cationic polymerization of silicon-containing epoxy resins. *Journal of Polymer Science Part A: Polymer Chemistry* **1990**, *28* (3), 479-503. DOI: 10.1002/pola.1990.080280303.

(45) Crivello, J. V.; Bulut, U. Dual photo- and thermally initiated cationic polymerization of epoxy monomers. *J. Polym. Sci. Part A: Polym. Chem.* **2006**, *44*, 6750-6764.

(46) Crivello, J. V. Synergistic effects in hybrid free radical/cationic photopolymerizations. *J. Polym. Sci. Part A: Polym. Chem.* **2007**, *45* (16), 3759-3769. DOI: 10.1002/pola.22126.

(47) Crivello, J. V. Cationic photopolymerization of alkyl glycidyl ethers. *J. Polym. Sci. Part A Polym. Chem.* **2006**, *44*, 3036-3052.

(48) Rajaraman, S. K., Mowers, W.A., Crivello, J.V. Interaction of epoxy and vinyl ethers during photoinitiated cationic polymerization. *Journal of Polymer Science Part A: Polymer Chemistry* **1999**, *37* (21), 4007-4018. DOI: 10.1002/(SICI)1099-0518(19991101)37:21<4007::AID-POLA15>3.0.CO;2-8.

(49) Sangermano, M. Advances in cationic photopolymerization. *Pure and Appl. Chem.* **2012**, *84* (10), 2089-2101. DOI: 10.1351/pac-con-12-04-11.

(50) Crivello, J. V.; Falk, B.; Zonca Jr., M. R. Photoinduced Cationic Ring-Opening Frontal Polymerizations of Oxetanes and Oxiranes. *J. Poly. Sci. Part A. Polym. Chem.* **2004**, *42*, 1630-1646.

(51) Nelson, E. W.; Jacobs, J. L.; Scranton, A. B.; Anseth, K. S.; Bowman, C. N. Photo-differential scanning calorimetry studies of cationic polymerizations of divinyl ethers. *Polymer* **1995**, *36* (24), 4651-4656. DOI: 10.1016/0032-3861(95)96832-s.

(52) Sangermano, M.; Razza, N.; Crivello, J. V. Cationic UV-Curing: Technology and Applications. *Macromolecular Materials and Engineering* **2014**, *299* (7), 775-793. DOI: 10.1002/mame.201300349.

(53) Gachet, B.; Lecompère, M.; Croutxé-Barghorn, C.; Burr, D.; L'Hostis, G.; Allonas, X. Highly reactive photothermal initiating system based on sulfonium salts for the photoinduced thermal frontal cationic polymerization of epoxides: a way to create carbon-fiber reinforced polymers. *RSC Adv.* **2020**, *10* (68), 41915-41920. DOI: 10.1039/d0ra07561b.

(54) Bomze, D.; Knaack, P.; Koch, T.; Jin, H.; Liska, R. Radical induced cationic frontal polymerization as a versatile tool for epoxy curing and composite production. *J. Polym. Sci. Part A: Polym Chem.* **2016**, *54* (23), 3751-3759. DOI: 10.1002/pola.28274.

(55) Klikovits, N.; Knaack, P.; Bomze, D.; Krossing, I.; Liska, R. Novel photoacid generators for cationic photopolymerization. *Polym. Chem.* **2017**, *8* (30), 4414-4421. DOI: 10.1039/C7PY00855D.

(56) Knaack, P.; Klikovits, N.; Tran, A. D.; Bomze, D.; Liska, R. Radical induced cationic frontal polymerization in thin layers. *J. Polym. Sci. Part A: Polym Chem.* **2019**, *57* (11), 1155-1159. DOI: 10.1002/pola.29375.

(57) Taschner, R.; Knaack, P.; Liska, R. Bismuthonium- and pyrylium-based radical induced cationic frontal polymerization of epoxides. *Journal of Polymer Science* **2021**, *59* (16), 1841. DOI: 10.1002/pol.20210196.

(58) Tran, A. D.; Koch, T.; Liska, R.; Knaack, P. Radical-induced cationic frontal polymerisation for prepreg technology. *Monatsh Chem* **2021**, *152*, 151-165. DOI: 10.1007/s00706-020-02726-y.

(59) Malik, M. S.; Wolfahrt, M.; Sangermano, M.; Schlögl, S. Effect of a Dicycloaliphatic Epoxide on the Thermo-Mechanical Properties of Alkyl, Aryl Epoxide Monomers Cured via

UV-Induced Cationic Frontal Polymerization. *Macromolecular Materials and Engineering* **2022**, *307* (7), 2100976. DOI: 10.1002/mame.202100976.

(60) Odian, G. *Principles of Polymerization*; Wiley, 2004.

(61) Login, R. B. Vinyl Ether Monomers and Polymers. In *Kirk-Othmer Encyclopedia of Chemical Technology*, 2000.

(62) Chatani, S.; Kloxin, C. J.; Bowman, C. N. The power of light in polymer science: photochemical processes to manipulate polymer formation, structure, and properties. *Polym. Chem.* **2014**, *5* (7), 2187-2201. DOI: 10.1039/c3py01334k.

(63) Trusiano, G.; Vitale, A.; Bonneaud, C.; Pugliese, D.; Dalle Vacche, S.; Joly-Duhamel, C.; Friesen, C. M.; Bongiovanni, R. Vinyl ethers and epoxides photoinduced copolymerization with perfluoropolyalkylether monomers. *Colloid and Polymer Science* **2020**, *299*, 509-521. DOI: 10.1007/s00396-020-04723-3.

(64) Sangermano, M.; Bongiovanni, R.; Malucelli, G.; Priola, A. Cationic photopolymerisation of divinylethers systems containing hydroxyvinylethers. *Polymer Bulletin* **1999**, *42* (6), 641-648. DOI: 10.1007/s002890050513.

(65) Stanislovaityte, E.; Priola, A.; Sangermano, M.; Malucelli, G.; Simokaitiene, J.; Lazauskaite, R.; Grazulevicius, J. V. Cationic photopolymerization of bisphenol-A-based vinyl ether systems. *Progress in Organic Coatings* **2009**, *65* (3), 337-340. DOI: 10.1016/j.porgcoat.2009.02.001.

(66) Conlon, D.; General Electric Corp, R.; Development Center, S. N. Y. Photoinitiated cationic polymerization with multifunctional vinyl ether monomers. *J. Radiat. Curing* **1983**, *10:1*, 6-13.

(67) Kwon, S.; Chun, H.; Mah, S. Photo-induced living cationic polymerization of isobutyl vinyl ether in the presence of various combinations of halides of diphenyliodonium and zinc salts in methylene chloride. *Fibers and Polymers* **2004**, *5* (4), 253-258. DOI: 10.1007/bf02875521.

(68) Sangermano, M.; Malucelli, G.; Morel, F.; Decker, C.; Priola, A. Cationic photopolymerization of vinyl ether systems: influence of the presence of hydrogen donor additives. *European Polymer Journal* **1999**, *35* (4), 639-645. DOI: 10.1016/S0014-3057(98)00168-2.

(69) Klikovits, N.; Liska, R.; D'Anna, A.; Sangermano, M. Successful UV-Induced RICFP of Epoxy-Composites. *Macromol. Chem. Phys.* **2017**, *218*, 1700313. DOI: 10.1002/macp.201700313.

(70) Sangermano, M.; Antonazzo, I.; Sisca, L.; Carello, M. Photoinduced cationic frontal polymerization of epoxy–carbon fibre composites. *Polym Int.* **2019**, *68* (10), 1662-1665. DOI: 10.1002/pi.5875.

(71) Xin, Y.; Xiao, S.; Pang, Y.; Zou, Y. NIR-sensitized cationic frontal polymerization of vinyl ether and epoxy monomers. *Prog. Org. Coat.* **2021**, *153*, 106149. DOI: 10.1016/j.porgcoat.2021.106149.

(72) Lecompère, M.; Allonas, X.; Maréchal, D.; Criqui, A. Versatility of Pyrylium Salt/Vinyl Ether Initiating System for Epoxide Dual-Cure Polymerization: Kick-Starting Effect of the Coinitiator. *Macromolecular Rapid Communications* **2017**, *38* (13), 1600660. DOI: 10.1002/marc.201600660.

(73) Goldfeder, P. M.; Volpert, V. A.; Ilyashenko, V. M.; Khan, A. M.; Pojman, J. A.; Solovyov, S. E. Mathematical Modeling of Free-Radical Polymerization Fronts. *J. Phys. Chem. B* **1997**, *101*, 3474-3482.

(74) Pojman, J. A.; Griffith, J.; Nichols, H. A. Binary Frontal Polymerization: Velocity Dependence on Initial Composition. *e-Polymers* **2004**, *13*, 1-7.

(75) Pojman, J. A.; Elcan, W.; Khan, A. M.; Mathias, L. Binary Polymerization Fronts: A New Method to Produce Simultaneous Interpenetrating Polymer Networks (SINs). *J. Polym. Sci. Part A: Polym. Chem.* **1997**, *35*, 227-230.

(76) J.A Dougherty, J. V. C. Photoinitiated Cationic Polymerization of Vinyl Ether-Epoxy Blends. *Journal of Radiation Curing* **1995**, *22* (2), 19-23.

(77) Decker, C.; Bianchi, C.; Decker, D.; Morel, F. Photoinitiated polymerization of vinyl ether-based systems. *Progress in Organic Coatings* **2001**, *42* (3), 253-266. DOI: 10.1016/S0300-9440(01)00203-X.

(78) Scherzer, T.; Buchmeiser, M. R. Photoinitiated Cationic Polymerization of Cycloaliphatic Epoxide/Vinyl Ether Systems Studied by Near-Infrared Reflection Spectroscopy. *Macromolecular Chemistry and Physics* **2007**, *208* (9), 946-954. DOI: 10.1002/macp.200600649.

(79) María González González, J. C. C. a. J. B. Applications of FTIR on Epoxy Resins – Identification, Monitoring the Curing Process, Phase Separation and Water Uptake. In *Infrared Spectroscopy - Materials Science, Engineering and Technology*, Theophanides, T. Ed.; IntechOpen, 2012.

(80) Ernö Pretsch, P. B., Martin Badertscher. *Structure Determination of Organic Compounds*; Springer-Verlag Berlin Heidelberg, 2009.

(81) Ficek, B. A. The potential of cationic photopolymerization's long lived active centers, PhD Dissertation, University of Iowa, Iowa City, IA, 2008.

(82) Kaalberg, S.; Jessop, J. L. P. Enhancing cationic ring-opening photopolymerization of cycloaliphatic epoxides via dark cure and oxetanes. *Journal of Polymer Science Part A: Polymer Chemistry* **2018**, *56* (13), 1436-1445. DOI: 10.1002/pola.29024.

(83) Eom, H. S.; Jessop, J. L. P.; Scranton, A. B. Photoinitiated cationic copolymerizations: Effects of the oligomer structure and composition. *Polymer* **2013**, *54* (16), 4134-4142. DOI: 10.1016/j.polymer.2013.05.061.

(84) Raspoet, G.; Nguyen, M. T.; McGarraghy, M.; Hegarty, A. F. The Alcoholysis Reaction of Isocyanates Giving Urethanes: Evidence for a Multimolecular Mechanism. *The Journal of Organic Chemistry* **1998**, *63* (20), 6878-6885. DOI: 10.1021/jo9806411.

(85) Teong, S. P.; Chua, A. Y. H.; Deng, S.; Li, X.; Zhang, Y. Direct vinylation of natural alcohols and derivatives with calcium carbide. *Green Chemistry* **2017**, *19* (7), 1659-1662. DOI: 10.1039/c6gc03579e.

(86) Pojman, J. A. Cure-on-Demand Composites by Frontal Polymerization. In *Encyclopedia of Materials: Plastics and Polymers*, Hashmi, M. S. J. Ed.; Elsevier, 2022; pp 85-100.

(87) Ranger Industries. *QuickCure Clay*. 2021. https://rangerink.com/ (accessed March 15, 2021).

(88) Crivello, J. V. Hybrid Free Radical/Cationic Frontal Photopolymerizations. *J. Polym. Sci. Part A Polym. Chem.* **2007**, *45*, 4331–4340.

(89) Schissel, S. M.; Jessop, J. L. P. Enhancing epoxide kinetics and tuning polymer properties using hydroxyl-containing (meth)acrylates in hybrid photopolymerizations. *Polymer* **2019**, *161*, 78-91. DOI: 10.1016/j.polymer.2018.12.010.

(90) Dillman, B. F. The kinetics and physical properties of epoxides, acrylates, and hybrid epoxy-acrylate photopolymerization systems, PhD Dissertation, University of Iowa, Iowa City, IA, 2013.

(91) He, Y.; Xiao, M.; Wu, F.; Nie, J. Photopolymerization kinetics of cycloaliphatic epoxide–acrylate hybrid monomer. *Polymer International* **2007**, *56* (10), 1292-1297. DOI: 10.1002/pi.2278.

(92) Braun, H.; Yagci, Y.; Nuyken, O. Copolymerization of butyl vinyl ether and methyl methacrylate by combination of radical and radical promoted cationic mechanisms. *European Polymer Journal* **2002**, *38* (1), 151-156. DOI: 10.1016/s0014-3057(01)00170-7.

(93) Bevington, J. C.; Huckerby, T. N.; Jenkins, A. D. The Copolymerization Activity of Some Vinyl Ethers. *Journal of Macromolecular Science, Part A* **1999**, *36* (12), 1907-1922. DOI: 10.1081/MA-100101633.

(94) Cai, Y.; Jessop, J. L. P. Decreased oxygen inhibition in photopolymerized acrylate/epoxide hybrid polymer coatings as demonstrated by Raman spectroscopy. *Polymer* **2006**, *47* (19), 6560-6566. DOI: 10.1016/j.polymer.2006.07.031.

(95) Bowden, G.; Garbey, M.; Ilyashenko, V. M.; Pojman, J. A.; Solovyov, S.; Taik, A.; Volpert, V. The Effect of Convection on a Propagating Front with a Solid Product: Comparison of Theory and Experiments. *J. Phys. Chem. B* **1997**, *101*, 678-686. DOI: 10.1021/jp962354b.

(96) Viner, V.; Viner, G. Effect of filler choice on a binary frontal polymerization system. *J. Phys. Chem. B* **2011**, *115* (21), 6862-6867. DOI: 10.1021/jp112365a.

(97) Pojman, J. A. Mathematical modeling of frontal polymerization. *Mathematical Modelling of Natural Phenomena* **2019**, *14* (6), 604. DOI: 10.1051/mmnp/2019059.

(98) Fiori, S.; Mariani, A.; Ricco, L.; Russo, S. First Synthesis of a Polyurethane by Frontal Polymerization. *Macromolecules* **2003**, *36*, 2674-2679. DOI: 10.1021/ma0211941.

(99) Groce, B. R.; Gary, D. P.; Cantrell, J. K.; Pojman, J. A. Front velocity dependence on vinyl ether and initiator concentration in radical-induced cationic frontal polymerization of epoxies. *J. Polym. Sci.* **2021**, *59* (15), 1678-1685. DOI: 10.1002/pol.20210183.

(100) Zabihi, O.; Ahmadi, M.; Nikafshar, S.; Chandrakumar Preyeswary, K.; Naebe, M. A technical review on epoxy-clay nanocomposites: Structure, properties, and their applications in fiber reinforced composites. *Composites Part B: Engineering* **2018**, *135*, 1-24. DOI: 10.1016/j.compositesb.2017.09.066.

(101) Basara, C.; Yilmazer, U.; Bayram, G. Synthesis and characterization of epoxy based nanocomposites. *Journal of Applied Polymer Science* **2005**, *98* (3), 1081-1086. DOI: 10.1002/app.22242.

(102) Solomon, D. H.; Swift, J. D. Reactions catalyzed by minerals. Part II. Chain termination in free-radical polymerizations. *J. Appl. Polym. Sci.* **1967**, *11* (12), 2567-2575. DOI: 10.1002/app.1967.070111216.

(103) Solomon, D. Clay minerals as electron acceptors and/or electron donors in organic reactions. *Clays and Clay Minerals* **1968**, *16* (1), 31-39. DOI: 10.1346/CCMN.1968.0160105.

(104) Nason, C.; Pojman, J. A.; Hoyle, C. The Effect of a Trithiol and Inorganic Fillers on the Photo- Induced Thermal Frontal Polymerization of a Triacrylate. *J. Polym. Sci. Part A Polym. Chem.* **2008**, *46*, 8091-8096. DOI: 10.1002/pola.23106.

(105) Ma, Q.; Zhang, Y.; Launay, V.; Le Dot, M.; Liu, S.; Lalevée, J. How to overcome the light penetration issue in photopolymerization? An example for the preparation of high content iron-containing opaque composites and application in 3D printing. *European Polymer Journal* **2022**, *165*, 111011. DOI: 10.1016/j.eurpolymj.2022.111011.

(106) Garra, P.; Dietlin, C.; Morlet-Savary, F.; Dumur, F.; Gigmes, D.; Fouassier, J.-P.; Lalevee, J. Photopolymerization processes of thick films and in shadow areas: a review for the access to composites. *Polym. Chem.* **2017**, *8* (46), 7088-7101, 10.1039/C7PY01778B. DOI: 10.1039/C7PY01778B.

(107) Jacquet, A.; Geatches, D. L.; Clark, S. J.; Greenwell, H. C. Understanding Cationic Polymer Adsorption on Mineral Surfaces: Kaolinite in Cement Aggregates. *Minerals* **2018**, *8* (4), 130. DOI: 10.3390/min8040130.

(108) Theng, B. K. G. *Clay Mineral Catalysis of Organic Reactions*; Chapman and Hall/CRC, 2018. DOI: 10.1201/9780429465789.

(109) Ziólkowska, D.; Shyichuk, A.; Karwasz, I.; Witkowska, M. Adsorption of Cationic and Anionic Dyes onto Commercial Kaolin. *Adsorption Science & Technology* **2009**, *27* (2), 205-214. DOI: 10.1260/026361709789625306.

(110) Kumari, N.; Mohan, C. Basics of Clay Minerals and Their Characteristic Properties. IntechOpen, 2021.

(111) Zweifel, H. *Plastics Additves Handbook*; Hanser Gardner, 2001.

(112) McCabe, R. W.; Adams, J. M. Chapter 4.3 - Clay Minerals as Catalysts. In *Developments in Clay Science*, Bergaya, F., Lagaly, G. Eds.; Vol. 5; Elsevier, 2013; pp 491-538.

(113) Goli, E.; Parikh, N. A.; Yourdkhani, M.; Hibbard, N. G.; Moore, J. S.; Sottos, N. R.; Geubelle, P. H. Frontal polymerization of unidirectional carbon-fiber-reinforced composites. *Composites Part A: Applied Science and Manufacturing* **2020**, *130*, 105689. DOI: 10.1016/j.compositesa.2019.105689.

(114) Hanumantha Rao, K.; Forssberg, K. S. E.; Forsling, W. Interfacial interactions and mechanical properties of mineral filled polymer composites: wollastonite in PMMA polymer matrix. *Colloids and Surfaces A: Physicochemical and Engineering Aspects* **1998**, *133* (1), 107-117. DOI: 10.1016/S0927-7757(97)00130-1.

(115) Komadel, P. Acid activated clays: Materials in continuous demand. *Appl. Clay Sci.* **2016**, *131*, 84-99. DOI: 10.1016/j.clay.2016.05.001.

(116) Adams, J. M.; Clapp, T. V.; Clement, D. E. Catalysis by montmorillonites. *Clay Minerals* **1983**, *18* (4), 411-421. DOI: 10.1180/claymin.1983.018.4.06.

(117) Yahiaoui, A.; Belbachir, M.; Hachemaoui, A. Cationic Polymerization of 1,2-Epoxypropane by an Acid Exchanged Montmorillonite Clay in the Presence of Ethylene Glycol. *International Journal of Molecular Sciences* **2003**, *4* (11), 572-585. DOI: 10.3390/i4110572.

(118) Allonas, X.; Lecompère, M.; Gachet, B.; Criqui, A.; Maréchal, D.; Croutxé-Barghorn, C. Pyridines as retarding agents in photoinduced thermal frontal cationic polymerization of epoxydes. *Polymer Chemistry* **2021**, *12*, 6846-6853. DOI: 10.1039/d1py01332g.

(119) Falk, B.; Zonca, M. R.; Crivello, J. V. Photoactivated Cationic Frontal Polymerization. *Macromolecular Symposia* **2005**, *226*, 97-108.

(120) Crivello, J. V. Investigation of the photoactivated frontal polymerization of oxetanes using optical pyrometry. *Polymer* **2005**, *46* (26), 12109-12117.

(121) McEwen, W. E.; DeMassa, J. W. Acid generation in the thermal decomposition of diaryliodonium salts. *Heteroatom Chemistry* **1996**, *7* (5), 349-354. DOI: 10.1002/(SICI)1098-1071(199610)7:5<349::AID-HC10>3.0.CO;2-Q.

(122) Taschner, R. Onium Salts for Cationic Polymerization and Ring-opening Metathesis Polymerization, PhD Dissertation, TU Wien, Vienna, Austria, 2023. DOI: 10.34726/hss.2023.71648.

(123) Malik, M. S.; Wolfahrt, M.; Schlögl, S. Redox cationic frontal polymerization: a new strategy towards fast and efficient curing of defect-free fiber reinforced polymer composites. *RSC Advances* **2023**, *13* (41), 28993-29003. DOI: 10.1039/d3ra05976f.

(124) Pojman, J. A. Self Organization in Synthetic Polymeric Systems. *Annals New York Acad. Sci.* **1999**, *879*, 194-214.

(125) Alzate-Sanchez, D. M.; Cencer, M. M.; Rogalski, M.; Kersh, M. E.; Sottos, N.; Moore, J. S. Anisotropic Foams via Frontal Polymerization. *Adv Mater* **2021**, *34* (8), 2105821. DOI: 10.1002/adma.202105821.

(126) Maréchal, D.; Allonas, X.; Lecompère, M.; Criqui, A. Novel Dual-Cure Initiating System for Cationic Polymerization of Epoxides. *Macromolecular Chemistry and Physics* **2016**, *217* (10), 1169-1173. DOI: 10.1002/macp.201500523.

(127) Gao, Y.; Rodriguez Koett, L. E.; Hemmer, J.; Gai, T.; Parikh, N. A.; Sottos, N. R.; Geubelle, P. H. Frontal Polymerization of Thin Layers on a Thermally Insulating Substrate. *ACS Applied Polymer Materials* **2022**, *4*, 4919-4927. DOI: 10.1021/acsapm.2c00497.

(128) Gary, D. P.; Ngo, D.; Bui, A.; Belgodere, J. A.; Pojman, J. A. Cure-on-demand ultra-high solid non-skid coatings through frontal polymerization. *CoatingsTech* **2023**, *Jan-Feb*, 34-44.

(129) Damonte, G.; Maddalena, L.; Fina, A.; Cavallo, D.; Müller, A. J.; Caputo, M. R.; Mariani, A.; Monticelli, O. On novel hydrogels based on poly(2-hydroxyethyl acrylate) and polycaprolactone with improved mechanical properties prepared by frontal polymerization. *European Polymer Journal* **2022**, *171*. DOI: 10.1016/j.eurpolymj.2022.111226.

(130) Li, B.; Zhou, M.; Cheng, M.; Liu, J.; Xu, X.; Xie, X. Rapid preparation of ZnO nanocomposite hydrogels by frontal polymerization of a ternary DES and performance study. *RSC Adv* **2022**, *12* (20), 12871-12877. DOI: 10.1039/d2ra01626e

(131) Martínez-Serrano, R. D.; Ugone, V.; Porcu, P.; Vonlanthen, M.; Sorroza-Martínez, K.; Cuétara-Guadarrama, F.; Illescas, J.; Zhu, X.-X.; Rivera, E. Novel porphyrin-containing hydrogels obtained by frontal polymerization: Synthesis, characterization and optical properties. *Polymer* **2022**, *247*, 124785. DOI: 10.1016/j.polymer.2022.124785.

(132) Yang, Y.; Hu, J.; Liu, J. D.; Qin, Y.; Mao, J.; Liang, Y.; Wang, G.; Shen, H.; Wang, C. F.; Chen, S. Rapid synthesis of biocompatible bilayer hydrogels via frontal polymerization. *Journal of Polymer Science* **2022**, *60* (19), 2784-2793. DOI: 10.1002/pol.20220184.

(133) Li, B.; Xu, X.; Hu, Z.; Li, Y.; Zhou, M.; Liu, J.; Jiang, Y.; Wang, P. Rapid preparation of N-CNTs/P(AA-co-AM) composite hydrogel via frontal polymerization and its mechanical and conductive properties. *RSC Advances* **2022**, *12* (30), 19022-19028. DOI: 10.1039/d2ra02003c.

(134) Ziaee, M.; Johnson, J. W.; Yourdkhani, M. 3D Printing of Short-Carbon-Fiber-Reinforced Thermoset Polymer Composites via Frontal Polymerization. *ACS Appl Mater Interfaces* **2022**, *14* (14), 16694-16702. DOI: 10.1021/acsami.2c02076.

(135) Zhao, S.; Li, J.; An, M.; Jin, P.; Zhang, X.; Luo, Y. Energy-efficient manufacturing of polymers with tunable mechanical properties by frontal ring-opening metathesis polymerization. *Polymers for Advanced Technologies* **2023**, *34* (1), 441- 445. DOI: 10.1002/pat.5895.

(136) Noè, C.; Hakkarainen, M.; Malburet, S.; Graillot, A.; Adekunle, K.; Skrifvars, M.; Sangermano, M. Frontal-Photopolymerization of Fully Biobased Epoxy Composites. *Macromolecular Materials and Engineering* **2022**, *307*, 2100864. DOI: 10.1002/mame.202100864.

(137) Hu, G.; Fu, W.; Ma, Y.; Zhou, J.; Liang, H.; Kang, X.; Qi, X. Rapid Preparation of MWCNTs/Epoxy Resin Nanocomposites by Photoinduced Frontal Polymerization. *Materials (Basel, Switzerland)* **2020**, *13* (24), 5838. DOI: 10.3390/ma13245838.

(138) Zhang, Z.; Gao, C.; Liu, R.; Li, W.; Qiu, J.; Wang, S. Catalyzed frontal polymerization-aided 3D printing of epoxy thermosets. *Additive Manufacturing Letters* **2022**, *2*, 100030. DOI: 10.1016/j.addlet.2022.100030.

(139) Zhang, Z.; Liu, R.; Li, W.; Liu, Y.; Luo, H.; Zeng, L.; Qiu, J.; Wang, S. Direct writing of continuous carbon fibers/epoxy thermoset composites with high-strength and low energy-consumption. *Additive Manufacturing* **2021**, *47*, 102348. DOI: 10.1016/j.addma.2021.102348.

(140) Zhang, Z.; Gao, C.; Liu, R.; Qiu, J.; Pei, Z.; Wang, S. 3D Printing of Frontal-polymerized Multiscale Epoxy Thermoset and Composites. *Manufacturing Letters* **2022**, *33*, 640-643. DOI: 10.1016/j.mfglet.2022.07.079.

(141) Gao, C.; Liu, R.; Li, W.; Qiu, J.; Wang, S. Collaborative printing and in-situ frontal curing of highly-viscous thermosetting composites. *Journal of Manufacturing Processes* **2023**, *89*, 1-9. DOI: 10.1016/j.jmapro.2023.01.048.

(142) Chen, Z.; Ziaee, M.; Yourdkhani, M.; Zhang, X. Multiphysics Modeling of Frontal Polymerization-Assisted Layer-by-Layer Additive Manufacturing of Thermoset Polymer Components. *Additive Manufacturing* **2022**, *59*, 103182. DOI: 10.1016/j.addma.2022.103182.

(143) Yoong Ahm Kim, T. H., Morinobu Endo, Mildred S. Dresselhaus. Carbon Nanofibers. In *Springer Handbook of Nanomaterials*, Vajtai, R. Ed.; Springer-Verlag Berlin Heidelberg, 2013.

(144) Hiremath, N.; Bhat, G. High-performance carbon nanofibers and nanotubes. In *Structure and Properties of High-Performance Fibers*, Bhat, G. Ed.; Woodhead Publishing, 2017; pp 79-109.

(145) Turani, M.; Baggio, A.; Casalegno, V.; Salvo, M.; Sangermano, M. An Epoxy Adhesive Crosslinked through Radical-Induced Cationic Frontal Polymerization. *Macromolecular Materials and Engineering* **2021**, *306* (12), 2100495. DOI: 10.1002/mame.202100495.

(146) Yapici, F., Ozcifci, A., Esen, R., and Kurt, S. The effect of grain angle and species on thermal conductivity of some selected wood species. *BioRes.* **2011**, *6* (3), 2757-2762.

VITA

Brecklyn R. Groce was born and raised in Pensacola, Florida, where he received his B.S. in Chemistry at the University of West Florida in May 2019. He began his Ph.D. studies at Louisiana State University in August 2019, working in Dr. John Pojman's research team. His work at LSU spanned many published projects in frontal polymerization and collaborations with primary investigators at LSU and other domestic and international universities. He additionally mentored multiple undergraduate and high school students on independent projects. He will pursue his interest in academia and begin a postdoctoral research position at Vrije Universiteit Brussel in Brussels, Belgium.